Pure

Bangor University

DOCTOR OF PHILOSOPHY

Behaviour and operation of pumped storage hydro plants.

Mansoor, Saad

Award date:
2000

Link to publication

General rights
Copyright and moral rights for the publications made accessible in the public portal are retained by the authors and/or other copyright owners and it is a condition of accessing publications that users recognise and abide by the legal requirements associated with these rights.

- Users may download and print one copy of any publication from the public portal for the purpose of private study or research.
- You may not further distribute the material or use it for any profit-making activity or commercial gain
- You may freely distribute the URL identifying the publication in the public portal ?

Take down policy
If you believe that this document breaches copyright please contact us providing details, and we will remove access to the work immediately and investigate your claim.

Download date: 02. Apr. 2025

Behaviour and Operation of Pumped Storage Hydro Plants

Thesis submitted to the University of Wales
in candidature for the degree of Doctor of Philosophy

I'W DDEFNYDDIO YN Y
LLYFRGELL YN UNIG

TO BE CONSULTED IN THE
LIBRARY ONLY

April 2000

By
Sa'ad Mansoor

Prifysgol Cymru · University of Wales

School of Informatics

P.C.B LLYFRGELL
U.W.B LIBRARY

SUMMARY

The thesis describes the development of a generic nonlinear computer model of a pumped storage hydroelectric scheme. The model combines the hydraulic, electrical and control systems. In particular, this model includes the water hammer effects, the hydraulic coupling in the common water supply tunnel, the power system stiffness and the electrical coupling between the generator and the power system.

The benefit of the simulation is that it gives insight into the plant characteristics and improves understanding of the physical phenomena involved. A specific case of the model for Dinorwig power station is tested against the plant responses and establishes a good degree of confidence in the simulation. The model is used to evaluate governor performance and establish stability boundaries for various operating conditions. The model is also used to design a new black-start regime which allows Dinorwig to energise the power system after blackout, with individual units picking up incremental loads up to 15% of machine rating while ensuring that frequency deviations remains within limits. Another application of the model is to explain why a period of sustained power oscillation occurred at Dinorwig and to identify under what circumstances this can take place.

Linearised system models are used for governor tuning and root locus and Bode plot methods applied to establish the optimum governor settings for different operation conditions. The results demonstrate the significance of hydraulic coupling and the power system (grid) size on governor tuning.

The final part of the work addresses conversion of the model to run in real-time and interfacing it with an actual unit governor. The results demonstrate the practicality of the hardware-in-the-loop simulation as a technique for safely implementing and testing new controllers or enhancements to the current controller.

ACKNOWLEDGEMENTS

I am grateful for the support and encouragement offered by my supervisor, Dr. Dewi Jones, throughout the course of this project. It has been a great privilege to work for him.

Thanks to Professor David Bradley, now at University of Abertay, for giving me the opportunity to study for a PhD here at Bangor and for his guidance and support during my studies.

I would like to thank Dr. Capell Aris at First Hydro Company, Llanberis, for his help, advice and generously supporting me throughout the project. Thanks are also due to Glyn Jones, Arwel Jones and Darryl Nottingham.

I would like to thank all my friends, who made my time here at Bangor so much fun.

I am grateful to the Engineering and Physical Science Research Council (EPSRC) for the financial support, which made it possible for the project reported in this thesis to be developed.

Finally, I must thank my long suffering wife, Karen, and my sons William and Peter for all their support over the years.

List of Symbols

a : Velocity of sound in water

A : Penstock cross section area

a_{ij} : Partial derivative

A_s : Surge tank cross section area

A_t : Turbine gain

b : System frequency response characteristic (stiffness)

C_s : Storage constant of the surge tank

d : Penstock diameter

D : Load damping

D_n : Turbine damping

D_{pf} & D_{qf} : Frequency sensitivity parameters

E : Elastic modulus of the penstock material

e : Thickness of the penstock wall

E_1 & E_2 : Generator voltage

F : Friction loss in the penstock

f : Frequency

f_0 : Rated frequency

f_{fl} : Steady state frequency at full-load

f_{nl} : Steady state frequency at no-load

f_p : Penstock head loss coefficient

f_r : Friction factor

f_t : Turbine head loss coefficient

g, (G) : Guide vane position

g_a : Acceleration due to gravity

G_{fl} : Guide vane position at full-load

G_{nl} : Guide vane position at no-load

H : Inertia constant

h : The head at the turbine admission

h_0 : The static head of water column

h_f : The head loss due to friction

h_s : The surge tank head

J : Combined moment of inertia of the generator and turbine

k : Bulk modulus of the water

K_d : Derivative gain

K_i : Integral gain

K_p : Proportional gain

l : Length of the tunnel

m : Turbine torque

M : Power system inertia

n : Turbine speed

n_m Rotor speed

P : Active power

P_{12} : Power exchange between the machines

P_m : Turbine output power

P_n : Number of generator poles

P_{tie} : Tie line power

q : Turbine flow

Q : Reactive power

q_{nl} : Turbine no-load flow

q_s : Flow into the surge tank

R : Droop setting

s : Laplace complex frequency variable

t : Time

T_{acc} : Accelerating torque

T_d : Derivative action time

T_e : Wave travel time

T_{et} : Wave travel time from the manifold to the surge tank

T_{ep} : Wave travel time from the turbine to the manifold

T_{elec} : Electromagnetic torque

T_i : Integral action time

T_m : Mechanical starting time

T_{mech} : Mechanical torque

T_s : Synchronising coefficient

T_{sa} : Sampling period

T_{st} : Surge tank period

T_w : Water starting time

T_{wp} : Penstock water starting time

T_{wT} : Tunnel water starting time

v : The water velocity

V : Voltage

X_T : Reactance between two generators

Z_0 : Normalised impedance of the penstock

η : Turbine efficiency

ρ : Water density

ζ : Damping factor

δ : Torque angle

δ_m : Mechanical torque angle of the rotor

ω_m : Mechanical angular velocity

ω_n : Natural frequency

Base values used in thesis

Turbine rating :	310 MW
Generator rating :	330 MW
Static head h_0 :	513 m
Turbine flow q :	65 m^3/s
Turbine speed n :	500 rpm
Rated frequency f_0 :	50 Hz

Contents

Chapter 1

Introduction

1.1 Dinorwig Power Station

Successful operation of a power system depends largely on the engineer's ability to provide reliable and uninterrupted service to loads. Stable operation of a power system depends on the ability to continuously match the electrical output of the generating units to the electrical load of the system. Ideally, the loads must be fed at constant voltage and frequency at all times. In practical terms this means that both voltage and frequency must be held within close tolerance so that the consumer's equipment may operate satisfactorily. For instance, a large drop in frequency could result in high magnetising currents in induction motors and transformers.

This thesis describes a computer simulation of Dinorwig power station. Dinorwig is the largest pumped storage scheme in Europe and the first in the world specially designed to deliver its full output in less than 16 seconds. The power station complex is built beneath the old Dinorwig state quarry, between an upper reservoir (Marchlyn Mawr) and a lower reservoir (Llyn Peris). Water falling from the upper reservoir is used to drive turbo-generators, which supply the British national grid[#] with electricity. During off-peak periods, the water is pumped back into the upper reservoir for future use. Pumping is achieved by using the turbo-generators in reverse as a motorised pump.

[#] This term is used to describe the power system

The role of the Dinorwig is primarily to regulate the frequency of the electricity supply on the grid against disturbances due to changing load conditions. The station's configuration varies widely depending on operational demand. When a sudden demand for power occurs, Dinorwig provides short-term supply while a base load (coal or nuclear) station is brought on-line; this is usually done under manual operation. Dinorwig is also used for continuous frequency regulation, which is achieved by measuring the grid frequency (nominally 50Hz) and actuating the turbine's guide vane by means of a digital electronic governor.

Changes in the financial and regulatory structure of the industry are placing increasing demands on power generators to supply cheap, high quality electricity. For Dinorwig, maintaining financial profitability requires improved accuracy and speed of response to short-term grid load perturbations. This means that advanced control techniques must be used in order to realise the full potential of the plant over a wide range of operating conditions; this leads, in turn, to a need for an authentic dynamic model which fully captures the plant characteristics. There are many reasons for constructing simulation models, e.g. Fasol & Pohl [1] describe how a simulation was used during commissioning of a new hydroelectric plant in Austria and Fasol [2] describes how a simulation assisted in the modernisation of old hydroelectric plant.

1.2 Station Operation

The major components of the system are shown in Figure 1-1. The unit governor receives information on the system frequency and power which, together with the requisite set values, is used to control the turbine guide vanes to regulate the flow of water through the penstock in order to match the system power requirements and regulate the grid frequency. The governor also receives a power reference signal, which is used to provide a feed-forward estimate of the gate opening needed for a given change in generated power. This signal gives a rapid initial response after which the final gate position is determined by governor action.

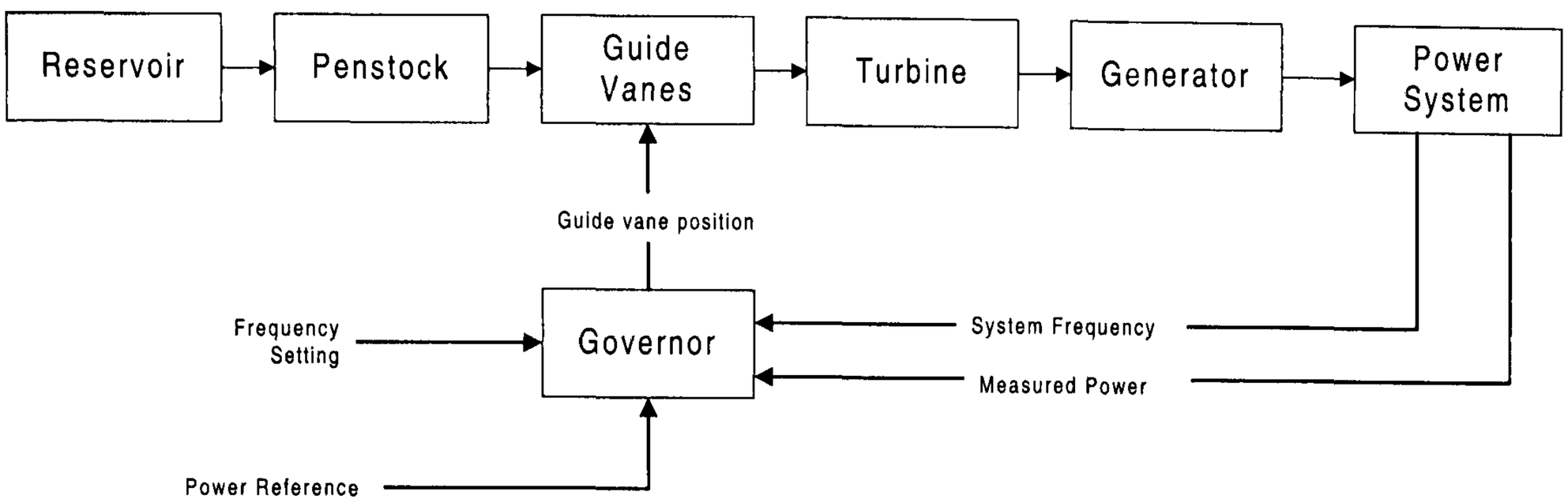

Figure 1-1: *System block diagram*

1.3 Operational Modes

Dinorwig's operations benefit the power system by peak lopping i.e. by generating at times of peak demand and pumping at low demand. Dinorwig is intended to fulfil the three generating roles that involve governor/load control [3]:

Frequency regulation (part-load): The primary operating regime of the Dinorwig station when used for system frequency control is the part-load response mode. In this mode, the demand load on the machine is set by the station operators to a nominal value, typically 50% of full load (150MW at Dinorwig) with subsequent load variations occurring in response to changes in system frequency. Choosing a 150MW set point ensures that the unit operates with a high efficiency. In practice, all units are banned from operating between 110-140MW due to vibration problems in the draft tube of the Francis turbines [4].

Dead-band response: In this operational mode a frequency dead-band of 0.5Hz is included to make the unit insensitive to system frequency changes. Usually the unit is brought on line to 150MW or 288MW as requested by NGC[#].

Immediate reserve: Dinorwig can provide reserve services on very short timescales, whilst spinning in air or at standstill. The station is required to meet a loss of generation equal to 1320MW from spinning-in-water state, without help from any other plant or

---

[#] National Grid Company owns and operates the electricity transmission system in England and Wales

allowing the frequency to drop to 48.5Hz (when the load would be shed by automatic low frequency relay operation).

1.4 Thesis Outline

1.4.1 Aims

The aim of this work is to develop a complete nonlinear simulation model of Dinorwig, using the MATLAB®/SIMULINK® software package. Although generic in nature, the model is structured to accommodate the special features of Dinorwig, which include the interaction of several machines operating with the power system and the effect of multiple penstocks fed from a common water supply tunnel. The main benefits sought from this simulation project are as follows:

- Improved insight into the plant characteristics and understanding of the physical phenomena as a result of constructing the model.
- Improved station response (speed and quality of the electricity supplied) by tuning the governor for various operating conditions and development of a new control strategy.
- Response prediction during the design of new control systems and parameter sensitivity analyses.
- Development of a new black-start regime (start-up from shut down without external supply) to be implemented at Dinorwig.
- Prevision of a hardware-in-the-loop (HIL) version, which provides a tuning strategy and a 'low-risk' route to implementation.
- A facility for operator training.

1.4.2 Structure

An introduction to the physical characteristics of the Dinorwig hydraulic system is given in Chapter 2. Different types of system models are examined and the advantages of using nonlinear models for simulation studies are discussed. The effect of water elasticity and the hydraulic coupling between units sharing a common tunnel is considered and why

they should be incorporated into the simulation model of Dinorwig is explained. Other features of the system are also introduced such as types of pressure control system and surge tanks. Finally, an evaluation of the parameters of the hydraulic system at Dinorwig is presented.

Chapter 3 gives an overview of characteristics of the various components of the power system. Emphasis is given to the transient behaviour in which the system is described mathematically by ordinary differential equations. Because Dinorwig's main activity is frequency regulation, more attention is paid to active (rather than reactive) power control. The effects of the system stiffness, load dynamics and the coupling between the generating units are introduced.

In chapter 4 an analytical approach is applied to obtain transfer functions for the control system and the guide vane dynamics. System identification techniques consisting of frequency and step response measurements are used to verify the analytical models. These tests revealed several unexpected features which were subsequently included in the simulation.

Chapters 2, 3 and 4 together describe models for system components and Chapter 5 integrates them into a complete novel nonlinear Simulink model. This approach provides a cost-effective and rapid method of analysing the responses of Dinorwig power station because it explores the link between the power system and individual units in a way not previously possible. The results show the limitation of the linearised models used for simulation studies. The chapter concludes by presenting two methods of verification - first by comparing with a real plant response and secondly by comparing with an independent model of Dinorwig.

Chapter 6 details the research undertaken into the governor tuning and how this could be used to improve the response of Dinorwig and establish stability boundaries for different operation modes. Current research into governor tuning methods is reviewed. The study shows that there is a high level of interaction between the governor settings and power system loading which implies that, in order to achieve optimum performance, the governor loop gains should be continually adjusted to take account of power system loading. Furthermore, the unit operation modes affect the governor loop gains and suggest that gain scheduling could be used to achieve optimum system response.

Chapter 7 illustrates the application of the simulation. A novel black-start scheme for Dinorwig is designed using the model. The new scheme enhances the station's

capabilities to load pick, and endorses Dinorwig's importance to the British national grid restoration plan. The model is also used to investigate undesirable responses of the station and help find a remedy, such as the case of oscillatory behaviour that occurred at Dinorwig during special operating conditions. The outcome of this study led to a change in Dinorwig's operational strategy. The model is later used to establish a relationship between the power system loading and the governor gain settings, based on Dinorwig's response to different power system sizes. The results show the effectiveness of the simulation for analysing station performance and enhancing its operation.

Chapter 8 demonstrate the practicality of real-time hardware-in-the-loop testing as a technique for testing a control system. This arrangement provides a safe path for investigating the effects of changing the strategy of the control system before being implemented into Dinorwig. This is a novel application of simulation, because this type of system has traditionally not been thought of in power system control engineering terms. Tests were carried out and the results concluded that real-time control is possible for such an arrangement.

Finally, Chapter 9 draws general conclusions on this research and suggests possibilities for the direction and nature of future work.

1.4.3 Contributions to published literature

- S. P. Mansoor, D. A. Bradley, C. Aris, and G. Jones, "The Development of a Hardware-in-the-Loop Simulation of a Pump Storage Hydro Power Station," *Proceedings of Mechatronics'98*, pp. 633-638, 1998.

- S. P. Mansoor, D. A. Bradley, C. Aris, and G. Jones, "The Influence of the Grid on the Response of Pump Storage Hydro-Power Station," *in Proc. the 2nd IMACS Int. Conf. On: Circuits, Systems and computers*, pp. 618-622, 1998.

- S. P. Mansoor, D. A. Bradley, C. Aris, and G. Jones, "The Influence of the Grid on the Response of Pump Storage Hydro-Power Station," *World Scientific*, vol. Recent Advances in Circuits and Systems, pp. 259-263, 1998.

- S. P. Mansoor, D. I. Jones, D. A. Bradley, C. Aris, and G. Jones, "Stability of a Pump Storage Hydro-Power Station Connected to a Power System," *in Proc. IEEE power Winter Meeting 1999, New York*, pp. 646-650, 1999.

- S. P. Mansoor, "Modelling of a Multiple Pump-Storage Units connected to a Power System," *in. Proc of the Institute of Physics PREP"99*, pp. 412-415, 1999.
- S. P. Mansoor, D. I. Jones, D. A. Bradley, C. Aris, and G. Jones, "Modelling of a Pumped Storage Hydro Power Station for Stability Studies", *Int. Journal on Hydropower & Dams "Hydropower into the Next Century"*, pp. 535-544, 1999.
- S. P. Mansoor, D. I. Jones, D. A. Bradley, C. Aris, and G. Jones, "Simulation of Oscillatory Behaviour at Dinorwig Pumped Storage Hydro Power Station," *Int. Journal on Hydropower & Dams "Hydropower into the Next Century"*, pp. 587-594, 1999.
- S. P. Mansoor, D. I. Jones, D. A. Bradley, C. Aris, and G. Jones, "Computer simulation of a fast-response hydroelectric power station" has been in press for publication in the *"IFAC Journal "Control Engineering Practice"*.

Chapter 2

Hydraulic System Model

2.1 Introduction

This chapter examines the characteristics of the hydraulic prime mover based on the fundamental relationships between the elements of the system. Models of the hydraulic system are developed systematically with increasing complexity suitable for their representation in system dynamic studies. Section 2.2 describes the effects of the characteristics of the water column on the performance of the hydraulic turbine. These include the effects of water inertia, water compressibility and pipe wall elasticity in the penstock or pressure tunnel feeding the turbine. Water column inertia causes changes in the turbine flow to lag behind changes in the turbine guide vane opening. This introduces phase lag into the speed-governing loop and hence has a destabilising effect on the generating unit. Pipe wall elasticity causes travelling waves of pressure and flow in the pipe. These are of little consequence when the penstock is short in relation to the wave velocity but can build up to destructive levels in cases where resonance between the penstock and the control system causes standing waves and local magnification of pressure oscillation.

The work then proceeds to analyse the hydraulic coupling due to a common tunnel supplying multiple penstocks. A solution to pressure variation the system due to guide vane movement in is introduced and incorporated in the model. In Section 2.4 linearised models of the hydraulic system are obtained for use in the control design study in

Chapter 6. The Dinorwig pumped storage scheme is constructed as shown in Figure 2-1. It has a simple layout consisting of the upper reservoir, a low pressure tunnel and a high pressure tunnel. The high-pressure tunnel is bifurcated into six individual penstocks, each supplying a turbine unit. Hence, the total flow in the common tunnel will depend upon the number of units in operation. Figure 2-1 shows the data used in Section 2.6 for evaluation of the system parameters and then, later in the thesis, they are utilised in the simulation studies.

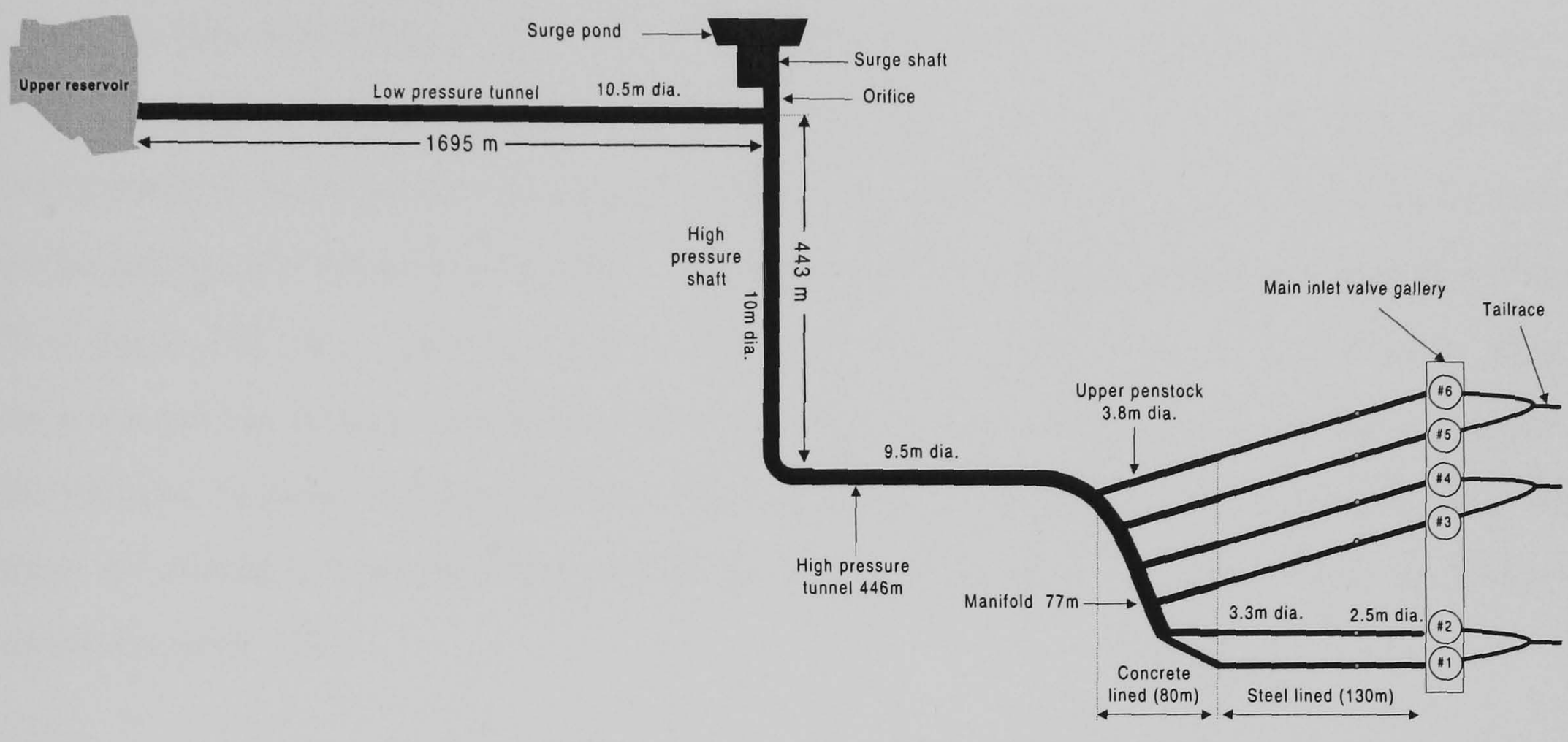

Figure 2-1: *Dinorwig hydraulic system*

2.2 Turbine Model

The oldest form of energy conversion is by the use of waterpower; the turbine converts the potential energy of the water into the rotational kinetic energy of the turbine. In the traditional hydroelectric scheme the energy is obtained free of cost as the water comes from a high level reservoir into the turbine in which the water energy is converted directly to mechanical energy. In the turbine, the tangential momentum of the water passing through a runner's blade will be changed in direction and a tangential force on the runner is produced. The runner therefore rotates and the energy is transferred from the water to the runner and hence to the output shaft. The water is discharged with reduced energy. The hydraulic turbine may be classified into one of two general categories: impulse and reaction [5].

Impulse turbine

The impulse turbine has one or more fixed nozzles, in each of which the pressure is converted to the kinetic energy of a water jet. The jets of water then impinge on the moving plates of the runner where they lose practically all their kinetic energy. The velocity of the water at discharge is only sufficient to enable it to move clear of the runner. The important feature of the impulse turbine is that there is no change of static pressure across the runner. The only hydraulic turbine of the impulse type is the Pelton wheel, as shown in Figure 2-2. The rotor consists of a circular disc with several "buckets" evenly spaced around its periphery. The splitter ridge in the centre of each bucket divides the oncoming water jet into two equal portions and after flowing around the inner surface of the bucket, the water leaves with a velocity opposite in direction to the original jet. The flow partly fills the buckets, and the water remains in contact with the atmosphere. Thus once the jet has been produced the static pressure of the water is atmospheric throughout the turbine. Impulse turbines are best suited to applications with high hydraulic head, and they are characterised by high reliability, low maintenance cost and high efficiency, which exceeds 90%.

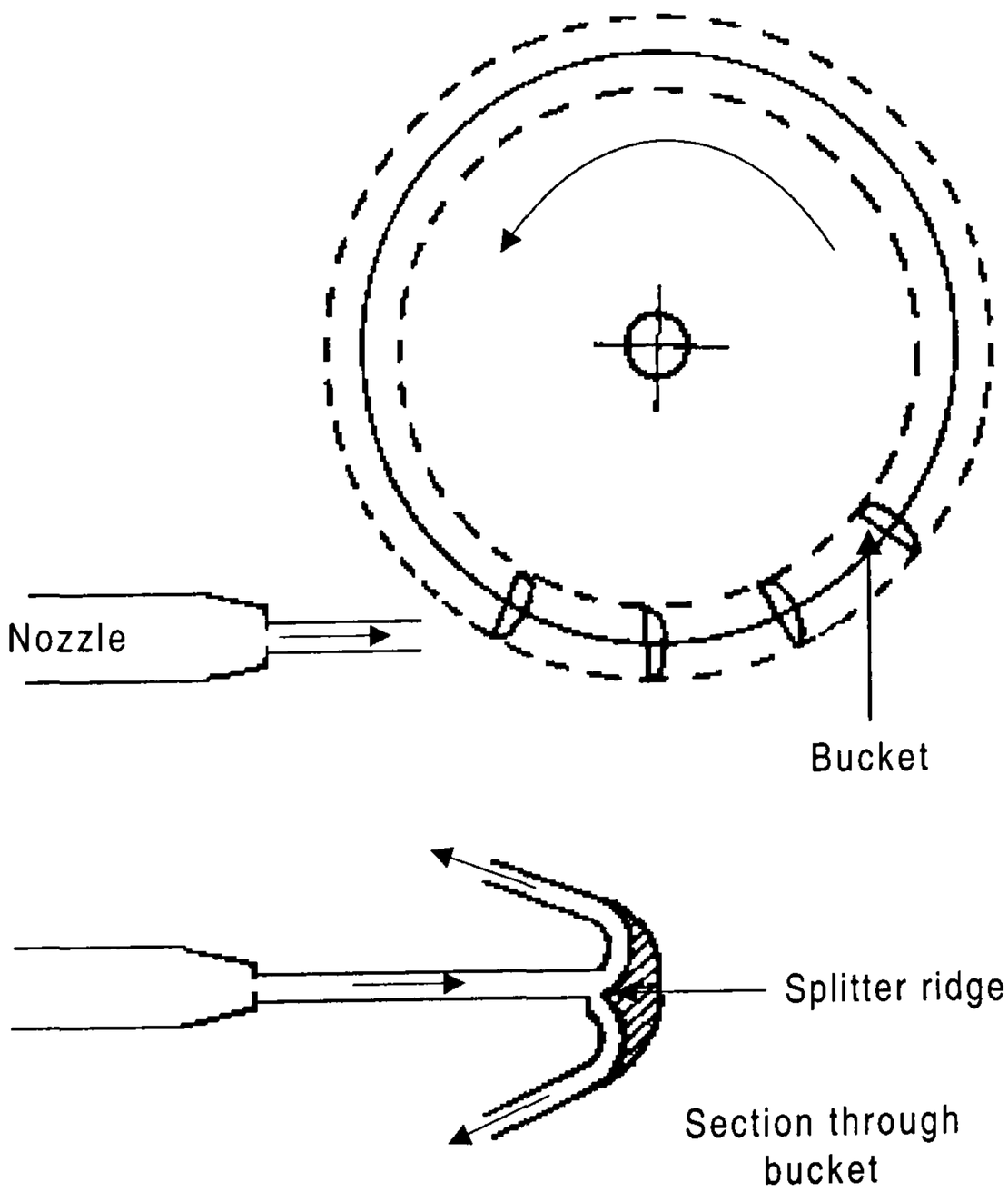

Figure 2-2: *Impulse turbine*

Reaction turbines

In the reaction turbine, the water is fed to the runner all around the circumference from a volute casing through a ring of guide vanes. To keep the pressure losses in the runner at a minimum, it is necessary for the runner to be always full with water (in contrast to the impulse turbine where only a few of the runner blades are in use at any moment). Therefore reaction turbines are able to deal with a larger quantity of water for a given runner size.

The classifications of turbines are based on the predominant direction of water flow through the runner. In a radial-flow turbine the path is wholly or mainly in the plane of the rotation, the water enters the rotator at one radius and leaves at a different radius – the Francis turbine is an example of this type. If however the main flow direction is parallel to the axis of rotation, then the turbine is said to be an axial-flow turbine – the *Kaplan* or *Propeller* turbines are examples of this type. The number of runner blades varies with the hydraulic head – the higher the head the more blades there are in the runner. The *Propeller* turbine has fixed blades while the blade pitch in *Kaplan* turbines is automatically adjusted by the means of an oil driven piston located in the main shaft. The control is designed such that the blade angle varies automatically with the guide vane opening to produce a maximum possible efficiency for a given operating condition. The fixed *Propeller* turbine has a good efficiency at the optimum design point but it decreases sharply with the reduction of flow. Because of the adjustable blades feature, the *Kaplan* turbine has a relatively flat efficiency curve over a wide range of flow. If the flow is partly radial and partly axial, the term mixed flow turbine is used.

Dinorwig power station is equipped with reversible pump-turbines of the Francis type, as illustrated in Figure 2-3. The water enters a spiral casing (volute) which surrounds the runner, whose cross sectional area decreases along the water path in such a way as to keep the water velocity constant in magnitude. Departing the volute the water is directed on to the runner by the guide vanes mounted all around the periphery of the runner. Each vane is pivoted and all will be turned in synchronism to alter the flow rate throughout the turbine, and hence the power output as required by governor action. The runner blades deflect the water so that its angular momentum is changed. From the centre of the runner, the water is turned into the axial direction and flows to the tailrace via the

draft tube. To ensure the hydraulic turbine is full of water, the lower end of the draft tube is always submerged below the water level in the tailrace.

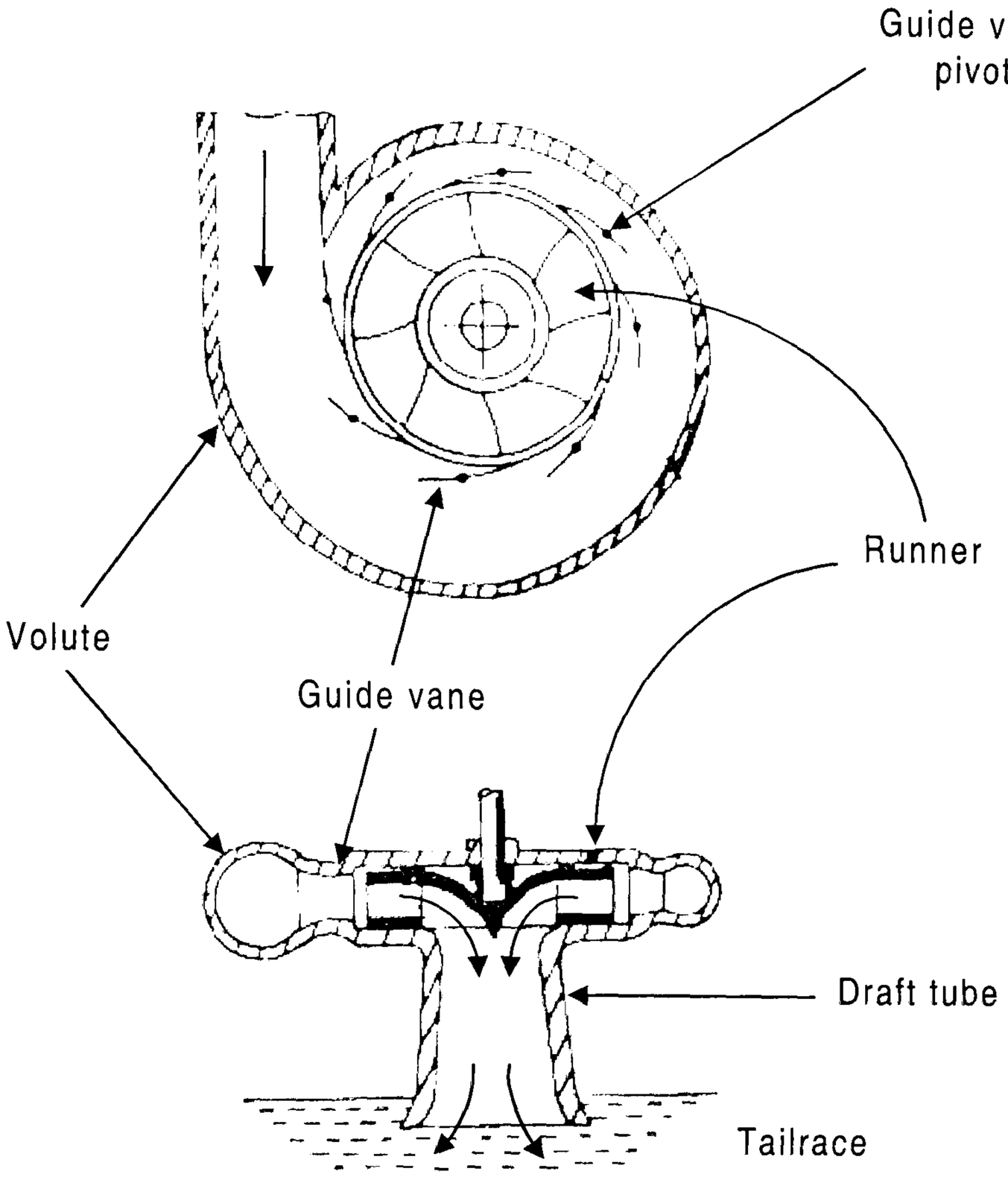

Figure 2-3: *Francis turbine*

The mechanical power (P_m) available from an ideal hydraulic turbine is the product of hydraulic head available (h) and mass flow rate (q) but in practice this is reduced by an efficiency factor, η, to account for power losses. The turbine torque at rated speed and head is almost linearly related to guide vane position for most turbines in the range from no-load to rated load but only approximately in the range from fully closed guide vane to no load guide vane, as shown in Figure 2-4. The turbine model is based on the equation for steady state operation relating the output power to water flow and head [6].

$$P_m = \eta q \rho g_a h \tag{2-1}$$

where[#]:

P_m = Turbine output power

η = The turbine efficiency

ρ = Water density

g_a = Acceleration due to gravity, m^2/s

h = The head at the turbine admission, m

q = Actual turbine flow, m^3/s

The fact that the turbine is not 100% efficient is taken into account by subtracting the no-load flow q_{nl} from the net flow to give the effective flow which, when multiplied by the head, produces mechanical power. There is also a turbine damping effect, which is a function of guide vane opening, to be included. Therefore the per unit turbine power, P_m can be expressed as:

$$P_m = A_t h(q - q_{nl}) - D_n G \Delta n \tag{2-2}$$

The turbine MW rating is used as power base, q_{base} is chosen as the turbine flow rate, with guide vanes fully open (guide vane position =1) and h_{base} is equal to the static head of water column h_0. The base values used throughout the thesis are shown in the symbol table. The parameter D_n accounts for the effect of the speed variation Δn on the turbine efficiency; typical values of D_n fall in the range $0.5 \leq D_n \leq 2.0$. The turbine gain A_t is obtained from the ratio of effective gate position to the actual gate position and can be calculated using equation (2-3).

$$A_t = \frac{1}{G_{fl} - G_{nl}} \times \frac{\text{Turbine MW rating}}{\text{Generator MW rating}} \tag{2-3}$$

where G_{fl} is the guide vane position at full load and G_{nl} is the guide vane position at no-load both are calculated at rated speed and head. The relationship between idealised and real guide vane position is shown in Figure 2-4.

[#] SI units are used in this thesis for physical quantities although the models are mostly expressed in the per-unit system.

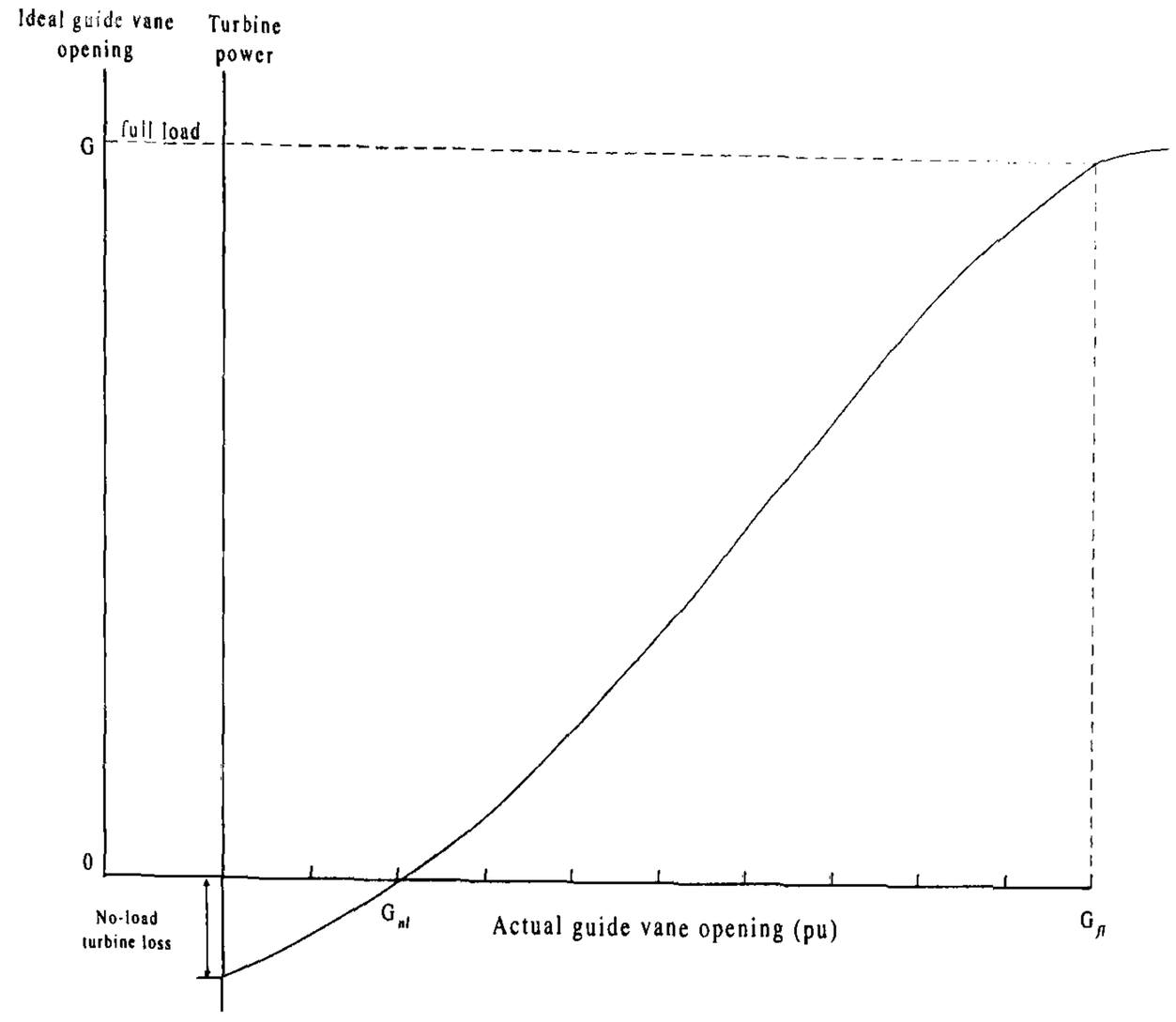

Figure 2-4: *Typical torque/guide vane characteristic*

The turbine characteristics define base flow through the relationship between the flow (q), guide vane (G) position and head (h). The per unit flow rate through the turbine using q_{base} as the turbine flow rate and h_{base} is equal to the static head h_0, is given by its valve characteristic,

$$\bar{q} = \bar{G}\sqrt{\bar{h}} \tag{2-4}$$

A linearised representation of the turbine can be established using the turbine data obtained by testing the system. The power developed by the turbine is a function of flow through it, the guide vane position and the utilised head. Therefore, the behaviour of the turbine may be characterised by the variation in flow (q) and output torque (m) relative to speed (n), guide vane opening (g) and the head (h). Figure 2-5 shows the 4-quadrant operating characteristics for one of Dinorwig's pump turbines [7]. These curves are obtained by testing the turbine for particular guide vane opening, the speed is varied and the turbine flow and torque are measured. The tests are repeated for various guide vane openings, from these curves it can be establish what the speed of the turbine should be, at any guide vane opening in order to give the best efficiency for that guide vane position.

For small variations around an operating point the turbine can be represented by the following linearised Taylor series approximations relating the flow and torque to head, speed and guide vane position [8].

$$\Delta q = a_{11}\Delta h + a_{12}\Delta n + a_{13}\Delta g \tag{2-5}$$

$$\Delta m = a_{21}\Delta h + a_{22}\Delta n + a_{23}\Delta g \tag{2-6}$$

The parameters a_{ij} are the partial derivatives of flow and torque with respect to head speed and guide vane position respectively. They remain constant for variation near the operating point (q_0, m_0). Their value depends upon the initial steady state point of the turbine and they can be measured accurately by experiment.

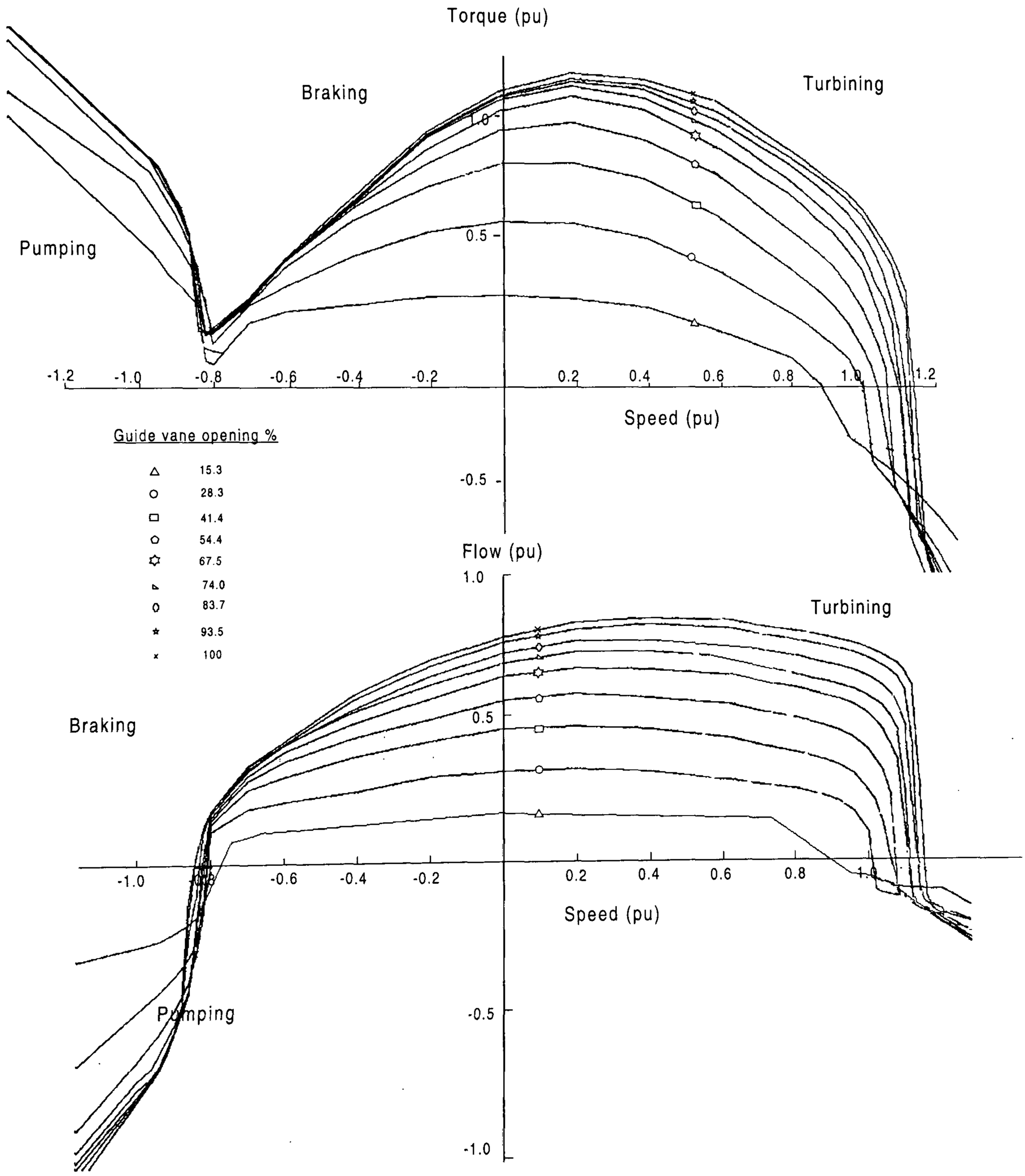

Figure 2-5: *Pump-Turbine characteristic*

Changes in turbine power output are essentially determined by two components, one related to turbine guide vane position and the other to changes in speed. Since the extent of the anticipated frequency variations (and hence the associated speed changes) are generally very small, especially when the plant is connected to the power system, they may be assumed to be insignificant. Variation of flow with the rated speed a_{12} is very small, as shown in the turbine characteristic of Figure 2-5, therefore it is possible to neglect it. The deviation of the mechanical torque with speed a_{22} is known as turbine self-regulation, which is negative with an absolute value near unity. For an ideal loss-less turbine operating at rated speed and head, the partial derivatives versus load are deduced as [9].

$$a_{11} = 0.5 \qquad a_{12} = 0 \qquad a_{13} = 1$$

$$a_{21} = 1.5 \qquad a_{22} = -1 \qquad a_{23} = \frac{\partial m}{\partial g}$$

The turbine representation depends mainly on the coefficient a_{23}. This coefficient is a critical parameter for an accurate approximation of the unit dynamics; a_{23} varies widely from the ideal value of unity. It can be measured precisely from the torque/guide vane characteristic, a curve that is readily found by test [10]. At Dinorwig, a test was carried out to determine the power output versus guide vane opening for different head conditions as shown in Figure 2-6 [11]. This relationship was used to evaluate the Dinorwig turbine gain when operating at rated speed and head. Dinorwig turbine rating is 310MW and the generator rating is 330MW thus using equation (2-3) results in $A_t = 1.12$, which is used in the simulation later in the thesis.

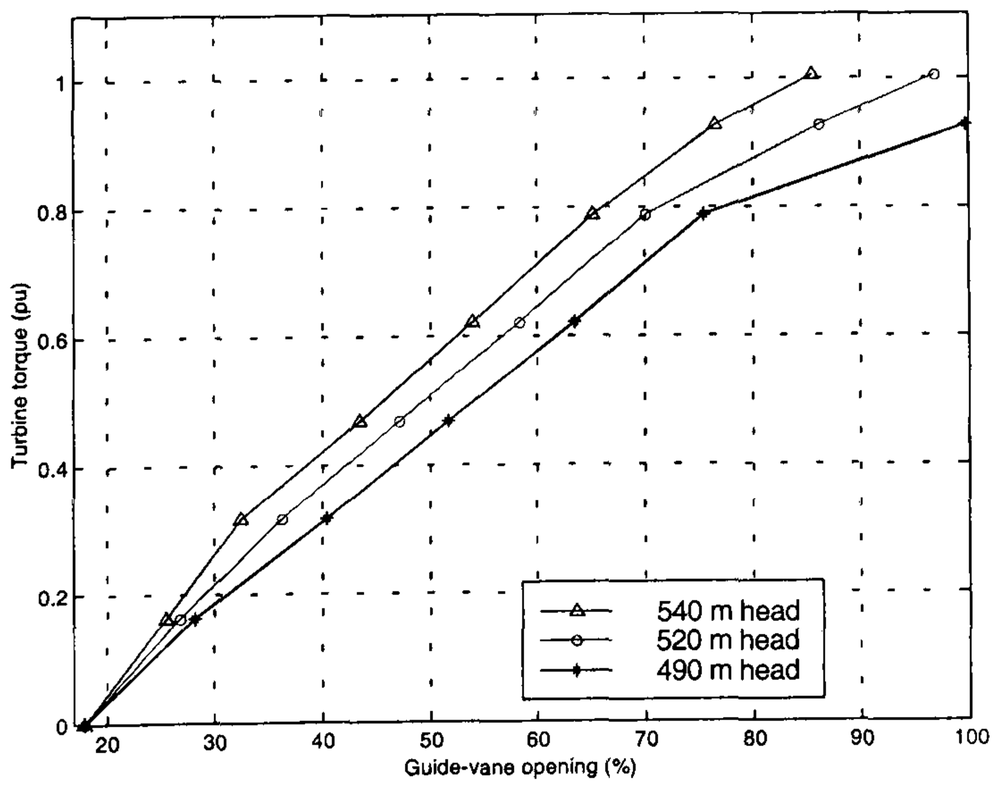

Figure 2-6: *Torque/guide vane characteristic for Dinorwig*

2.3 Modelling the Water Column

The performance of a hydraulic turbine is greatly influenced by the characteristics of the water column which feeds it; these include the effects of water inertia, water compressibility and pipe wall elasticity in the penstock. The effect of water inertia is to cause changes in turbine flow to lag behind changes in the guide vane opening. In fact, the power has a transient response which is initially in the opposite sense to that intended by changing the guide vane position. Although the turbine guide vane opening may change rapidly, the water column inertia prevents the flow from changing as rapidly. Consequently, after a rapid increase in guide vane opening, and before the flow has had time to change appreciably, the velocity of water into the wheel drops because of the increased area of the guide vane opening. The power transfer to the wheel actually drops before it increases to its required steady state value. This is the most prominent factor, which makes a hydraulic turbine such an uncooperative component in a speed control system [12].

Pipe wall elasticity causes travelling waves of pressure and flow in the water - a phenomenon commonly referred to as water hammer. Water hammer occurs when a change in pressure, above or below normal pressure, is caused by a sudden change in the rate of water flow. Because sudden changes in the demand for water occur during load fluctuation, water hammer occurs at all points in the penstock between the forebay and the turbine. Under severe conditions, the effect can damage or destroy valves, turbine guide vanes and the penstocks.

2.3.1 Single penstock modelling

A simple hydropower plant consists of a single conduit supplying a turbine-generating unit, and the initial model development is restricted to this case with an inelastic water column. The turbine and penstock characteristics are determined by three basic equations relating to the velocity of water in the penstock, acceleration of the water column under the influence of gravity and the production of mechanical power in the turbine. First, a non-linear representation is developed which is appropriate when large changes in speed and power are to be considered, such as in islanding, load rejection and system restoration studies.

The basic water column model represents a single penstock with a very large or no surge tank. The penstock is modelled on the assumption that the water acts as an incompressible fluid so that here the water hammer effect may be neglected. Consider here a rigid conduit of length *l* and cross-section area A, where the penstock head losses h_f due to the friction of water against the penstock wall are proportional to flow (q) squared.

$$h_f = f_p q^2 \tag{2-7}$$

where f_p, is the head loss coefficient in the penstock due to friction [13]. The loss coefficients in different parts of the Dinorwig hydraulic system are calculated in Section 2.6.3.

Assuming that the water in the penstock can be treated approximately as a solid mass, the rate of change of flow can be related to the head of water using Newton's 2nd law of motion. This state that "*An object's acceleration is proportional to the net force, and the object's mass is the proportionality factor between the force and the acceleration*" The force on the water mass is

$$(h_0 - h - h_f)\rho g_a A = \rho A l \frac{dv}{dt} \tag{2-8}$$

where

h_0 = The static head of water column, m

h = The head at the turbine admission, m

h_f = The head loss due to friction, m

f_p = head loss coefficient, $m/(m^3/s)^2$

v = The water velocity, m/s

The rate of change of the flow in the penstock can be determined as:

$$\frac{dq}{dt} = (h_0 - h - h_f)\frac{g_a A}{l} \tag{2-9}$$

Equation (2-9) can be written in per unit form in order to normalise system representation. Compared to the use of physical units, the per unit format offers computational simplicity by eliminating units and expressing the system quantities as dimensionless ratios. The base values are chosen so that the principle variables will be equal to one per unit under

rated conditions. Here the base head h_{base} is chosen to be the available static head h_0 which is equal to the reservoir head minus the tailrace head, and the base flow q_{base} is equal to the turbine flow with guide vane fully open. Expressing equation (2-9) in per unit yields

$$\frac{d\bar{q}}{dt} = (\bar{1} - \bar{h} - \bar{h_f}) \ \frac{h_{base} g_a A}{l q_{base}} \tag{2-10}$$

$$\frac{d\bar{q}}{dt} = \frac{(\bar{1} - \bar{h} - \bar{h_f})}{T_w} \tag{2-11}$$

where $T_w = \dfrac{l q_{base}}{h_{base} g_a A} = \dfrac{l v_{base}}{h_{base} g_a}$ is the water inertia time constant, sometimes known as the water starting time.

The water starting time represents the time required for a head h_{base} to accelerate the water in the penstock from standstill to the velocity v_{base}. This is calculated between turbine inlet and the forebay or the surge tank if a large one exists [14]. Consider a simple penstock supplied from an open reservoir discharging into the atmosphere as shown in Figure 2-7. Opening the guide vane in a time Δt causes the velocity of the water in the penstock to increase by Δv and the head at the turbine inlet to drop by Δh.

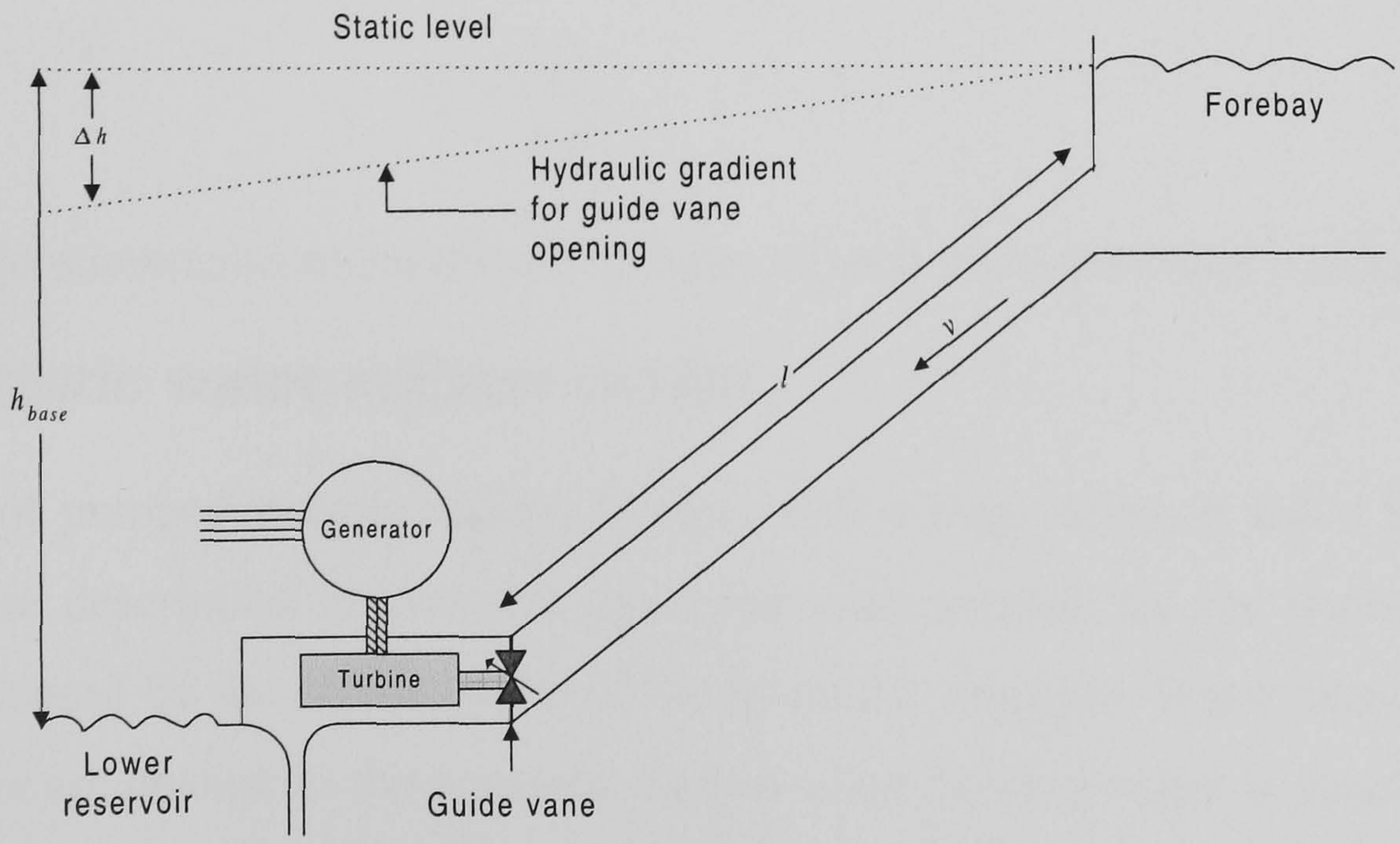

Figure 2-7: *Schematic of pump storage plant*

The acceleration of water due to change in head at the turbine, characterised by Newton's 2nd law of motion may be expressed as

$$\rho A l \frac{d\Delta v}{dt} = -\rho g_a A \Delta h \tag{2-12}$$

The acceleration equation can be converted to per unit form by dividing by v_{base} and h_{base} to give:

$$\left(\frac{l v_{base}}{g_a h_{base}} \right) \frac{d\Delta \bar{v}}{dt} = -\Delta \bar{h} \tag{2-13}$$

Writing in terms of per unit variables

$$T_w \frac{d\Delta \bar{v}}{dt} = -\Delta \bar{h} \tag{2-14}$$

This equation represents an important characteristic of the hydraulic plant. Inspection of equation (2-14) shows that, if the guide vane is closed, a back pressure will arise causing the water to decelerate. That is, if there is a positive pressure change, there will be a negative acceleration change. Similarly, a negative pressure change will cause a positive acceleration change. The maximum acceleration occurs immediately after the guide vane opening because the entire difference in pressure is available for accelerating the water. For a non-uniform penstock with different cross sectional areas, the water inertia time constant is calculated as [15]:

$$T_w = \frac{\sum l v}{g_a h} \tag{2-15}$$

where $\sum lv$ is the summation of length and velocity of sections in the water passage.

2.3.2 Elastic water column model

The majority of pumped storage stations operate with a long penstock and a high head and an accurate description of penstock dynamics must account for the water hammer phenomenon caused by the characteristic of the hydraulic line [16]. Water hammer is the result of a pressure change in the penstock caused when flowing water is decelerated or accelerated by closing or opening the guide vane or changing the velocity of the water rapidly in some other manner. The phenomenon is characterised by a series of positive

and negative pressure waves, which travel back and forth in the penstock until they are damped out by friction.

To investigate the effect of the water elasticity on the hydraulic system, consider the case of water flowing with a certain velocity in a penstock being brought to rest by closing the turbine guide vane. If the water was entirely incompressible and the penstock wall perfectly rigid, then all the particles in the entire column of water would have to decelerate together. From Newton's 2nd law of motion, the more rapid the deceleration the greater would be the corresponding force, and with an instantaneous closure of the guide vane all the water would be stopped instantaneously and the force would be infinite which is clearly impossible. In fact, even the water is to some extent compressible and so its particles do not decelerate uniformly. A rapid closure of the guide vane would not bring the entire column of water to a halt immediately. Only those particles of water in contact with the guide vane would be stopped at once and the others would come to rest later.

Consider a rigid penstock, when a guide vane is suddenly closed the pressure head immediately upstream of the guide vane is increased, causing a high-pressure wave to propagate to the upper reservoir (or the surge tank if one exists). The water particles nearest to the guide vane are compressed by the water above it. The water will continue to move at the original velocity and successive elements of water are compressed. The action of compression moves upstream as a wave until it reaches the open water surface. The pressure wave moves at velocity, a, which is the velocity of sound in water. The time taken for the pressure wave to travel the length of the penstock to the open surface is called the wave travel time T_e, which is given as:

$$T_e = \frac{l}{a} \tag{2-16}$$

The kinetic energy of the moving water is converted to elastic energy in compressing the water and stretching the penstock. The last water element will expand at the open water surface to its original state followed by other elements, causing a negative pressure wave.

As the wave travels downstream, conditions change from an increased water pressure head back to the normal pressure when the wave reaches the guide vane at time, $t = 2T_e$. The water moving away from the guide vane will cause a reduction in pressure and a negative pressure wave moves upstream to the open water surface [17]. The periodic fluctuation following a sudden guide vane closure is shown schematically in

Figure 2-8. In practice, water friction will act within the water and at the boundaries so that the pressure wave will be attenuated.

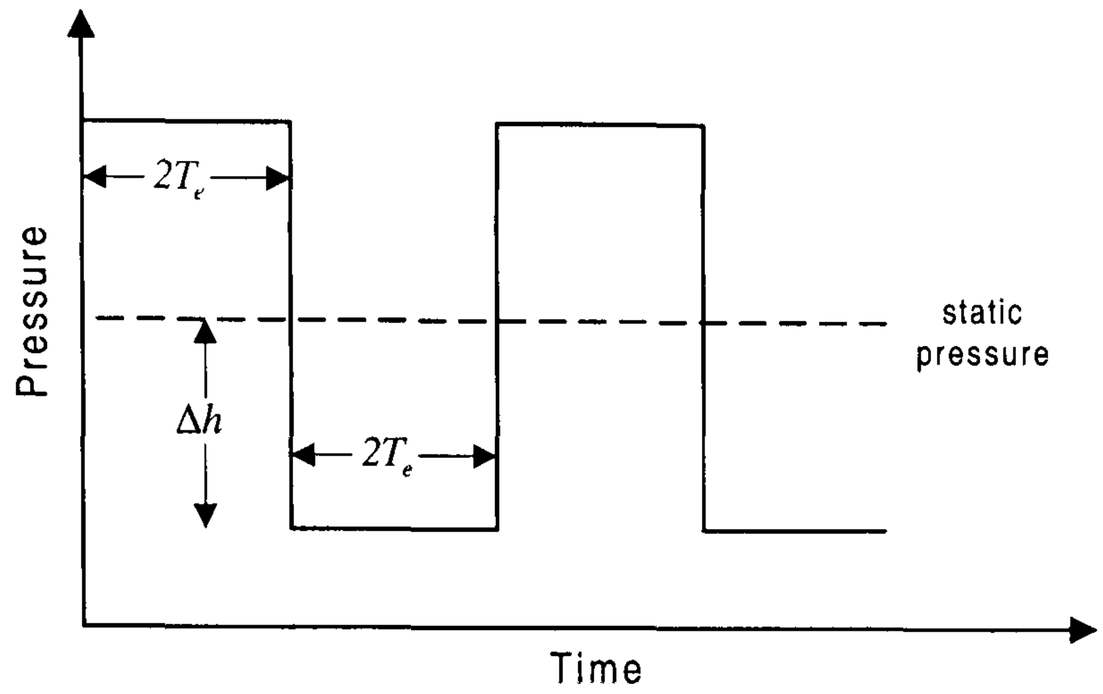

Figure 2-8: *Pressure wave at the guide vane due to sudden closure*

Pressure waves in the penstock can be modelled by treating it as a hydraulic transmission line terminated by an open circuit at the turbine end and a short circuit at the reservoir [18]. Assuming the penstock to be a uniform conduit supplied from a large reservoir, the incremental head and flow at the turbine inlet are related as shown in the transfer function (2-17).

$$\frac{H(s)}{Q(s)} = -\frac{T_w}{T_e}\tanh\left(T_e s + F\right) \tag{2-17}$$

where

F = Friction losses in the penstock

s = Laplace complex frequency variable

2.3.3 Combined turbine / penstock

2.3.3.1 Inelastic water column

The hydraulic system can be modelled by combining equations (2-2) for the turbine and (2-11) for the inelastic water column. The block diagram of Figure 2-9 is a nonlinear representation showing how the generated power depends on the guide vane position. Note that the power also depends on additional inputs Δn, h_0 and q_{nl} but that these change slowly compared to the primary control input. The value for water starting time of the

penstock (T_w) is obtained at rated conditions using rated head and rated flow as the base values.

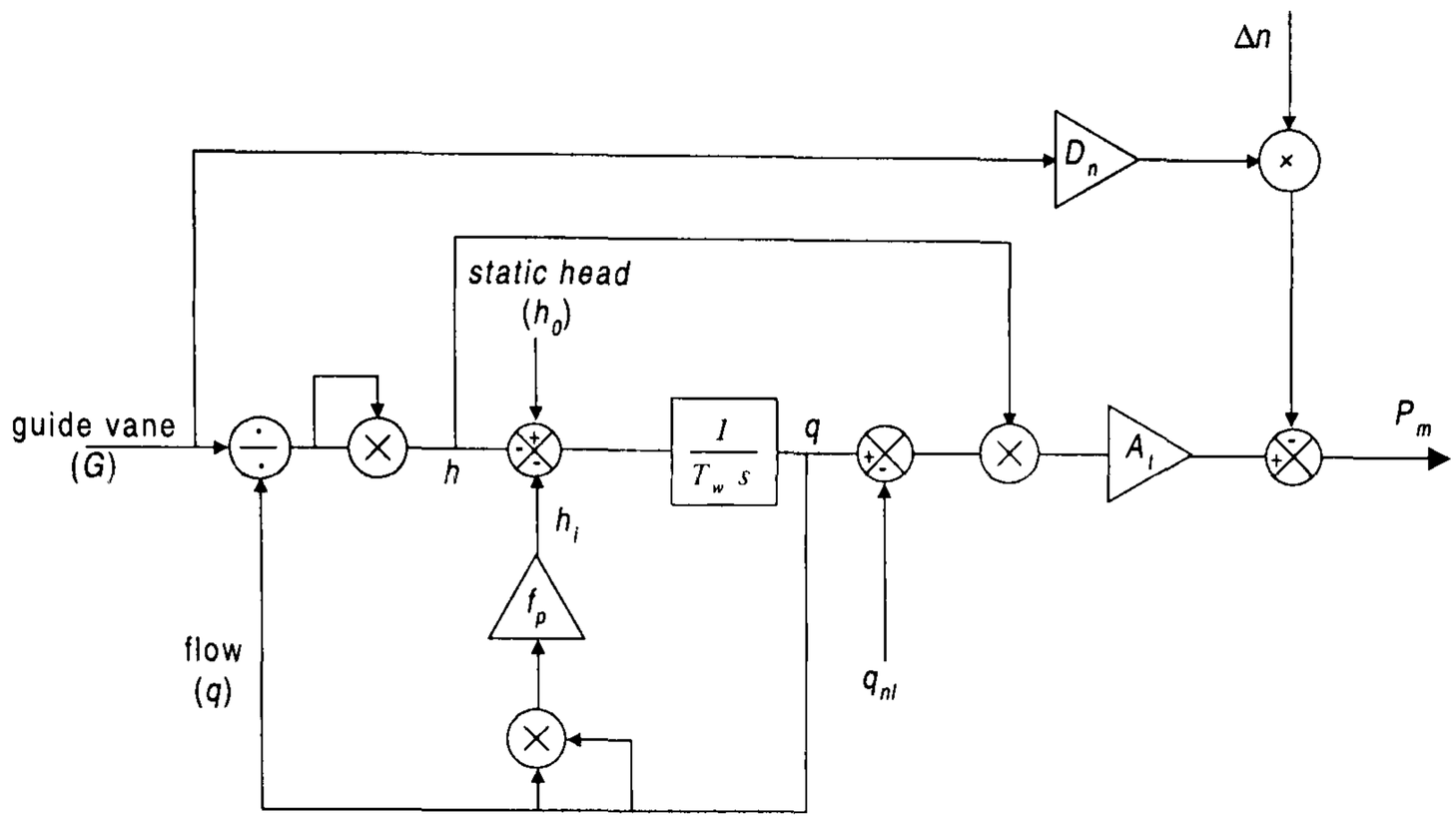

Figure 2-9: *Inelastic water column model of penstock and turbine*

2.3.3.2 Elastic water column

Whilst modelling the hydraulic system using the assumption of inelastic water columns is adequate for a short penstock, there is sometimes need to consider the effects which cause travelling waves of pressure in the penstock. The nonlinear hydraulic system including water hammer effects can be modelled by combining the turbine equation (2-11) and equation (2-17) for the elastic water column. Figure 2-10 shows the block diagram of the system, where the dynamics of the turbine power are functions of the head across the turbine and the guide vane opening.

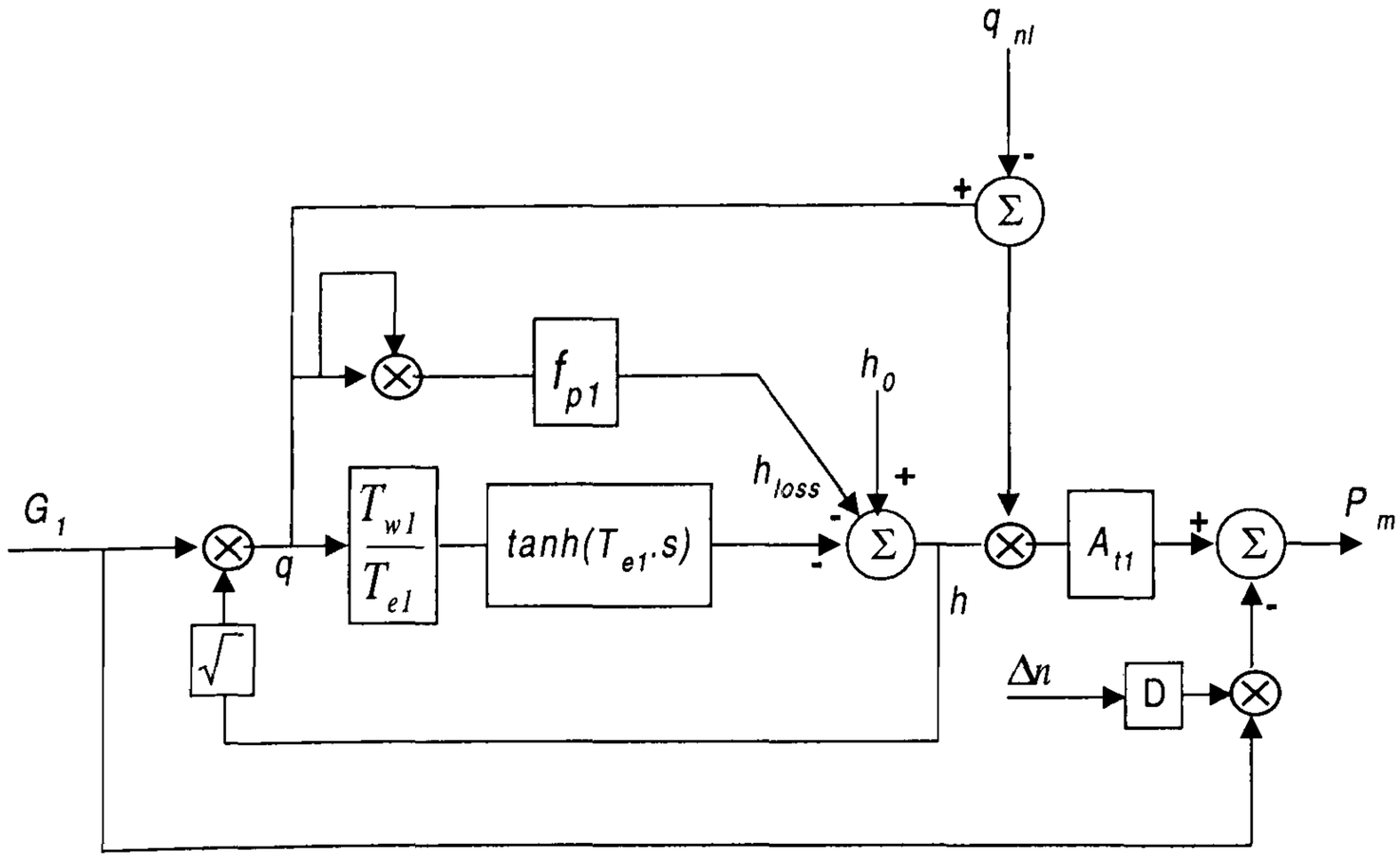

Figure 2-10: *Nonlinear model of turbine with elastic water column*

2.3.4 Multiple penstock model

The hydraulic turbine models presented hitherto are based on a single conduit analysis. There are cases, however, where all the turbines of a hydropower plant share a common tunnel, which is subsequently bifurcated to form the penstocks leading to individual turbines. This is the case at Dinorwig. Due to the common tunnel, a hydraulic coupling between the individual units is introduced and the dynamics of each turbine depends on the control action taken on every unit of the plant. This is of great importance because the generators of the same plant are also electrically coupled. Therefore, a closer examination of the dynamics of the coupled hydraulic turbines is required.

To probe into the nature of the coupling effects, consider the case of multiple units operating at full load connected to an infinite bus and one unit being taken off load. This is accomplished at Dinorwig by setting the power generating reference to zero, causing the guide vane to be ramped down. As the guide vane of the unit coming off line is being closed, the turbine head for that unit increases. With the guide vanes of the remaining units almost stationary, the initial rise in the turbine head for the unit coming off-line will result in a decreased flow to this unit. At the same time, it will produce an increase in the flows for the remaining units, because the total flow in the common tunnel cannot be changed instantaneously. The increase of head at the turbines will simultaneously cause a decrease in the rate of flow through the tunnel until the final flow conditions reach a new steady state [19]. Qualitatively, then, it is clear that hydraulic coupling leads to interaction between the individual machines. Again, two modelling approaches can be taken depending on the characteristic of the water columns. The initial approach neglects water compressibility while the second approach assumes an elastic water column.

2.3.4.1 Inelastic water column

For short-medium penstocks, it is well known [19] that the dynamics of the hydraulic turbine can be analysed with little loss of accuracy by neglecting the compressibility of the water. The flow at the common tunnel can be calculated using the continuity equation:

$$q = \sum_{i=1}^{j} q_i$$

where: j =number of units and q_i = flow in the penstock i.

The total flow in the common tunnel must be equal to the sum of the flows in the individual penstocks. The momentum equation for the water at the common tunnel can be written using the representation of equation (2-9).

$$h_0 - h = \frac{l}{g_a A}\left(\frac{dq_1}{dt} + \frac{dq_2}{dt} + \cdots\cdots + \frac{dq_n}{dt} \right) \tag{2-18}$$

Writing (2-18) in per unit notation based on the rated flow q_{i0} yield

$$h_0 - h = \frac{l}{g_a A}\left(q_{10}\frac{d\overline{q_1}}{dt} + q_{20}\frac{d\overline{q_2}}{dt} + \cdots\cdots + q_{n0}\frac{d\overline{q_n}}{dt} \right) \tag{2-19}$$

where $\overline{q_n} = \dfrac{q_n}{q_{n0}}$

The momentum of water in an individual penstock is:

$$h - h_f = \frac{l_i}{A_i g}\left(q_{i0}\frac{d\overline{q_i}}{dt} \right) \tag{2-20}$$

Using equation (2-20) to eliminate h in equation (2-19) and expressing the head in per unit form by dividing by the rated static head h_0, a matrix expression representing the special case of Dinorwig where $q_{10} = q_{20} \cdots = q_{n0}$, can be written as shown in equation (2-21).

$$\begin{bmatrix} 1-\overline{h_1} \\ 1-\overline{h_2} \\ \vdots \\ 1-\overline{h_n} \end{bmatrix} = \begin{bmatrix} T_{wT}+T_{w1} & T_{wT} & \cdots & T_{wT} \\ T_{wT} & T_{wT}+T_{w2} & \cdots & T_{wT} \\ \vdots & \vdots & \vdots & \vdots \\ T_{wT} & T_{wT} & \cdots & T_{wT}+T_{wn} \end{bmatrix} \begin{bmatrix} \overline{\dot{q}_1} \\ \overline{\dot{q}_2} \\ \vdots \\ \overline{\dot{q}_n} \end{bmatrix} \tag{2-21}$$

where:

T_{wn} = The water starting time for the penstock of the n^{th} unit, the rated flow for the n^{th} unit is used to calculate this value.

T_{wT} = The water starting time for the common tunnel only, the rated flow for the n^{th} unit is used to calculate this value.

2.3.4.2 Elastic water column

The effects of water compressibility can be introduced into a multiple penstock model in a similar manner to the single penstock representation. The model now incorporates the nonlinear single penstock model shown in Figure 2-10. The coupling effect of the tunnel is included by using the same form of transfer function between the head and the flow that, for the tunnel, is the sum of the flows in the individual penstocks. The nonlinear model of the hydro-turbine including the hydraulic interaction model is illustrated in Figure 2-11. The head loss in the upper tunnel is proportional to the coefficient f_t times flow rate times absolute value of flow rate to maintain direction of head loss where the flow can reverse.

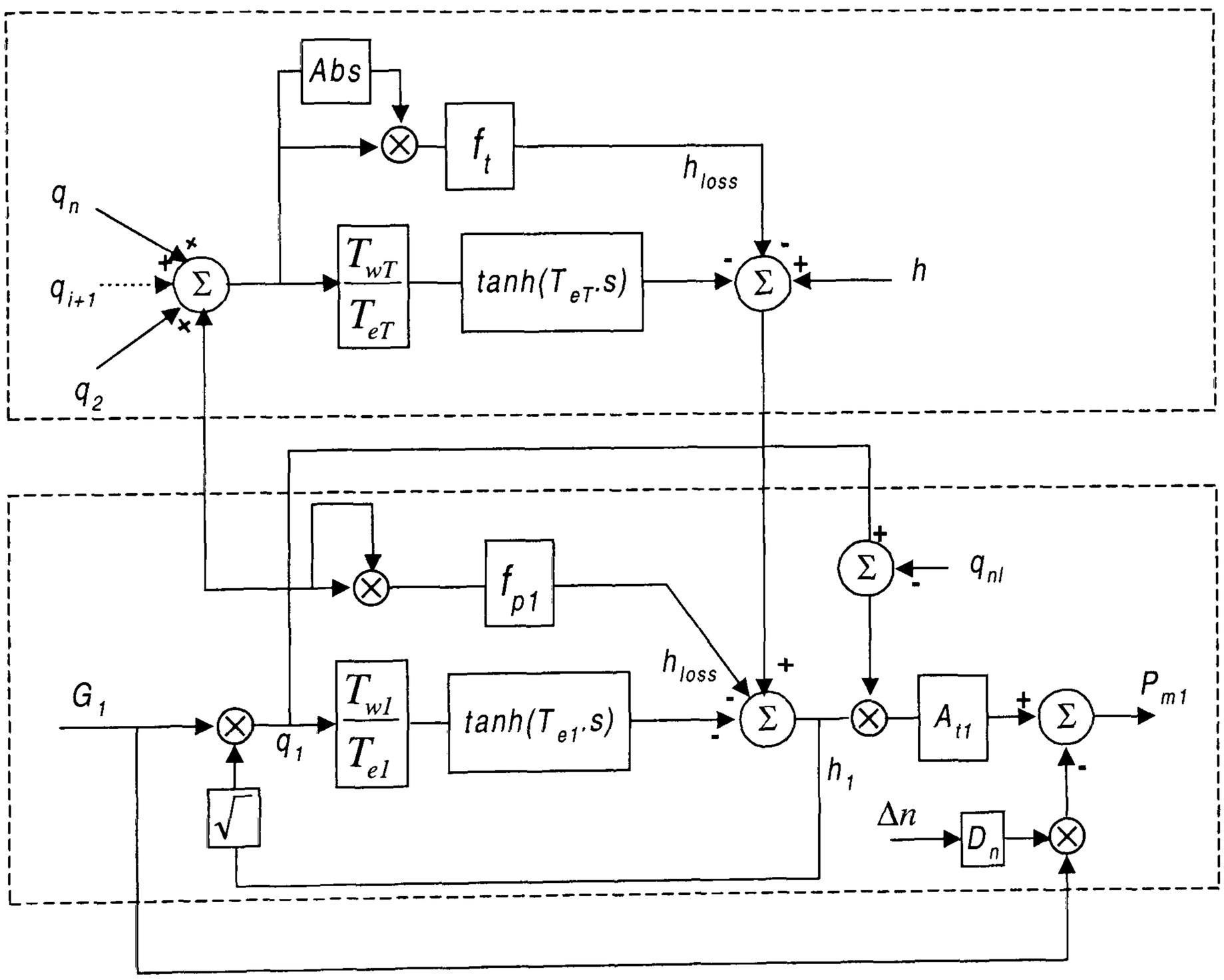

Figure 2-11: *Nonlinear model of multiple penstocks supplied from a common tunnel*

2.4 Linearised Models

Much insight into the salient dynamic characteristics of this model can be obtained by considering a linearised representation. This is used for small signal analysis and control design studies.

2.4.1 Inelastic water column

The inelastic water column transfer function is obtained by linearising the basic penstock–turbine equations, (2-4) and (2-11) as presented in Appendix-I. This results in the first order transfer function of equation (2-22) relating small changes in the mechanical power to changes in the guide vane opening. Note that the water time constant T_w here corresponds to the operating condition rather than the rated condition. Thus to model the unit correctly in stability simulations, it is necessary to adjust the value of T_w each time the initial operating conditions are changed [20].

$$\frac{\Delta P_m(s)}{\Delta G(s)} = \frac{1 - T_w s}{1 + 0.5 T_w s} \tag{2-22}$$

The transfer function (2-22) has a zero is in the right half of the s-plane located at $s = 1/T_w$, which represents a non-minimum phase system [21]. The system's outstanding dynamic characteristic is illustrated in Figure 2-12, this shows the change in the turbine mechanical power for a step change in the guide vane position applied at $t = 0$ for a system with a water time constant $T_w = 3s$. A transient change in power occurs which is opposite to the direction of change in guide vane position and the change in the turbine power is twice as large and in the opposite direction to the final change. The subsequent power increase depends on the value of T_w, as the water accelerates until the flow reaches the new steady state value that establishes the new power output.

The initial and final power values for a unit step change in guide vane position can be determined as follows. The initial value theorem gives [21].

$$P_m(0) = \lim_{s \to \infty} s \frac{1}{s} \left[\frac{1 - T_w s}{1 + 0.5 T_w s} \right] = -2$$

while the final value theorem gives,

$$P_m(\infty) = \lim_{s\to 0} s\frac{1}{s}\left[\frac{1-T_w s}{1+0.5T_w s}\right] = 1$$

The step time response can be calculated from the inverse Laplace transform of equation (2-22).

$$P_m(\mathrm{s}) = \mathcal{L}^{-1}\left[\frac{(1-T_w s)}{s(1+0.5T_w s)}\right]$$

from which the power generated for unity guide vane opening is given by:

$$\Delta P_m(t) = 1 - 3e^{-\frac{2t}{T_w}}$$

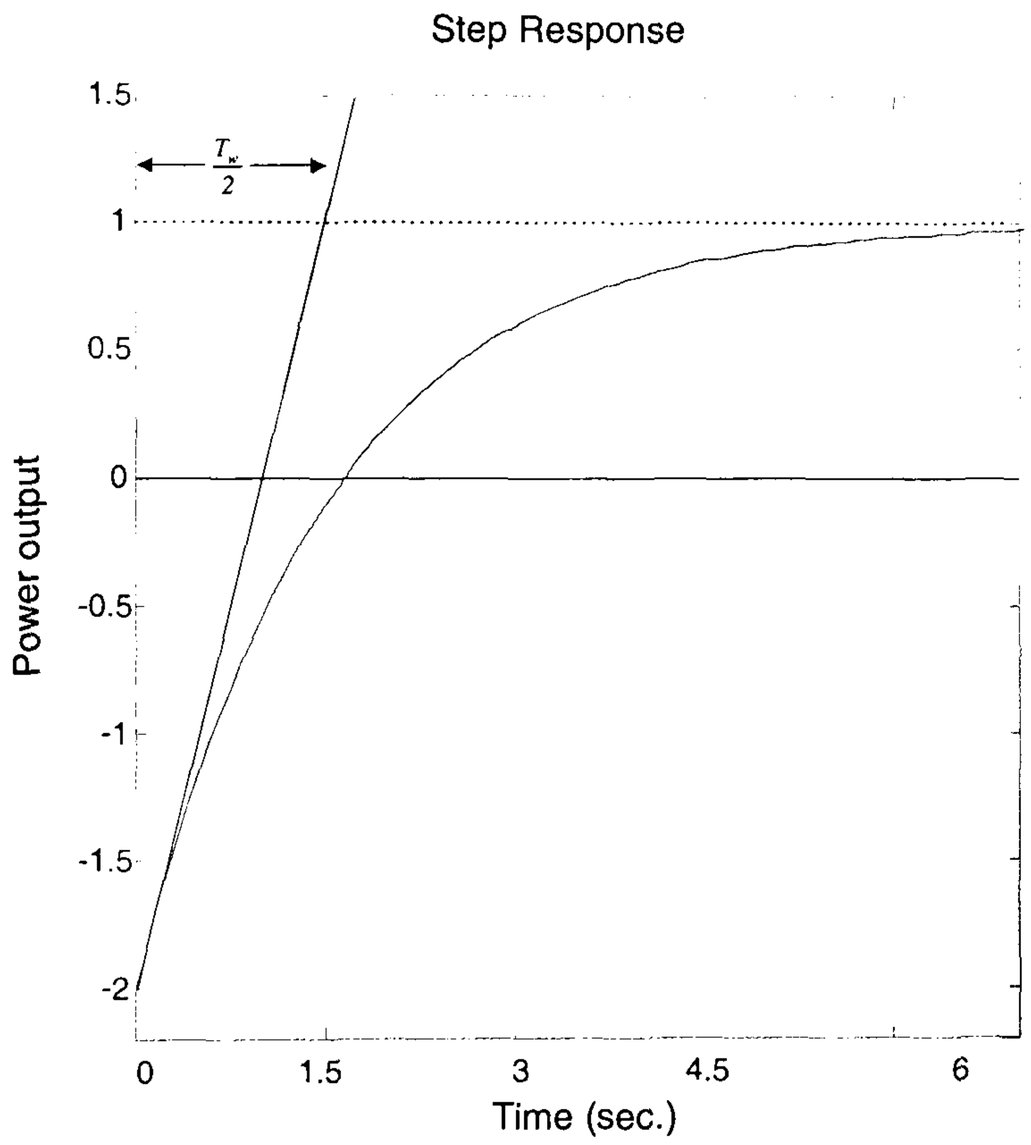

Figure 2-12: *Turbine power change due to step guide vane opening*

2.4.2 Elastic water column

A linearised model for the turbine with elastic water column can be assembled by combining equation (2-17) with equations (2-5) and (2-6) to yield equation (2-23), the transfer function relating the incremental torque or power output to changes in guide vane position.

$$\frac{\Delta P_m(s)}{\Delta G(s)} = \frac{a_{23} + (a_{11}a_{23} - a_{21}a_{13})\dfrac{T_m}{T_e}\tanh(T_e s + F)}{1 + a_{11}\dfrac{T_m}{T_e}\tanh(T_e s + F)} \tag{2-23}$$

A close examination of the transfer function reveals that its gain varies between two limiting values:

Low limit $\left|\dfrac{\Delta P_m(0)}{\Delta G(0)}\right| = a_{23}$

High limit $\left|\dfrac{\Delta P_m(\infty)}{\Delta G(\infty)}\right| = \dfrac{|a_{11}a_{23} - a_{21}a_{13}|}{a_{11}}$

Using the ideal turbine parameter values summarised in Section 2.2 and ignoring the friction losses by setting the friction coefficient F = 0, then equation (2-23) can rewritten to yield the transfer function:

$$\frac{\Delta P_m(s)}{\Delta G(s)} = \frac{1 - Z_0\tanh(T_e)}{1 + 0.5Z_0\tanh(T_e)} \tag{2-24}$$

where $Z_0 = \dfrac{T_w}{T_e}$ is the normalised impedance of the penstock.

Equation (2-24) is a distributed-parameter model and it is difficult to use it for system stability studies, therefore, the general approach is to approximate it with a reduced-order model. The first approach is to use a Maclaurin series to obtain an n^{th} order rational transfer function, which approximates the irrational transfer function of equation (2-23). Series approximation methods must be applied with caution as the order of the approximation is increased in pursuit of model accuracy. A fourth order series is found to be the highest useful approximation because including further terms makes the transfer function unstable although the original transfer function of equation (2-20) is stable [22]. The fourth order transfer function can be written as:

$$\frac{\Delta P_m(s)}{\Delta G(s)} = \frac{1 - T_w s + 0.5T_e^2 s^2 - 0.167T_e^2 T_w s^3 + 0.04167T_e^4 s^4}{1 + 0.5T_w s + 0.5T_e^2 s^2 + 0.0834T_e^2 T_w s^3 + 0.04167\,T_e^4 s^4} \tag{2-25}$$

The representation of equation (2-23) could alternatively be modified by forming the lumped parameter approximation. This is performed by expanding the transfer function into the general nth-order model, using the relationship:

$$\tanh(x) = \frac{1 - e^{-2x}}{1 + e^{-2x}} \tag{2-26}$$

This leads to the finite approximation [23],

$$\tanh(T_e s) = \frac{sT_e \prod_{n=1}^{n=\infty} \left[1 + \left(\frac{sT_e}{n\pi} \right)^2 \right]}{\prod_{n=1}^{n=\infty} \left[1 + \left(\frac{2sT_e}{(2n-1)\pi} \right)^2 \right]} \tag{2-27}$$

For n = 1 equation (2-27) can be written in the form of equation (2-28), which is a more accurate system representation.

$$\frac{\Delta P_m(s)}{\Delta G(s)} = \frac{1 - T_w s + \frac{4}{\pi^2} T_e^2 s^2 - \frac{T_w T_e^2}{\pi^2} s^3}{1 + 0.5 T_w s + \frac{4}{\pi^2} T_e^2 s^2 + 0.5 \frac{T_w T_e^2}{\pi^2} s^3} \tag{2-28}$$

Figure 2-13 shows the Bode plots for the transfer functions of equations (2-22), (2-25) and (2-28) assuming a water starting time $T_w = 2s$ and wave travel time $T_e = 1s$. It is clear that the linearised first order model is accurate at very low frequencies with significant errors at high frequencies compared to the representation of the lumped parameter model. The Maclaurin approximation matches the lumped parameter response for frequencies below 2 rad/s. The gain limits of the transfer function lies between $0 - 6.02dB$, (gain range 1–2) which agrees with the earlier prediction.

The classical representation of the system of equation (2-22) that represents a short-medium penstock can be derived by assuming T_e is very small. Thus, equation (2-25) can be rewritten as equation (2-28) and the first order reduced model can be obtained.

$$\frac{\Delta P_m(s)}{\Delta G(s)} = \frac{a_{23} - (1.5 - 0.5 a_{23}) T_w s}{1 + 0.5 T_w s} \tag{2-29}$$

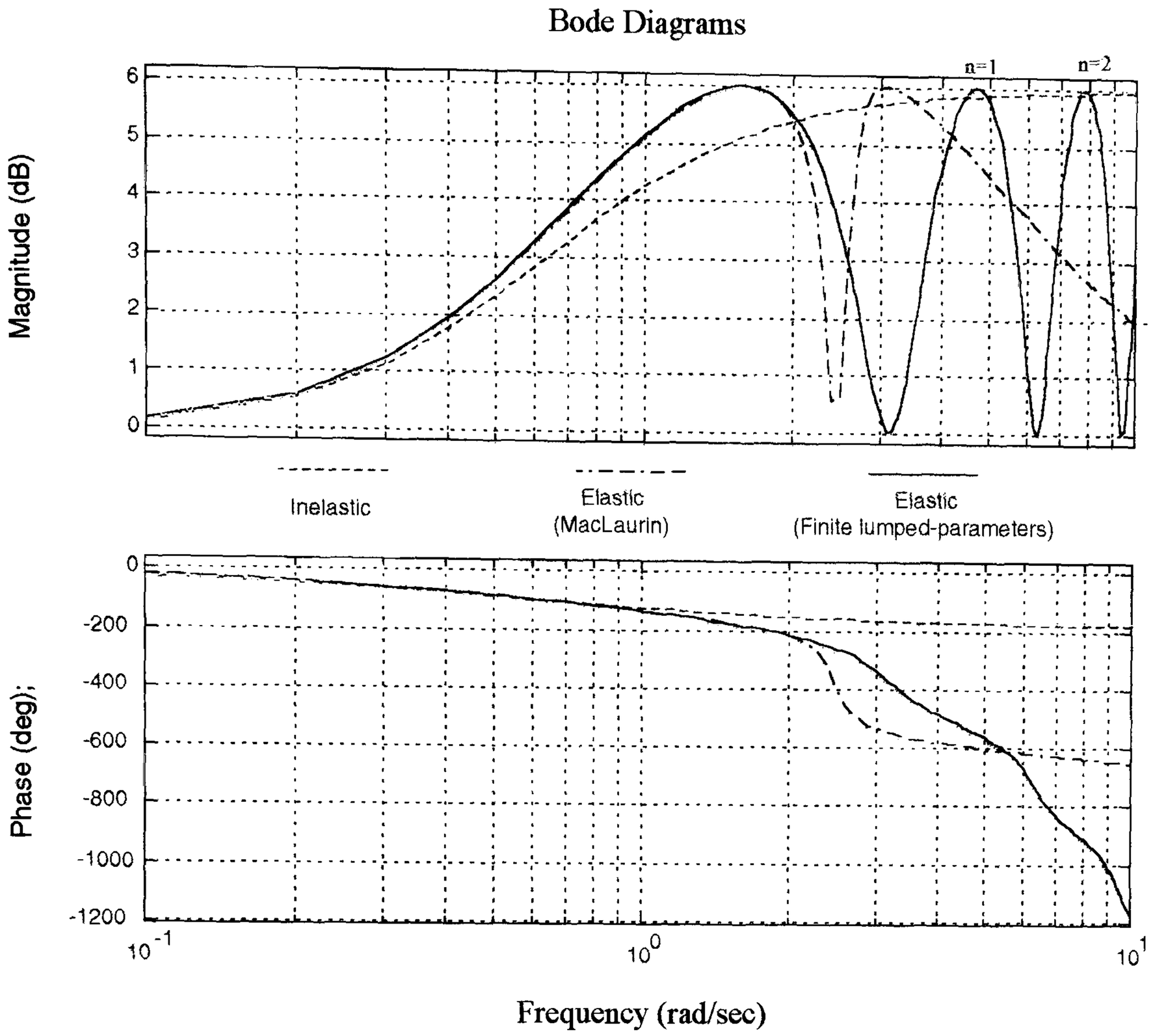

Figure 2-13: *Open loop frequency responses for the penstock-turbine*

2.5 Pressure Control Systems

2.5.1 Surge tanks

Hydraulic transients and pressure changes can be controlled in several ways. Two simple solutions are to ensure that the guide vane can only change position slowly and to provide a pressure relief valve.

- The simplest solution to reducing the pressure surge is to slow the closing time of the guide vane. Guide vane controls and governor regulation can limit the guide vane closure time so that there is no damaging pressure head rise. The pressure surge is a function of the inverse of the closing time. If a pipeline full of water is about 1000m long and it takes 10s to close the valve, both the pipe and valve experience a

relatively mild rise in pressure. If the valve is closed over a period of 5s the rise in pressure is higher [24].

- Another way to control the pressure is to install a pressure regulator valve near the turbine, which is used to dump water out of the hydraulic system into the lower reservoir. The relief valve can be connected to the turbine spiral case and controlled by the turbine guide vane mechanism to prevent excessive pressure by maintaining a nearly constant water velocity in the penstock. The relief valves are designed to open at a rate that limits pressure rise to an acceptable value [17].

- A common method of controlling pressure is to construct a surge tank. The surge tank prevents excessive pressure occurring by providing a storage volume into which the flow can pass. Surge tanks act as a forebay and shorten the distance for relief from the pressure wave. It provides flow stabilisation to the turbine, pressure regulation and improvement of speed control. If the load on the turbine is suddenly reduced, the governor will act to close the guide vane aiming to decrease the rate of water flow in the tunnel. The water flow in the tunnel cannot drop immediately to the new flow rate and the temporary surpluses of water go into the surge tank. Consequently, the water level in the surge tank rises and the back pressure increases causing the flow in the tunnel to be decelerated gradually. The surge tank also serves as an auxiliary supply to ensure that sufficient water is immediately available close to the turbine when there is a sudden increase in the electrical load. Three slightly different types of surge tanks, which are illustrated in Figure 2-14, are used in hydro plant [25].

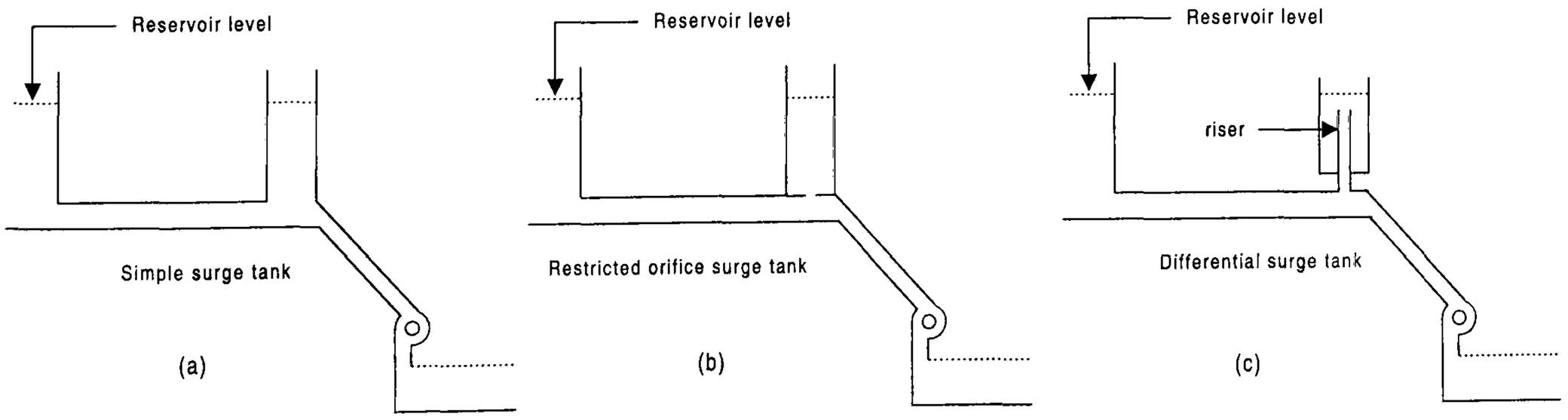

Figure 2-14: *Types of surge tanks*

- Figure 2-14(a) is a simple surge tank, consisting of a vertical standpipe connected to the penstock with an opening large enough so that there is no appreciable loss in head as the water enters the surge tank. This is the most efficient surge tank to provide a ready water supply to the turbine but it is the most hydraulically unstable.

- Figure 2-14(b) is a restricted orifice surge tank. This is connected in such a way that there is a restricted passage which resists the flow of water back and forth through the tank and the penstock. Appreciable head losses will develop in the water that flows into or out of the tank. Thus, the orifice tank has the disadvantage that it does not supply or accept excess water flow from the penstock, but it is more hydraulically stable.

- Figure 2-14(c) is a differential surge tank and is a combination of the two previous types. It consists of an internal riser of smaller diameter than the penstock, freely connected to it and a storage tank of larger diameter surrounding the riser pipe and connected to it by a restricted passage. The level of the stored water in the larger tank is independent of the accelerating head and the head acting on the turbine, both of these heads being determined by the water level in the smaller inner riser.

2.5.2 Modelling of the surge tank

At Dinorwig, the hydraulic transients and pressure changes are controlled by the use of a surge tank. This is in the form of an open reservoir located immediately above the high-pressure shaft, as shown in Figure 2-1 having a capacity of 27000m^2. An integral parapet in the pond floor leads into a 30m-diameter surge shaft. This connects the high-pressure shaft and pond via a 10m-diameter orifice shaft. Thus, the surge tank can be considered as a restricted orifice (throttled) type. Although large, the tank is still treated as a conduit for modelling purposes. Consequently, the system is composed of three-way compound conduits: the low-pressure tunnel, the high-pressure tunnel and the surge tank including the throttling orifice [26].

The surge tank model is derived from the continuity relation of flow at the tank junction, which can be written as [25]:

Flow down the upper tunnel q_t = flow into the surge tank q_s + flow to turbines q_p

The flow into the surge tank depends upon the area of the tank (A_s) and the rate of change of the tank level (h_s).

$$q_s = A_s \frac{d\ h_s}{dt} \tag{2-30}$$

The surge tank water level in per unit is calculated as:

$$h_s = \frac{q_s}{C_s.s} \tag{2-31}$$

where C_s is the storage constant of the surge tank, is defined as:

$$C_s = \frac{A_s h_{base}}{q_{base}} \quad \text{seconds} \tag{2-32}$$

The head losses in the orifice to the surge tank are proportional to the coefficient f_0 times flow rate times the absolute value of the flow rate (to maintain the direction of the head loss). Hence, the head on the lower penstock is the surge tank level (head) minus the head losses due to the orifice. The level of the surge tank defines the head across the lower penstock. The inclusion of the surge tank effect is warranted in cases where dynamic performance is being simulated over a few minutes of "real" time. Figure 2-15 shows the surge tank model as a block diagram.

The addition of the surge tank will give rise to a poorly damped oscillation between the tank and the reservoir. These oscillations are generally quite slow, of the order of a few minutes per cycle and can be neglected in studies of governing and load frequency control. In the lumped system (rigid column) theory, if the head loss in both the tunnel and the orifice are neglected, the surge oscillation in the surge tank has a period (T_{st}), which is the time interval between the turbine load change and the occurrence of the maximum surge. It can be computed from the following expression [27].

$$T_{st} = 2\pi\sqrt{\frac{lA_s}{gA}} \tag{2-33}$$

where:

l = length of the tunnel from the reservoir to the surge tank

A_s = Cross-sectional area of the surge tank

A = Cross-sectional area of the tunnel

The surge follows a damped sine wave and the maximum change in the water level occurs at 1/4 T_{st} after the start. At Dinorwig the surge tank period is 240 seconds and the storage constant of the surge tank $C_s = 960s$.

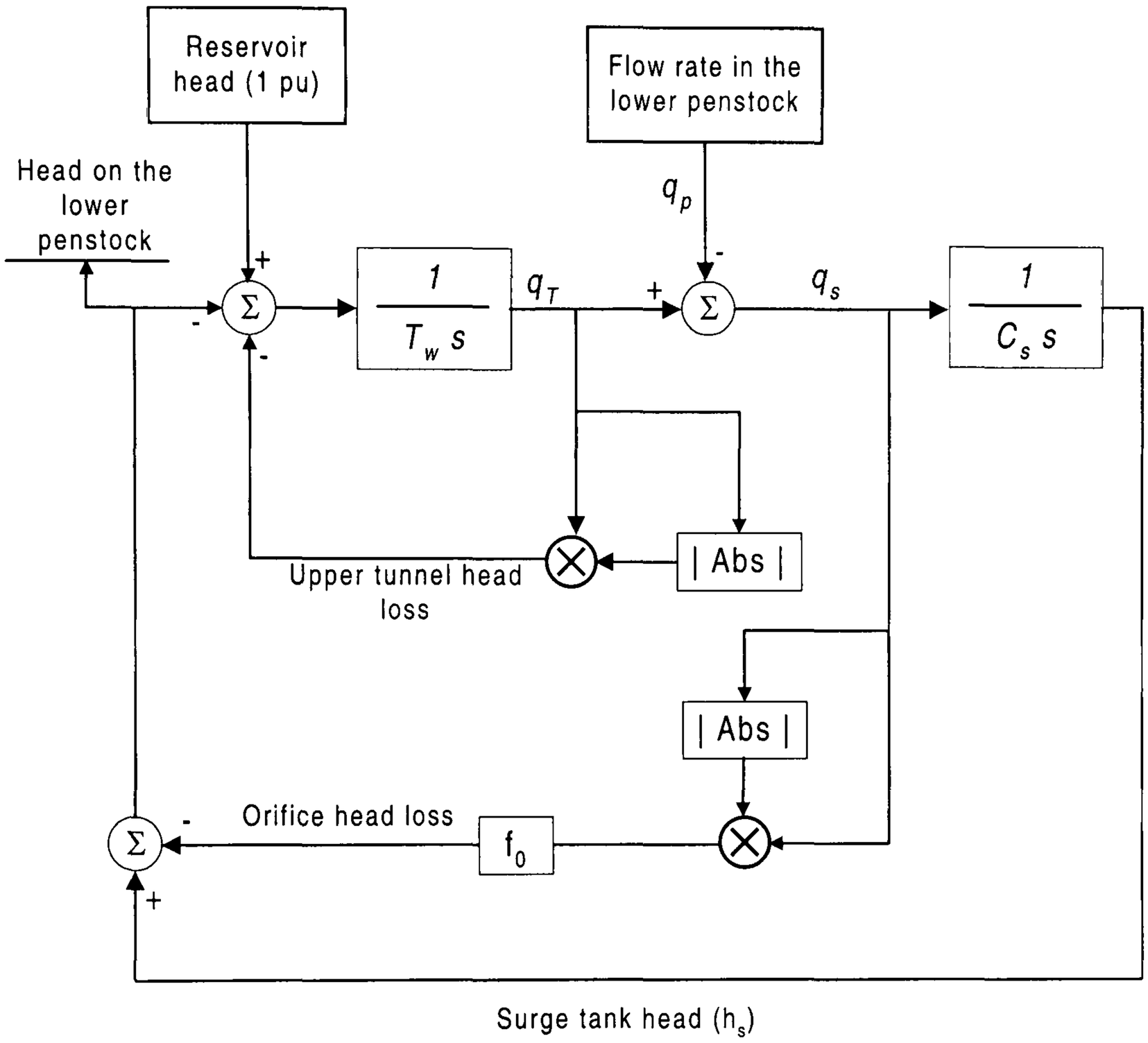

Figure 2-15: *Surge tank model*

2.6 Evaluation of Hydraulic Parameters for Dinorwig

2.6.1 Water starting time

The water starting time for rated conditions is calculated from the plant drawings and measured flows between the surge tank and the turbine inlet. Consequently, the water time constant becomes a function of the number of units that are on-line [20]. Starting at the surge tank the water is brought to the power station by a single tunnel of about 994m in length. At the end of this tunnel are individual penstocks of 210m in length. The static head used is 513m. The maximum generating flow (six units operating at full load) in the common tunnel is measured to be 390 (m^3/s). Table 2-1 summarises the calculation of water starting time for each section of the hydraulic system base on equation (2-15). The water starting time for a unit varies from 0.69s when one unit is on-line to 2.72s when all the six units are on line.

Table 2-1: Dinorwig water starting time

Section	One unit	Two units	Three units	Four units	Five units	Six units
L.P shaft	0.24	0.48	0.73	0.97	1.22	1.46
H.P shaft	0.07	0.14	0.21	0.28	0.36	0.42
H.P tunnel	0.078	0.156	0.234	0.312	0.390	0.468
Tunnel T_{wT}	0.388	0.776	1.174	1.562	1.97	2.348
	Unit 1	Unit 2	Unit 3	Unit 4	Unit 5	Unit 6
Manifold concrete	0.054	0.054	0.053	0.063	0.083	0.11
Penstock concrete	0.034	0.034	0.04	0.048	0.051	0.057
Penstock steel	0.166	0.166	0.166	0.166	0.166	0.166
Main inlet valve	0.0526	0.0526	0.0526	0.0526	0.0526	0.0526
Penstocks T_{wp}	0.3066	0.3066	0.3116	0.3296	0.3526	0.3856

2.6.2 Wave travel time

The wave travel (propagation) time T_e is dependent on the length of the tunnel and the velocity of sound in the water. Its value is determined by equation (2-34).

$$T_e = \frac{l}{a} \tag{2-34}$$

According to Parmakian [28] the velocity of pressure wave propagation in a pipe a is given by the following formula:

$$a = \sqrt{\frac{1}{\rho\left(\frac{1}{k} + \frac{d}{eE}\right)}} \tag{2-35}$$

where:

ρ = The water density

k = Bulk modulus of the water

d = Penstock diameter

e = Thickness of the penstock wall

E = Elastic modulus of the penstock material

For a perfectly rigid pipe, the velocity with which a wave is propagated relative to the liquid is the same as the velocity of sound in an infinite expanse of the liquid. Thus, equation (2-35) can be rewritten to represent a rigid pipe condition.

$$a = \sqrt{\frac{k}{\rho}} \tag{2-36}$$

The bulk modulus of water is 2.05×10^{9} N/m^2 and so the wave velocity for a rigid pipe is:

$$a = \sqrt{\frac{2.05\times10^{9}\ \text{N/m}^2}{10^{3}\ \text{kg/m}^3}} = 1432\ \text{m/s}$$

The tunnels at Dinorwig are concrete lined in the rock, and the thickness of the tunnel wall is much greater than the diameter of tunnel. Thus, it is possible to apply the rigid pipe approximation of the wave velocity to calculate the wave's travel time for each section of the hydraulic system. This was calculated and found to be:

Wave time from the manifold to the surge tank T_{et} = 0.642s

Wave time from the turbine end to the manifold T_{ep} = 0.146s

2.6.3 Head loss coefficients

The flow in the penstock is usually turbulent and hence highly complex. Water flowing through a penstock will cause a pressure decrease in the direction of flow. The pressure drop over a length of the penstock it can be expressed in terms of the head loss h_f as [29].

$$h_f = f_r\left(\frac{l}{d}\right)\left(\frac{v^2}{2g_a}\right) \tag{2-37}$$

where f is the friction factor and d is the penstock diameter.

This expression is called the Darcy-Wiesbanch form and the factor ($v^2/2g$) is called the velocity head. The head loss depends upon the water velocity in the penstock and consequently on the number of units in operation if they are supplied from a common tunnel. The head loss coefficient f_p, used earlier in the modelling of the water column is calculated using expression (2-7).

The head losses calculated for Dinorwig are given in Table 2-2, which represent the hydraulic pressure losses for the plant when a single unit operating at full load draws a water flow of 65 (m^3/s). The friction factor " f " is a function of the Reynolds number and of the relative roughness of the pipe and is calculated graphically. The data for the friction factor were supplied by the mechanical department at the First Hydro Company (FHC) [30].

Table 2-2: Head loss for Dinorwig hydraulic system

Section	Diameter m	Length m	Velocity m/s^3	f_r (Moody)	h_f m	f_p $m/(m^3/s)^2$
L.P tunnel	10.5	1695	0.75	0.0151	0.05	1.65e-5
H.P shaft	10	412	0.82	0.0147	0.0277	4.9e-6
H.P tunnel	9.5	446	0.917	0.0154	0.031	7.33e-6
Manifold	9.5	77	0.917	0.0154	0.0053	1.25e-6
Penstock concrete	3.8	50	5.73	0.0189	0.416	9.85e-5
Penstock steel	3.3	110	7.6	0.0108	1.059	2.5e-4
M.I.V	2.5	20	13.24	0.0117	0.75	1.78e-4

The flow in the common tunnel depends upon the number of units dispatched and the total hydraulic loss therefore increases with the number of units running. The total hydraulic loss and the head loss coefficients corresponding to the number of units operating are summarised in Table 2-3.

Table 2-3 Dinorwig data used in the simulation studies

Total head loss (1 unit)	2.36 m
Total head loss (2 unit)	2.7 m
Total head loss (3 unit)	3.34 m
Total head loss (4 unit)	4.2m
Total head loss (5 unit)	5.3 m
Total head loss (6 unit)	6.7 m
Head loss coefficient f_t Common tunnel	2.873e-5 $[m/(m^3/s)^2]$
Head loss coefficient f_p Individual penstock	5.2e- 4 $[m/(m^3/s)^2]$

2.7 Conclusions

Mathematical models are of fundamental importance in understanding any physical system Any mathematical description of a system implies some degree of approximation or some qualifying assumption so knowledge of these assumptions and the range of conditions over which the models are valid is equally important. In this chapter, the hydraulic system was analysed where the specific area of discussion included the water hammer phenomenon, its effect on the water column dynamics, the hydraulic coupling between units connected to a common tunnel, and the method used to calculate the hydraulic parameters for Dinorwig.

The nonlinear models are required for simulation studies where the speed and the power changes are large, such as governor performance evaluation, islanding, load rejection and system restoration studies. Linearised models are useful for control system tuning using linear analysis techniques (frequency response, root locus, etc). They are not adequate for time domain simulation because, in addition to being limited to small perturbations, where the value of water starting time must be adjusted each time the dispatch of units changes because it is calculated using the unit's rated conditions. However, this problem can be avoided by using the nonlinear models.

In Chapter 5, the nonlinear models are combined with the power system (developed in chapter 3) and governor system (developed in Chapter 4) models to produce a complete generic model of the plant suitable for a wide range of studies. The opportunity to apply system identification techniques to verify the models were limited due to the time constraints of the project and the availability of the station to carry out the tests. The linear models are used in Chapter 6 to establish the station stability boundaries for a variety of operating conditions.

Chapter 3

Power System Dynamics

3.1 Introduction

This chapter focuses on the characteristics and modelling of the individual elements of the power system. For reliable service, a power system must remain stable and capable of withstanding a wide range of disturbances. Power systems are identified by the physical layout of the generators and loads in addition to commercial boundaries. The flows of active and reactive power in the transmission lines are independent of each other as the active power depends on the angle by which the sending end leads the receiving end, while the reactive power depends on the voltage magnitudes. Since we are interested in modelling the effect of Dinorwig on the stability of the power system, this chapter concentrates on active power control. Therefore, the power system models constructed here are used for frequency control.

Section 3.2 of this chapter deals with a single unit supplying an isolated load where a generator model based on the equation of motion of a synchronous machine is introduced. This is followed by an explanation of the different types of load and their representation for stability studies while Section 3.3 considers an unit operating in parallel with a large power system. Operating within a large system induces an electrical coupling between the unit and the power system; this effect is also investigated and included in the model. The remainder of the chapter examines the control of active power for a large power system, which is commonly referred to as load frequency control.

3.2 Isolated Operation

The simplest power system representation is the case of a single generator supplying an isolated load (islanding). This can occur in emergencies such as power system restoration, or dividing the power system into small islanding systems. In the case of large interconnected power systems, all generating units operating as frequency regulators will contribute to the overall change in generation irrespective of the location of the load change. In the case of small, isolated load operation the unit must hold the system frequency constant. This is an important distinction because the criteria for system stability differ from those for an unit connected to a large power system. This will allow an understanding of the dynamics of the generator for different loading conditions.

3.2.1 Generator mechanical model

The dynamic behaviour of the generators within a power system is of fundamental importance to the overall quality of the power supply. The synchronous generator converts mechanical power to electrical power at a specific voltage and frequency. The source of the mechanical power, the prime mover, may be a diesel engine, a steam turbine or a water turbine in the case of Dinorwig. Whatever the source, it must have the basic property that its speed is almost constant regardless of the power demand. The analysis of any power system to determine its transient stability involves the mechanical properties of the machines because, after any disturbance, they must adjust the angle of their rotors to meet the conditions of power transfer imposed. The electric dynamics have very short time constant compared to hydrodynamics and can be ignored.

Dinorwig power station is mainly used for load/frequency control and since the system frequency is dependent on the active power balance, the generator model is based on its response to frequency changes. However if voltage stability is to be investigated this involves the addition of AVR's, excitation system and PSS (power system stabilizer) into the generator model.

The mechanical equations of a rotating machine are very well established and they are based on the swing equation of the rotating inertia. For the purpose of control analysis, the generating unit is modelled by linear differential equations, which describe their response to small perturbations. The swing equation relates the machine's rotor torque angle to the acceleration torque, which is the difference between the shaft torque

and electromagnetic torque [31]. Constant shaft speed for a given machine is maintained when there is equilibrium between the mechanical shaft and braking electrical torques. Any imbalance between the torques will cause the acceleration or deceleration of the machine according to the laws of motion of a rotating body.

$$T_{acc} = J\frac{d^2\delta_m}{dt^2} = T_{mech} - T_{elec} \tag{3-1}$$

where:

T_{acc} = Accelerating torque, N.m.

J = Combined moment of inertia of the generator and turbine, $Kg.m^2$

δ_m = Mechanical torque angle of the rotor, rad.

t = Time, seconds

T_{mech} = Mechanical torque, N.m.

T_{elec} = Electromagnetic torque, N.m

The mechanical angular velocity ω_m is the time derivative of the torque angle. Rewriting (3-1) yields,

$$J\frac{d\omega_m}{dt} = T_{mech} - T_{elec} \tag{3-2}$$

The kinetic energy of a rotating body is equal to ½ J ω_m^2, thus equation (3-2) can be normalised in terms of the per unit inertia constant H, which is defined as the kinetic energy of the machine at rated speed per machine volt-ampere rating. Using ω_{m0} to denote rated angular velocity in mechanical radians per second gives

$$\frac{2HVA_{base}}{\omega_{m0}^2}\frac{d\omega_m}{dt} = T_{mech} - T_{elec} \tag{3-3}$$

The angular velocity of the rotor in electric rad/sec ω is related to the rotor mechanical angular velocity by $\omega = \frac{\omega_m}{p_n}$, where p_n is the number of generator poles. The equation of motion in per unit form can be written using the angular velocity of the rotor in electric rad/sec.

$$2H\frac{d\overline{\omega}}{dt} = \overline{T}_{mech} - \overline{T}_{elec} \tag{3-4}$$

Noting that $T_{base} = \dfrac{VA_{base}}{\omega_{m0}}$.

It is preferable to express the relationship of equation (3-4) in term of mechanical and electrical power rather than torque. Since the power is equal to torque times angular velocity, P=Tω, expanding for small oscillations around the operating point and neglecting the second order terms gives,

$$\Delta\overline{P} = \overline{\omega_0}\Delta\overline{T} + \overline{T_0}\Delta\overline{\omega} \tag{3-5}$$

Therefore,

$$\Delta\overline{P}_m - \Delta\overline{P}_e = \overline{\omega}_0(\Delta\overline{T}_{mec} - \Delta\overline{T}_{elec}) + (\overline{T}_{mec0} - \overline{T}_{elec0})\Delta\overline{\omega} \tag{3-6}$$

At steady state, the mechanical torque is equal to the electrical torque ($T_{mec0} \cong T_{elec0}$). Combining equations (3-4) and (3-5), the deviation in per unit speed Δω of the rotor as a function of deviations in the mechanical and electrical powers can be represented as

$$\Delta\overline{P}_m - \Delta\overline{P}_e = 2Hs\Delta\overline{\omega} \tag{3-7}$$

Mechanical starting time

The mechanical starting time of the machine T_m, can be calculated using equation (3-4) where,

$$\frac{d\overline{\omega}}{dt} = \frac{\overline{T}_{acc}}{2H}$$

Let T_m be the time required by the rated torque to accelerate the rotor from stand still to rated speed. Integrating with respect to time with ω = 1.0 pu, and T_{acc} = 1.0 pu results in:

$$1.0 = \frac{1}{2H}\int_0^{T_m} 1.0dt$$

Therefore, the mechanical starting time T_m = 2H.

As defined earlier the machine inertia constant H is given by,

$$H = \frac{\text{Stored energy at rated speed}}{\text{MVA}_{\text{rating}}}$$

where the stored energy at rated speed = $\frac{1}{2} J\omega_{m0}^2 \times 10^{-6}$MW.s, and the rated speed $\omega_{m0} = \frac{2\pi \ n_m}{60}$ rad/sec; where n_m is the rotor speed in revolution per minute.

Therefore,

$$H = 5.4775 \times 10^{-9} \frac{\text{Jn}_m^2}{\text{MVA}}$$

At Dinorwig the total rotating inertia of the turbine generator H = 3.995, hence the machine starting time T_m = 7.99s [32].

3.2.2 Load modelling

The term load can be defined as a device connected to a power system (bus) that consumes reactive or active power. Load modelling is qualitatively different from generator modelling. It is relatively simple to construct models of any of the typical load component such as lamps, heaters, and refrigerators. However, this is only a small part of the problem because the exact composition of the load is often very difficult to estimate. Load composition changes continuously reflecting customer patterns of using various appliances and devices. It depends on weather, consumer life style and many other factors. Even if the load composition were known exactly, it would be impractical to represent each individual load component.

In power system stability, the common practice is to represent the composite load characteristic as seen from bulk power delivery points. As illustrated in Figure 3-1, the aggregated load is categorised into load classes and each category is represented in terms of load component. Historically, load characteristics are divided into two categories static and dynamic [33]. Their effects on system stability are discussed separately in this section.

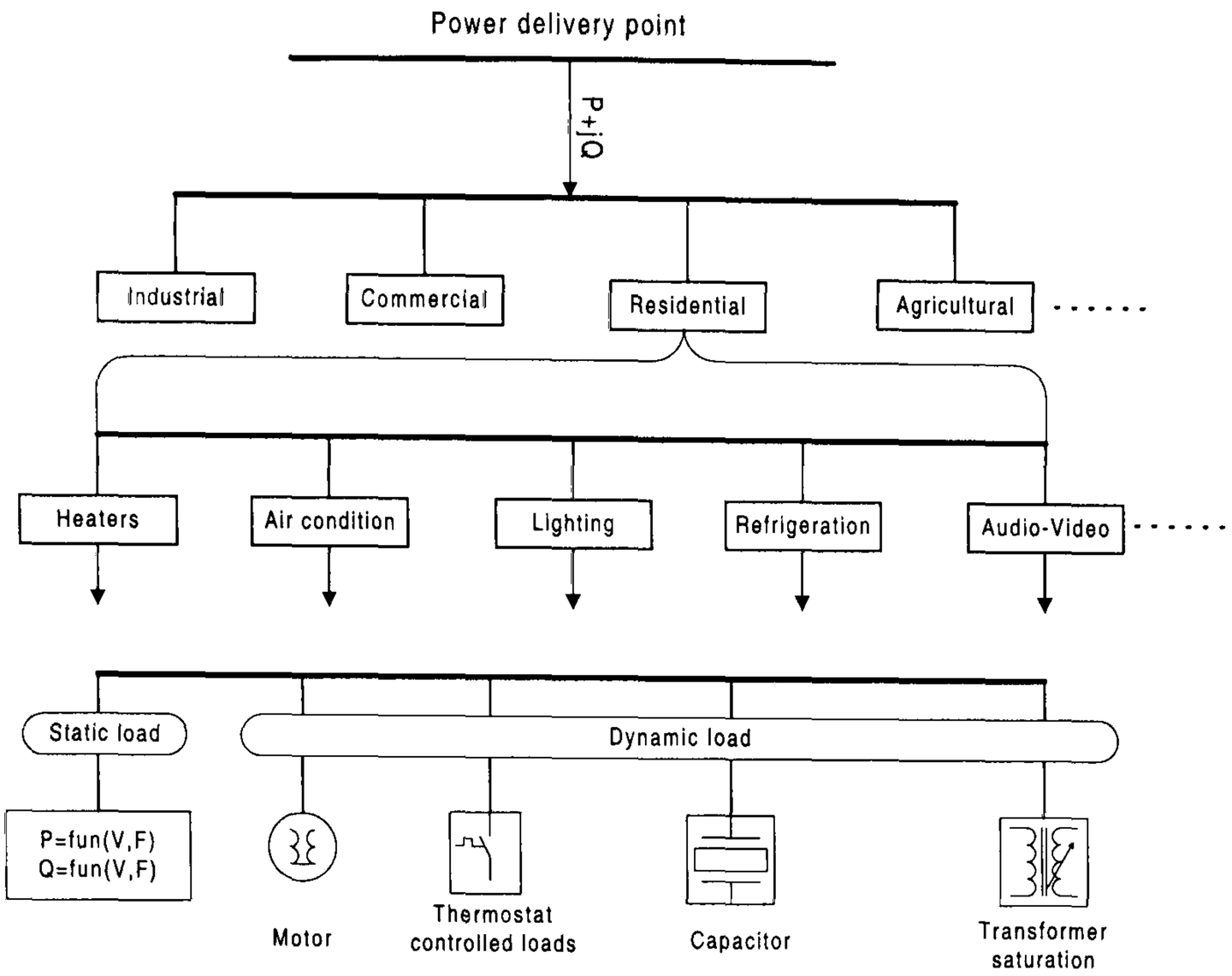

Figure 3-1: *Component based load modelling*

Static model

A static model expresses the active and reactive powers as functions of the bus voltage and frequency at any instant of time. It is common to represent the load by separately considering the active power (P) and reactive power (Q); both can be represented by a combination of constant impedance, current and power elements. Polynomials or other algebraic functions can reasonably represent static loads. The representation is based on the frequency and voltage dependence of the load observed over a rather limited range of variation and often is based only on the measured slopes ($\partial P/\partial f$) and ($\partial Q/\partial f$). This is because these quantities are still the best-known and most generally available data. Traditionally, the model has represented the relationship between power and voltage as an exponential equation, usually in the following form:

$$P = P_0\left(\frac{V}{V_0}\right)^a$$
$$Q = Q_0\left(\frac{V}{V_0}\right)^b \qquad (3\text{-}8)$$

The exponents are $a = \partial P/\partial V$ and $b = \partial Q/\partial V$, at $V=V_0$, where the subscript "$_0$" identifies the values of the respective variables at the initial operating conditions. Berg [34] has identified the parameters for different loads and established that 'a' lies between 0 and 2, and 'b' lies between 0 and 3.

The static load model that includes frequency dependence is usually represented by multiplying the exponential load model by a frequency sensitivity factor, which yields the general load equations.

$$P = P_0\left(\frac{V}{V_0}\right)^a (1 + D_{pf}\Delta f)$$
$$Q = Q_0\left(\frac{V}{V_0}\right)^b (1 + D_{qf}\Delta f) \quad (3\text{-}9)$$

where P_0, Q_0, are the connected loads at normal frequency, D_{pf} and D_{qf} are the frequency sensitivity parameters of the model and D_{pf} ranges from 0 to 3 and D_{qf} ranges from -2 to 0, depending on the type of load.

The static load models can be classified into three different representations [35], as demonstrated graphically in Figure 3-2.

- **Constant power model** – the power does not vary with changes in voltage magnitude, which is also called the constant MVA model; this is obtained by setting the exponents to "0".
- **Constant impedance model** – the power varies directly with the square of the voltage magnitude, the model is constructed by setting the exponents to "2".
- **Constant current model** – the power varies directly with the voltage magnitude, the model is constructed by setting the exponents to "1".

The range of frequency and voltage excursions depends on the nature of the disturbances. Accidental loss of generation will lead to a collapse in the frequency and voltage whereas loss of the load will cause an increase in the frequency and the voltage of the power system.

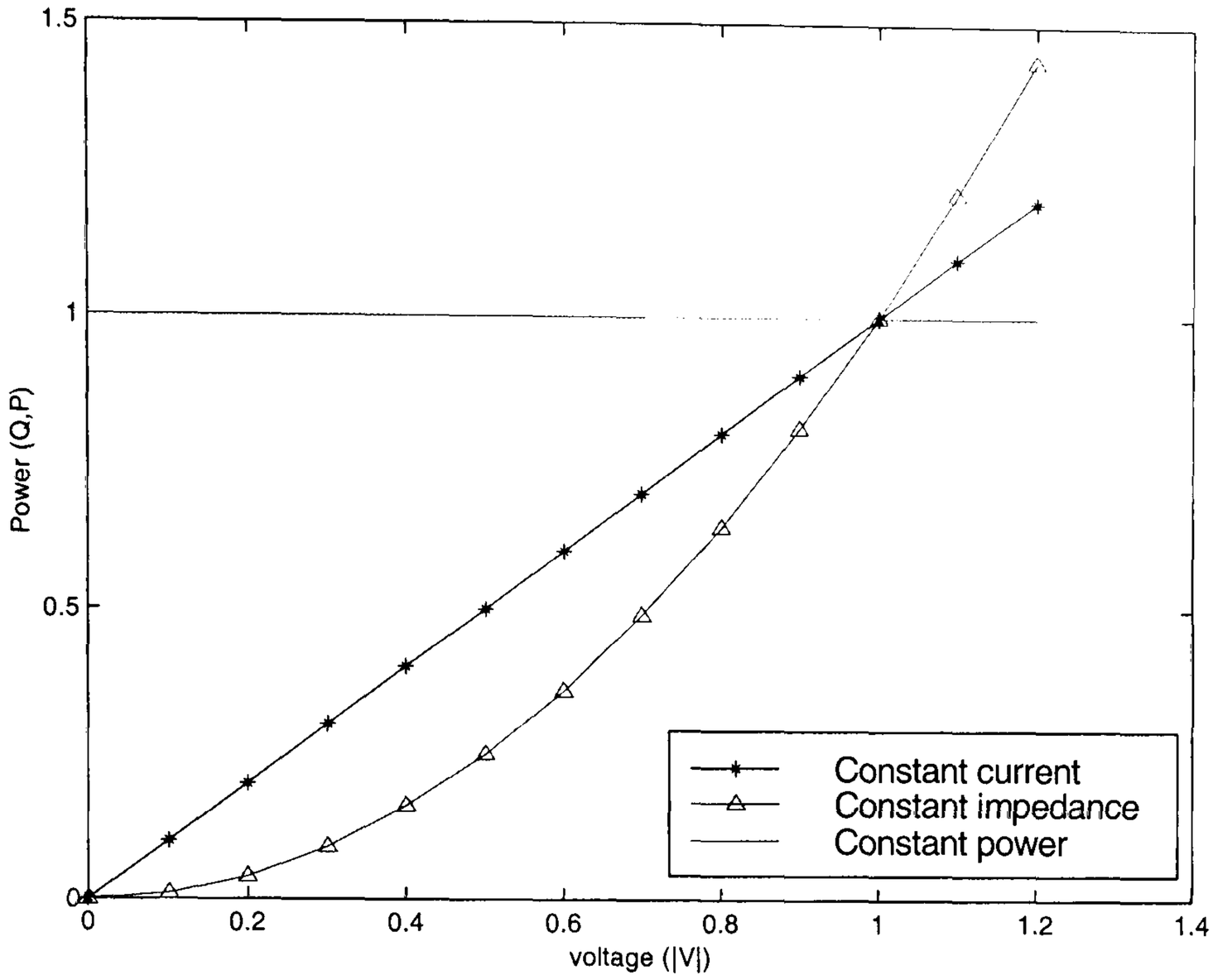

Figure 3-2: *Characteristics for different load models*

Dynamic model

A dynamic model expresses the active and reactive powers at any instant of time as functions of the bus voltage and frequency at past and present instants of time. The response of most composite loads to frequency and voltage changes is fast, and a steady state response is reached very quickly. The case of static models is justified in such conditions. There are, however, many components of power systems which respond relatively slowly. Studies of inter-area oscillations and long term stability often require load dynamics to be modelled.

3.2.3 Generator loading

In some extreme circumstance, the generator may be required to supply an isolated load and it is necessary to enhance the generator model to account for the load power characteristics of the local load. The most commonly accepted static model is to represent active power as constant current and reactive power as constant impedance [36]. Throughout the thesis, these models are used when analysing a single unit supplying an isolated load. This representation is used in Chapter 7 to investigate the black start regime at Dinorwig. As described earlier most loads consist of a large quantity of diverse

equipment and since we are interested in the short-term stability of the system, it is adequate to use the static load models of equation (3-9). Assuming the system voltage remains constant and using the constant current model the active power can be expressed as:

$$P_L = P_0 + P_0 D_{pf} \Delta f \tag{3-10}$$

Equation (3-10) is developed for small signal analysis and neglecting the second order terms yields equation (3-11) that separately represents the non-frequency sensitive load change and frequency sensitive load change.

$$\Delta P_L = \Delta P_0 + D\Delta f \tag{3-11}$$

The damping term $D = P_0 D_{pf}$, is proportional to the connected load and the load frequency sensitivity parameter. Thus, the damping will be close to zero if the unit is lightly loaded. Combining the load equation (3-11) with the generator representation of equation (3-7) yields a transfer function describing the mechanical motion of a single machine connected to a load with damping D.

$$\Delta \overline{P}_m - \Delta \overline{P}_e = (T_m s + \overline{D})\Delta \overline{\omega} \tag{3-12}$$

3.3 Parallel Operation

In today's world, an isolated generator supplying its own load independently is very rare. The usual situation is that the generators are operating in parallel (synchronised) sharing the load of the power system. Operating is this manner increases the reliability of the power system because the failure of any generator will not lead to total power loss. Moreover, having a large number of generators in parallel allows a bigger load to be supplied and permits the shutdown of some generators for maintenance.

3.3.1 Electrical coupling between generators

There is considerable electrical coupling between a generator connected in parallel to another generator or to a power system. To investigate this effect, consider an electrical system represented by two generators connected in parallel across a reactance X_T with their resistances neglected. Figure 3-3 illustrates the system representation. The reactance X_T consists of the sum of the armature reactance and the coil's self-inductance of each

generator. The classical model of a generator as described in Section 3.2.1 is used in this analysis. Generator #1 operates at a voltage E_1 and rotor angle δ_1. Similarly, Generator #2 operates at a voltage E_2 and rotor angle δ_2. In steady state the two generators will be operating at base frequency and any load imposed on the system will affect the frequency of both generators. Since the generators are operating in parallel, the power-angle expression of equation (3-13) is used to calculate the power exchange between the two units. This power will act as a load on machine #1 and as a generation to machine #2 [37].

$$P_{12} = \frac{E_1 E_2}{X_T} \sin \delta \tag{3-13}$$

where:

P_{12} = Power exchange between the machines

E_1 & E_2 = Generator voltage

X_T = The total reactance between the two generators

δ = Torque angle (δ_1- δ_2)

Since we are interested in small changes around the operating point, equation (3-13) can be linearised around the operating conditions represented by $\delta = \delta_0$ to yield

$$\Delta P_{12} = \frac{E_1 E_2}{X_T} \cos \delta_0 (\Delta \delta) \tag{3-14}$$

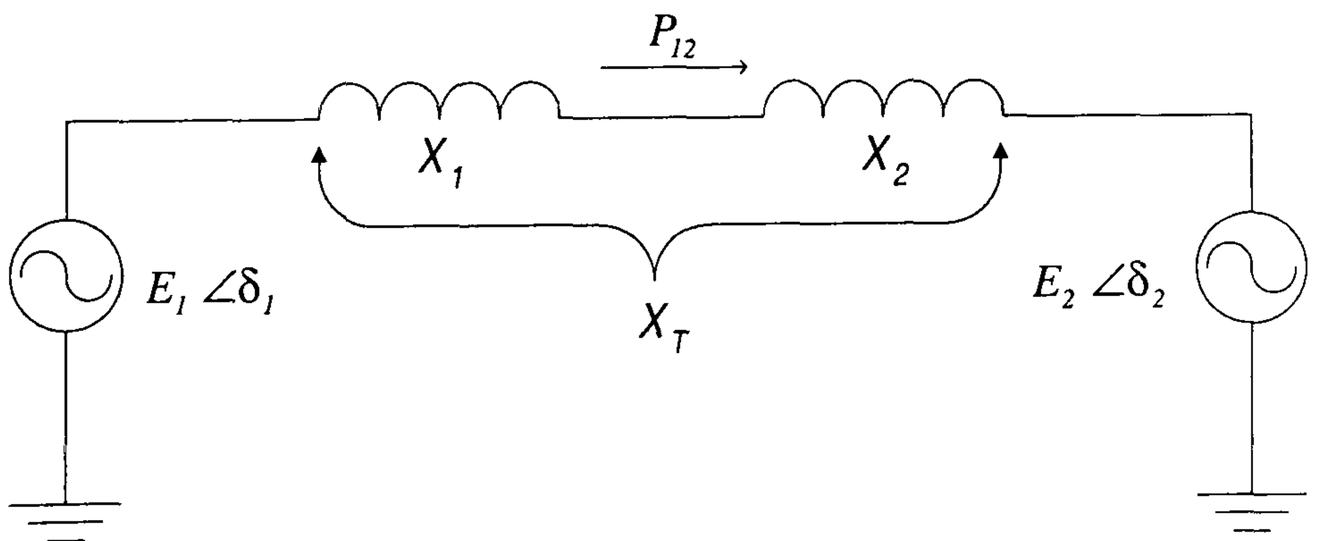

Figure 3-3: *Parallel generators model*

The deviation in the torque angle $\Delta\delta$ is calculated by integrating the difference in frequency between the two machines. For a torque angle in radians, the frequency

deviation is multiplied by $2\pi f_0$. Figure 3-4 shows the block diagram of two generators operating in parallel sharing a load with a damping coefficient (D). The model developed is used for internal machine oscillation studies and is implemented in Chapter 5, to describe a unit connected in parallel with the power system. This representation is also implemented used in Chapter 7 to simulate a black-start operation at Dinorwig where two units are used to pick up cold loads during restoration of the power system.

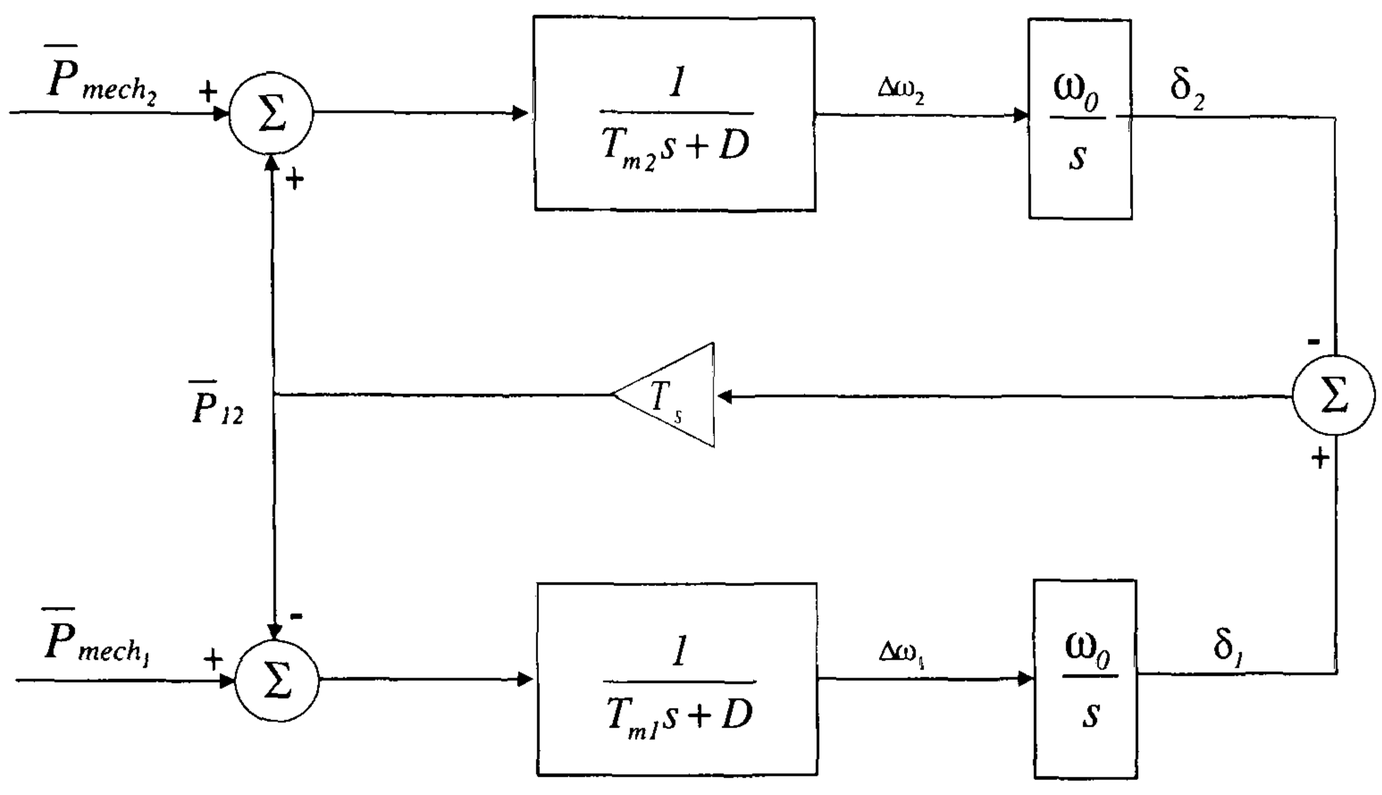

Figure 3-4: *Block diagram of two generators operating in parallel*

The strength of the electrical coupling depends on the synchronising coefficient T_s of the power transmission line, which is a measure of the incremental change in power resulting from an incremental change in the power angle.

$$T_s = \frac{\Delta P}{\Delta \delta} = \frac{E_1 E_2}{X_T} \cos \delta_0 \tag{3-15}$$

The strength of coupling approaches zero when operating close to the stability limits ($\delta = 90^{\circ}$). Therefore, it is not desirable to operate the line near to its power limit.

Substituting equation (3-15) in equation (3-14) yields,

$$\Delta P_{12}(s) = \frac{2\pi T_s}{s}\left[\Delta F_1(s) - \Delta F_2(s)\right] \tag{3-16}$$

Using the representation of Figure 3-4 the characteristic equation of a generator operating in parallel can be written as equation (3-17).

$$s^2 + s\frac{D}{T_m} + \frac{T_s \omega_0}{T_m} = 0 \tag{3-17}$$

Comparing equation (3-17) with the general representation of a 2nd order system, the undamped natural frequency ω_n and the damping ratio ζ of the generator are given by:

$$\omega_n = \sqrt{\frac{T_s \omega_0}{T_m}}$$
$$\zeta = \frac{D}{2\sqrt{T_m T_s \omega_0}} \qquad (3\text{-}18)$$

An increase in the machine inertia constant decreases both the natural frequency and the damping ratio. Conversely, increasing the synchronous torque coefficient increases the natural frequency and decreases the damping ratio. An increase in the damping coefficient increases the damping ratio without affecting the natural frequency. Figure 3-5 shows the behaviour of interconnected generators to a sudden load change in generator #2 assuming no change in prime mover power (no governor action). Since the generators are operating in parallel, they will share the total load ΔP_L and the power exchange between the generators will be equal to half of the applied load. The final steady state deviations of frequency in both generators settle at a value of $\Delta P_L/2D$. The natural oscillation frequency of the speed and power exchange can be calculated using equation (3-18).

The change in electric torque of a synchronous machine following a perturbation can be resolved into two components – the synchronising torque component and the damping torque component. System stability depends on both components of torque of each synchronous machine. Lack of adequate synchronising torque results in instability through a periodic drift in rotor angle, the rotor angle continues to increase steadily until synchronisation is lost, this form of instability is referred to as first-swing instability.

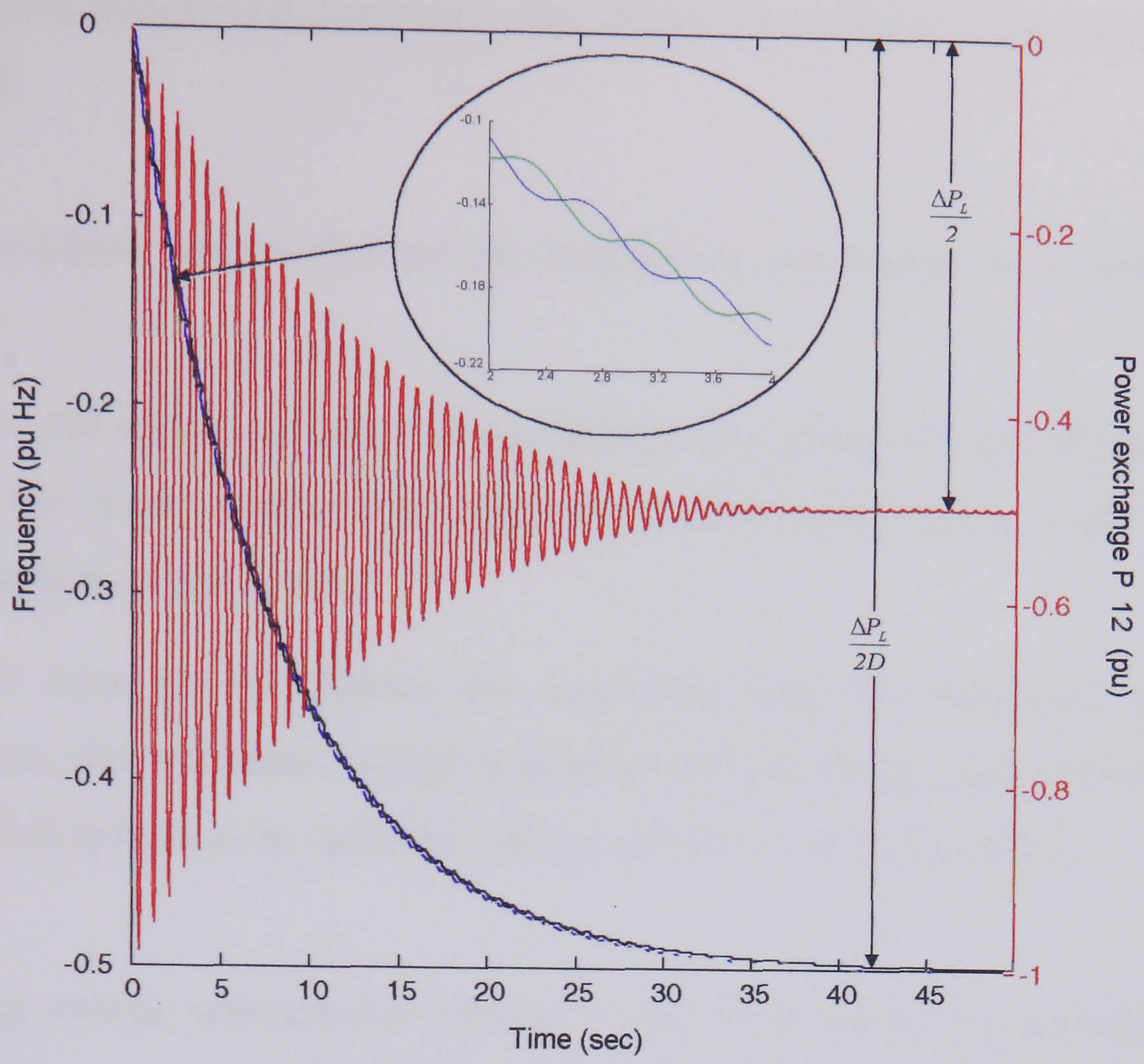

Figure 3-5: *The effect of loading interconnected generators*

3.4 Power System Model

A stable power system is one in which the synchronous generators, when perturbed, either return to their original states if there is no load change or modify the generation to match the load change. The perturbation may cause an oscillatory transient but, with a stable system, the oscillation will be damped. These oscillations appear as fluctuations in the power flow over the transmission line. A reliable power system maintains a constant voltage and frequency at all times. In practice, both voltage and frequency must be held within close tolerance so that the consumer's equipment operates satisfactorily.

Two types of stability analysis are associated with a power system. Recovery from a sudden large disturbance is referred to as *transient stability*. Typically, the disturbances are short circuits of different types which occur on the transmission lines and bus and transformer faults. The period of interest is usually limited to 3-10 seconds following the disturbance. On the other hand, *small signal stability* is the ability of the power system to maintain synchronism despite the occurrence of small disturbances. This type of stability

is largely due to insufficient damping in the system and different types of oscillation can be identified:

- Local machine: the oscillations are localised to one station or a small part of the system.
- Tie line: this relates the effect of oscillations of a group of coupled machines at one part of the power system with machines at other parts, due to week ties between different parts of the system.
- Control: here the oscillations are associated with the behaviour of the speed governors, the automatic voltage regulation and the HVDC link converters. Tuning the control system to an optimum setting will overcome this problem.

An electrical energy transmission system is characterised by its nominal frequency, voltage profile and load flow [38]. In any such system, the demanded real (P_L) and reactive (Q_L) powers change throughout the day. However, over short periods of typically a few minutes, they can be considered constants with superimposed first order disturbances ΔP_L and ΔQ_L. The changes in the generated power, ΔP_G and ΔQ_G must match the load disturbances if the exact nominal state is to be maintained. Due to the random nature of the load fluctuation, this cannot be achieved fully and the goal is then to regulate the system to within sufficiently small tolerances of the nominal. Therefore controlling system behaviour can be divided into two more or less independent problems:

Megawatt-frequency control (P-F control)

For satisfactory operation of the power system, the frequency should remain nearly constant. Relatively close control of frequency ensures constant speed of motors; the frequency of a power system is dependent on active power balance, as frequency is a common factor throughout the system. A change in the active power demand at one point is reflected throughout the system by a change in frequency. Thus, the frequency error is the most sensitive indicator that a real power mismatch has occurred - an increase or decrease in the real power generated is required in response.

Megavar-voltage control (Q-V control)

The control of voltage level is accomplished by controlling the production, absorption and flow of the reactive power at all levels of the system. The generating units provide the basic means of voltage control. The synchronous generator can generate or absorb reactive power depending on its excitation. When overexcited they supply reactive power, and when overexcited they absorb reactive power. A change in voltage magnitude is the most sensitive indicator that reactive power mismatch has occurred – an increase or decrease in the reactive power generated is required in response.

Dinorwig is configured to operate as a power/frequency (P-F) controller thus it is sufficient to implement the frequency changes and ignore the voltage changes. In order to establish a model of the power system to be used in conjunction with the hydraulic system, consider a controlled region of the power system connected via a tie line to a neighbouring region. Assume that the controlled region experiences a real load change of magnitude ΔP_L and that a change ΔP_G in generated power occurs due to the action of the frequency control machine. The net power surplus (ΔP) is given by:

$$\Delta P = \Delta P_G - \Delta P_L \tag{3-19}$$

The surplus power can be absorbed by the system in one of three ways:

- Changes to the system kinetic energy, which is generally associated with a change in system frequency.
- Increased power export to the neighbouring area via the tie lines.
- Increased load consumption.

The sensitivity of a system load to frequency is expressed by the load damping factor D, which represents the change in the power for a given change in the frequency in an interconnected system. Typical values of D are 1% to 2%; a value of D=2 implies that a 1% change in frequency would cause a 2% change in load. The smaller the changes in frequency for a given load change, the stiffer the system. The per unit area transfer function using the total load as power base and 50 Hz as frequency base, can now be represented as follow:

$$\frac{\Delta \overline{F}(s)}{\Delta \overline{P}_G(s) - \Delta \overline{P}_L(s) - \Delta \overline{P}_{tie}(s)} = \frac{1}{\overline{D} + \overline{M}s} \tag{3-20}$$

where M is the combined inertia constant of the local machine and the effective rotating inertia of all the other machines connected via the power system.

The inertia constant of the power system can be estimated using the measured transients of the frequency. Inoue et al [39] have used the frequency transient responses which occur during events such as load rejection tests. A polynomial approximation was applied to the waveform of the transient in estimating the inertia constant. The result shows that the inertia constant in Japan is around 11 to 18 seconds. There is also a suggestion that there is a positive correlation between the inertia constant and the load damping D, which affects the value of the inertia for a given system loading. In the absence of a speed control governor (blocked governor) and the tie line, the inertia and the damping constants determine the system response to a load change, as the steady state frequency deviation is calculated as $\Delta f_{ss} = \frac{-\Delta P_L}{D}$.

3.5 Load Frequency Control

The characteristic of synchronous generators requires that they rotate at a fixed speed. If two or more generators are connected on the same electrical system (utility grid) they will operating as if they are on the same shaft. The real power generated depends on the prime mover torque, which is controlled in a hydraulic turbine by the guide vane position.

Two types of control schemes are used for most generator drives. The first type is called isochronous (constant speed) control where the governor continues to adjust the generator output until the measured frequency matches the set point precisely. An isochronous governor scheme works satisfactorily when a generator is supplying an isolated load or in a relatively small power system, where one generator only is used to respond to load changes. Isochronous governors are not used in multimachine systems because of the need for proper load sharing between the machines, since they will counteract each other in trying to control system frequency to their own setting. Isochronous speed control would cause an individual turbine to load up completely if its reference is slightly higher than the power system or to totally unload if its reference is slightly lower than the power system [40].

The second type is droop control (speed regulation) where the governor opens the guide vanes to a fixed position determine by the relationship between speed (frequency)

of the power system and a speed reference. The speed droop operates as a steady state offset with regard to a constant frequency reference. The turbine speed cannot be changed when the generator is locked to a power system but it is possible to change the speed reference of the governor. Therefore, all the control machines will pick up load if the power system frequency falls and will drop load if the power system frequency rises. Whatever governor mechanism is present on a turbine; it will always be adjusted to provide a slightly drooping characteristic with increasing load. The value of the speed droop (R) determines the speed versus load characteristic of the generating unit as shown in Figure 3-6.

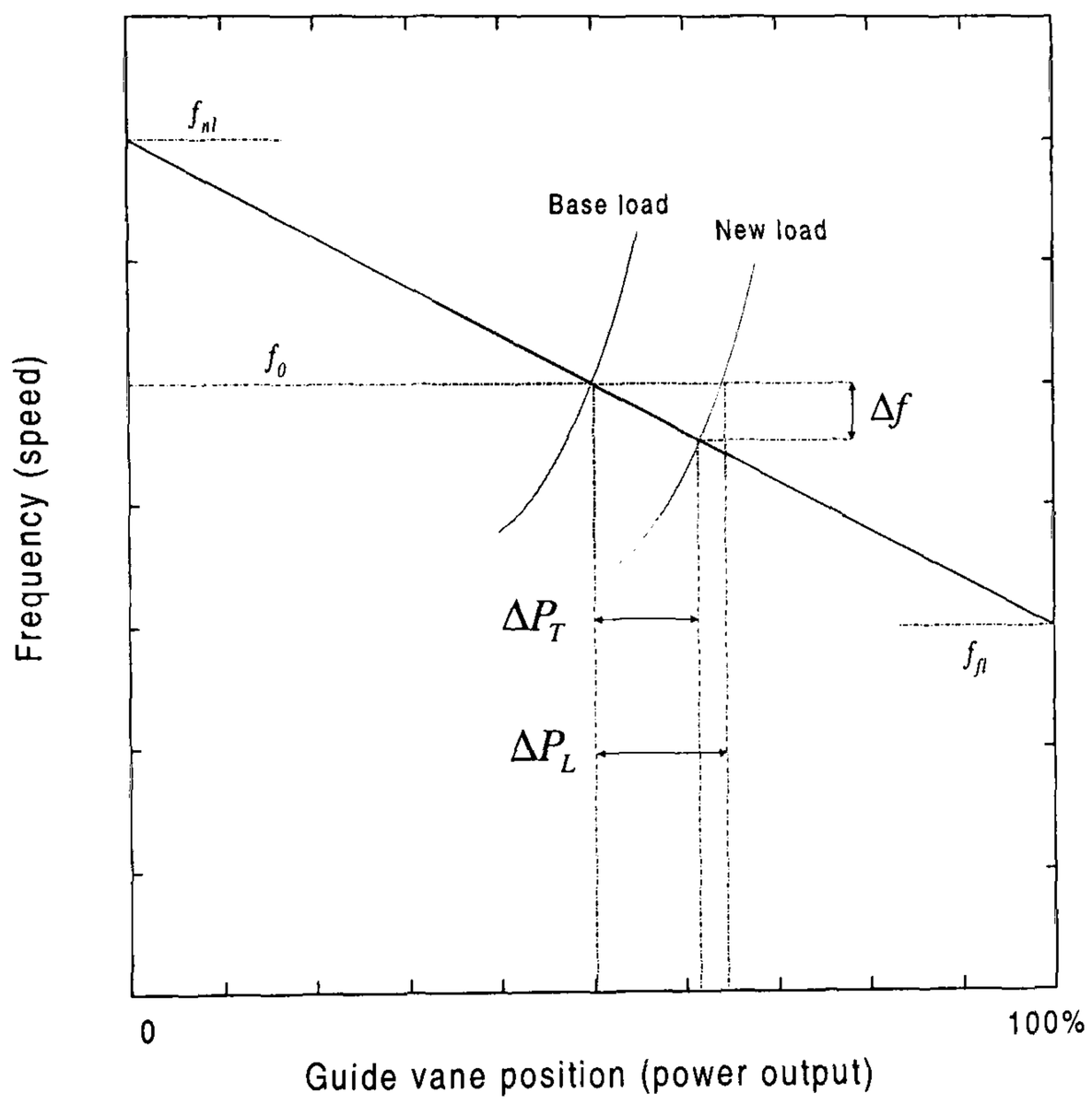

Figure 3-6: *Characteristics of governor with speed droop*

The speed droop of a unit is defined by the equation,

$$R\% = \frac{\Delta f \quad (\Delta w)}{\Delta P} = \frac{f_{nl} - f_{fl}}{f_0} \times 100 \tag{3-21}$$

where[#]:

[#] SI units are used in this thesis for physical quantities although the models are mostly expressed in the per-unit system.

f_{nl} = Steady state frequency at no load

f_{fl} = Steady state frequency at full load

f_0 = Rated frequency

A typical droop or "speed regulation" characteristic is 4% in the UK, which means that a frequency deviation of 4% causes 100% change in the generator output.

The load frequency control characteristic of the power system depends on the collective effects of all the droops of the speed governors and on the frequency characteristics of the load damping D of equation (3-20). The steady state frequency deviation following a load change ΔP_L for a power system with units operating in speed droop mode is given by,

$$\Delta f_{ss} = \frac{-\Delta P_L}{\left(\frac{1}{R_1} + \cdots + \frac{1}{R_n}\right) + D} = \frac{-\Delta P_L}{\beta} \tag{3-22}$$

where n = the number of units operating with speed governor.

The power system frequency response characteristic "β", which is referred to as the stiffness, is normally expressed by MW/Hz. The physical significance of β can be stated as follows; if a power system was subject to a step load change, it would experience a static frequency drop inversely proportional to its stiffness. The smaller the changes in frequency for a given load change the stiffer the system. Figure 3-6 illustrates the steady-state relationship between load change, frequency change and the increase in power output provided by the governor action. The power output increase of each individual unit under governor control is given by:

$$\Delta P_T = -\frac{\Delta f_{ss}}{R_{unit}} \tag{3-23}$$

The power system equation (3-20) is rewritten to include the stiffness "β" thus, the transfer function of the power system which relates the change in frequency to a change in power is given by:

$$\frac{\Delta\overline{F}(s)}{\Delta\overline{P}_G(s)-\Delta\overline{P}_L(s)} = \frac{1}{\overline{M}s+\overline{\beta}} \tag{3-24}$$

The linearised equation (3-24) is used to represent the power system for load frequency control. This is justifiable because the study is based on analysing the effect of Dinorwig's operation on the power system and the amount of power that is involved is very small compared to the total power system size. Therefore, it is justifiable to assume that there is no change in the system operating point and the perturbations due to Dinorwig are around that point.

3.6 Conclusions

This chapter has presented the background to power system dynamics, as appropriate for use in a modelling study of a power system. The complexities of the models depend on the type of transient and the system being investigated. Since we are mostly concerned about the frequency control of the power system more effort has been placed on the active power flow in the system.

Generally, the components of the power system that influence the electrical torque include the network state before and after the transient, the loads and their characteristics, the synchronous generator, the speed governor and other supplementary controls such as tie-line power flows. A linearised model representing the power system was developed for use in frequency control analysis of Dinorwig plant. The justification for using the linearised model in the simulation is that the effect of Dinorwig generation is small compared to the total power system loading; it is therefore possible to assume that the system variation is close to its operating point. The models assembled here are then integrated with those developed in Chapter 2 and the governor model described in the next chapter to build a generic model for the Dinorwig pumped storage plant as described in Chapter 5.

Chapter
4

Speed Governor

4.1 Introduction

Having described the dynamic characteristics of the hydraulic prime mover (penstock/turbine) and the electrical power system, this chapter proceeds to describe the next link in the chain, the primary speed/load control -historically known as the speed governor. Referring back to Figure 1-1, the unit governor receives information on the system frequency and power demand then acts to regulate the flow of water through the penstock by controlling the turbine guide vanes in order to restore the frequency to its set value.

The emphasis in this chapter is initially to develop models of the governor and the guide vane dynamics based on an analytical approach. Subsequently, system identification techniques are used to verify and revise these models. A frequency response measurement is used to obtain the Dinorwig governor model which includes the additional internal functions in the PLC diagram such as filters and extra operational loops. The work proceeds with a transient analysis based on a step response test carried out on the guide vane to obtain an approximate model.

4.2 The Three Term (PID) Controller

One of the most widely used control laws in hydro power station governing systems is the PID type controller, where the PID stands for Proportional-Integral-Derivative. It can be implemented mechanically, pneumatically, electrically or as is most common today, a computer-based device. This is the case at Dinorwig. They are easy to adjust and configure, in addition to providing possibilities of improvement in operation and control. The main advantage of using a digital controller is that it allows the governing system to be more sensitive to small errors and it is capable of fast action. In addition, digital controllers are accurately reproducible and produce an identical response from all the units on line in contrast to the variability mechanical or electrical governors. Since the three PID parameters are separately adjustable, it can be tuned to meet the needs of the plant.

The proportional term of the controller produces a control signal proportional to the error in the system, so that $u(t) = K_p e(t)$. Typically, given a step change in set point, low values of K_p give rise to stable responses but large steady-state errors. Higher values of K_p give better steady-state performance, but worse transient response. Therefore, the proportional action is used to reduce the steady state error, although increasing the gain K_p decreases the system time constant and damping. The proportional action can never eliminate the steady state error in the system because some (small) error must be present in order to produce a control output.

A common way of reducing the steady state error is by incorporating integral action into the controller. Here, the control signal generated is proportional to the integral of the error signal, that is $u(t) = K_i \int e(t)\,dt$, where K_i is the integral gain. While an error exists, the integrator tends to increase control action, thus driving the plant towards the demand output. Then, when the error disappears, the continuing integrator output can be used to maintain the control action necessary for steady-state conditions. Although the steady-state error may be reduced to zero, such performance is achieved at the expense of stability. This is because the integral term increases oscillation amplitude and settling time by introducing extra 90^{o} of phase lag at all frequencies, thus reducing the gain and the phase margins. To reduce the oscillation a third term can be added, which gives a control signal proportional to the time derivative (rate of change) of the error signal,

$u(t) = K_d \frac{de(t)}{dt}$, where K_d is the derivative gain. Since the output signal responds only to the rate of change of error, it has no effect upon steady–state operation (rate of change is zero). Pure derivative feedback is not practical to implement and it is usually used in conjunction with proportional and/or integral gains to increase the damping of the system. During a transient, the 90^{o} phase lead introduced by the zero at the origin of the s-plane increases the system's phase margin and hence increases the damping of the system. This increase in the damping will allow higher values of K_p and K_i to be used than would otherwise be the case. The overall controller transfer function is [41]:

$$G_c(s) = K_p + \frac{K_i}{s} + K_d s \tag{4-1}$$

Often, the controller is represented in terms of the interactions created as

$$G_c(s) = K_p\left[1 + \frac{1}{sT_i} + sT_d\right] \tag{4-2}$$

where:

T_i = Integral action time (reset time) $= \frac{K_p}{K_i}$

T_d = Derivative action time (rate time) $= \frac{K_d}{K_p}$

4.2.1 Digital PID representation

The principle of PID control applies also to digital control and the controller is transformed into discrete time using Tustin's method (bilinear approximation) to yield:

$$G_c(z) = K_p + K_i \frac{T_{sa}(z+1)}{2(z-1)} + K_d \frac{2(z-1)}{T_{sa}(z+1)} \tag{4-3}$$

where:

$z = e^{sT}$

T_{sa} = Sampling period

The sampling period selection is usually limited by the speed of the computer and physical consideration of the system. The sampling frequency must be at least equal to twice the value of the highest significant frequency in the signal. Sampling rates used in practice are generally much higher and may be between 4 and 20 times the system bandwidth. It is not necessary to sample all parts of the process at the fastest rate and the Dinorwig PLC governor uses different sampling times as follows [42]:

50 ms: Frequency measurement, frequency control and test terminals.

200 ms: Operating mode, selection of parameters and fault monitoring.

2000 ms: Auxiliary circuits.

4.2.2 Dinorwig Governor configuration

The unit governor has the general configuration shown in Figure 4-1 where the speed and power control loops are integrated, with the power loop providing the permanent droop on the speed. The system comprises two main control loops as follows:

- A frequency control loop, in which the frequency deviation is fed to the controller whose output, is used to adjust the turbine guide vane position. An adjustable frequency dead-band, typically of 0.5Hz, would be included in this loop to limit the response and prevent hunting

- A power control loop in which the power output deviation is multiplied by the speed regulation droop (R) and fed into the proportional and integral sections of the governor thus creating a compensating signal for the frequency deviation. The derivative action is not used in this loop.

A hydraulic turbine, because of its particular response characteristics, requires a governor with transient droop characteristics for stable speed control response. Conventionally, this is implemented in a mechanical-hydraulic governor. The term transient droop implies that for fast transient conditions (deviations in frequency) the governor exhibits a high regulation (low droop gain), while for slow transients the governor has low regulation (high droop gain) [14]. At Dinorwig, this is implemented by setting the governor to operate with two droop settings; 1% for high regulation and 4% for low regulation. They are set on a control panel by the station operator at the request of the NGC.

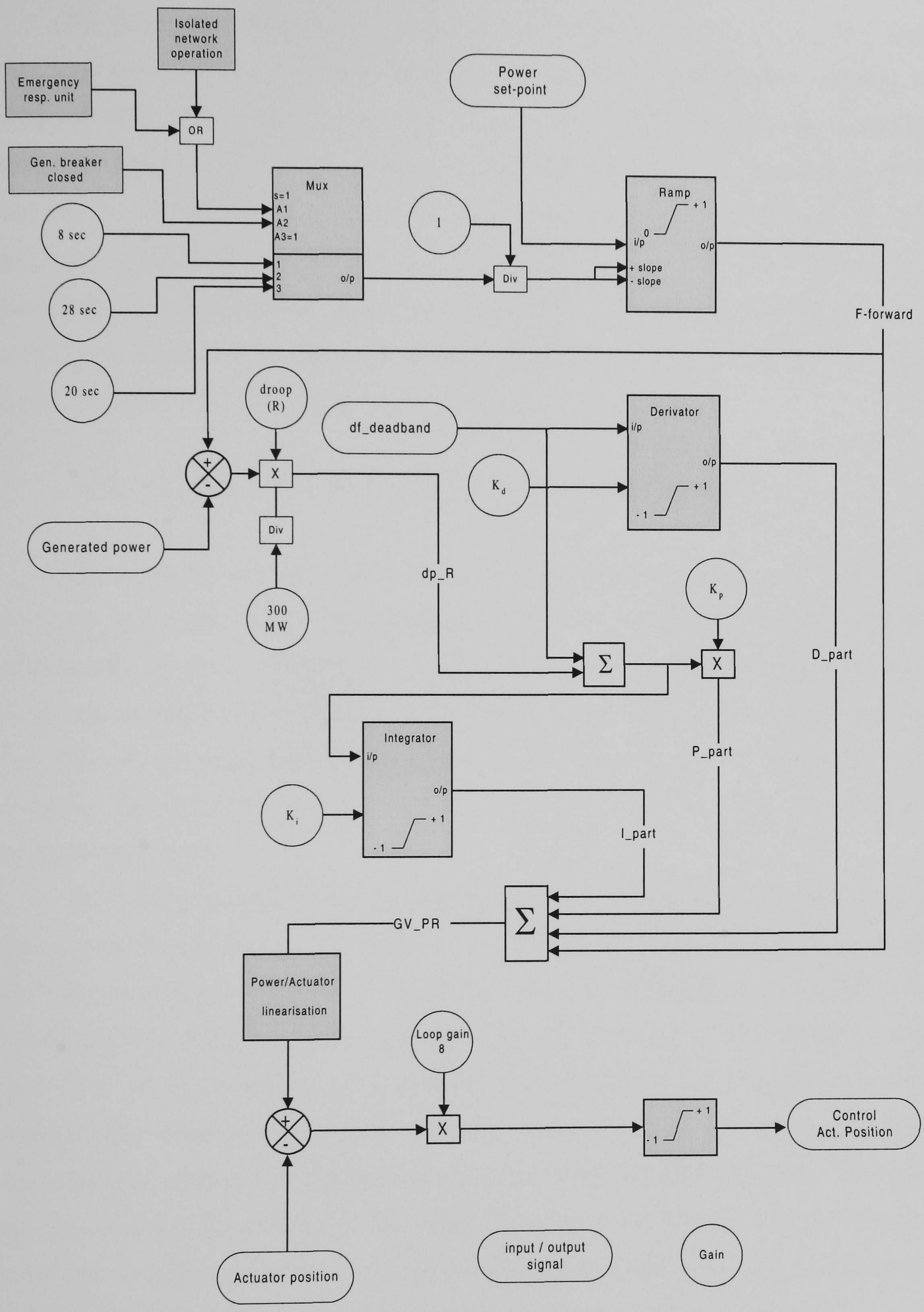

Figure 4-1: *Dinorwig PLC diagram*

The power reference signal is used to inject a feed-forward signal, which sets the reference position for guide vane opening. This enables a rapid initial response to be achieved after which the governor acts to trim the guide vane position to obtain the required output power. By this means, the response time from closed to fully open is 28 seconds in normal operation and 8 seconds under emergency conditions. The power reference signal is also used to define the operating point for the unit when used in the part–load response mode for frequency regulation. The output signals from the P, I parts and D are summed with the feed forward signal to produce the guide vane position reference signal (GV_PR) which can be written as:

$$GV\_PR = \left[(df + dp \times R)(K_p + \frac{K_i}{s}) + df \times K_d s + \text{feed forward} \right] \tag{4-4}$$

The governor normally operates with a power feedback loop so it is necessary to compensate for the non-linear relationship between guide vane opening and power (torque) as shown in Figure 2-6. The compensation is brought about by using a linearisation function in the PLC's programme. The function is defined by 3 co-ordinates for different net head (490-520-546 meters), 10 co-ordinates for power and 30 co-ordinates for resulting actuator position. The values between these co-ordinates are interpolated linearly.

The reference guide vane position reference is then compared with the position signal from the actuator and the deviation signal is converted into a hydraulic signal using an E/H (electrical to hydraulic) transducer. The hydraulic signal drives the actuator servomotors to adjust the guide vane position. The deviation signal influences the E/H transducer so that it deflects in proportion to the amplitude of the signal from neutral position. The deflection of the E/H convertor causes the actuator servomotor to move in the closing or opening direction depending on the direction of the deflection. The speed of the servomotor is proportional to the deflection of the E/H convertor. The servo loop gain parameter is adjusted during the commissioning period and a suitable response to step disturbances in the actuator loop is obtained by setting the gain to a value of 8.

4.3 System Identification

System identification is an important step to verify the theoretical model with experimental data, since even the best theoretical models are only approximations to the real system. The identification process fits a model to the recorded experimental data by assigning suitable numerical values to its parameters. System identification can be grouped into **non–parametric** methods and **parametric** methods**.**

Non–parametric methods determine the time and the frequency response of a linear time invariant system without prior knowledge of the model structure of a system. They are often used as a preliminary tool to get an initial estimate of the model structure of a system with unknown dynamics. There are different kinds of experimental data for generating a model, which can be classified as transient analysis (step or an impulse response), frequency analysis, spectral analysis (pseudo-random binary sequence "PRBS") and correlation analysis; all these methods are easy to apply but often sensitive to noise.

Parametric methods can be characterised as a mapping from recorded data to an estimated parameter vector (curve-fitting techniques). They can be applied to off-line or on-line estimation. The most common type of linear system model is the so-called **ARMAX**[#] model. Estimation of the parameters of this model is usually done by the least-squares method in which a certain quadratic criterion, based upon the system output measurement and the parameters to be estimated, is optimised to minimise the fit error [43].

The critical first steps in system identification are the design of experiments and collection of data. Making an experiment on an industrial plant always involves a large economic risk. The experiment must be planned carefully and executed with caution to ensure that normal operation is undisturbed while obtaining the data. An efficient experiment is possible if the process and the disturbances are known very well a *priori*. The major steps in a practical identification study are summarised in Figure 4-2.

[#]ARMAX is acronym for auto-regressive moving average exogenous variable.

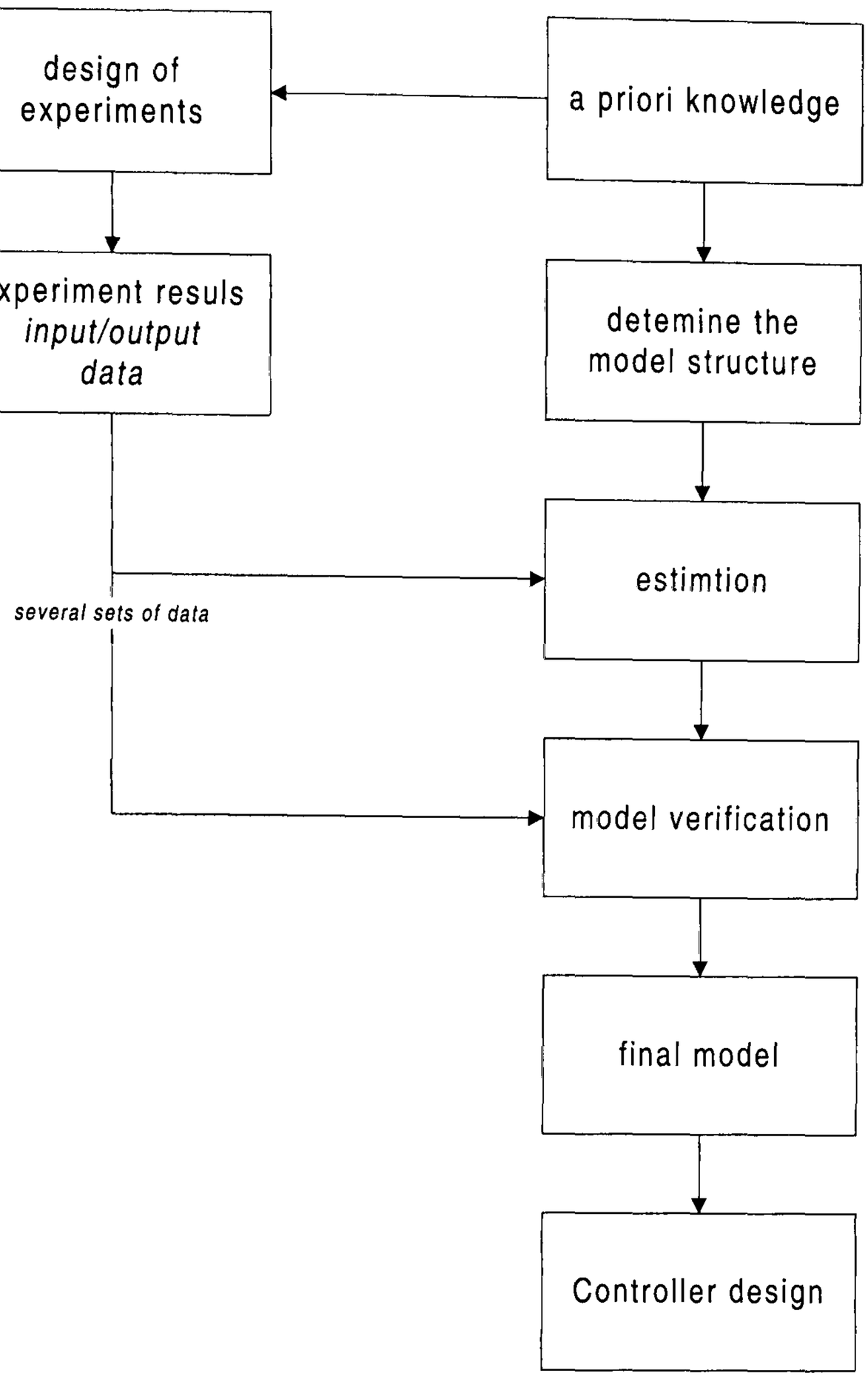

Figure 4-2: *System identification process*

Collecting the data (observing the system): the first step in identification consists of collecting observations of the process variables (inputs and outputs). The input–output data are some times recorded during a specifically designed experiment, where the user may determine which signal to measure and when to measure them. The object of experimental design is to make these choices so that, subject to practical constraints that may, the data contains maximum information.

Selecting a model set: a specific model is selected, on the basis of observations - this is probably the most important and most difficult choice within the system identification procedure. It is here that a *priori* knowledge and engineering intuition and insight have to be combined with formal properties of models. In the case of Dinorwig, the set of models of the hydraulic system is constructed from basic physical laws.

Choosing a selection criterion: any model only approximates the true system behaviour so the intended use of the model will largely determine the selection criteria in order to optimise its desirable features.

Computing model parameters: the assessment of a model's quality is typically based on how it performs when attempting to reproduce the measured data. The computation of the model parameters can be seen as an optimisation problem (the selection of the "best" model).

Model validation: validation is a trial to test whether the model is "good enough", that is, whether it is valid for its purpose. This involves various procedures to assess how the model relates to observed data, to prior knowledge, and its intended use. Deficient model behaviour in these respects causes the model to be rejected, while good performances will develop a certain confidence in the model.

4.3.1 Governor frequency response test

To verify the mathematical model of the governor described in equation (4-1) an open loop frequency test was conducted on the spare governor at Dinorwig using a Solartron 1253 gain-phase analyser [44]. The principle of this test is simple – a sinusoidal signal of varying frequency is applied to the system and the output is measured in terms of both magnitude and phase relative to the input. The system gain is then calculated at each frequency as the ratio of output to input magnitudes. The results are then plotted as a Bode diagram, from which a system transfer function can be deduced.

The governor used in the test is a digital ABB-HPC 640 controller as utilised at Dinorwig for all six operating units. The input signal to the governor is the power system frequency. The signal is in the shape of successive pulses of constant amplitude with time intervals dependent upon the value of the frequency. The frequency is sampled every 50ms and the output signal is measured using the mean average value over ten cycles. The generator output of the gain-phase analyser is a voltage signal therefore it was necessary to convert it to a pulsed frequency and this was achieved by using an AD537 V/F converter [45]. The converter is a controlled oscillator whose output signal has a frequency proportional to the input voltage.

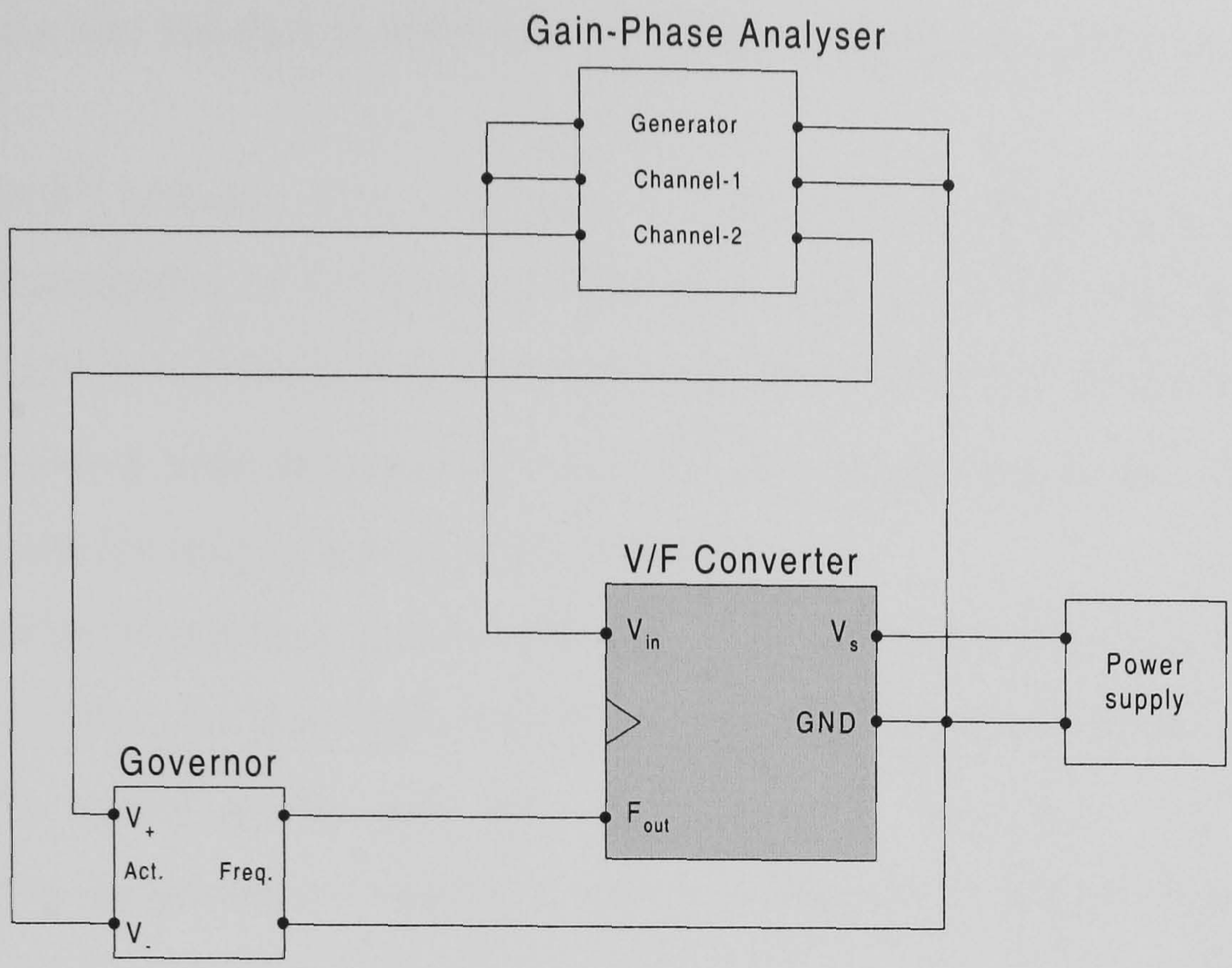

Figure 4-3: *Test connection*

The governor output to the actuator is a voltage signal whose magnitude varies by ±10V, which represents the actuator position from fully open to fully closed. No signal conversion is required here as the analyser compares the two voltage signals. Figure 4-3, shows the hardware connections for the system under test, where the voltage generator is connected to the V/F converter and its output signal used to supply the frequency input to the governor. One analyser channel is used to monitor the voltage input to the V-F converter and the other monitors the actuator signal of the governor. The gain-phase analyser generator was set to a –5.14V bias, which is a steady state DC offset corresponding to 50Hz output of the V/F converter, which is the nominal frequency of the power system. A frequency error signal (± Δf) was superimposed on the 50 Hz and this was implemented by setting the amplitude (rms) of the AC component of the generator output to 20mV equivalent to ± 0.3Hz. The frequency range chosen was from 0.02Hz-1.26Hz swept at 18 points from the low to high frequency.

Test results

The swept frequency test was carried out using gain settings for isolated-operation mode, $K_p = 2.5$, $K_i = 0.8$ and $K_d = 4$, while the droop was set to zero to disconnect the power feedback loop. A system transfer function was obtained by fitting asymptotic

approximations into the data to determine the corner frequencies and hence the pole-zero locations.

MATLAB® software [46] was used to write a program to plot the frequency response characteristics of the governor using the data collected from the analyser as shown in Figure 4-4. Initially the Bode gain plot has a slope of -20dB/decade and the phase plot shows a constant phase shift of -90^{o}, so that the system has a pole at $s = 0$, which represents the integral action of the controller.

The system proportional gain is represented by the horizontal line and it is apparent that the value of the gain is ≈ 27dB, which is higher than expected (7.95dB corresponds to $K_p = 2.5$). The source of the extra gain is the internal servo loop gain of 8 (18dB) implemented in the governor software as shown in Figure 4-1. Three corner frequencies can be determined at frequencies $\omega_1 = \frac{1}{T_i} \simeq 0.325$ rad/sec, $\omega_2 = \frac{1}{T_d} \simeq 0.625$ rad/sec and $\omega_3 \simeq 3.25$ rad/sec. The break point due to the integral effect occurs at ω_1, which represents the ratio between the integral and proportional gains.

It can be seen that there is a decrease in the phase below ω_1 and to prevent this from affecting the overall system's phase margin it is necessary to locate ω_1 below the cross over frequency of the system. Meanwhile the next break point is due to the derivative effect and occurs at ω_2, which is the ratio between the proportional and the derivative gains. Here the phase is increasing above ω_2 therefore it is desirable to locate ω_2 so that the increase in the phase occurs near the crossover frequency to insure high phase margin. This causes a stabilising effect on the system response and reduces the overshoot. The purpose of the derivative action is to extend the crossover frequency beyond the constraints imposed on the PI type controller.

At frequency ω_3 there is an additional 20dB per decade roll-off indicating the presence of a second filter term. Investigation revealed a low pass filter with time constant $T_f = 0.3$ implemented to limit the derivative action. Whilst the derivative term causes the gain to increase with frequency, thereby improving the phase margin, it also has the undesirable effect of increasing the high frequency gain, making the system more noise sensitive and encouraging undesirable natural resonance effects. For this reason, the

derivative action is usually cut off at some point between the system bandwidth and the frequency of first resonance.

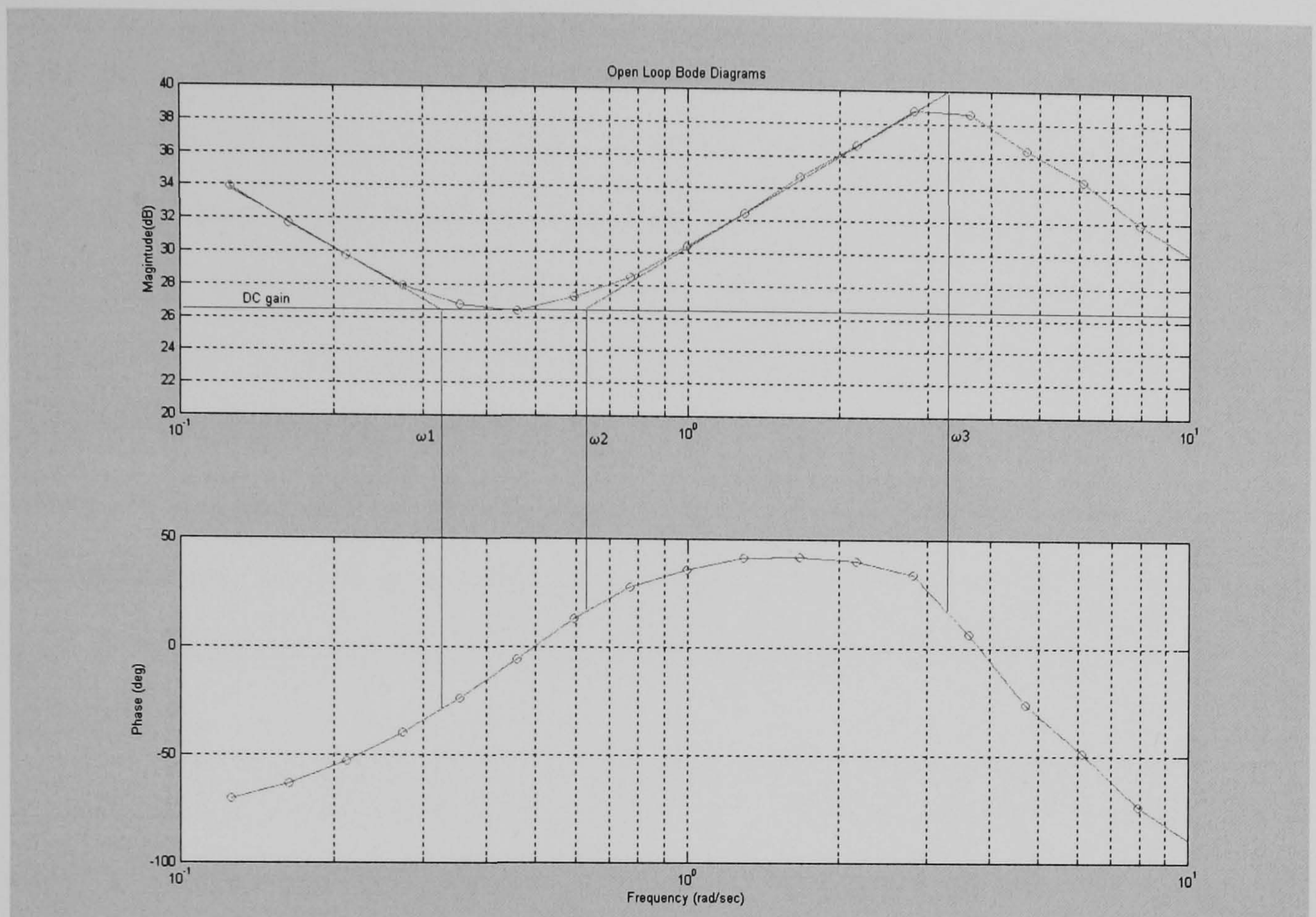

Figure 4-4: *Test frequency response of the governor*

It was also necessary to model the signal conditioning included by the control system manufacturer that takes a 10 cycle running average of the measured power system frequency. This was represented by the transfer function:

$$\frac{\Delta F_a(z)}{\Delta F(z)} = \frac{\sum_{j=0}^{9} z^j}{10z^9} \tag{4-5}$$

where:

F_a = Average frequency

F = Power system frequency

To verify the revised governor model its frequency response was compared with the experimental results. The Bode plot was obtained by combining the discrete transfer function of the PID compensator (including the derivative limiter filter) as represented by equation (4-6), with the averaging filter of equation (4-5).

$$G_c(z) = \left. \frac{15.7z^2 - 31z + 15.3}{z^2 - 1.85z + 0.848} \right|_{Tsa=0.05} \tag{4-6}$$

Equation (4-6) is derived using the same PID gains as the experiment and a sampling period of 50ms. The results shown in Figure 4-5 exhibit good agreement between the revised model and the experimental results in both magnitude and phase. Some discrepancies remain between the two responses especially at high frequencies ~ 5+ rad/sec. This is thought to be due to the noise present during the test and the saturation of the guide vane position signal. The test was repeated using different PID gain parameters and the results when compared with the model were found to exhibit similar agreement to the previous test. The verification procedure was considered complete at this point and the revised governor model shown in Figure 4-6 is used in subsequent work.

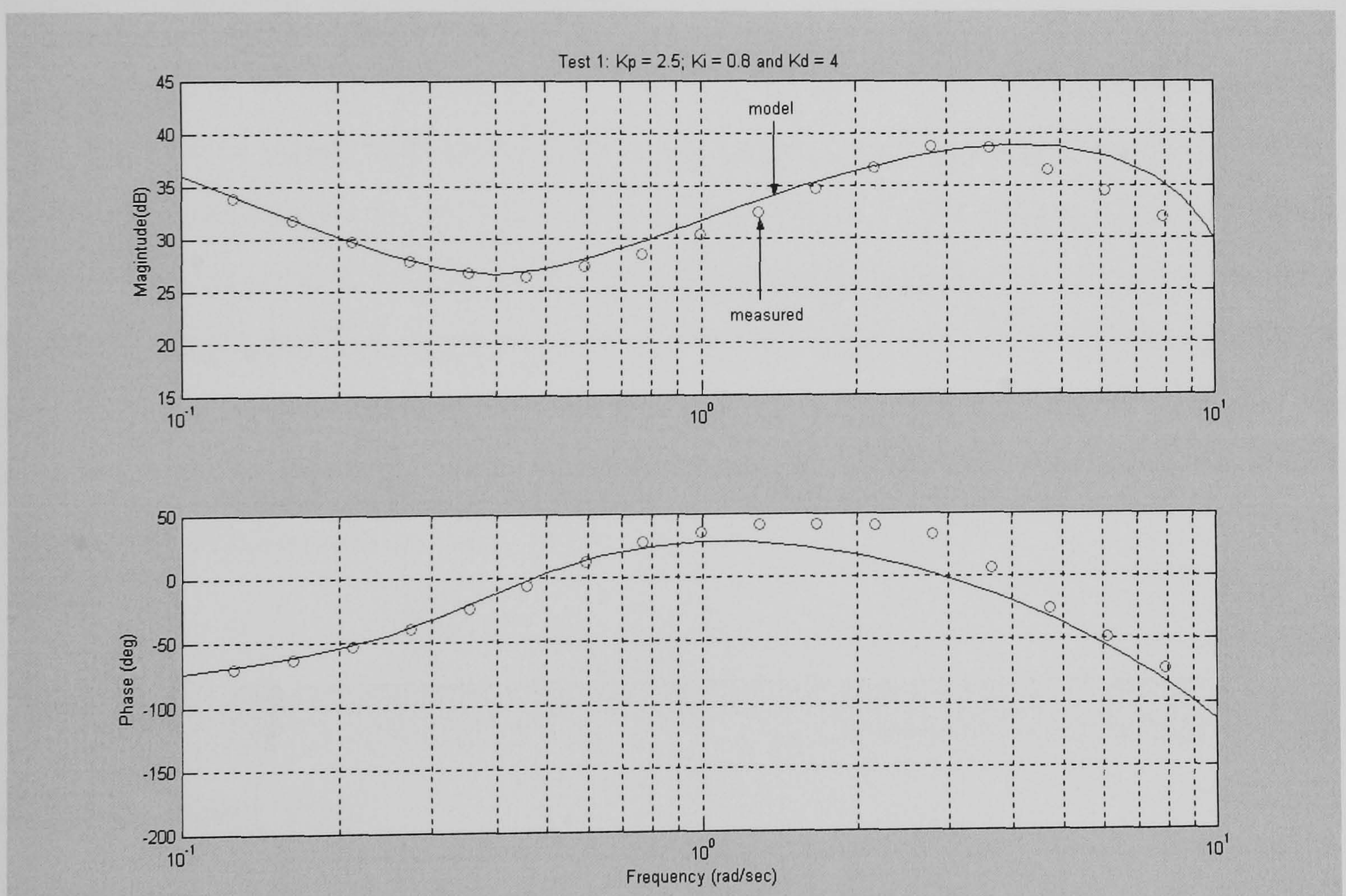

Figure 4-5: *Frequency response of the governor*

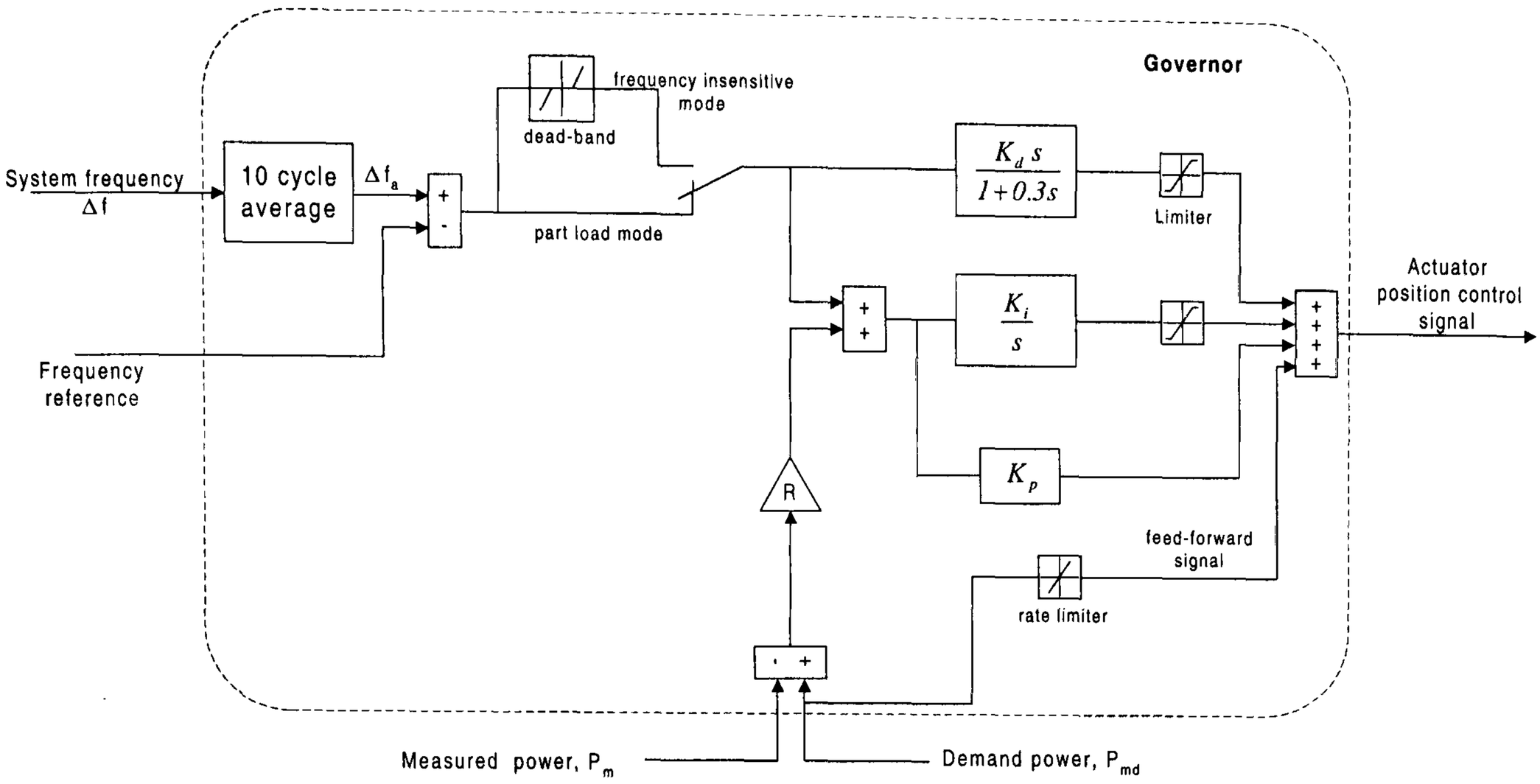

Figure 4-6: *Control loop model for the governor*

4.3.2 Guide vane modelling

The water flow into the turbine is controlled by the guide vane whose position depends upon the control signal from the governor. The guide vane dynamics are represented as a two-stage actuator with an internal feedback loop. The governor output (electrical signal) is converted by an E/H transducer to drive the actuator servomotors and hence to adjust the guide vane's position. In general, the guide vane dynamics can be represented by the transfer function of equation (4-7), which relates the desired and the actual positions. The time constants T_1 and T_2 are determined by the pressure/flow characteristics of the guide vane and its actuator servomotors [47].

$$\frac{Y(s)}{U(s)} = \frac{1}{(T_1 s + 1)(T_2 s + 1)} \tag{4-7}$$

4.3.2.1 Step test

A step response test was carried out on the guide vane to identify the low-order approximation model of the two-stage servomotors from an off line input/output data test record. This method is chosen because it is quick and relatively easy to implement and all the signals required to perform the test are available in the governor cubicle. The test yields information about the steady state and transient response.

The test is performed by using a step-input signal as a guide vane position reference and then recording both the actuator and the guide vane position. Meanwhile the actuator feedback loop is used to adjust the guide vane position. Figure 4-7(a) shows the actuator step response which is smooth and monotonic. This can be represented by a sum of exponentials as shown in equation (4-8) [48].

$$y(t) = y(\infty) + Ae^{-\alpha t} + Be^{-\beta t} + \text{----------} \tag{4-8}$$

Assuming that - α is the slowest pole in the system, it is possible to write

$$y(t) - y(\infty) \cong Ae^{-\alpha t} \tag{4-9}$$

Because $y(\infty) > y$ as shown in Figure 4-7(a) the equation can be solved as

$$\log_{10}[y(\infty) - y(t)] = \log_{10}(-A) - \alpha t \log_{10}(e) \tag{4-10}$$

Figure 4-7(b) shows the plot of $\log_{10}[y(\infty) - y(t)]$, which is an equation of a line whose slope determines α and intercept determines A. Using this method the parameter values were estimated to be $A = -1.1$ and $\alpha = 5.1$. The next pole is found by subtracting $1 - Ae^{-\alpha t}$ from the data, and then $\log_{10}$ of the result is plotted as shown in Figure 4-7(c). Following the same procedure, the parameter values are estimated to be $B = 0.1$ and $\beta = 3.8$. Combining the results, an expression for the response is estimated as:

$$y(t) = 1 - 1.1e^{-5.1t} + 0.1e^{-3.8t} \tag{4-11}$$

Equation (4-11) is plotted as solid line in Figure 4-7(a) and shows a reasonable fit to the data and no further terms were calculated. From y(t) we compute,

$$Y(s) = \frac{1}{s} - \frac{1.1}{(s+5.1)} + \frac{0.1}{(s+3.8)}$$

$$Y(s) = \frac{(s+5.1)(s+3.8) - 1.1(s+3.8) + 0.1(s+5.1)}{s(s+5.1)(s+3.8)}$$

Solving will result in a low order transfer function

$$G(s) = \frac{1}{(0.19s+1)} \tag{4-12}$$

The process was repeated to determine the transfer function of the second stage servomotor which was found to be a first order system with a time constant of $T_2 = 0.4$.

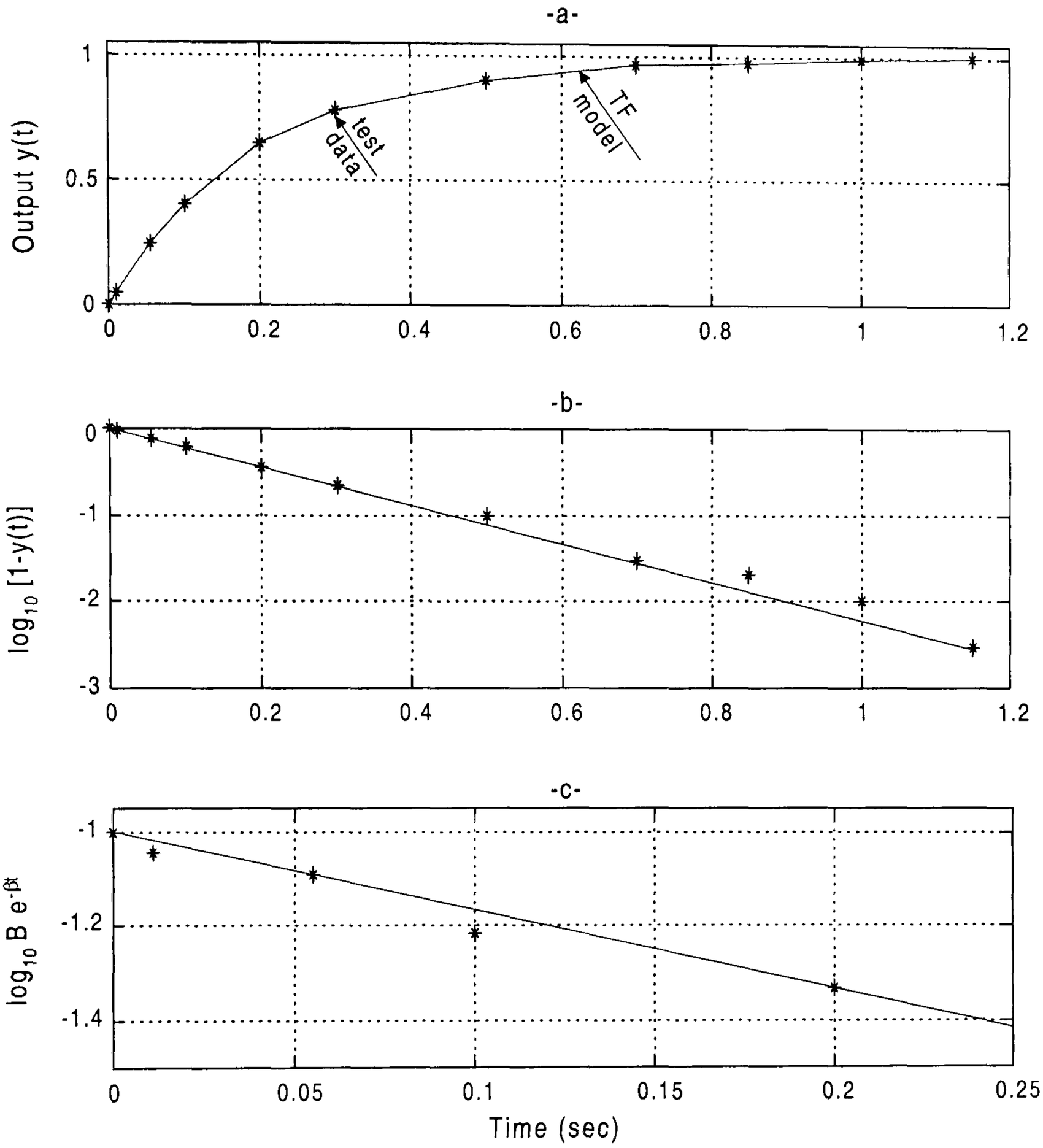

Figure 4-7: *Actuator response*

4.3.2.2 Non-linearity

The guide vane dynamics contain a nonlinearity due to its movement limitation that imposes upper and lower bounds on the corresponding model variable. When the input signal is within the range specified by the Lower limit (fully closed) and Upper limit (fully open) parameters, the input signal passes through unchanged. When the input signal is outside these bounds, the signal is clipped to the upper or lower bound. The model of

the guide vane dynamics used in the simulation including the required saturation blocks is shown in Figure 4-8.

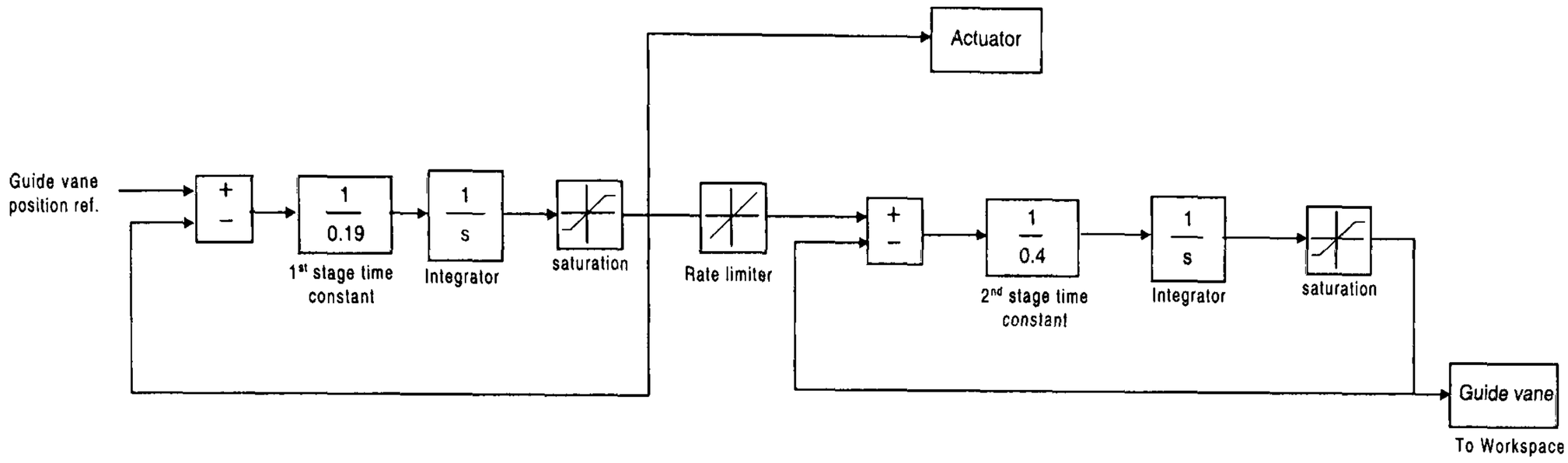

Figure 4-8: *Simulation model of the guide vane*

A further test was carried out to verify the guide vane model by applying a feed-forward signal to the servo loop. This signal was ramped for 7 seconds to fully open the guide vane then after 8 seconds; another signal was applied to close the guide vane. The results are shown in Figure 4-9(a) where it can be seen that the actuator and the guide vane start opening at the same time and the actuator is opening at a faster rate than the guide vane. The actuator is fully opened in 7 seconds while the guide vane response trails by 3 seconds and to compensate for this effect in the model a rate limiter is introduced between the actuator and the guide vane loop as shown in Figure 4-8.

A similar test was conducted on the model and the results of the simulation run are presented in Figure 4-9(b). The only discrepancy between the two responses occurs during closing down because the guide vane slows down before it is fully closed in order to limit the pressure in the system. This effect is not incorporated in the model of Figure 4-8, which is used to represent the guide vane dynamics in the thesis.

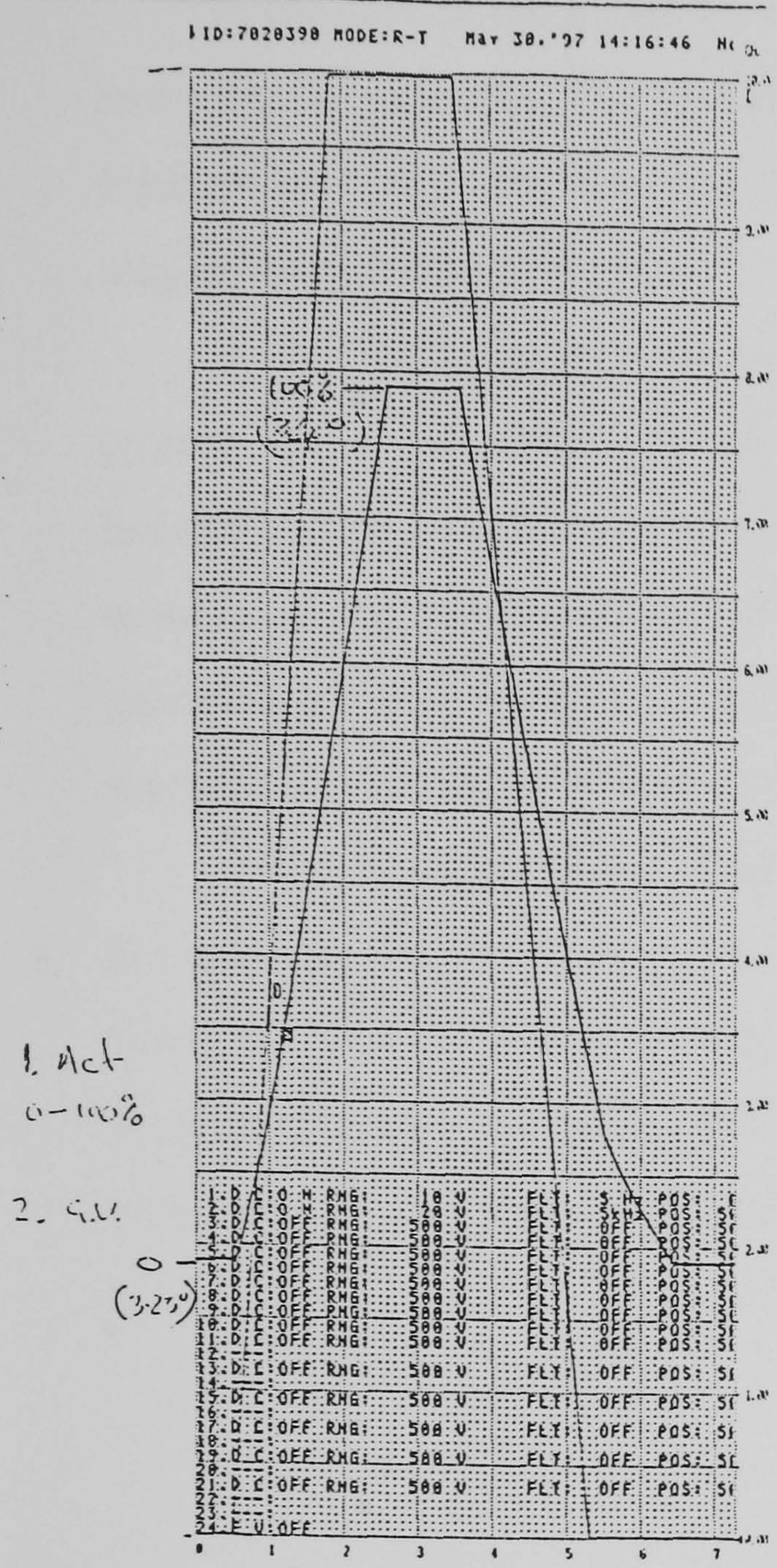

-a-

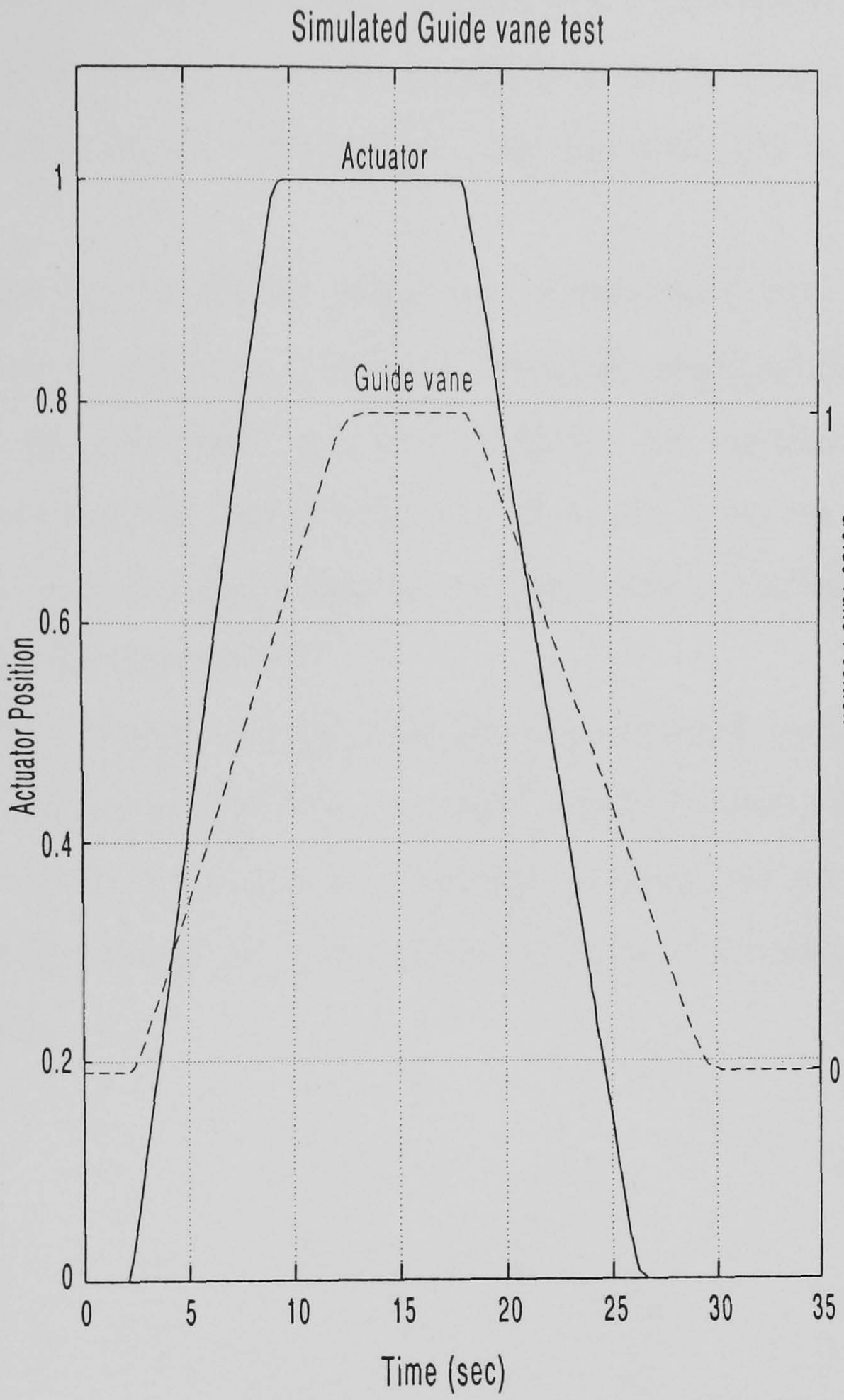

-b-

Figure 4-9: *Guide vane test*

4.4 Conclusions

The first part of the chapter concentrated on extracting the salient dynamic features (those relevant to the simulation) from the complex PLC programme. This was achieved by implying system identification techniques to establish accurate models of the governor and the guide vanes. The results demonstrate that it is essential to verify the system mathematical models because the uncertainty about exactly how the program functions and what the parameter values are can lead to errors.

In the case of the governor a frequency analysis method was chosen although it was more time consuming. The test result in identifying an averaging filter due to frequency measurement and the derivative action limiter filter which were not included in the original mathematical models.

A step response test was chosen to identify the guide vane dynamics. Firstly, the system has a low order and the step response results in an adequate approximation. Secondly, the frequency response analysis could not be considered for commercial reasons as the length of the test would have resulted in loss of revenue due to lost generation. Third, the power oscillation in the system due to the guide vane's continuous movement would have been unacceptable to the NGC.

The governor and the guide vane models derived using the experimental approach are used in the next chapter in conjunction with the hydraulic models developed in Chapter 2 and the power system models of Chapter 3 to assemble a generic nonlinear model of pumped storage hydro station. This model is later used in Chapter 7 for dynamic simulation and system stability studies.

Chapter 5

Model Integration and Verification

5.1 Introduction

This chapter presents a systematic integration of the models derived in previous chapters into a complete nonlinear model of the system. A decision was made with FHC to base the simulation activity around the MATLAB®/SIMULINK® tools which is easy to integrate with the dSPACE® tool to perform on-line or hardware-in-the-loop simulation in Chapter 8. The main goal of this work is to construct an off-line nonlinear model of Dinorwig to be used to enhance the station performance and to provide a comprehensive model for development of a new control system in future (see Chapter 9). In Section 5.2.1 a model of a unit supplied from a single penstock is developed. A review of linearised dynamic models generally used for predicting hydropower station response illustrates their shortcomings when applied to a fast-response station. This is followed by constructing a nonlinear model by adding the water hammer effect, the control system and the dynamics of the electrical power system. Section 5.2.2 extends the integration of the model by including the hydraulic coupling effects due to the common tunnel and the surge tank to complete model of Dinorwig connected to the power system. Section 5.3 presents the steps taken to verify the model behaviour which includes comparison with an independent model and real-plant responses.

5.2 Model Integration

5.2.1 Single penstock plant

Historically, models of hydropower stations have concentrated on the behaviour of low to medium head base load stations connected to an isolated load. They have tended to use relatively simple representations of the hydraulic and mechanical systems, such as shown in Figure 5-1. In this model [49] the turbine/penstock combination is represented by the classical transfer function of equation (2-22) relating changes in the mechanical power to changes in the guide vane opening which assumes an ideal turbine operated at rated flow and head and uses the water starting time (T_w) to represent the transient behaviour of the hydraulics.

The speed governor is modelled as a standard PID controller as described in Section 4.2 and the generator dynamics are represented by the "swing" equation, which relates the rotating machine inertia (T_m) to acceleration torque. The load is represented by the constant current model of equation (3-9) where the loading condition depends upon the value of the load damping D.

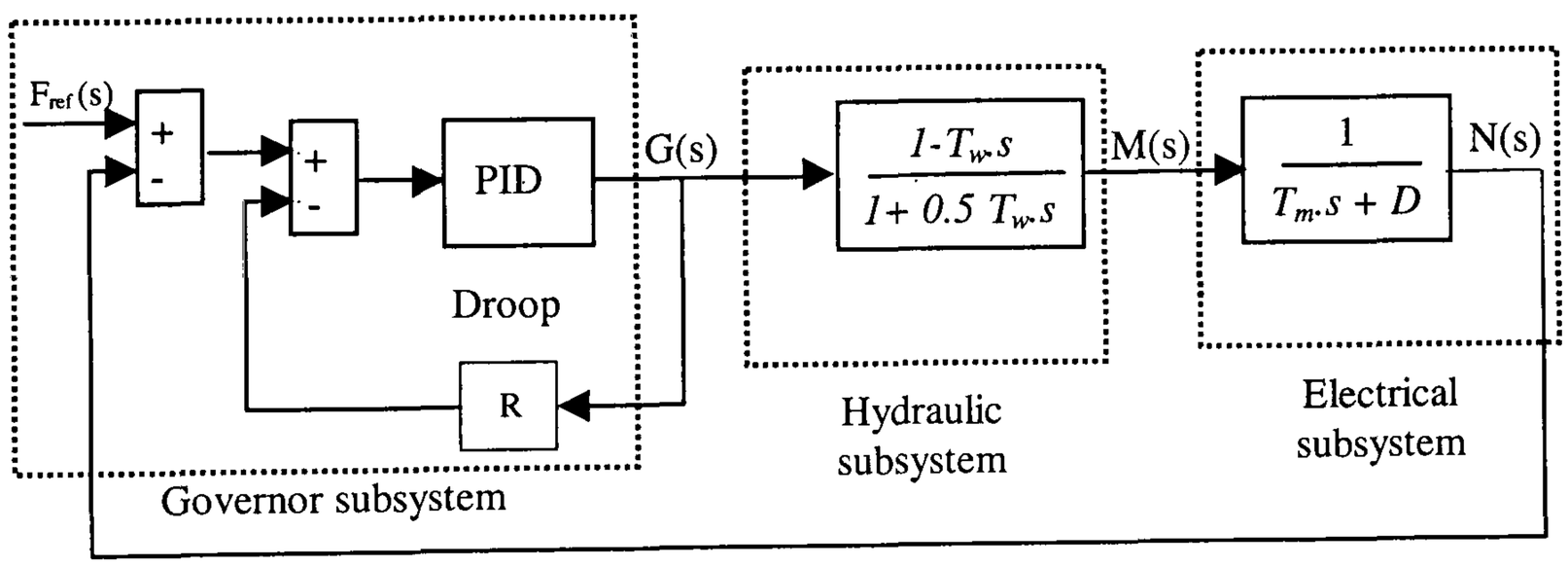

Figure 5-1: *Block diagram of dynamics suitable for a base load hydropower station*

5.2.1.1 Limitation of the linearised model

Although this model has been used for many studies, the inherent approximations hold only for low-medium head conditions and it is not suitable for many fast response stations, which tend to operate with a high head. A simple illustration of the limitations of this type of model is shown in Figure 5-2, where the unit was subject to an initial 30%

(0.3 p.u.) increase in load demand, followed a short time later by a further 50% (0.5 p.u.) increase.

The initial part of the curves in Figure 5-2 show that the station acts to pick up the 30% load to restore the system frequency back to its nominal value. However, when the response to the subsequent 50% increase in demand load is considered, the inaccuracy of the model becomes clear as the guide vane opening exceeds 1.0 p.u, (which is physically impossible) before settling down to a final load figure of 80%.

The water starting time for the penstock T_w is calculated using equation (2-15), which, in the linear representation, is calculated from the initial value of flow. Thus for simulation studies, the linearised penstock model requires different values for T_w to reflect changes in water flow rate [50]. The linear model is valid only as long as the unit's load does not deviate greatly from the initial load. For the nonlinear model, the value of T_w is calculated from the value of the flow at rated conditions. The change in the effective time constant is implicit within the nonlinear expressions and the model is valid for all operation conditions.

The need for a model that accurately reflects the true system conditions is clear. This implies the inclusion of factors such as the influence of the power system, limits on guide vane opening and the water hammer phenomenon resulting from the guide vane movement, especially where the penstock may be considered elastic.

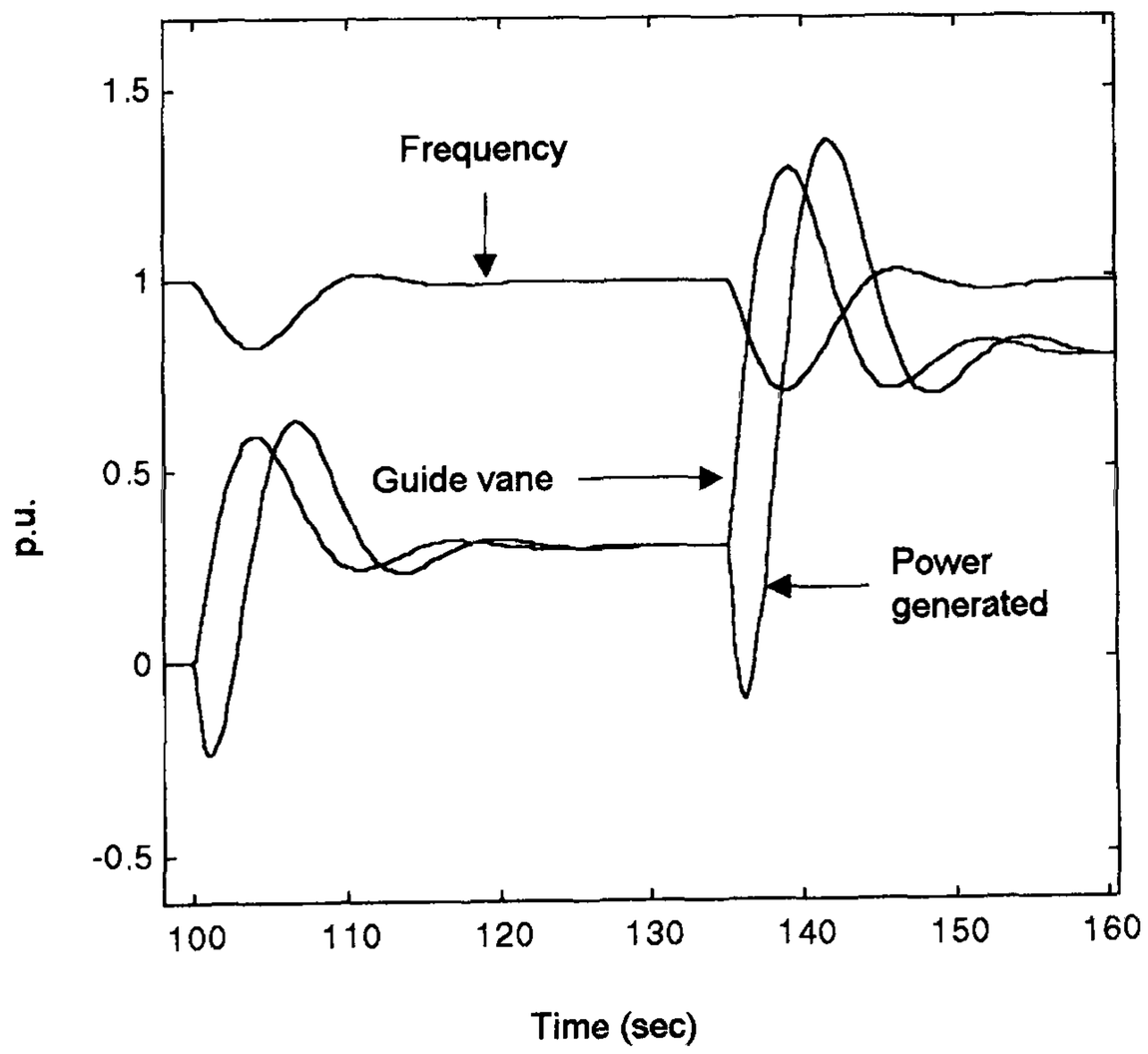

Figure 5-2: *Unit response of a hydropower station to step changes in demand load*

5.2.1.2 Enhanced nonlinear model

The approach to modelling a system requires an ability to break the problem down into smaller elements that can be addressed individually. Here, this is apparent in the way the hydraulic, electrical and control systems were initially modelled as separate subsystems in chapters 2, 3 and 4 respectively. However, having modelled each of these individually, they must then be integrated together to form a model of the whole system. The system integration was implemented by collecting the low-level Simulink blocks into three different subsystems as follows:

- Hydraulic subsystem: consisting of the water column, the surge tank (if utilised) and the guide vane dynamics.
- Electrical subsystem: consisting of the power system, the generator, the power transferred between the two and the load perturbation.
- Control subsystem: consisting of the speed governor.

Stations operating with high head and long penstocks experience pressure changes in the penstock due to the water hammer phenomenon. In Chapter 2, these effects were considered in detail and a conclusion was made to include them into the turbine-penstock dynamics. As a result, a nonlinear hydraulic system was assembled as described in Section 2.3.3.2, where the turbine power is function of head across the turbine and the guide vane opening. In the model, the travelling wave effects are represented by the equation,

$$\frac{H(s)}{Q(s)} = -\frac{T_w}{T_e}\tanh\left(T_e s + F\right) \tag{5-1}$$

The guide vane dynamics were integrated using the model shown in Figure 4-8, which is developed from an experimental data. In the meantime, an improved speed governor representation based on experimental data illustrated in Figure 4-6 is used where the feed-forward signal is added into the control loop.

The primary purpose of development of the plant model is to analyses it response to load/frequency control, hence the influence of the power system size and the effect other plants operating in frequency control mode should be included in the model. This is

achieved by using the representation of equation (3-24), which relates the system frequency change with stiffness. Generally, in the analysis of load-frequency controls, the intermachine oscillations is not considered as the interest is based on the collective performance of all generators in the system. However, if we are interested in a specific plant performance then the electrical coupling between the machine and a power system could be included.

At steady state the unit and the power system will be operating at base frequency, hence if load appears it will affect the frequency of the system. It is shown at Section 3.3.1 that the power exchange between the unit and the power system $P_{Gi}(t)$ is equal to instantaneous shaft angle difference between the machine and the power system. Once all these enhancements are applied, a generic model of single tunnel hydropower plant is assembled as shown in Figure 5-3. The parameter B_c represents the MW base conversion between the unit and the power system.

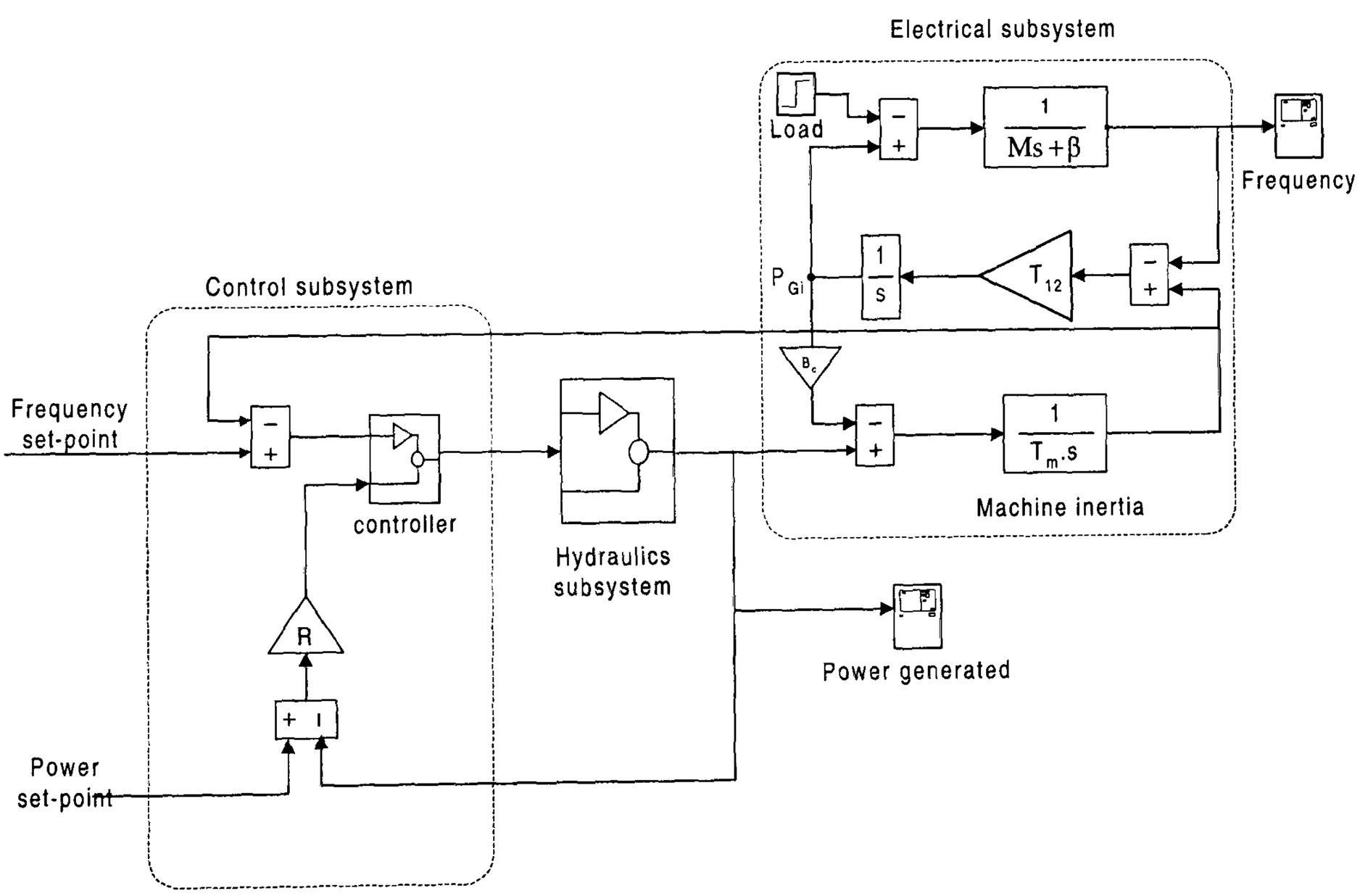

Figure 5-3: *Single tunnel hydropower plant connected to the power system*

The function tanh(T_es) in equation (5-1) can be simulated using the relationship,

$$\tanh(T_e.s) = \frac{1 - e^{-2T_e s}}{1 + e^{-2T_e s}} \tag{5-2}$$

The term $e^{-2T_e s}$ represents a time delay which can be implemented in SIMULINK® by means of a transport delay block. However, using this representation causes algebraic loops constraints which stop the simulation. Therefore, another solution was required and a Padé approximation to the time delay $e^{-2T_e s}$ was considered. The results of the approximation were compared with the frequency response of tanh(T_es) as shown in Figure 5-4. It can be seen that increasing the order of the approximation improves the match to the frequency but unfortunately it has the disadvantage of causing time-domain oscillations. This is demonstrated in Figure 5-5 where the step response of tanh(T_es) is compared with that of the sixth order Padé approximation where large high frequency oscillations are evident. This causes the simulation to become unstable. An alternative is to use a second order approximation but its frequency response exhibits a shift of 0.2 rad/s in the resonant peak and it is accurate only for frequencies below 1.3 rad/s. Consequently, it was decided not to use this method of approximation and a third approach was considered.

A low order polynomial approximation was found by converting equation (5-2) to its equivalent z-transform, which was then used to obtain a continuous representation of the system. Using this method, a second order approximation was obtained which gives a better response than the Padé approximation as demonstrated by its frequency and step responses of Figure 5-4 and Figure 5-5 respectively. The function of equation (5-2) is replaced in the simulation by the low order polynomial approximation and gives a satisfactory representation of the travelling wave effect while avoiding the introduction of high frequency oscillatory artefacts and consequent problems with poor numerical stability associated with a high order approximation. These are:

$$\tanh(T_e.s) = \frac{3.59s}{s^2 + 5.21} \qquad \text{for the main tunnel } (T_e = 0.642)$$

$$\tanh(T_e.s) = \frac{16.67s}{s^2 + 112.6} \qquad \text{for the j}^{th} \text{ penstock } (T_e = 0.146)$$

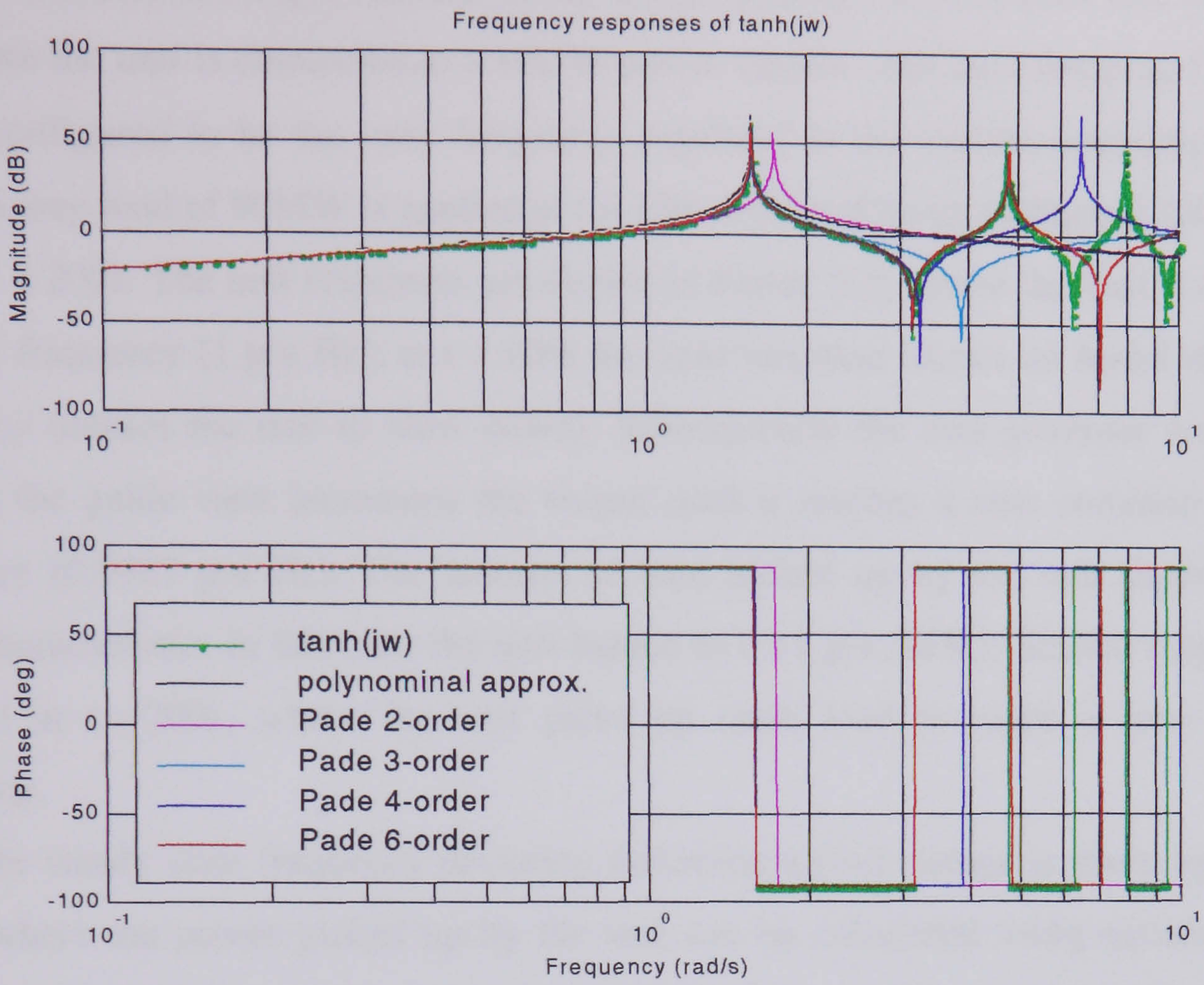

Figure 5-4: *Frequency responses of tanh ($T_e s$)*

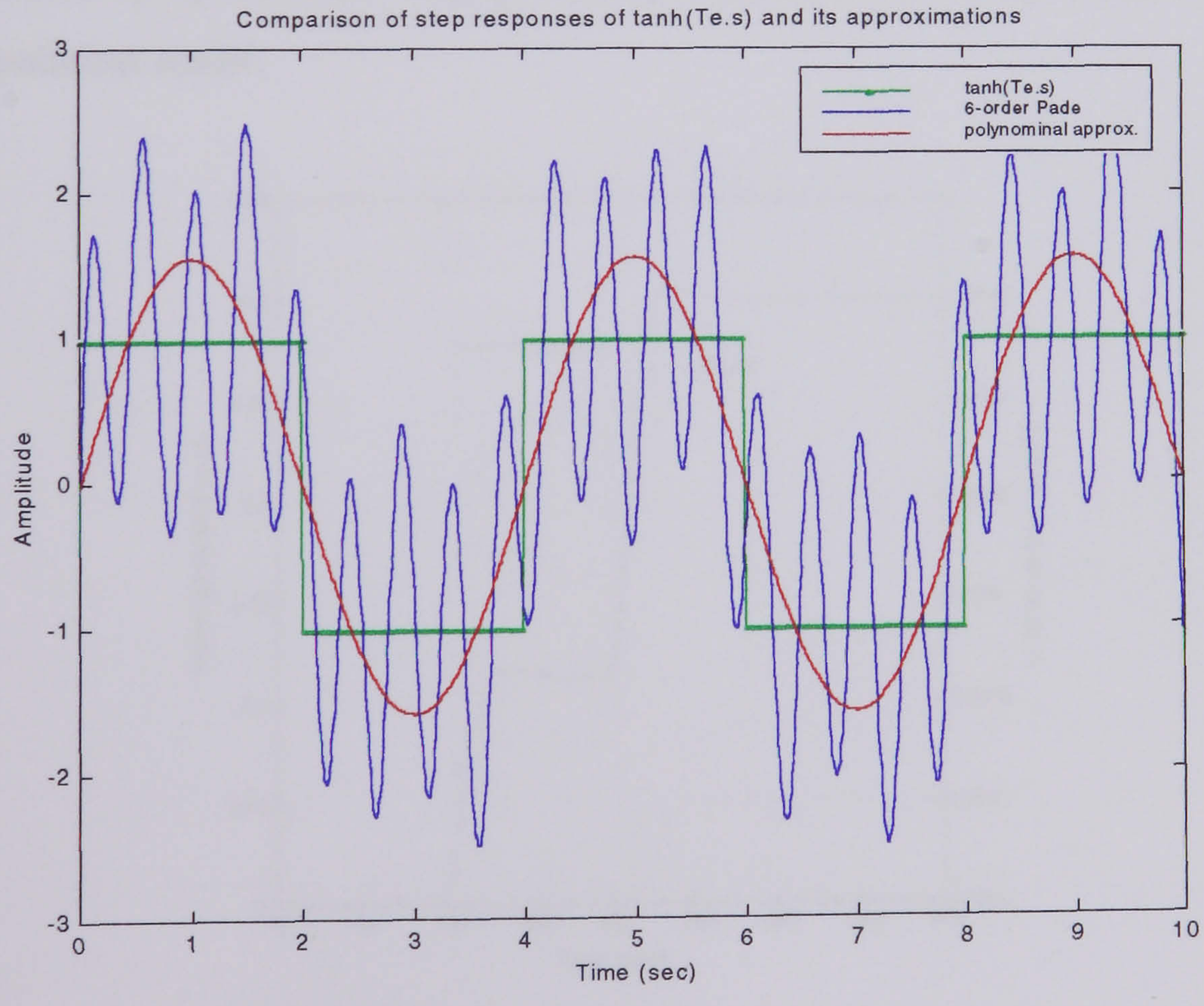

Figure 5-5: *Step responses of tanh ($T_e s$)*

To illustrate the improvements in the model structure a simulation test was carried out, where the unit is connected to a 40GW power system with load damping D = 1. The unit is configured to be the only frequency regulator in the system operating with 1% droop. A step load of 90MW is applied at t = 100s followed by an additional 120MW step load at t = 200s. The unit responses are shown in Figure 5-6, where the unit is initially at nominal frequency (1 p.u Hz), at t = 100s the load insertion causes an initial drop in the frequency (causes the unit to slow down). Subsequently the unit governor responds by opening the guide vane increasing the output until it reaches a new common operating frequency (0.9987 p.u Hz). The amount of load picked up by the unit depends on its droop characteristic; in this case the unit loaded to 0.11 p.u (MW). Similar responses are obtained at t = 200s, where the unit picks up extra load to reach a new operating frequency.

The steady state frequency deviation following a load change is given by equation (3-22) where the power picked up by the unit can be calculated using equation (3-23). Applying the equations on the system scenario result in steady state frequency deviation of 0.0013 p.u (Hz) after the first load and 0.0017 p.u (Hz) after the second load, while the total load picked up by the unit is equal to 0.3 p.u (MW) of its rating, these values agrees with the simulation result.

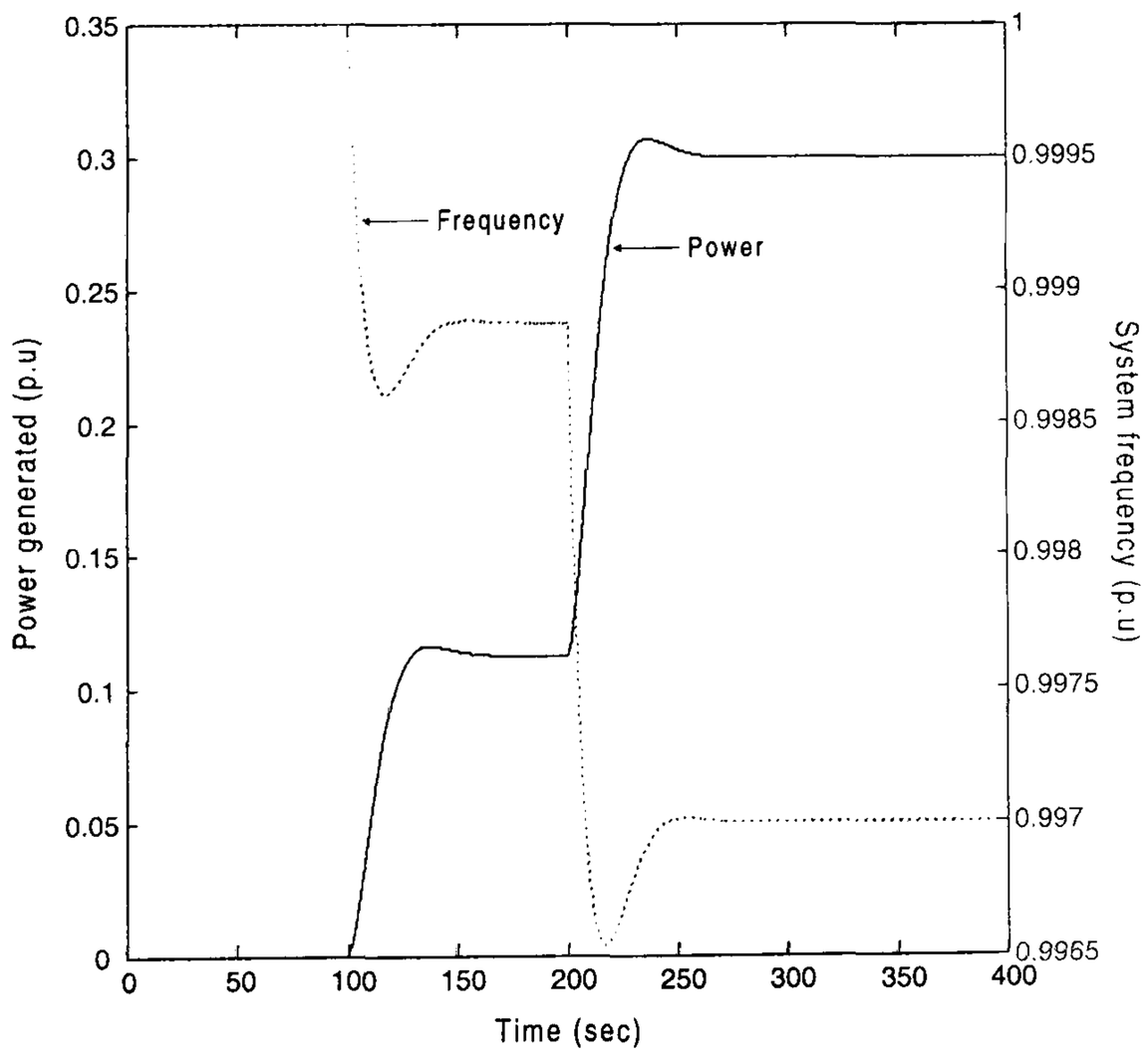

Figure 5-6: *Unit response to step changes in system demand load*

5.2.2 Multiple penstocks plant

The preceding discussion represents the initial stage of model development. However, as explained in Chapter 2, the Dinorwig station has a single tunnel with surge chamber, which splits into six separate penstocks supplying individual turbines. The approach used to integrate the system is similar to the one used for the single penstock model, where the model was broken down into small elements (subsystems). However, the system complexity prevents the hydraulic system from being represented as a single subsystem and this applies to the electrical system too. Therefore, it was decided to create a subsystem for each of the following elements:

- Unit individual penstock;
- Low pressure tunnel and the surge tank;
- High pressure tunnel;
- Unit controller;
- Electrical coupling between the unit and the power system;
- The power system.

Combining all subsystems together results in a model of the Dinorwig plant as shown in Figure 5-7. In the Simulink model, the individual penstocks and the high pressure tunnel are represented by the elastic water column developed in Section 2.3.4.2 where the effects of the hydraulic coupling and water hammer are included. Meanwhile the low pressure tunnel and the surge tank subsystem is based on the model of Figure 2-15 which describes the low pressure tunnel as an inelastic water column, because the surge tank alleviates the travelling wave effects. The unit controller subsystem considered here is also based on the Dinorwig governor of Figure 4-6, where two feedback loops (power and frequency) are included. This subsystem also includes the guide vane dynamics shown in Figure 4-8. Consequently, the subsystem output signal is used to adjust the guide vane position of the penstock subsystem.

As before the electrical coupling subsystem is implemented by comparing the power system frequency with the unit frequency, which is then multiplied by the integral of the synchronising coefficient to yield the power exchange between the unit and the

power system. Again the power system is represented by equation (3-24), which shows the effect of system loading on frequency.

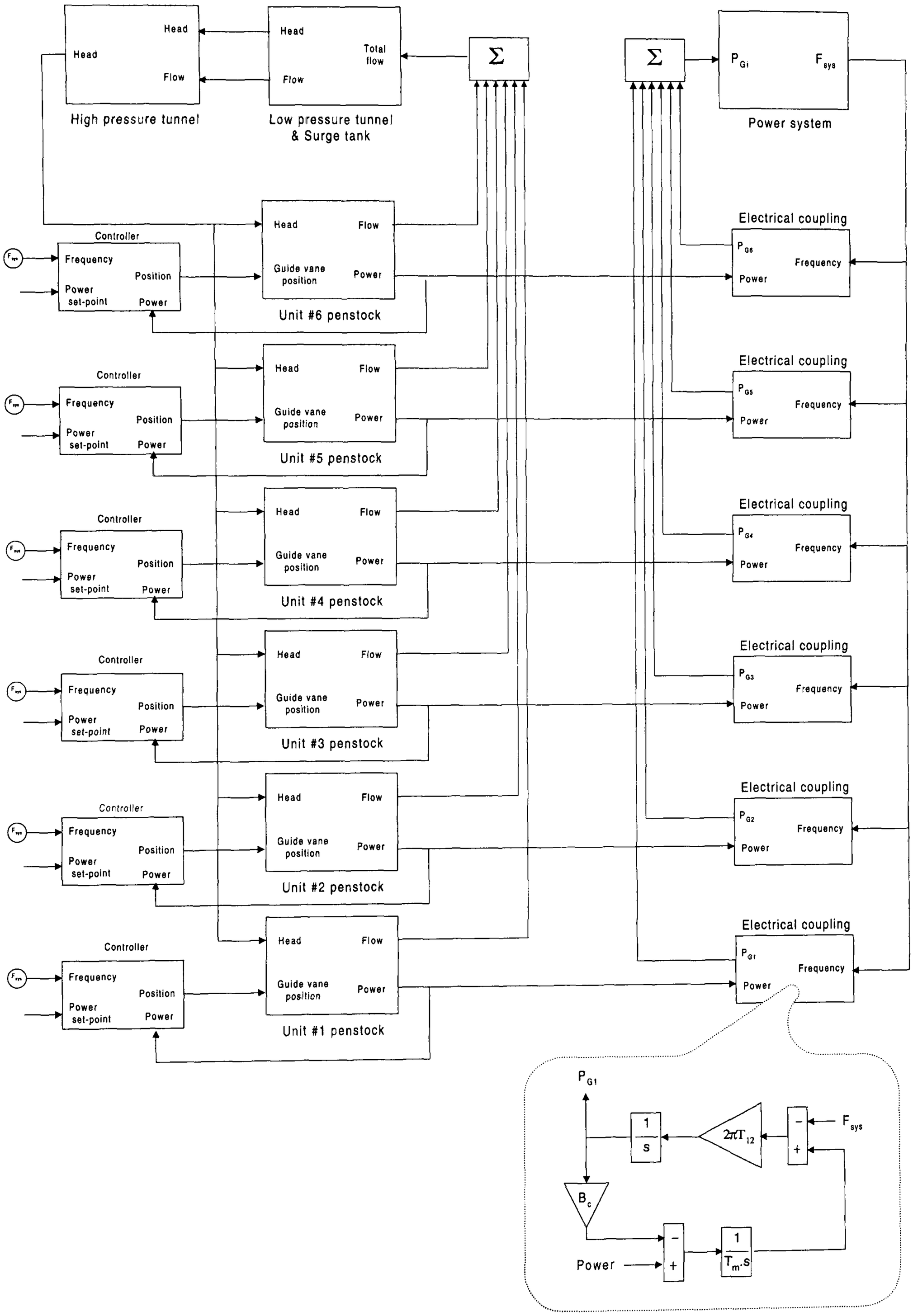

Figure 5-7: *The overall nonlinear multiple penstock off-line-model structure*

5.3 Model Verification

Before using the simulation to investigate plant behaviour and hence to predict the effect of control parameter changes, it is necessary to confirm that its response agrees with the real plant. However, for financial and regulatory reasons there are tight constraints on the field tests which can be performed on the working plant. Thus, it was not feasible to apply system identification techniques such as those described in Section 4.3 on the plant and alternative methods are considered based on simulation analysis to verify the model.

5.3.1 Comparison with linear response

Initially, the response of the simulation was compared with that of the linear model to check that its qualitative behaviour and time scale were correct. For comparison purposes the governor representation was deactivated in both models, both no-load flow and speed deviations were set to zero in the travelling wave model. Figure 5-8 shows the simulation results when the models are subject to a large 4 p.u. step in guide vane position. The power increase predicted by both models has a similar form and time constant (note that non-minimum phase behaviour is exhibited). The non-linear model, however, predicts an output power oscillation as expected due to the travelling wave effects in the water column, which are entirely absent in the linearised model.

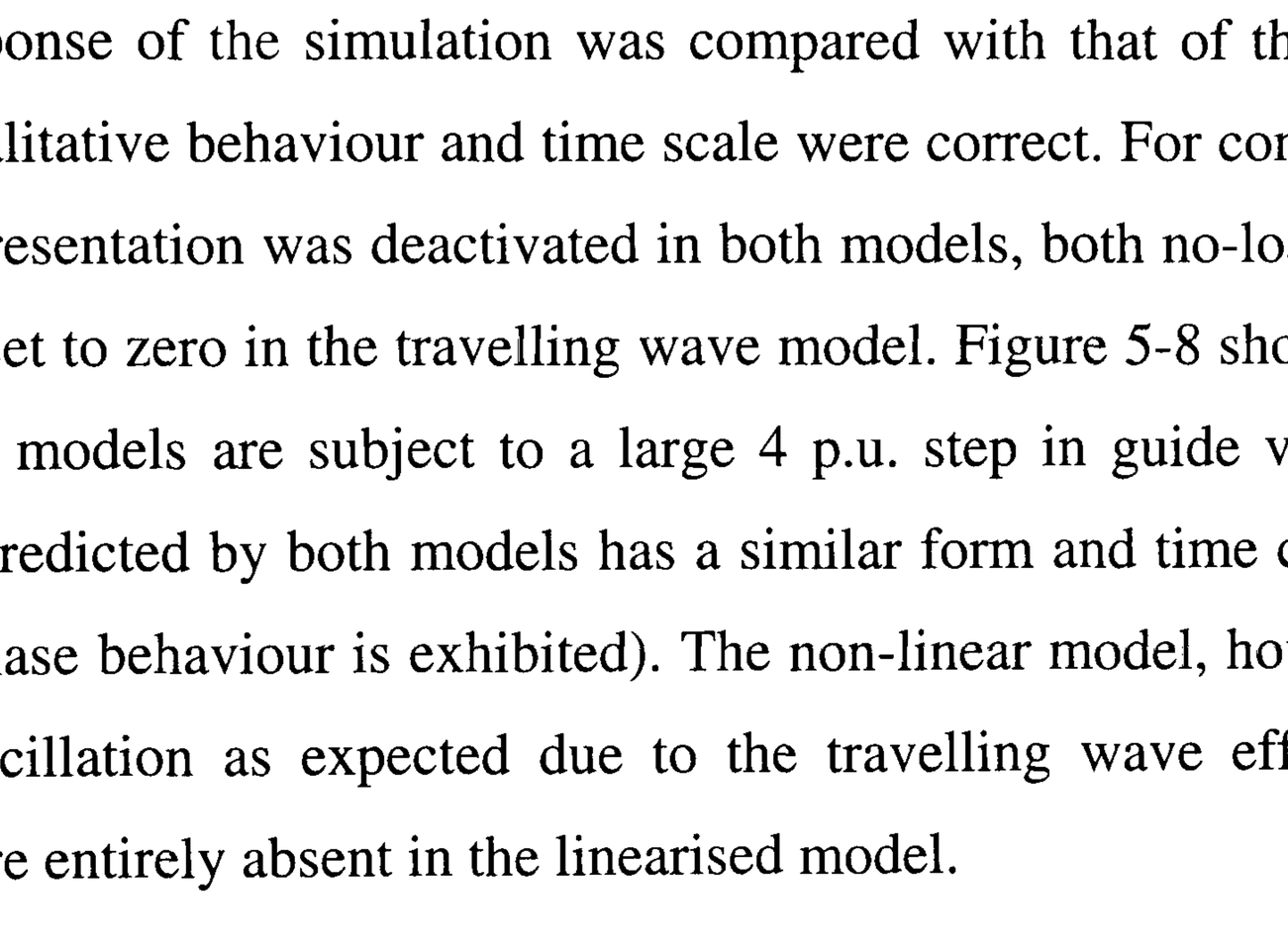

Figure 5-8: *Comparison between linear and non-linear model responses*

5.3.2 Simulation of hydraulic coupling between units

The effect of hydraulic coupling in the supply tunnel is confirmed by simulating a sequence of four units brought on-line in turn, with their governors blocked. The turbines head (pressure) variations are shown in Figure 5-9, where 20s ramp openings are used, as would be the case in practice. As the guide vane of the unit coming on-line is opened, its inlet pressure is seen to decrease as the flow increases. With the guide vanes on the other units held stationary, the flow to the remaining units is reduced because the total flow in the tunnel cannot change immediately; the consequent drop in pressure at those units is clear in Figure 5-9. Note that the pressure drop for the units coming online will be greater than for the remaining units and the hydraulic stiffness[#] is increased because of greater flow in the common tunnel when there are more units online. This test confirms that the simulation exhibits the expected nonlinear and multivariable behaviour. Although this does not constitute a systematic verification of the model, it does provide good evidence for its authenticity [51].

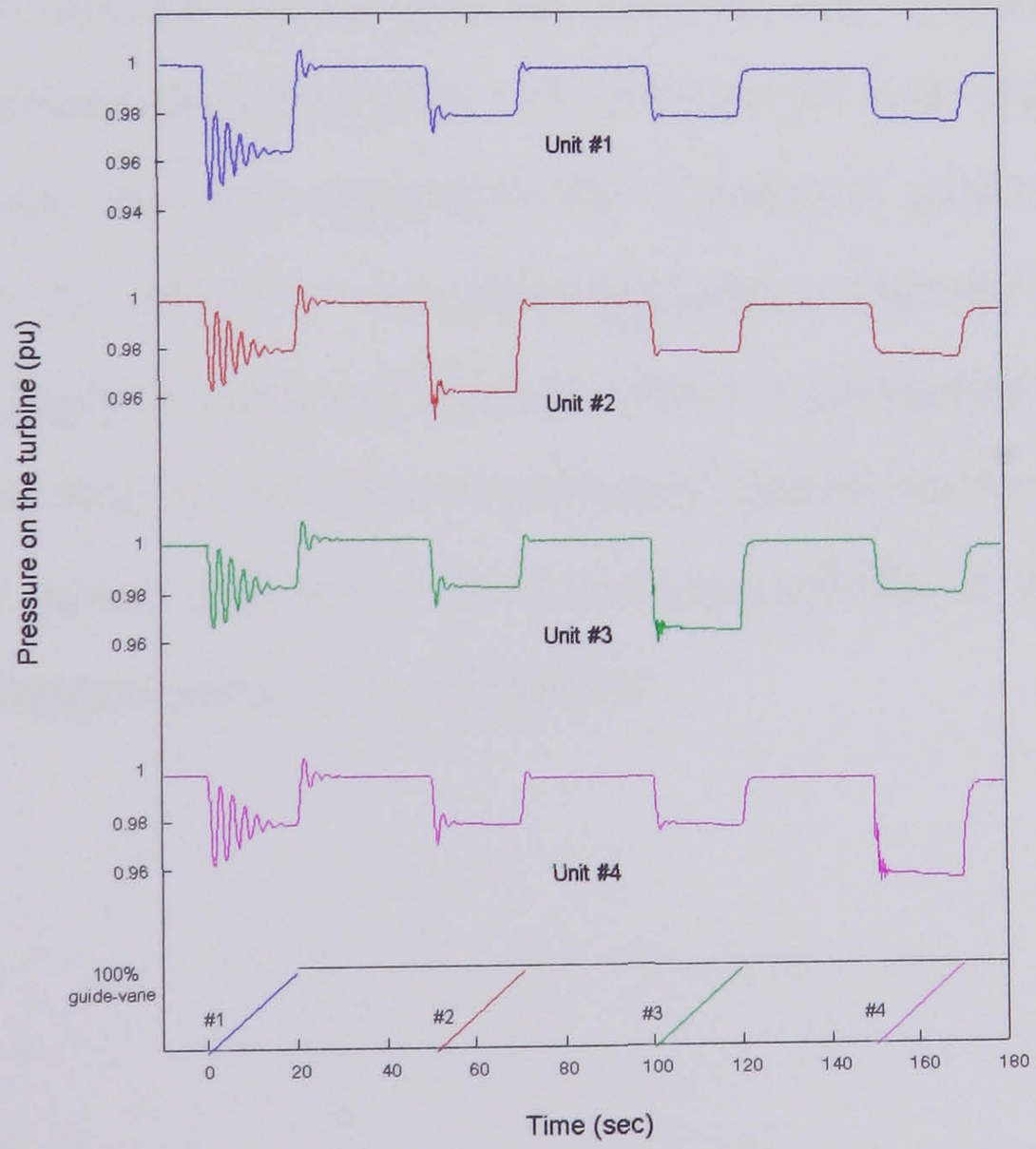

Figure 5-9: *Simulation result showing the hydraulic coupling effect*

[#]It is common nomenclature for power engineers to use the term "stiffness" although it is a viscous damping term.

5.3.3 Comparison with an independent model

The third element of model verification is comparison with responses predicted by an independent computer model based on an entirely different method of solution and separately developed code. The computer program called PTRAN was used to investigate the hydraulic system transient responses [52]. The program is based on the method of characteristics, which converts the quasi-linear, partial differential equations of motion and continuity, describing the unsteady flow of a fluid in any internal flow system, into ordinary differential equations relating pressure and flow at 89 nodes in the Dinorwig system.

An open loop response was calculated, for several well-defined conditions within the plant's working envelope, to emphasize the hydraulic effects between two units. The passive unit is generating 288MW at full head under steady state conditions, while the active unit is initially loaded to 100MW. Figure 5-10 presents the transient responses obtained using the PTRAN program. Once the active unit loading increases to 150MW, due to its guide vane opening in 2.626s, the passive unit generation initially falls by 10MW because of pressure drop and after ~ 4 seconds the unit returns to its steady state condition. The same scenario was applied to the simulation model and again the results are shown in Figure 5-10. There is very good agreement between the two responses for both the unit being brought on-line and the unit which is perturbed as a consequence. The major discrepancies are that the distributed parameter model predicts a rather longer delay in the response of the active unit and a more pronounced dip in the power output of the passive unit than the lumped parameter simulation.

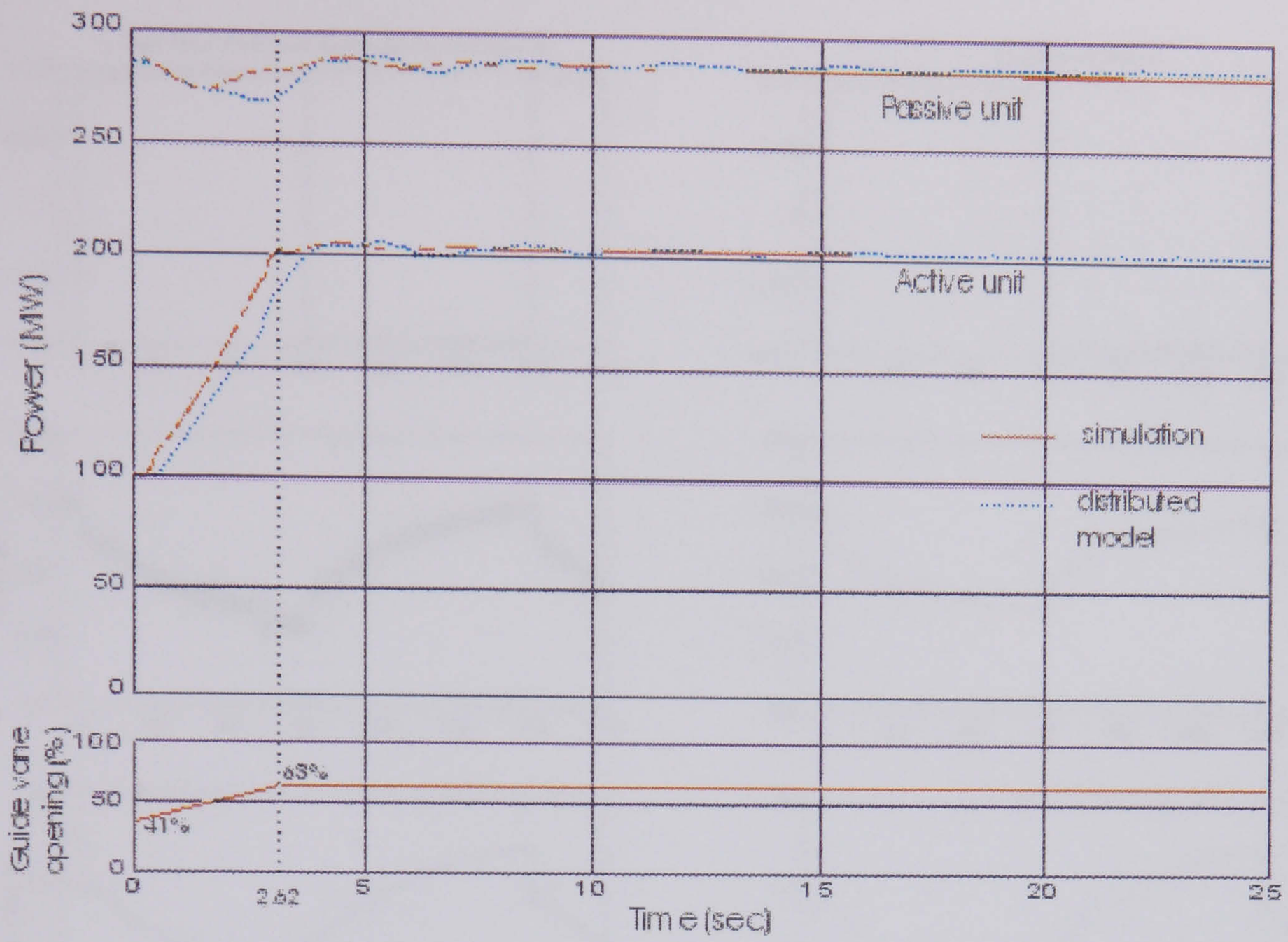

Figure 5-10: *Comparison of simulation results with an independent distributed parameter model*

5.3.4 Comparison with measured response

The final verification measure was to compare the simulation with the results of a test on the plant, which was possible because it is occasionally necessary for commercial purposes. This is a dynamic test usually carried out by NGC on Dinorwig plant to ensure compliance with the Grid Code and to establish the plant frequency response capability for commercial payment purposes. The tests involve injection of a simulated frequency error signal into the governor. In addition to the step as shown in the Figure 5-11, ramp injections are also carried out together with dead-band tests to check the robustness of the unit control system. Since the response characteristic of a unit varies depending on its loading level, tests are repeated at various critical loading points across the whole loading range.

The results shown (Test No.4) represent Unit #2 loaded with 220MW and operating at specific governor setting of $K_p = 20$, $K_i = 3$, $K_d = 4$ and droop of 1%, responding to an injection of $\pm$ 0.035Hz step error signal cycled every 60 second. The unit responds to the positive signal representing loss of load in the power system by shedding load of 30MW.

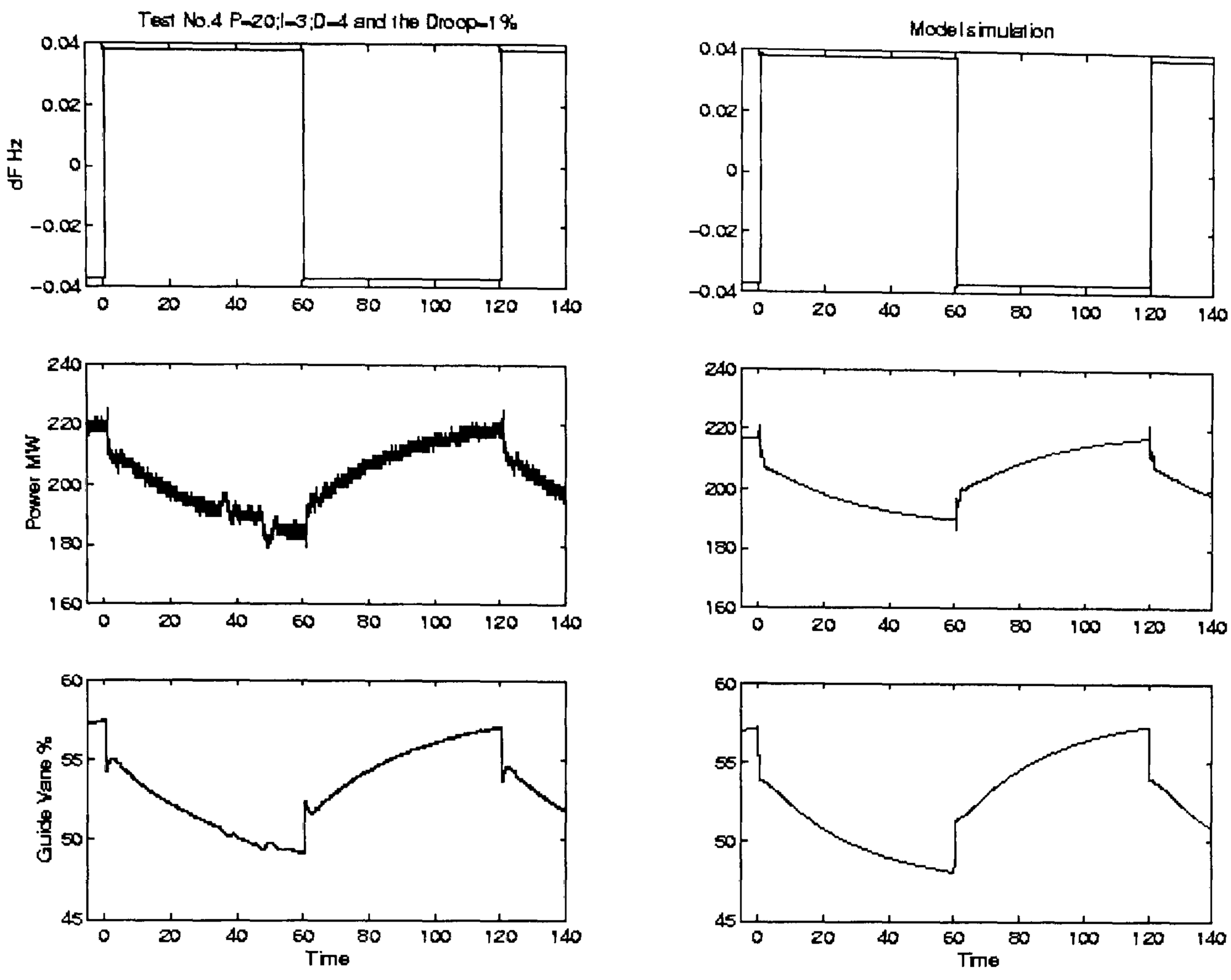

Figure 5-11: *Frequency response test*

The automatic reduction in the power output is termed High Frequency Response [53]. It is important that the generation output is reduced increasingly within 10s, to minimise the initial frequency peak. Meanwhile during the negative frequency cycle, which represents loss of generation in the power system the initial short-term automatic power output increase is termed Primary Response. It is important that the primary response from the synchronised generation is increased with time through automatic governor action in the period of 0-10 seconds after the incident and sustained for a further 20s, this is critical to minimise the initial frequency dip. The automatic positive power response in the subsequent frequency stabilisation phase beyond 30s after the incident is termed Secondary Response. The unit primary response increases the power by 18MW and the secondary response is stabilised with extra generation of 30MW.

An identical test setting was applied to the simulation and the results are shown in Figure 5-11. There is very good agreement for both the generated power and the guide vane opening although close inspection shows that the simulation output is rather better

damped than the measured response during the period immediately after the step is applied. The slight perturbation to be seen in the measured response in the interval 35-50 seconds is due to a change in the operational conditions of the plant (another unit being brought on-line at this time), this was not included in the simulation. Further tests using different sizes and types of frequency error signals are presented in Appendix-II. It is concluded that, whilst a systematic comparison with measured system responses over the complete working envelope would have been preferable, the measures taken provide sound evidence for the model's authenticity and the verification procedure has established a good degree of confidence in its use for further investigation.

5.4 Conclusions

This chapter has developed the integrated model of a pump storage station and applied it to the Dinorwig power station. The model includes representations of the hydrodynamics, control system and electrical power system. The real benefit of the simulation is that it gives better insight and improved understanding of the plant dynamics whose complex features cannot be fully understood in terms of linear models. Different verification measures such as comparison with real plant responses and an independent model were applied to establish a good degree of confidence in the veracity of the model. The model in this form is used to produce the results in Chapter 7.

While the model now includes the majority of the factors affecting the plant's dynamics, there are other secondary factors which could be incorporated at the expense of additional complexity. For instance, studies of interactions between turbine hydraulics including draft tube pulsation. In such cases, the model must correspond as closely as possible to the actual turbine and controls that exist at the plant.

Chapter 6

Governor Tuning

6.1 Introduction

Historically, the design of control systems for hydropower schemes has been done by means of linearised system transfer functions. The preceding chapters have shown that the plant is, in fact, highly nonlinear, time variant and multivariable so any law designed on the basis of a linearised representation is a compromise. Consideration of advanced control techniques which take these factors into account is beyond the scope of this thesis although it is intended that it should be addressed in future work (see Chapter 9).

Nevertheless, as this chapter will show, there remains scope for optimising the governor performance even within the limited structure of a PID controller. Here, the governor tuning (i.e. adjustment of the PID gains) is examined in terms of plant stability and dynamic performance. The primary objective of this chapter is to improve accuracy and speed of response of Dinorwig to short-term power system load perturbations. Optimisation of plant performance will enhance its financial combativeness to benefit FHC.

Different methods of governor tuning are introduced which not only indicate stability but also provide information on the adjustments needed to meet a given performance specification. Initially, the stability of a hydro unit configured to supply an isolated load is analysed using the Routh-Hurwitz criterion. The effect of the derivative

gain is analysed using the root locus method and it is shown that the derivative gain limits can be extended further than recommended by Hagihara et al [49].

The work proceeds to investigate the stability of Dinorwig when operating as a frequency regulator and the results show that the power system size influences the plant response. However, when operating with a dead-band (frequency insensitive mode), the response is mainly influenced by the droop setting. The stability limits were calculated using the gain and phase margins of the system.

6.2 Stability of the Unit in Isolated Operation

Generally, generating units are connected to power networks and the dynamics of the network must be considered during frequency (speed) control design. In the case of a small isolated network the unit must act to maintain the system frequency. Most units at some time may be required to supply isolated loads either deliberately or by accident. For instance a black-start operation may be required or the power system may split into smaller networks. Even when isolated, the dynamic characteristics of the load will vary and must be considered in control design [54]. In the derivation of the transfer function of the system for stability studies the following assumption are made:

- The hydro system operates with small load perturbations.
- The water is incompressible and no elastic effect in the penstock is considered. Moreover, the water time constant is held constant at full rated load value, not modified for part gate operation.
- The hydraulic coupling is ignored.
- The turbine is operating at a point on the power gate curve where a small change in gate position gives proportionate change in steady state torque. This assumes a linear relation between the guide vane opening and the power generated.
- The guide vane dynamics are assumed sufficiently fast to be omitted.

6.2.1 System representation

The block diagram shown in Figure 6-1 represents the plant used for steady state analysis. Using the solid mass approximation for short/medium head penstock, the linearised

representation of the hydraulic system of equation (2-22) is used in the analysis to represent the penstock-turbine dynamics. The generator is represented by its mechanical starting time of equation (3-7). Since we are interested in the frequency variation with power rather than voltage, the load dynamics are modelled by the constant power (MVA) model represented by equation (6-1) as described in Section 3.2.2. Depending on the load characteristic, the relationship between power and frequency can be represented by

$$P = P_0(1 + D_{pf}\Delta f) \tag{6-1}$$

Linearising around the operating point to represent a small perturbation and neglecting the 2nd order terms yields:

$$\Delta P = \Delta P_0 + P_0 D_{pf}\Delta f \tag{6-2}$$

where the load damping $D = P_0 D_{pf}$, is proportional to the connected load and the load's frequency sensitivity.

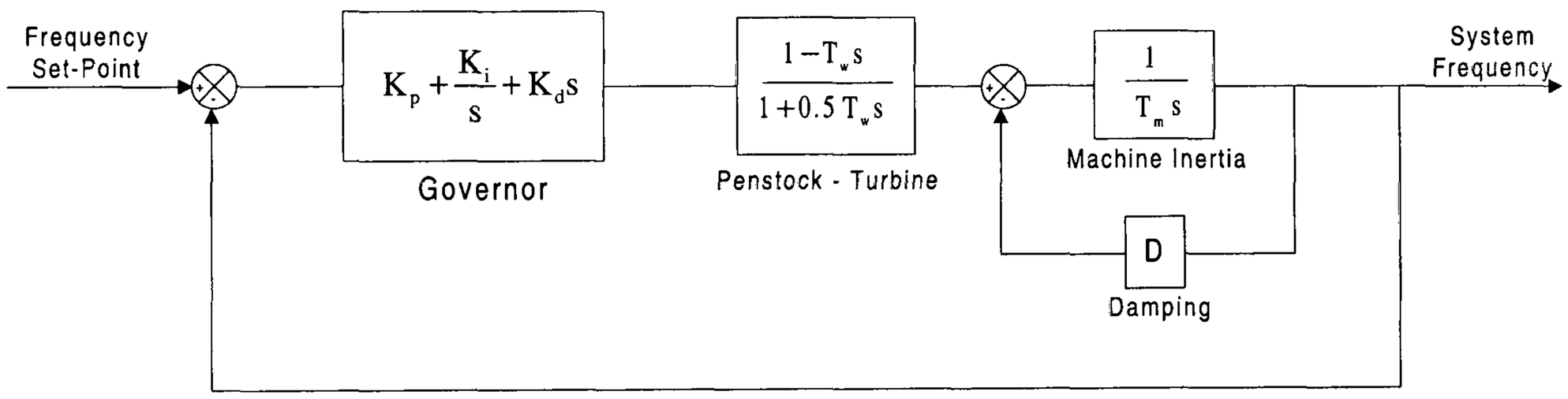

Figure 6-1: *Block diagram of a hydraulic turbine generating system.*

The system transfer function can then be written as:

$$G(s) = \frac{(K_p s + K_i + K_d s^2)(1 - T_w s)}{s(1 + 0.5T_w s)(T_m s + D)} \tag{6-3}$$

6.2.2 Routh-Hurwitz stability criterion

The transient response of a linear closed-loop system may be determined from the position of the closed-loop poles on the complex plane; the system becomes unstable as soon as one of the closed-loop poles is located in the right-hand half of the complex plane [21]. The closed-loop poles may be found by solving the characteristic equation (6-4).

$$1 + GH(s) = 0 \tag{6-4}$$

Routh's method determines the number of roots located in the right-hand half of the complex plane using only the coefficients of the characteristic equation without solving the equation for the roots themselves. The characteristic equation can be written in polynomial form as:

$$A(s) = A_0 s^n + A_1 s^{n-1} + A_2 s^{n-2} + A_3 s^{n-3} + - - - - - - - + A_{n-1} s + A_n \tag{6-5}$$

A necessary condition for stability of the system is that all the roots in equation (6-5) have a negative real part, which in turn requires that all $\{A_i\}$ coefficients are positive. If any of the coefficients are negative or zero it may be shown that there is either a closed-loop pole in the right hand half of the s-plane or there is one or more closed-loop poles on the imaginary axis. This is not, however, a sufficient test for stability.

The well-known Routh-Hurwitz test [48] requires the computation of a triangular array that is a function of $\{A_i\}$, a necessary and sufficient condition for stability is that all the elements in the first column of this array are positive. This condition can be used to obtain an analytical expression for the system's stability boundaries in terms of the plant and controller parameter values. Combining the transfer function of the governor with that of the controlled system shown in Figure 6-1, the characteristic equation can be written as:

$$\left[K_p + K_d s + \frac{K_i}{s}\right]\left[\frac{1 - T_w s}{1 + 0.5 T_w s}\right]\left[\frac{1}{T_m s + D}\right] + 1 = 0 \tag{6-6}$$

Appendix-III shows the solution of equation (6-6) to derive the system characteristic equation in the form:

$$A(s) = s^3(0.5 - X_3) + s^2(X_3 - X_1 + 1 + 0.5X_4) + s(X_1 - X_1X_2 + X_4) + X_1X_2 = 0 \tag{6-7}$$

Where $X_1 = \frac{K_p T_w}{T_m}$; $X_2 = \frac{K_i T_w}{K_p}$; $X_3 = \frac{K_d}{T_m}$; and the system regulation $X_4 = D\frac{T_w}{T_m}$

6.2.2.1 Routh's test

To determine the Routh array, the coefficients of the characteristic equation (6-7) are arranged in two rows, beginning with the first and the second coefficients and followed by the even-numbered and odd numbered coefficients. Therefore, the array for the system can be constructed as:

s^3:	A_0	A_2
s^2:	A_1	A_3
s:	$B_1 = -\dfrac{\det\begin{bmatrix} A_0 & A_2 \\ A_1 & A_3 \end{bmatrix}}{A_1}$	0
s^0:	$C_1 = -\dfrac{\det\begin{bmatrix} A_1 & A_3 \\ B_1 & 0 \end{bmatrix}}{B_1}$	

All the elements of the array A_0, A_1, A_2, A_3, B_1, C_1 must be positive to ensure a stable response so the following criterion must be fulfilled.

- A_0 will be positive if $0.5-X_3>0$ which means that $0.5>X_3$ therefore the derivative gain must be set to $K_d< 0.5T_m$.
- A_1 will be positive if: $1-X_1+X_3+0.5X_4>0$, which results in $X_1<1+X_3+0.5X_4$.
- A_2 will be positive if: $X_1-X_1X_2+X_4>0$, which results in $1+\dfrac{X_4}{X_1} > X_2$
- A_3 (C_1) will be positive if: $X_1 X_2>0$
- B_1 will be positive if $A_1A_2-A_0A_3 > 0$, which results in:

$$(1-X_1+X_3+0.5X_4)(X_1-X_1X_2+X_4)-(0.5-X_3)(X_1X_2)>0 \qquad (6\text{-}8)$$

If all the above conditions are satisfied, the stability boundaries of the system can be established by setting equation (6-8) to be equal to zero which results in:

$$X_1^2(X_2-1)+X_1(1-1.5X_2+X_3-0.5X_4-0.5X_4X_2)+(X_4+X_3X_4+0.5X_4^2)=0 \qquad (6\text{-}9)$$

6.2.2.2 Stability limits

MATLAB® was used to solve equation (6-9) and plot curves for various parameter values to establish the stability boundaries of the system. Figure 6-2(a) shows X_1 versus X_2 with changing X_3 from 0-0.4 in 0.1 steps, while setting X_4 to a fixed value of 0.2. All points lying within the region bounded by the curve and the axis are stable, and all points external to the region are unstable. The effect of X_3 is illustrated as the stability region is expanded by increasing the value of X_3 towards its stability limit, which is defined in condition 1 of the Routh-Hurwitz criterion, i.e. that $X_3<0.5$.

The benefit of defining the stability boundaries in terms of X_1 and X_2 is apparent from their definition, where it is seen that they are universal parameters and not related to any specific system parameters. Hovey [55][56] has considered the stability boundaries for a system governed by a PI type controller and operating with regulation X_4 set to zero. The self-regulation of the turbine and connected load acts to reduce the speed transient and to increase the stability of the unit. However, since the net amount of self regulation is not always precisely known, the assumption of a purely resistive load for an isolated system will result in a conservative evaluation of the regulating capabilities of a particular hydroelectric generating unit and governor.

The dotted line in Figure 6-2(a) represents Hovey's stability curve, where the operating point (H) for optimum transient response was chosen as $X_1 = 0.5$ and $X_2 = 0.25$. It can be seen that the governor setting chosen by Hovey is conservative and does not utilise the maximum capability of the generating system. Similarly Paynter [57] has recommended an operating point (P) for optimum transient response at $X_1 = 0.4$ and $X_2=0.169$. The stability boundaries of Dinorwig unit in terms of the PID gains of the governor are shown in Figure 6-2(b). The operating point "o" represents the PI gains currently in use at Dinorwig for isolated network operation (used for synchronisation process) $K_p = 2.5$ and $K_i = 0.8$. Using low values for the derivative gain ($K_d < 1.6$) yields an unstable response because the operating point will be outside the stability boundaries. Therefore to insure a stable damped response, higher derivative gain is required so the unit will be operating within the stability envelope. Currently the gain $K_d = 4$ is utilised in the governor which gives a maximum operating boundaries.

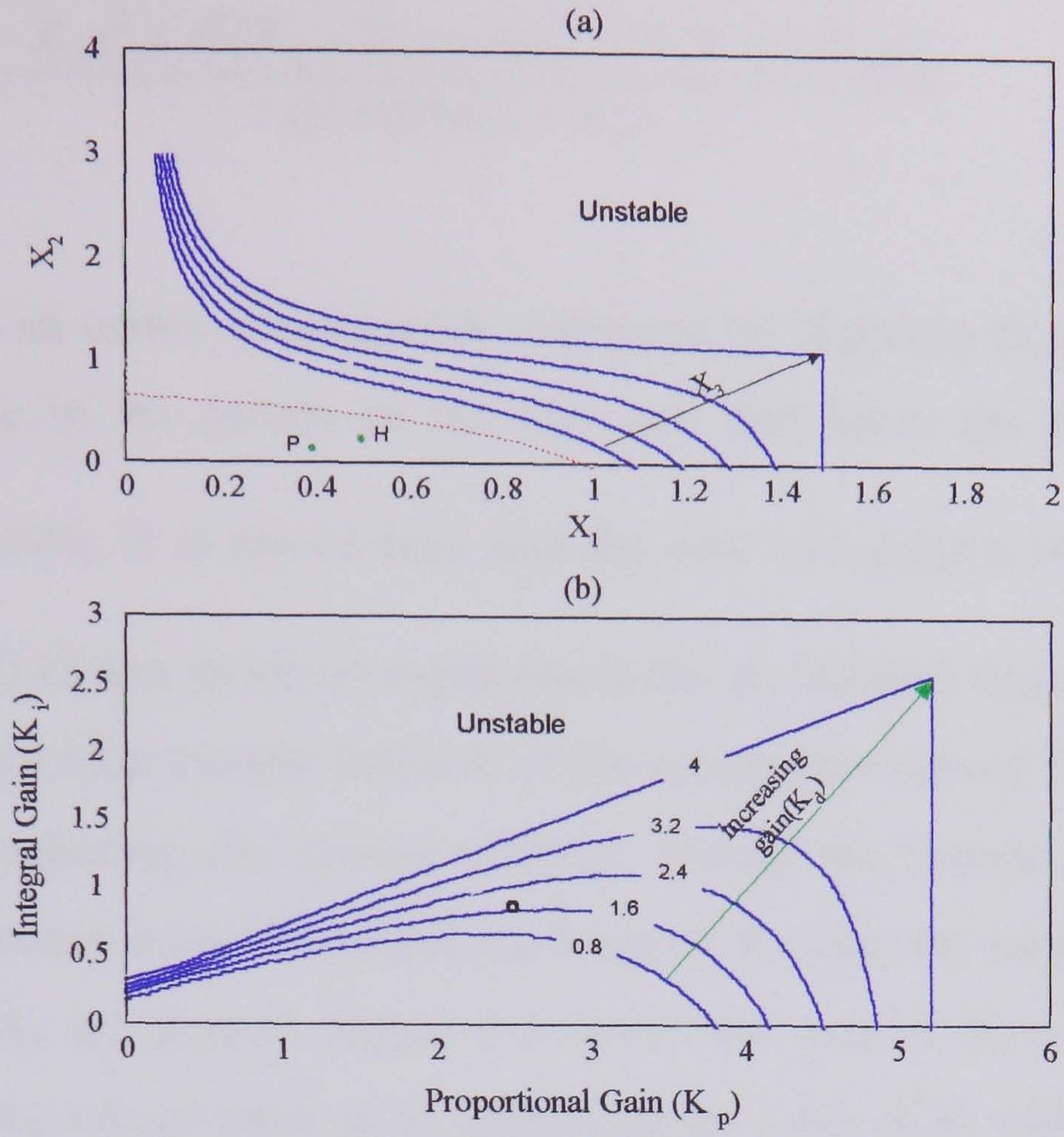

Figure 6-2: *Plots of stability boundaries for X4 = 0.2*

6.2.3 Root locus method

The effect of the governor gain parameters on the system dynamic behaviour of a unit supplying an isolated load is examined using the root locus method. The root locus shows how changes in the system's feedback gain or other system parameters influence the pole location. Roots that lie in the right half of the plane represent terms in the solution which will grow with time and thus indicate an unstable system. Roots that lie in the left half plane represent terms that die out and the further they are to the left, the faster these terms will disappear. To improve the transient response of the system it is necessary to move the roots to the left, thus increasing the damping. The distance of the complex roots from the real axis indicates the frequency of the oscillatory terms in the transient response. Those roots near the real axis have a low frequency while those further away will have a higher frequency [58].

The system representation of Figure 6-1 was used in the investigation. The open loop system transfer function as represented by equation (6-3) can be rewritten as equation (6-10) relating to the parameters X_1, X_2, X_3 and X_4 as shown in [Appendix-IV].

$$G(s) = \frac{-X_3 s^3 + s^2(X_3 - X_1) + s(X_1 - X_1 X_2) + X_1 X_2}{s(1+0.5s)(s+X_4)} \tag{6-10}$$

This work extends an earlier investigation conducted by Hagihara et al [49] where they predicted a change in the pattern of the root loci that limits the derivative gain to $K_d \le \frac{K_p T_w}{3}$. However, it is shown here that the root loci pattern changes occur at a higher value $X_3 = 0.45$ and yields an expansion in the K_d stability limits. The location of the roots of the open loop transfer function of the system represented by equation (6-10) will be used in evaluating the system stability. Setting the system regulation $X_4 = 0$ (i.e. assuming frequency insensitive load), the locus of the roots for varying X_1 and X_2 for typical values of X_3 are plotted. Figure 6-3 shows the case of $X_3 = 0$, the solid lines illustrate root loci for a fixed value of X_2, increasing the value of X_1 will lead the complex root to move toward the imaginary axis and eventually enter the unstable region.

The dashed lines illustrate the root loci for fixed values of X_1, which similarly move toward the imaginary axis and enter the unstable plane with increasing X_2. The points P and H mark the locations of the complex roots for optimum values of X_1 and X_2 as recommended by Paynter [57] and by Hovey [56] respectively. It can be seen that Paynter's operating point will result in a damping ratio $\zeta \approx 0.73$, which produces an overshoot of 5%, which represents good system tuning. Hovey's operating point has a damping ratio $\zeta \approx 0.38$, which results in a bigger overshoot.

The effect of the derivative gain on the root locus is investigated for the cases $X_3 = 1/3$ and $1/2$ are illustrated in Figure 6-4 and Figure 6-5 respectively. Adding X_3 expands the stability zone and for $X_3 = 1/3$ the optimum setting is marked as "M", giving a damping ratio $\zeta \approx 0.707$. Operating with $X_3 = 0.5$ results in a different pattern of root locus that moves the root toward the real axis with increasing X_1. The change in pattern of the root locus occurs when the value of $X_3 = 0.45$.

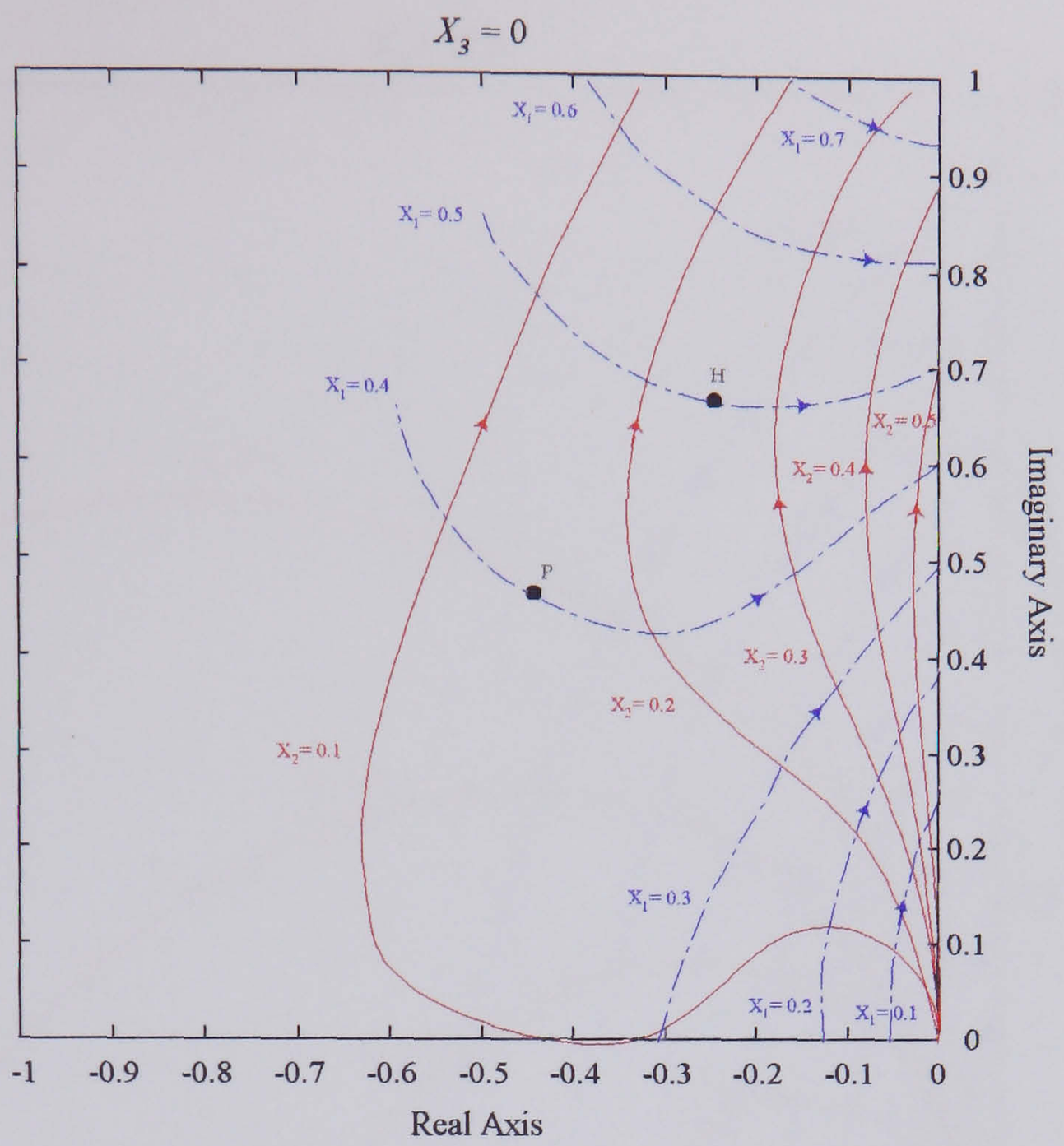

Figure 6-3: *Root loci of the system for $X_3 = 0$*

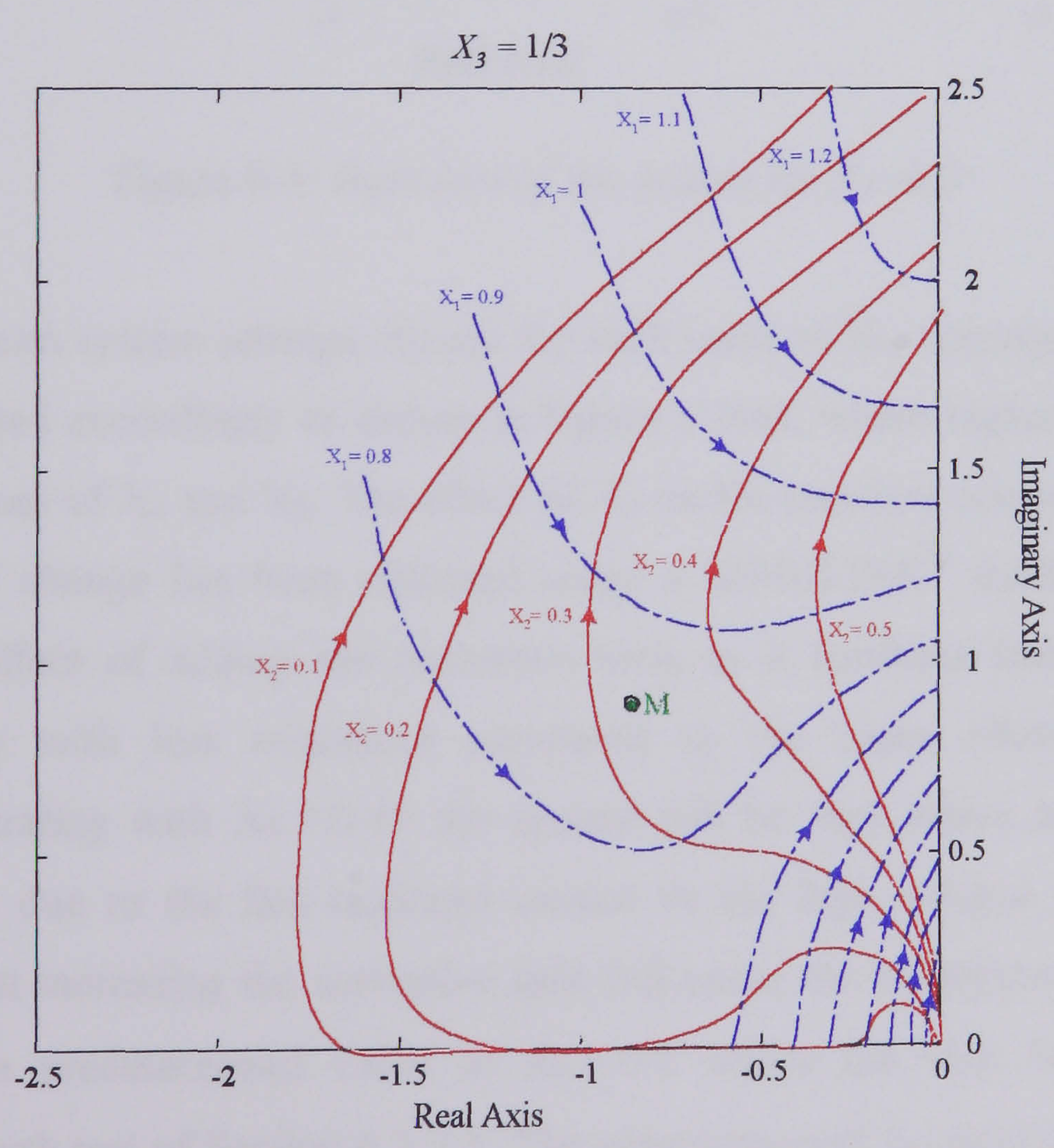

Figure 6-4: *Root loci of the system for X_3=0.3*

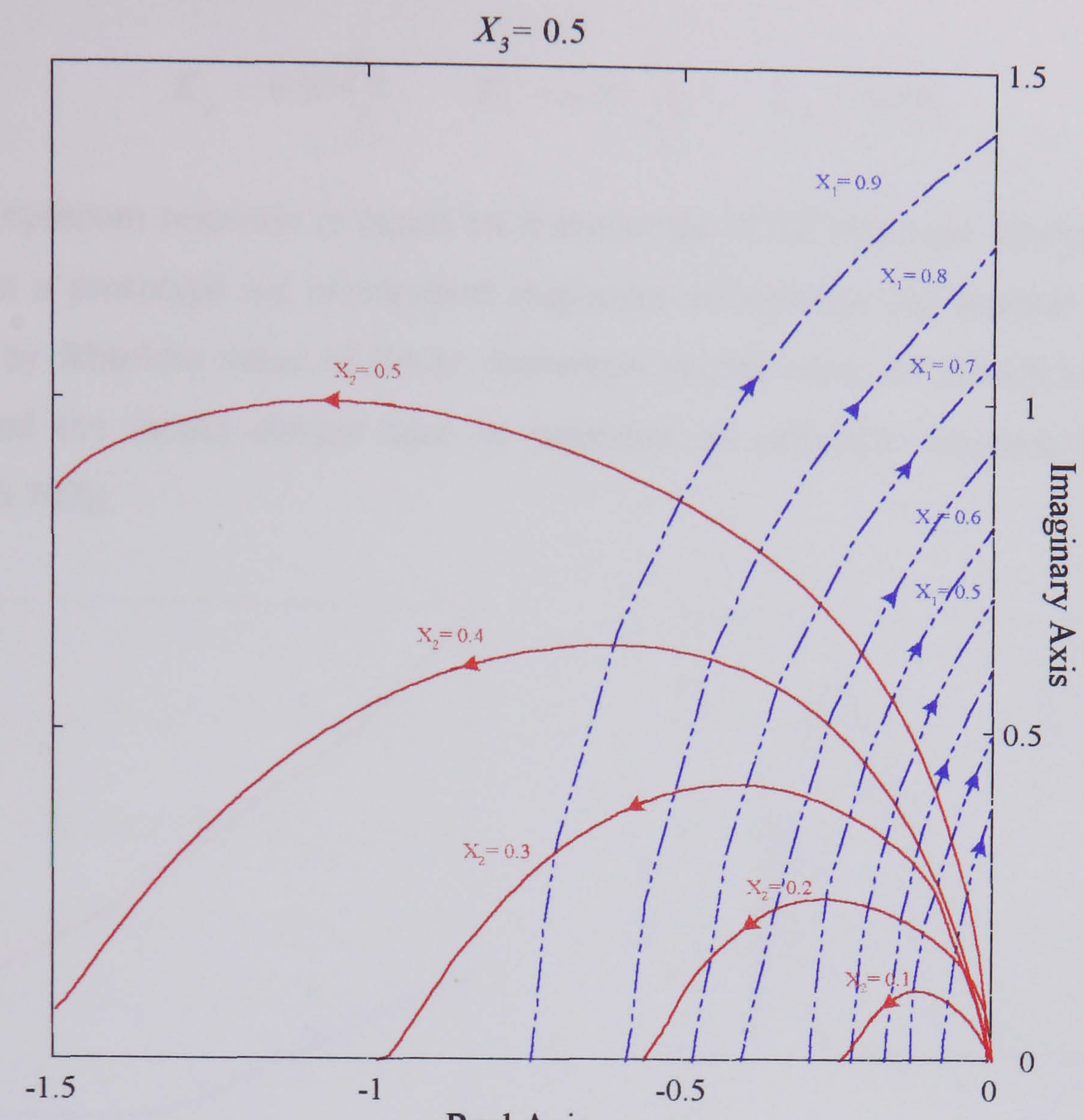

Figure 6-5: *Root loci of the system for X_3=0.5*

The optimum system settings change for each value of X_3; consequently, X_1 and X_2 should be adjusted accordingly as shown in Figure 6-6(a), where higher X_3 values result in increased values of X_1 and X_2. The effect of X_3 on the transient response of the system for a step load change has been obtained using a SIMULINK® model. Figure 6-6(b) illustrates the effect of adding the derivative term as it confirms that the system will stabilise rapidly with less overshoot compared to the cases where it is omitted. Meanwhile, operating with $X_3 = 0.45$ the system will be very active and may cause an extra overshoot due to the fast response caused by the high integral gain setting. The results imply that increasing the derivative gain will cause the enlargement of the stability boundaries to a predetermined value of $X_3 = 0.5$ where the final limits are reached according to Routh test of Section 6.2.2.1. The generating unit is required to deliver a fast response to load changes and selecting $X_3 = 0.4$ will achieve that aim. In this case, using Figure 6-6(a) the optimum PID gains are adjusted to:

$$K_p = 0.97\frac{T_m}{T_w} \qquad K_i = 0.39\frac{T_m}{T_w^2} \qquad K_d = 0.4T_m$$

The optimum response is based on a prototype ITAE response. Graham et al [59] worked out a prototype set of transient responses to minimise the **I**ntegral of the **T**ime multiplied by **A**bsolute value of **E**rror. Prototype models were developed based on pole location and the model chosen here to represent an optimum response has poles at (s+0.707±0.707j).

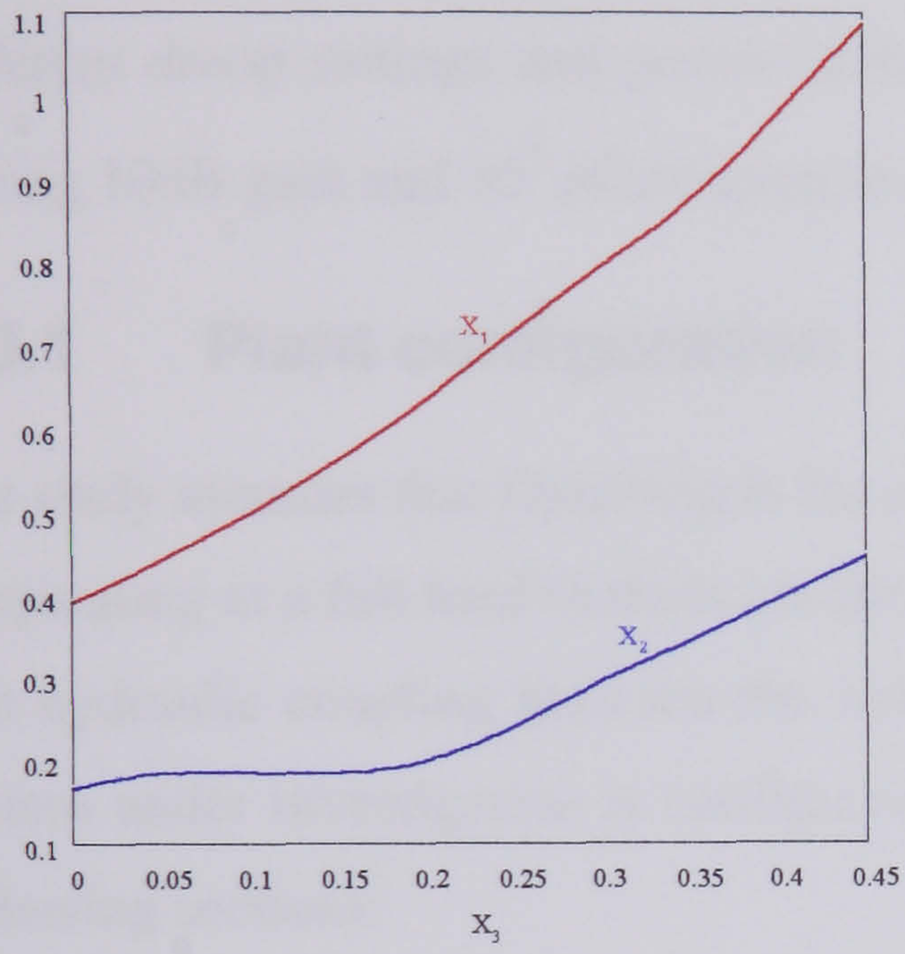

-a-

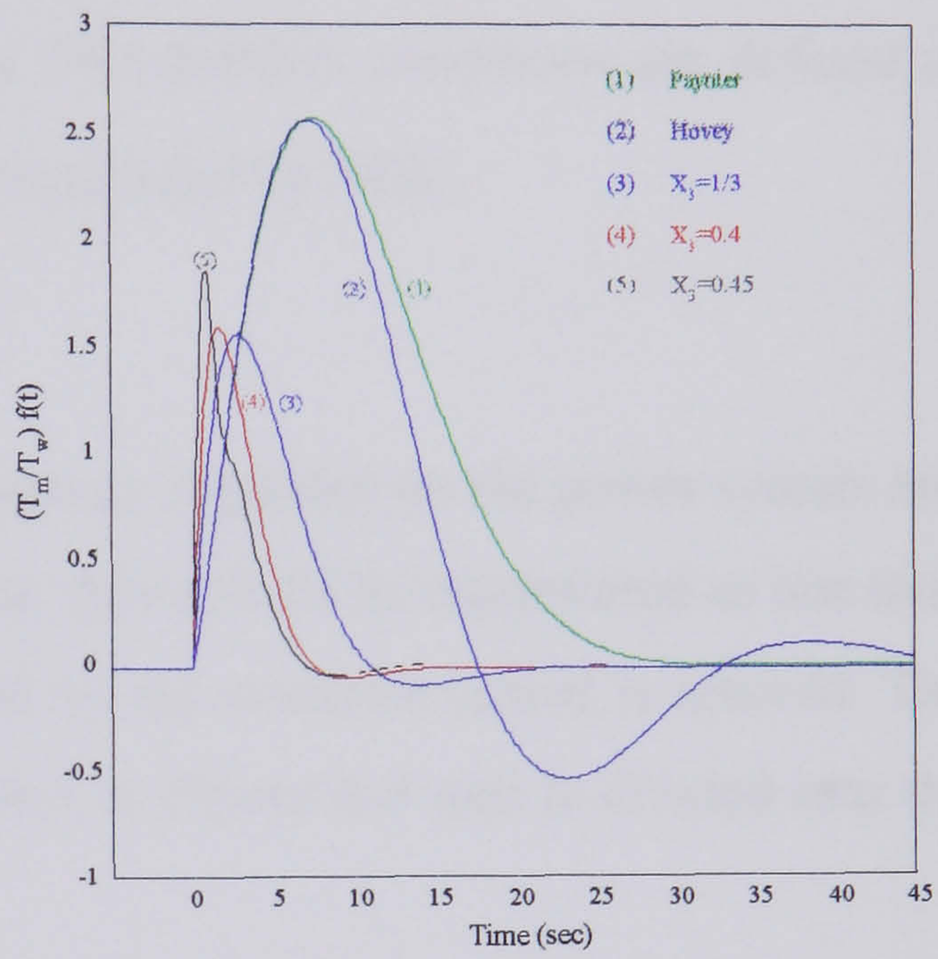

-b-

Figure 6-6: a-*Optimum values of X_1 and X_2 for different values of X_3.*

b-*Optimum Transient responses for $X_4 = 0$*

This analysis has extended the stability boundaries and provides tuning guidelines which yield a better response than popular methods currently used during plant commissioning.

6.3 Stability of Plant Connected to a Power System

The response of an unit when used for system frequency control is determined by the behaviour of its governor, the stiffness of the connected power system and the interaction between them. An investigation into the governor settings at Dinorwig was carried out in order to establish the optimum governor settings for different power system (grid) loading conditions, providing as close to an ideal response as possible without endangering the stability of system frequency control. The gain and phase margins of the open loop transfer function of the system were examined to determine the stability of the plant, for different droop settings and power system sizes. The stability conditions are defined as having 10dB gain and 30^{o} phase margins, as recommended by NGC.

6.3.1 Plant configuration

The study assumes that Dinorwig is the only frequency regulator on the power system and is operating at a full load (6 units on-line) and that they can all be represented as one unit. The hydraulic coupling between the units caused by the common tunnel is ignored. The system under investigation is configured as shown in Figure 6-8 and is divided into the following sections:

Speed Governor

The governor used is based on a typical PID controller consisting of two feedback loops as shown Figure 4-6. The droop considered here is the normal station setting of either 1% or 4%. The governor has an averaging filter for the power system frequency signal represented by equation (4-5) whose effect was included as an equivalent continuous transfer function. MATLAB® was used to find a best-fit transfer function. Figure 6-7 shows the result of the curve fitting obtained by using a continuous representation of equation (6-11).

$$G_{av}(s) = \left(\frac{1}{0.165s+1}\right)\left(\frac{1}{0.165s+1}\right) \tag{6-11}$$

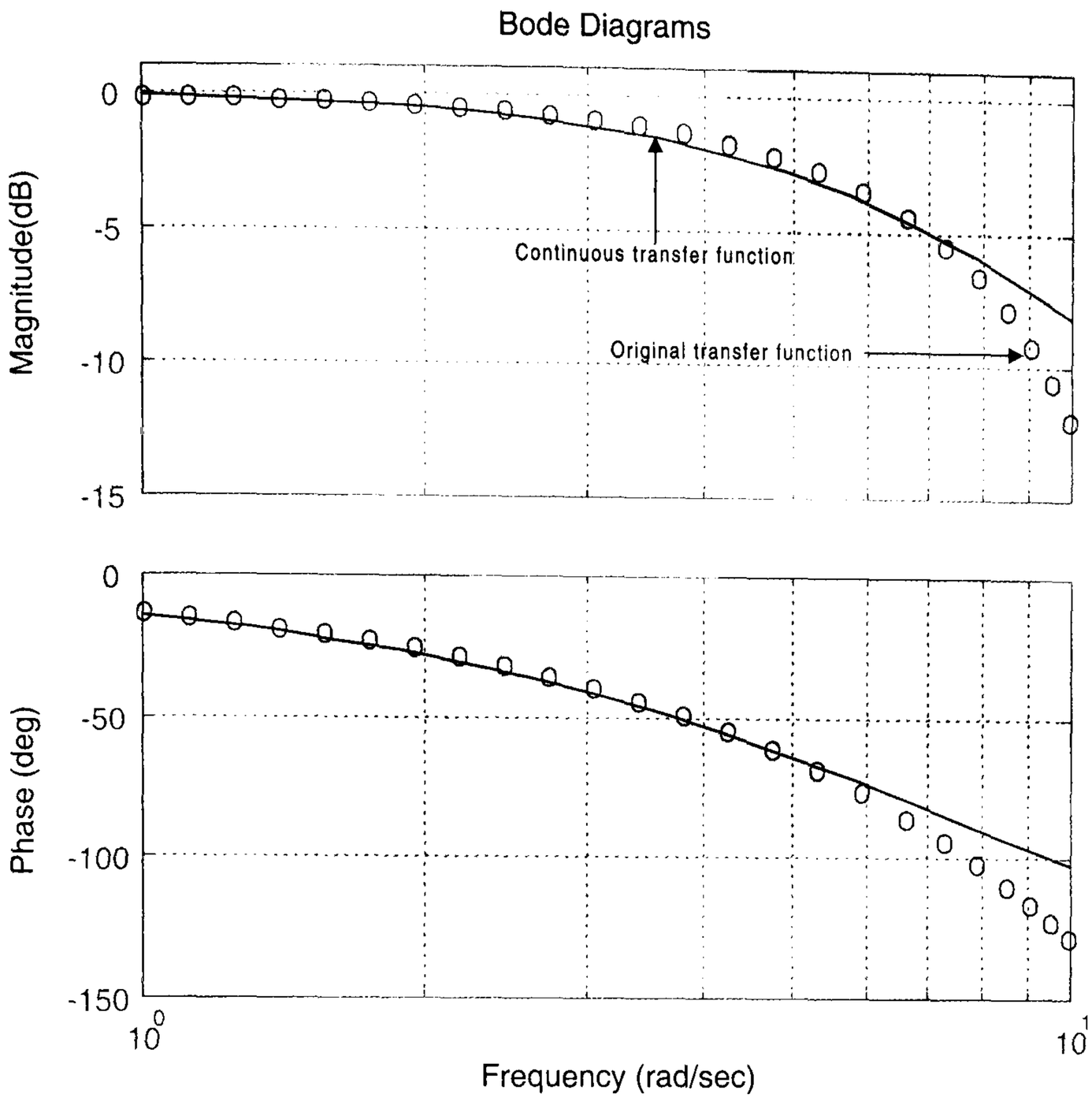

Figure 6-7: *Averaging filter frequency response*

Hydraulic system

The linearised model for the turbine with elastic water column represents the hydraulic system because Dinorwig has a long penstock with high head that leads to travelling wave effects in the system. The transfer function of equation (6-12) relating the power output to guide vane position is described in detail in Section 2.4.2.

$$\frac{P_m(s)}{G(s)} = \frac{1 - T_w s + \frac{4}{\pi^2} T_e^2 s^2 - \frac{T_w T_e^2}{\pi^2} s^3}{1 + 0.5 T_w s + \frac{4}{\pi^2} T_e^2 s^2 + 0.5 \frac{T_w T_e^2}{\pi^2} s^3} \tag{6-12}$$

The guide vane dynamics are represented by a two-stage actuator whose transfer functions are obtained from the step response test presented in Section 4.3.2.1.

Power system

The power system is assumed to be a single area with the tie line power set to zero so there is no power transfer to or from a second system. The linearised first order system

described in equation (3-20) was used to represent the total rotating inertia of the system (M) and the load / frequency damping (D).

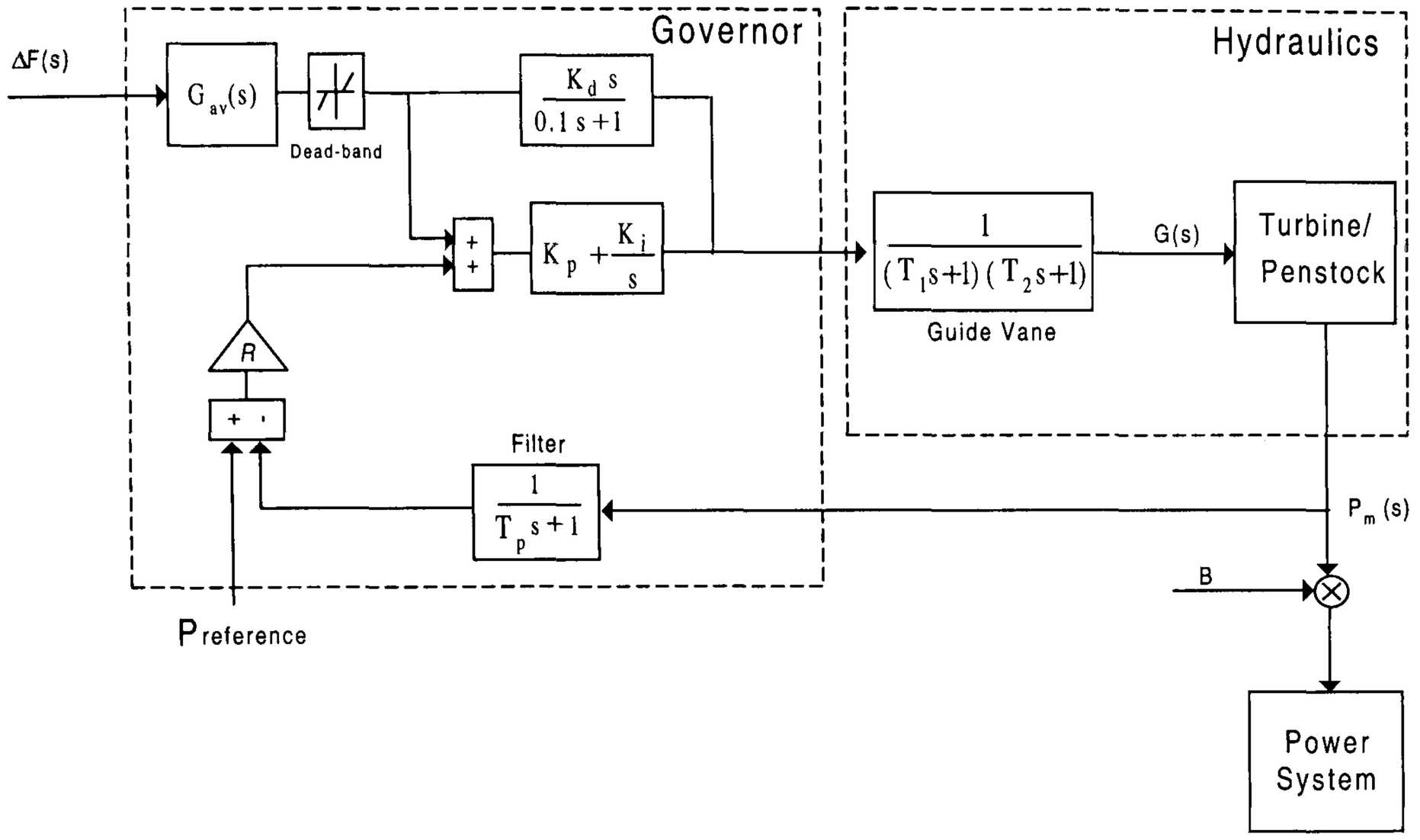

Figure 6-8: *System configuration*

The plant block diagram of Figure 6-8 was manipulated to obtain the transfer function between power and frequency. An alternative notation to the block diagram is given by the signal-flow graph introduced by Mason [60]. The method involves characterising the system by a network of directed branches and associated transfer functions connected at nodes. Using these rules, the complete plant transfer function can be written as:

$$\frac{\Delta P_m(s)}{\Delta F(s)} = \frac{(T_p s+1) G_{av}\left[K_p + \frac{K_i}{s} + \frac{K_d s}{0.3s+1}\right] A(s)}{(T_p s+1) + R\left(K_p + \frac{K_i}{s}\right) A(s)} \qquad (6\text{-}13)$$

where A(s) is the transfer function representing the dynamics of the guide vane and the turbine-penstock;

$$A(s) = \frac{1}{(T_1 s+1)(T_2 s+1)} \times \frac{1 - T_w s + \frac{4}{\pi^2} T_e^2 s^2 - \frac{T_w T_e^2}{\pi^2} s^3}{1 + 0.5 T_w s + \frac{4}{\pi^2} T_e^2 s^2 + 0.5 \frac{T_w T_e^2}{\pi^2} s^3}$$

6.3.2 Stability margins

A MATLAB® program was written to evaluate the performance of the control system at Dinorwig power station by determining the stability margins of the system for various operating conditions. Table 6-1 shows the system parameters used in the investigation, Dinorwig operates with two droop settings of 4% and 1%, therefore it is necessary to assess the effect of droop on the stability of the system. The open loop frequency response of the system was plotted for different K_p and K_i gains with $K_d = 10$ and for both droop settings; in each case the gain and phase margins were determined.

Table 6-1: System parameters

D :	load damping factor	1 pu MW/ 1 pu Hz
M :	inertia of the power system	10
P_m :	Power output of the plant	6×300MW
T_1 :	first stage actuator	0.19
T_2 :	second stage actuator	0.4
T_p :	power measurement filter	2

Figure 6-9(a) shows the gain margin for a 40GW system in which the fraction of the total generation capacity supplied by Dinorwig corresponds to a base conversion of B = 0.045. The gain margin is initially improved by increasing the proportional gain. However, once the peak value is reached, indicating the ideal setting for the controller, the gain margin starts to decline. Figure 6-9(b) reveals that increasing the proportional gain will improve the phase margin and that unsatisfactory stability margins can result from reducing the droop value to below 1% at low values of proportional gain. Hence increasing the integral gain to speed up the response will require an increase in the proportional gain to maintain the stability margins.

The effect of the power system size on the stability margins is shown in Figure 6-10(a), representing specific controller settings; $K_p = 10$, $K_i = 6$, and $K_d = 10$. It is apparent that the system loading has a significant effect on the response of the plant; since the margins expand with increased system loading. Therefore, when the power system is heavily loaded it is possible to increase the governor gain settings to speed up the unit response. The correlation between the power system size and the governor settings is

evident when applying a step input into the system as shown in Figure 6-10(b). High governor settings will cause the response to oscillate when operating with low power system loading, while the response will stabilise with larger power system size.

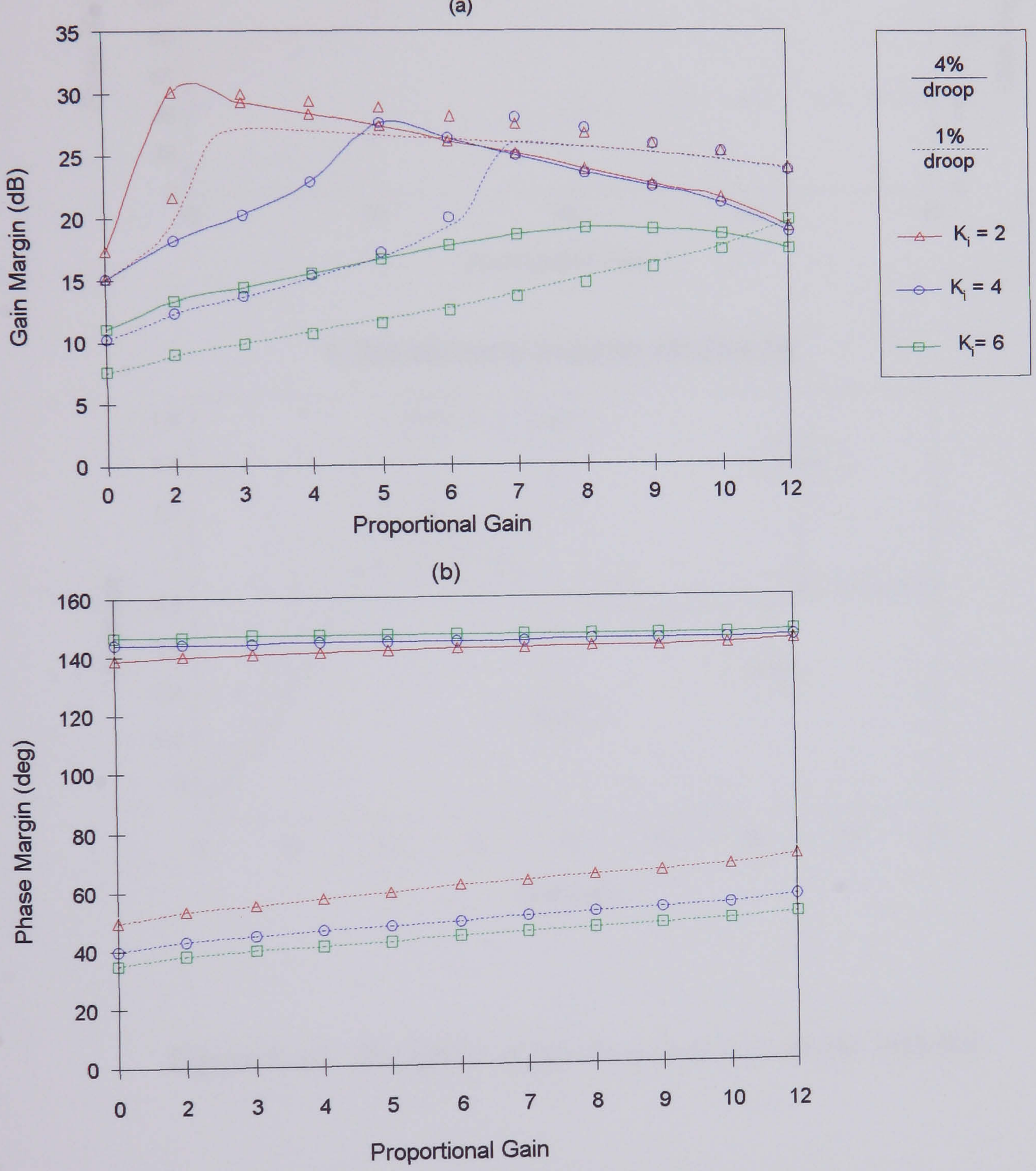

Figure 6-9: *Stability margins of the plant operating with 40GW power system*

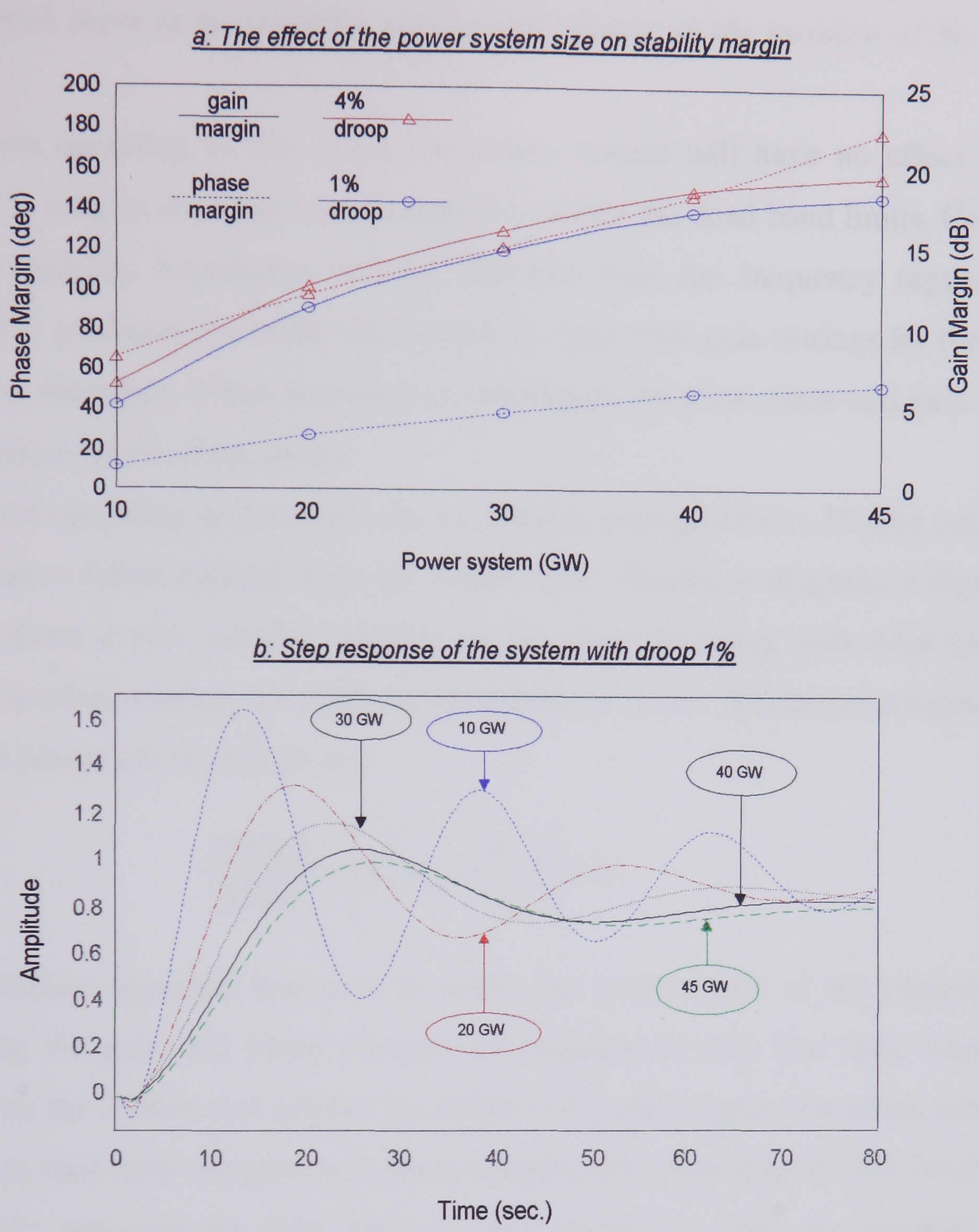

Figure 6-10: *The effect of power system size on the stability*

6.4 Stability of Plant Operating with a Dead-Band

For commercial reasons, Dinorwig is often used as a fast base load unit to increase the system generation (raise the frequency) temporarily until slower response units are brought on-line. This is achieved by the introduction of the dead-band of ± 0.5Hz on the frequency control loop (Figure 4-6) and setting the unit to supply a fixed amount of power (adjusted by the operator) usually at 288MW. The dead-band associated with a speed governor is defined as *the total magnitude of the change in steady-state speed (frequency)*

within which there is no resulting measurable change in the position of the guide vane [61].

When operating in this mode the power system will have no effect on the unit response as long as the frequency deviation is within the dead band limits. Consequently, the plant stability boundaries will be different from the frequency regulation mode. Dinorwig is configured to utilise the same P & I governor gain settings for both operating conditions, therefore, it was necessary to investigate the plant phase and gain margins for the alternative mode of operation.

When operating in this mode the governor is configured as a PI type controller with the derivative action omitted from the control loop. The block diagram of Figure 6-8 was used to obtain a new transfer function of the plant operating with dead-band on. The transfer function relating the plant power output to power deviation (compared with the power set point) can be written as:

$$\frac{\Delta P_m(s)}{\Delta P(s)} = \left[R\left(K_p + \frac{K_i}{s} \right) \right] A(s) \qquad (6\text{-}14)$$

A similar approach was used to assess the performance of the control system by identifying the gain and phase margins for equation (6-14). The open loop frequency response of the system was plotted for different K_p and K_i gains for droop settings of 1% and 4%; in each case the gain and phase margins were determined. The results shown in Figure 6-11 represent the plant margins when all the six units are operating with their dead–band on. It is evident that operating with low droop gain (1%) increases the margins of the system and hence its stability, however with high droop (4%) there is a dramatic decrease in the margins. The reason is that the droop represents a loop gain in the system as expressed by equation (6-14), thus using 4% droop means that the power error signal into the governor will be four times bigger than when operating with 1% droop yield. Meanwhile increasing the integral gain also results in a reduction in the margins and the correlation between the integral and the proportional gains is clear in the gain margin plot as there is a maximum gain for each value of K_i which occurs at a particular proportional gain.

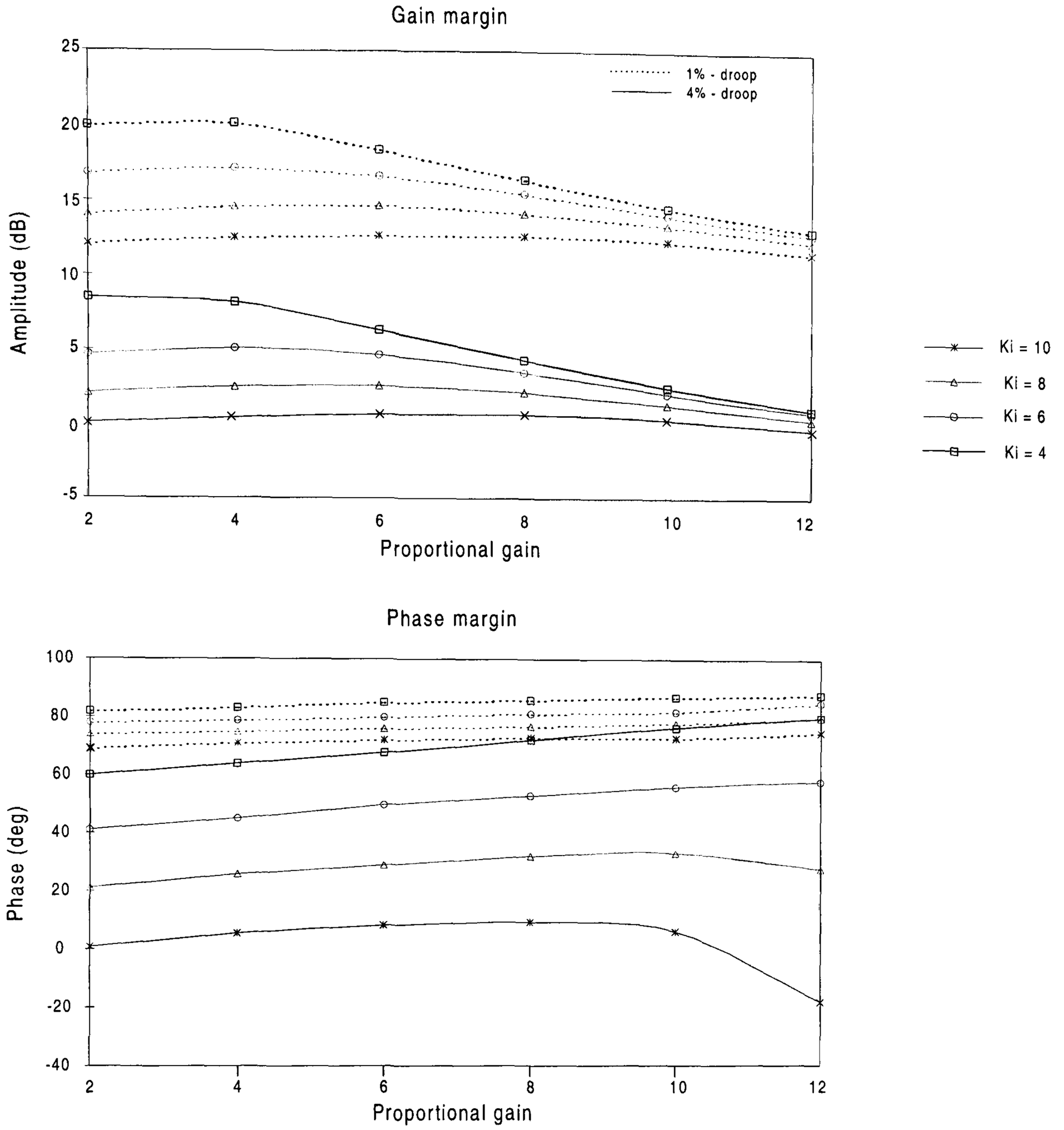

Figure 6-11: *Stability margins of the plant when operating with dead-band*

The effect of plant loading (number of units on-line) on the stability was also analysed, by identifying the margins for a single unit having dead-band on and its droop set to 4%. As before the margins are obtained for different governor gain settings and the results compared with the margins for six units on-line. The results shown in Figure 6-12 exhibit an increase in the margins due to the reduction in the number of units. Meanwhile, increasing the proportional gain will lead to a fall in the gain margins but an increase in the phase margins. The stability of the plant decreases when more units are operating with a high droop setting.

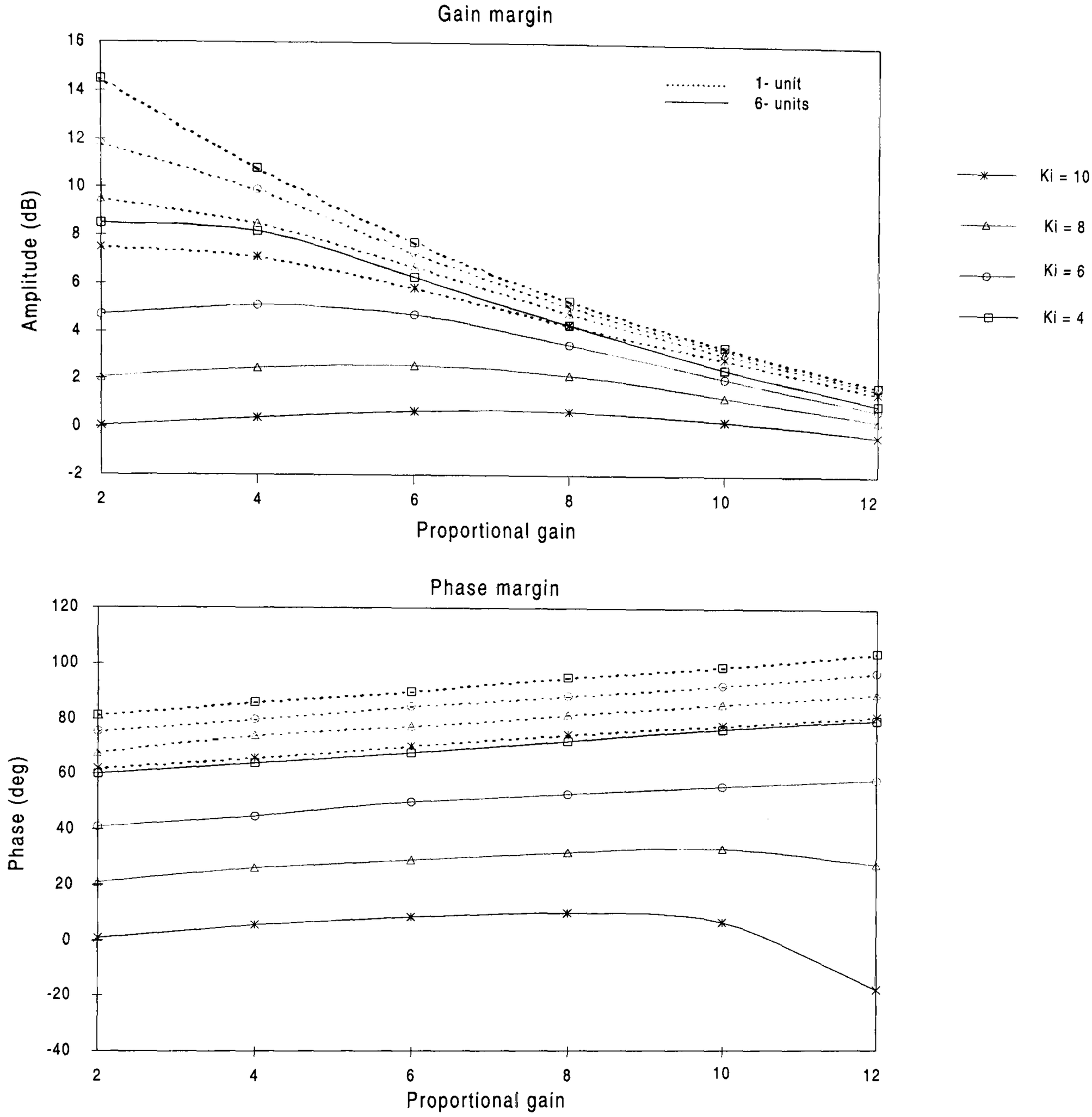

Figure 6-12: *The effect of the plant loading on the margins*

To the best of our knowledge, this is the first time that such a sensitivity study has been performed and it has considerably improved the understanding of how the station will react under different circumstances – both internal and external – and what could be done to compensate for varying conditions. The result has been published in [62].

6.5 Conclusions

Tuning the speed governor is a very important issue for control engineers in the power industry. A general guide for optimum adjustment of the gains of the governor for a unit supplying an isolated load (or a small power system) has been provided, where the

performance of the governor and hence the plant response can be improved by appropriate derivative gain. In the case of a plant regulating the frequency of a large power system, it has been demonstrated that the stability boundaries of the system expand as the power system size increases.

In the case of Dinorwig, to fulfil its commercial obligation it is essential to respond quickly to any changes in the power system loading. This could be achieved by operating close to the stability boundaries. Since Dinorwig's control strategy is based on using one set of gain settings for all operating conditions, when the power system size reduces this may cause operation to be near or even outside these boundaries. Ensuring stability under all circumstances requires conservative gain settings which are well away from optimum for normal operating conditions. Avoiding instability while maximising the commercial potential of the plant suggests that it is necessary to schedule the gains according to operating conditions. Currently, the only gain scheduling is:

- Winter / summer.
- Integral gain boost.

The original governor gains at Dinorwig were very conservative being based during commissioning on a relatively small power system. The results of this work have been implemented on the plant where the higher gains have resulted in faster and more accurate responses being achieved. However, gain scheduling for different power system sizes has not been implemented on the plant to date because the power system properties are not available - consultation with NGC would be necessary to make such data continuously available to the control system at Dinorwig.

Anther important factor for gain scheduling at Dinorwig is operation with dead-band on, where the speed of the response is determined by the power setting ramping time as the unit is <u>not</u> required to be very fast in this mode of operation. In this case, the power system size has no influence on the plant response and the main cause for instability is the droop. Operating with a high droop setting of 4% reduces the stability boundaries, especially when several units are on-line and operating in this mode. Therefore, to avoid the risk of instability it is recommended that the droop be set to 1% on these units in order to expand of the boundaries. The nonlinear simulation of oscillatory behaviour in Chapter 7 reinforces this conclusion. This recommendation is currently implemented as part of the control strategy at Dinorwig.

Chapter 7

Application of the Nonlinear Simulation

7.1 Introduction

The real benefit of simulation is that it gives better insight and improved understanding of the causes of recorded behaviour as well as an indication of how that behaviour can be moderated. In this context, the model is being used both to analyse the current system response, and also to improve stability and design a new control strategy. The chapter is divided into three sections; it starts with the development of a new black-start regime to be used to enhance the capability of the Dinorwig plant in power system restoration. Black-start is the ability of a power station to start-up from shut down without external electrical supply. In the event of complete loss of electricity supply, there is the need to return the system back on line as efficiently as possible using units with black-start capability. The new regime is based on two units operating in parallel - one used as a frequency regulator and the second as a load pickup unit. An investigation is conducted into the stability and frequency responses of the system during the cold load pickup in the early stages of power restoration. The results confirm that this arrangement will allow a load equivalent to 15% of the unit rating to be picked up without causing the frequency to swing outside its limits.

In the second section, the model is used to investigate specific operating conditions where a sustained power system frequency oscillation occurred during a particular event at Dinorwig. The simulation successfully reproduces the oscillatory phenomenon whose causes were not easily diagnosed from limited recorded data. Further, it indicates what measures should be taken to improve the control system to prevent such incidents from occurring again.

Finally, a model based analysis is used to identify the interaction between the machine governor and the power system in order to establish the influence of changes in system loading on governor performance and the settings required for near optimal performance under different system conditions. The advantage of using this approach is that the normal control techniques used for stability analysis are based on a linearised representation of the system and do not account for the effect of non-linearity on system response. Consequently, the analysis will be limited to a small envelope around the operational boundaries.

7.2 Power System Restoration

The restoration of a power system following a major supply failure can be supported by the availability of hydro power stations with an appropriate black-start capability. This requires that the station is capable of responding to incremental load changes while ensuring that frequency deviations remain within limits, placing an onerous duty on governor operation during load pickup. The normal operation of a power system may be disturbed in extreme circumstances by a major system fault.

The process of restoring the power supply is very complex and is achieved by re-energising the disconnected lines using plant in other parts of the system or by means of plant enabled for black-start operation. These plants have the ability to generate power without the need for a voltage source from an external network, relying exclusively on self-sustained auxiliary systems for this purpose [63].

7.2.1 Restoration plan

The system restoration plan developed for all hydro systems emphasises the switching operation and the response of prime movers to sudden load pickup. In this plan, due consideration is given to the time it takes to isolate and energise the necessary lines by

using central control systems to execute the switching operation programs. These programs are used to determine the response of the system and provide guidelines for load pickup based on the prevailing generation on-line, transmission configuration and system loading [64]. The restoration plan must account for a number of common concerns to ensure successful operation. These include:

- Immediate re-supply of station services.
- Time consuming nature of switching operations.
- Voltage rise on energising unloaded transmission lines.
- Frequency response of prime movers to a sudden load pick-up.

7.2.2 Black-Start operation

Pump storage hydro generators are designed to come on load faster than conventional generators. They can readily be used to control frequency and voltage in the attempt to slowly raise the generated power and support the restoration of the supply of power to base load plants over a relatively short time scale. This will then enable the base load plant to be brought back on line, completing the restoration of supply. A black-start regime requires strict control of frequency in order to reduce the extent of the frequency deviation caused by the connection of loads. Therefore, a balance must be maintained between load and generation to avoid excessive frequency deviations.

As with the introduction of large load increments there is always the risk that the system frequency moves outside the operating limits of the plant, causing the restoration process to collapse. The size of the load pick up that can be achieved depends upon the response of the pump storage plant in support of system restoration. It is therefore essential to establish the largest incremental increase in load which can be achieved without causing the system frequency to fall below its lower limit, enabling an acceptable frequency and voltage profile to be maintained during the restoration phase.

The conventional frequency control strategy used in normal operation is generally insufficient during the initial period of restoration following a major system fault, as the unit will be operating in an isolated mode. In these circumstances, the connection of excessive load might cause the frequency to drop below its limits. Delfino et al [36] have

suggested an approach based on the use of a special frequency controller operating in association with the machine governor for the restoration of the Italian power system. The auxiliary regulator provides an extra frequency error signal and, as soon as the frequency falls out of the dead-band range of 49.5Hz - 50.5Hz, the output of this regulator will be added to the conventional speed governor signal to control the gate position. However, in the case of Dinorwig the station is not equipped with the frequency regulator so a new system arrangement is considered here to support the power system restoration plan. The black-start capabilities of the station are improved in order to limit the frequency deviation due to cascading insertions of cold loads and in order to perform correct parallel operation with other units at the end of the restoration plan.

7.2.3 Dinorwig black-start configuration

The operation is based on two units connected in parallel; one is used as a frequency regulator whose governor is configured for isochronous control (zero speed droop regulation). The second unit, referred to as the power unit, is configured for conventional speed droop governor control with a droop setting between 1% and 4%. The frequency-regulating unit is used to control the frequency deviation by sharing the load after which it will reduce its output as the power unit takes up the entire load. The second, power controlled machine has a dead-band in its frequency response characteristic such that its governor will not respond to frequency changes within the limits of the dead-band, typically ± 0.5Hz. As load is inserted onto the system, this will be picked up by the frequency-controlled machine acting alone as long as the frequency variation is within the limits set by the dead-band. However, should the frequency variation exceed these limits, the power-controlled machine will act to pick up additional load.

7.2.4 System model

A system model is developed as shown in Figure 7-1 to be used to determine the maximum load increment that can be picked up by an individual generator while maintaining the system frequency between 48.5Hz and 51.5Hz to maintain the system stability. In the model, as in the real system, the units are initially synchronised so that as the load is picked up it will affect the output frequencies of both units, as well as the

system frequency. The unit controllers will therefore need information about the condition of both units in order to bring the frequency back to its steady state value.

The model shown in Figure 7-1, is obtained by rearranging the nonlinear single penstock model developed in Section 5.2.1.2. This is achieved by replacing the power system with a second unit supplied form the same tunnel. Meanwhile the electrical system consists of a basic model of the generators operating in parallel, as introduced in Section 3.3.1. The effect of load damping D is introduced into the machine loop. The power transferred between the two units P_{12} is represented by equation (3-16) where the synchronising coefficient T_{12} used is 0.707 assuming the operating power angle to be equal to 45^{o}. This will result in an intermachine oscillation of 0.81Hz, which is a typical value.

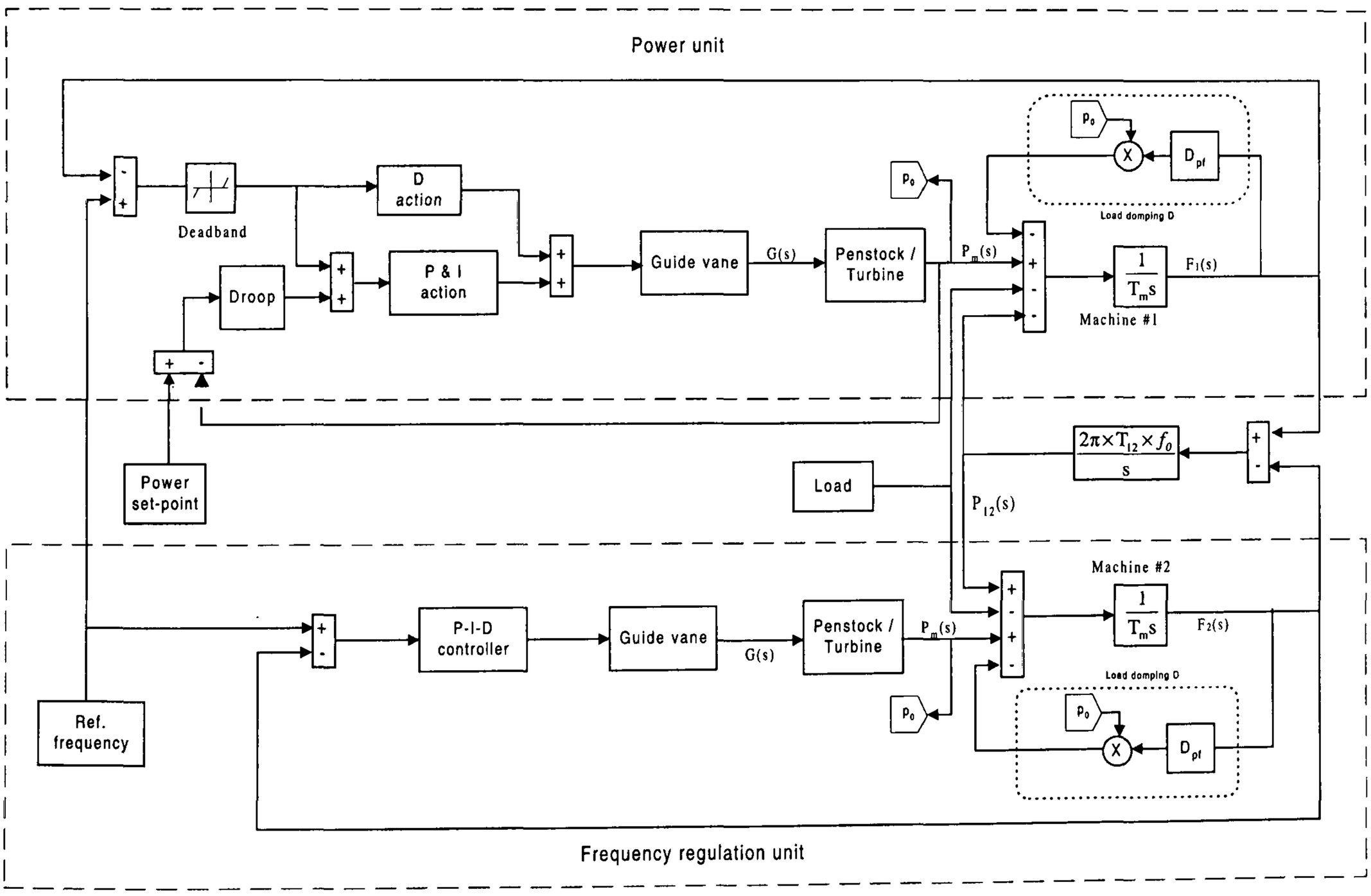

Figure 7-1: *Block diagram of the black-start system configuration*

7.2.5 System simulation

The governor gain settings for both units during the simulation are chosen to be identical to the Dinorwig parameters for isolated load operation. The load model used in the simulation is based on linear active power with load frequency coefficient $D_{pf} = 1$. Figure 7-2 then shows the response of a single pump storage unit operating without additional support to a black-start condition involving the insertion of step loads equal to 15% of the unit rating power, with 30 seconds intervals between each load insertion.

The simulation was repeated using two units configured for black-start operation. The result is shown in Figure 7-3 from which it can be seen that both units share the load to control the frequency deviation. Ultimately, the power unit will take the entire load as the frequency unit reduces its output. The frequency unit appears to be more dynamic when the deadband of ± 0.5Hz is introduced on the power unit while removing the deadband will influence the response of the power unit to respond to frequency changes.

The frequency deviation of the system due to load insertion for both single unit and the black-start configuration are shown Figure 7-4. From this it can be seen that the frequency drop is restricted to 49Hz in the black-start operation, maintaining system stability. In the case of single unit operation, the frequency drops to 47.5Hz, well outside the system frequency limits; the step load insertion would need to be restricted to less than 5% of the full unit rating to achieve stable operation.

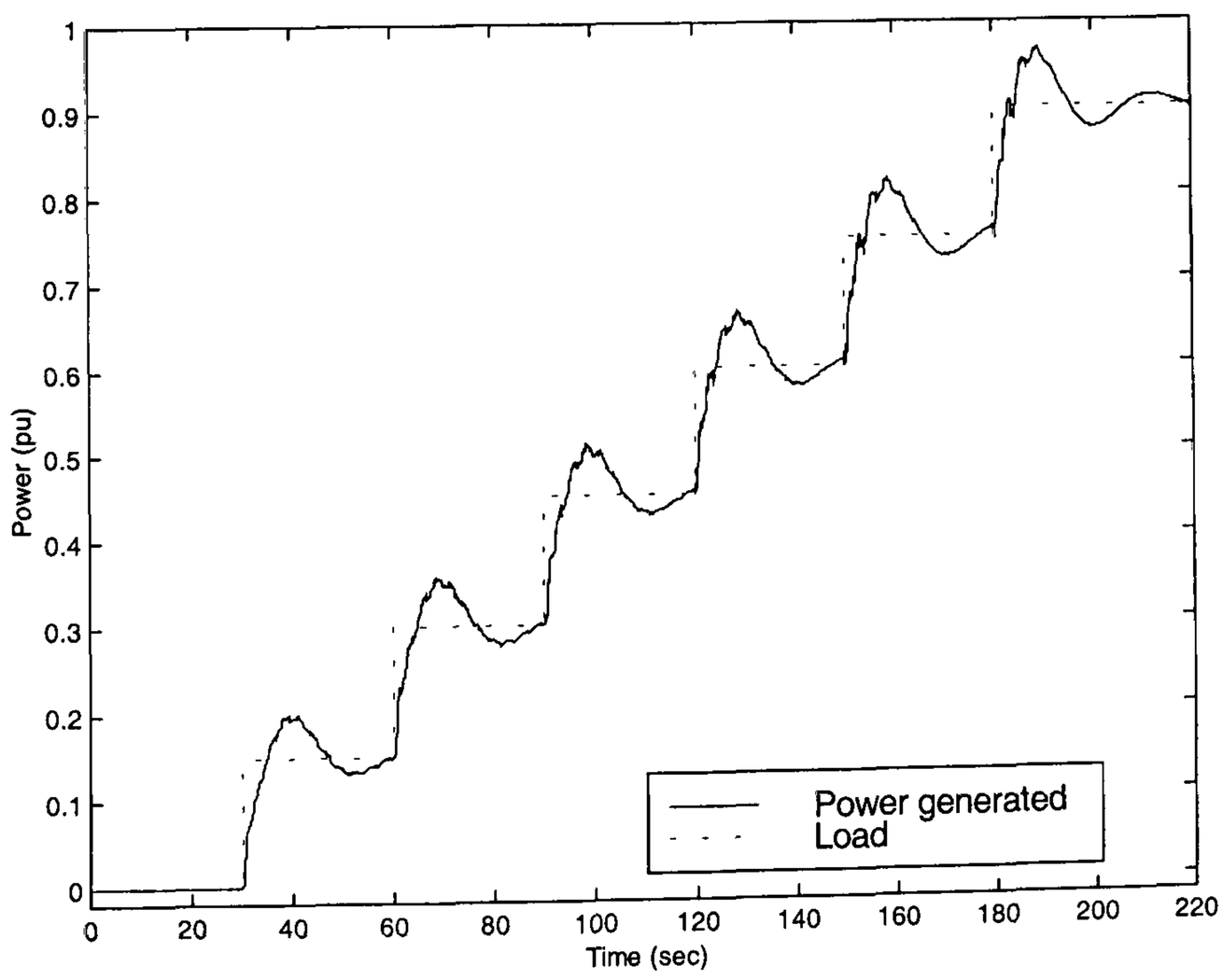

Figure 7-2: *Response of single unit to load insertion*

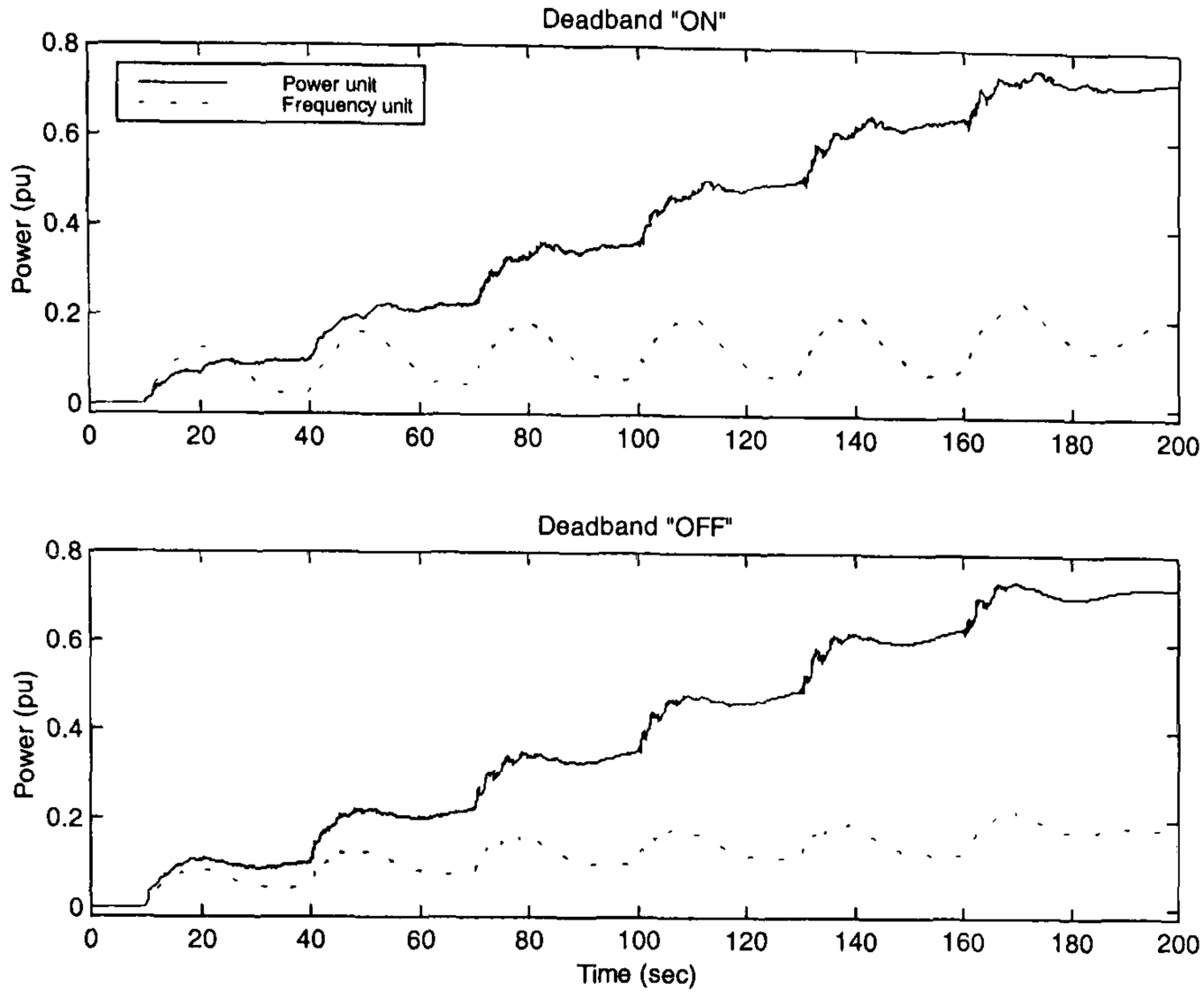

Figure 7-3: *Response of black-start units to load insertion*

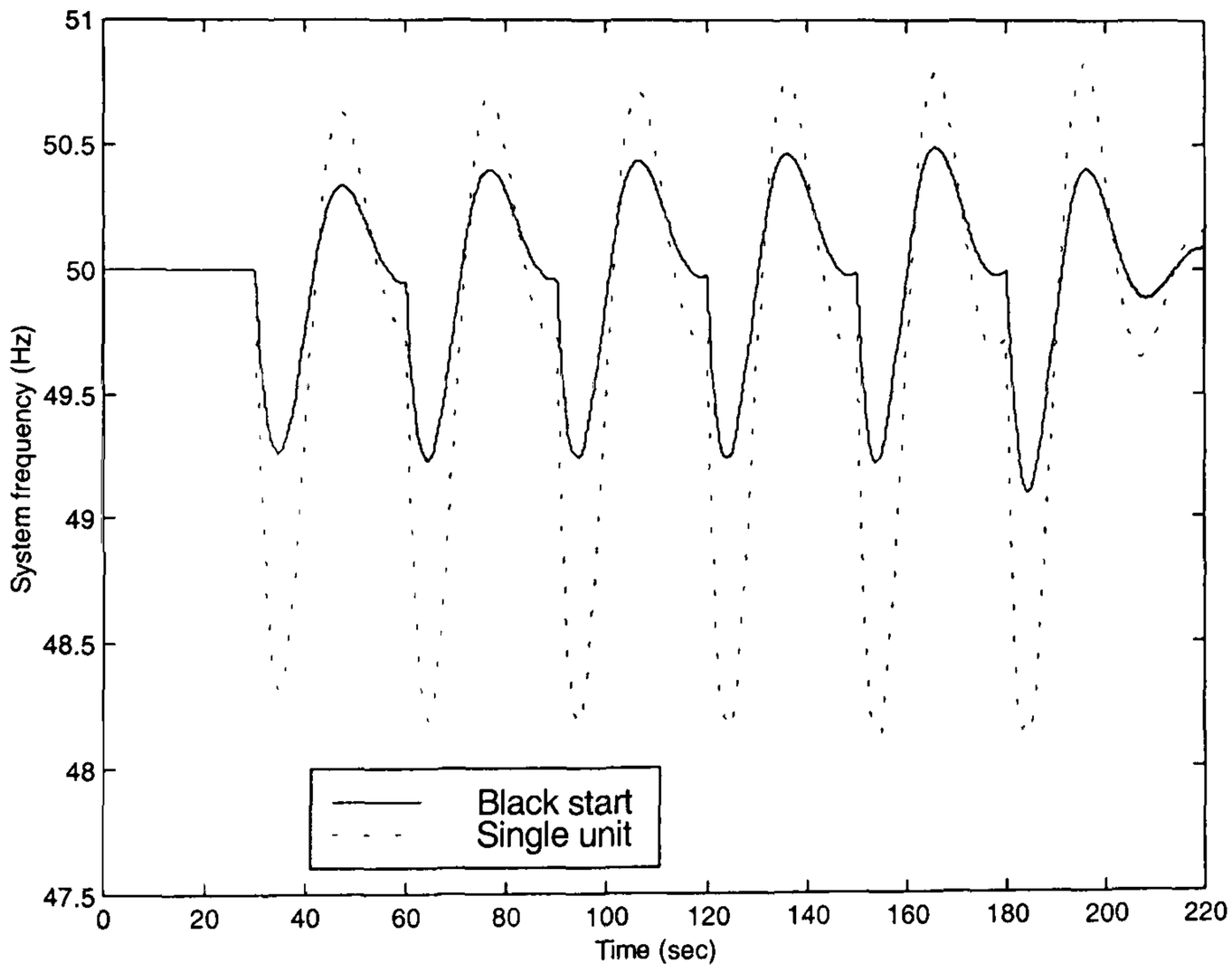

Figure 7-4: *Frequency decay due to the insertion of subsequent loads*

Load sharing between the two units for black-start operation is demonstrated in Figure 7-5, when the system is subject to a load insertion of 15%. Initially the units share the load but as the power unit takes up the load, the frequency unit reduces its output accordingly.

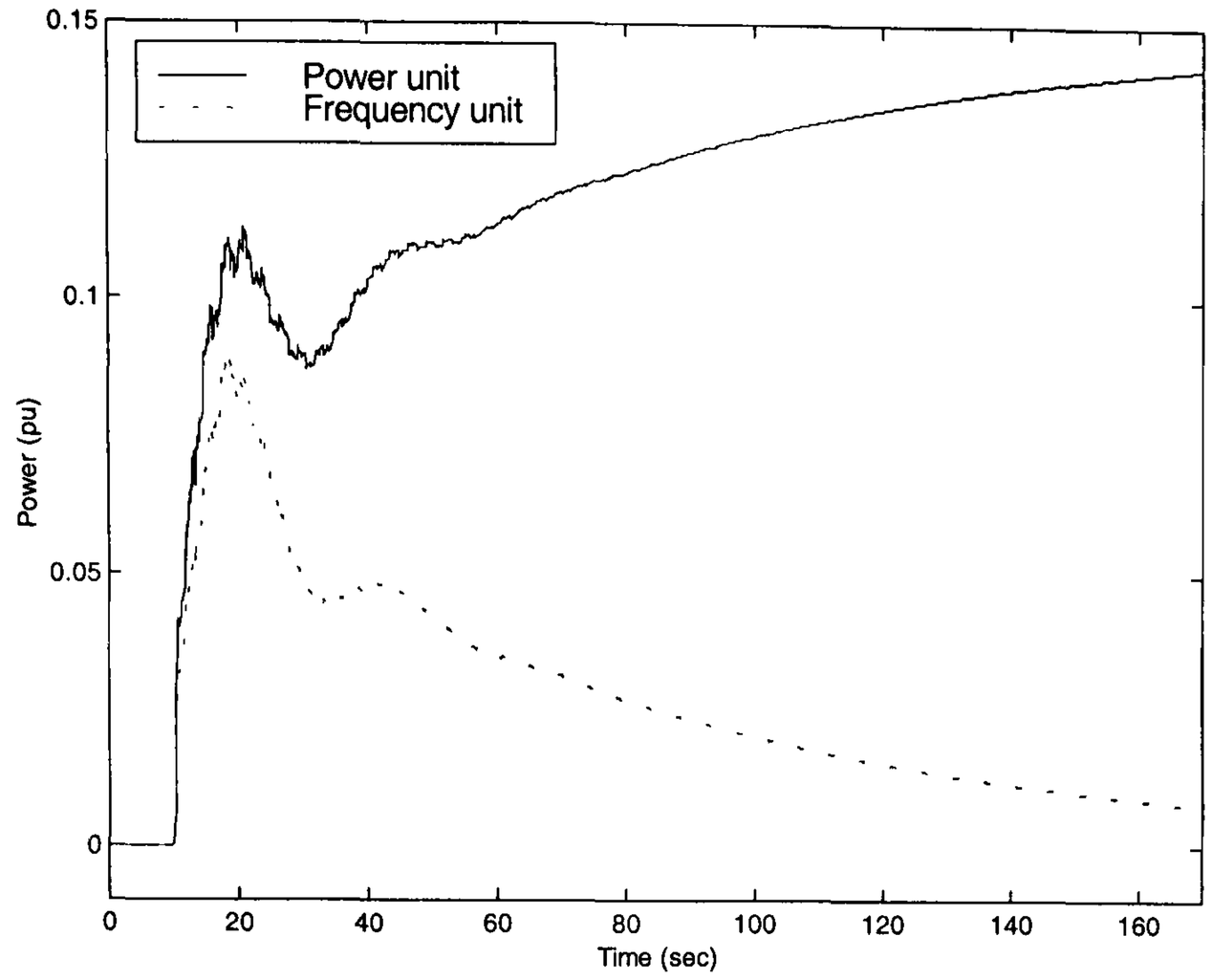

Figure 7-5: *Load sharing during black-start operation*

Black-start is an extremely onerous condition for a power system and one that requires control of both power and frequency if system frequency limits are to be maintained. The simulation studies show that a fast response pump storage hydro station can meet these conditions by using a pair of interconnected machines operating to control power and frequency.

7.3 Simulation of Oscillatory Behaviour

On rare occasions, Dinorwig has been subject to sustained oscillations of output power. For example, in one particular event during winter 1998/1999 oscillations occurred when the station was operating with four units online. Units #1 and #2 were in frequency-insensitive mode (dead-band on) with $K_p = 10$, $K_i = 12$ and droop 4% while units #3 and #4 were in part-load response mode (i.e. effectively regulating the power system frequency) with $K_p = 10$, $K_i = 12$, $K_d = 2$ and a droop of 4%.

The top graph of Figure 7-6 shows that afternoon's record of each unit's power output and the measured power system frequency is shown in the bottom graph. At time $t = 90s$, unit #5 is brought online in dead band response mode to pick up a load of 288MW. This action causes a rapid increase in power system frequency as this is delivered and some oscillation in the output power of unit #5 occurs, which slowly decays up to $t = 200s$. Both units #3 and #4 respond by decreasing the amount of power

generated. Shortly afterwards, the record shows that a steady upward trend in power system frequency begins while units #3 and #4 exhibit a steady decrease in generated power – this can only be due to a change on the power system loading, either because the demand is reducing or a base-load station is picking up the load. By t = 330s a distinct oscillation in the generated power is to be seen which affects all the units on-line and gradually increases in amplitude. By t = 420s a constant amplitude oscillation is established whose combined power variation exceeds 120MW and causes a 0.06Hz peak to peak swing in the power system frequency.

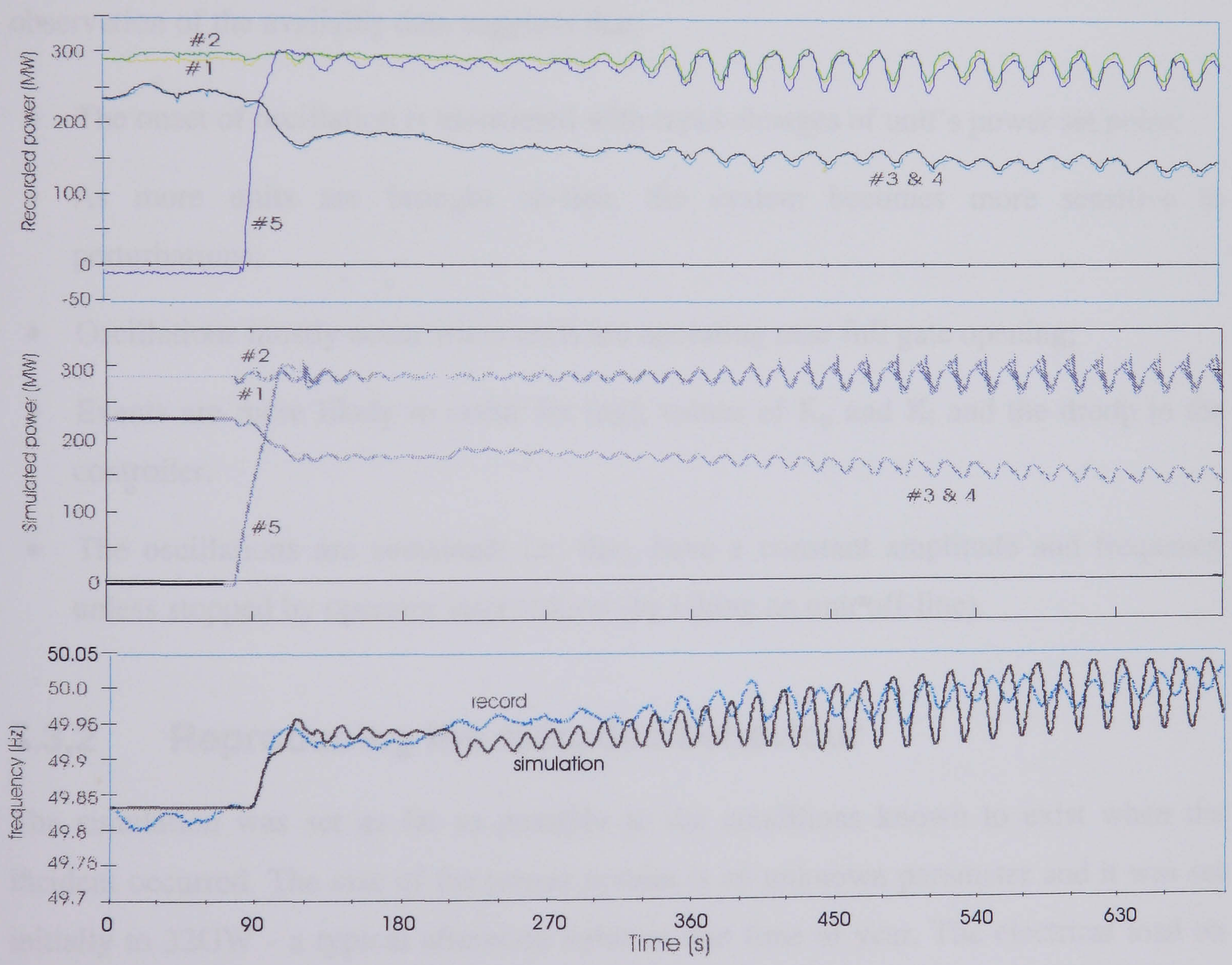

Figure 7-6: *Comparison of recorded and simulated power output and power system frequency*

7.3.1 Nature of the oscillatory behaviour

It is vital to understand why these oscillations occur so that such operating conditions can be avoided in the future and several possible causes were suggested by operations staff. However, the data available from this and similar events is very limited because they occur relatively rarely and then are remedied immediately by operator action so it is difficult to determine a pattern from the logged data. In particular, it is not possible to explain on the basis of linear, decoupled models of individual units why a synchronous and sustained oscillation occurs especially as it involves the frequency-insensitive units, whose governors do not react to changes in power system frequency at all. Nevertheless, observation of the available data suggests that:

- The onset of oscillation is associated with rapid changes of unit's power set point;
- As more units are brought on-line, the system becomes more sensitive to perturbations;
- Oscillations mostly occur when units are operating near full gate opening;
- Events are more likely to occur for high values of K_p and K_i and the droop in the controller.
- The oscillations are sustained; i.e. they have a constant amplitude and frequency unless stopped by operator intervention (by taking an unit off-line).

7.3.2 Reproducing the recorded behaviour

The simulation was set as far as possible to the conditions known to exist when the incident occurred. The size of the power system is an unknown parameter and it was set initially to 32GW - a typical afternoon value at that time of year. The electrical load on Dinorwig was set to match the steady state conditions at t = 90s in the record.

Figure 7-6 shows the result for simulated power generation in the middle graph and the simulated system frequency in the lower graph.

At time t = 90, unit #5 is ramped up to generate 288MW and after 20 seconds it reaches its set point. The simulated power and frequency are similar to the measured data. At t = 200s a simulated ramp reduction of load is initiated and the simulation responds in

the same manner as the record with the power system frequency increasing, generation from units #3 and #4 decreasing and a tendency to oscillate with a period of about 14s. By t = 200s the power waveform of all units is distinctly non-sinusoidal and a peak-to-peak frequency variation of 0.12Hz. Observation of the simulated gate vane positions shows that units #1, #2 and #5 are now in a limit cycle with the gate vanes striking the fully-open limits while the simulated turbine inlet pressures show that hydraulic coupling in the common tunnel causes the frequency-insensitive machines to synchronise their power oscillation.

The simulated frequency variation has twice the amplitude of the actual data and this is thought to be due to choosing smaller values for power system size and damping than existed in practice. The sharp edges in the oscillatory waveform of units #1, #2 and #5 are not seen in the record because the actual gate vane saturation characteristic is more gradual than the hard limit used in the simulation [65]. The simulation has identified the basic causes of the phenomenon as a combination of:

- Control saturation.
- Hydraulic coupling in the common tunnel, which causes local interaction between the units and reduces stability margin.
- Large water flow when several units are on-line which again reduces stability margin.
- High values of controller gains K_p and K_i.

Even the existence of this set of conditions does not necessarily induce oscillation – for instance, a large power system size would serve to restore sufficient stability margin to prevent its occurrence – but the limits of the operational envelope are better defined than was previously the case.

7.3.3 Sensitivity analysis

Once the basic phenomenon has been reproduced in the simulation, it is possible to investigate what factors influence its onset. Further simulations were carried out to identify the significance of some of the plant variables on the system response. The only parameters which are directly under the control of Dinorwig power station are the

controller parameters and further simulations were performed to investigate how these affect the response. Three options were considered: (i) changing the droop gain R, (ii) changing the control gains, K_p and K_i and (iii) addition of the derivative term with gain K_d into the power regulation loop when operating with dead-band.

(i) The effect of droop setting

To evaluate the effect of the droop setting the simulation was repeated with the same operating conditions but with the dead-band response units set to a droop of 1% instead of 4%. The simulation result of Figure 7-7 demonstrates that the reduced droop value acts to stabilise the system, as the unit's power output settle to a steady value and the power system frequency is stabilised near its set value. Operating with dead-band on makes the droop a system feedback loop gain which multiplies the power error signal - decreasing its value results in an increased stability margin.

This outcome coincides with an earlier prediction derived from the governor tuning analysis for units with dead-band on (see Section 6.4). It is concluded that, depending on the number of units on-line in this mode, operating with high droop gains causes a reduction of the stability boundaries. Since changing the droop setting is done by the station operator using the control panel, it is now the station operational strategy to bring dead-band units on-line with their droop set to 1%.

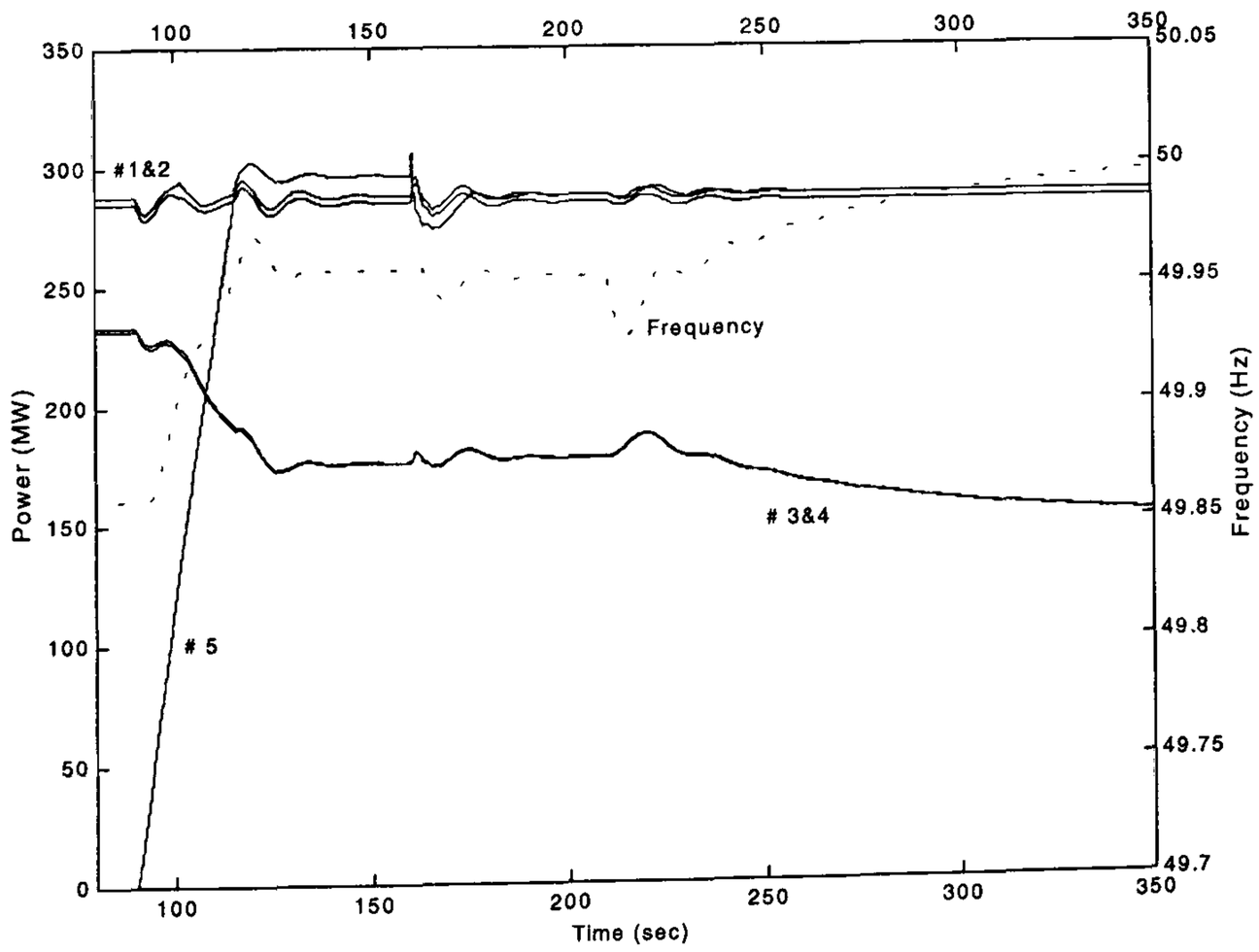

Figure 7-7: *Simulation showing power output and frequency with dead band units operating at droop = 1%*

(ii) Effect of the control gains

The effect of changing proportional and integral gains is shown in Figure 7-8. Here, the simulation is repeated for the same operating conditions with the governor settings for **all** the dead-band units reduced to $K_p = 8$ and $K_i = 7$. The result indicates that decreasing the values of PI gains yields a better stability bound, as the power output responses are asymptotically stable when the gains are substantially reduced. Currently the governor gains implemented are the same for both operations (part-load response and dead-band response) and de-tuning would compromise the commercial obligation to deliver a load change of 34MW in 10 seconds if the frequency falls by 0.1Hz. Thus, it is necessary to use the higher control gains in order to deliver a fast response to fulfil the station's commercial obligations.

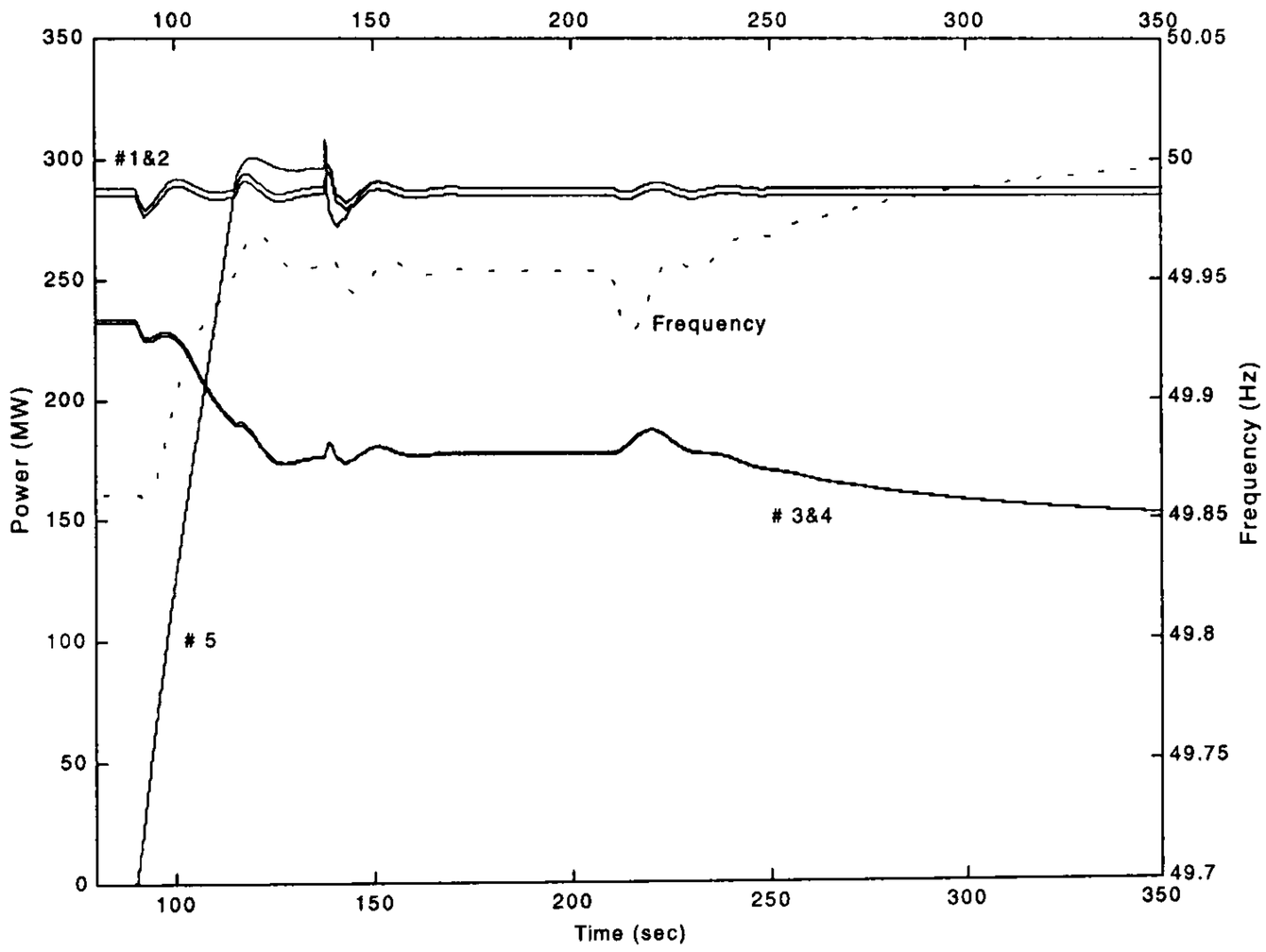

Figure 7-8: *Simulation run for governor gains* $K_p = 8$ *and* $K_i = 7$

(iii) The effect of introducing a derivative term

Derivative feedback is commonly used in conjunction with proportional and integral feedback to increase the damping and generally to improve the stability of the system. Noting once more that a unit in dead-band response mode is governed by a PI controller (the derivative gain being omitted from the power control loop), a derivative term was added to the control loop to form a PID type controller. The simulation was repeated to examine its effect. The results in Figure 7-9 were obtained using an identical operating

condition to Section 7.3.2 but with a derivative gain $K_d = 4$ for all units. It is evident that this will result in a stable damped response. The simulation has established that this action leads to an increase in the damping and, generally, to improved system stability and it is concluded that a PID type governor could be implemented on the speed regulation loop.

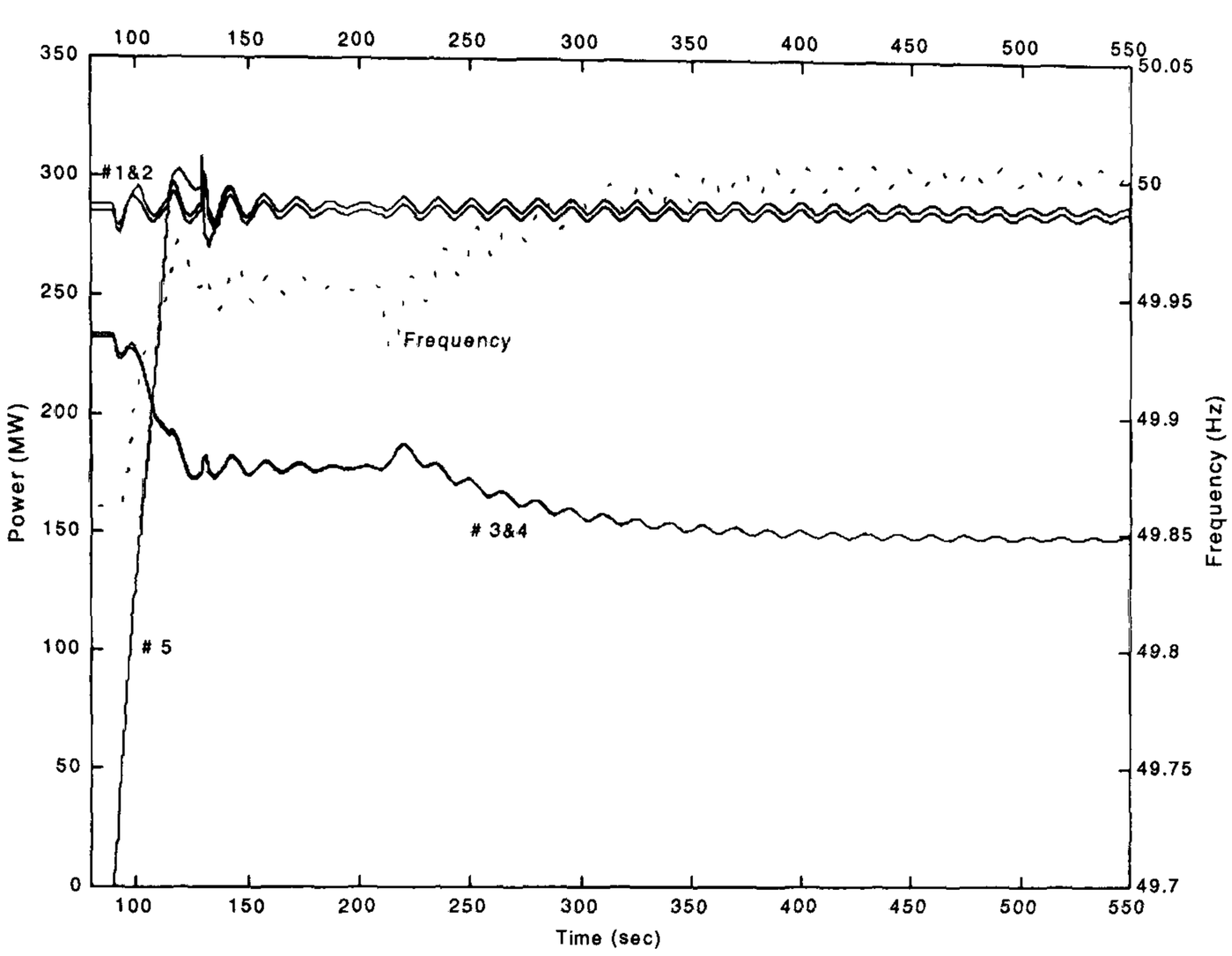

Figure 7-9: *Simulation run using derivative gain* $K_d = 4$

7.4 Power System Stability using the Nonlinear Simulation

As increasing demands are placed by system managers on the operation of Dinorwig there is a need to better define the station, and particularly machine, operating parameters in order to optimise performance under a wide range of power system, and station, conditions. In this context, the performance and setting of the machine governors is of particular importance as these provide the means by which the power produced by any individual machine is varied in response to changes in power system loading and hence in system frequency. However, observations and tests on the governors, for instance during the initial setting up and commissioning, have suggested that there is significant interaction between the governor settings required for optimal performance and the loading on the power system, and hence its stiffness.

Unfortunately, the nature of the station and its plant together with the costs, and indeed risks, associated with carrying out tests on individual machines means that it is not practical to carry out investigations at the level of detail that would be required to establish the optimum governor settings over the full range of system and station conditions. Considering this limitation on testing, the governor settings that have historically been used have tended to be conservative as they are determined based on a relatively limited set of trials during which the governor is adjusted. In order to allow a more comprehensive investigation of the behaviour of the machine governors, and hence to more thoroughly evaluate the interrelationships that exist between governor settings and power system conditions, the simulation has been used to investigate governor and machine behaviour with respect to a range of power system conditions.

7.4.1 Simulation results

The simulation is used to investigate the behaviour of a single unit operating as a frequency regulator (part-load) under a variety of conditions. This allows evaluation of the influence of power system conditions on governor settings. The simulation is conducted with the assumption that the unit is the only frequency regulator in the power system. The total system inertia was set to M = 10, while the load damping coefficient D = 1. The test was repeated to investigate the unit response to changes in the power system loading.

The relationship between the settings of the governor proportional-integral gains and the size of the power system size for stable operation is shown in Figure 7-10. The operational area lies between the low limits and the high limits, and an optimal setting can be chosen between the two boundaries. The low limits characterise a slow stable response based on the prototype ITAE[#] response for pole location (s+1) and the high limits represent a faster response based on prototype ITAE response for poles location at (s+0.7081) (s+0.521±1.068j) [59].

[#] ITAE = Integral of the Time multiplied by Absolute value of Error.

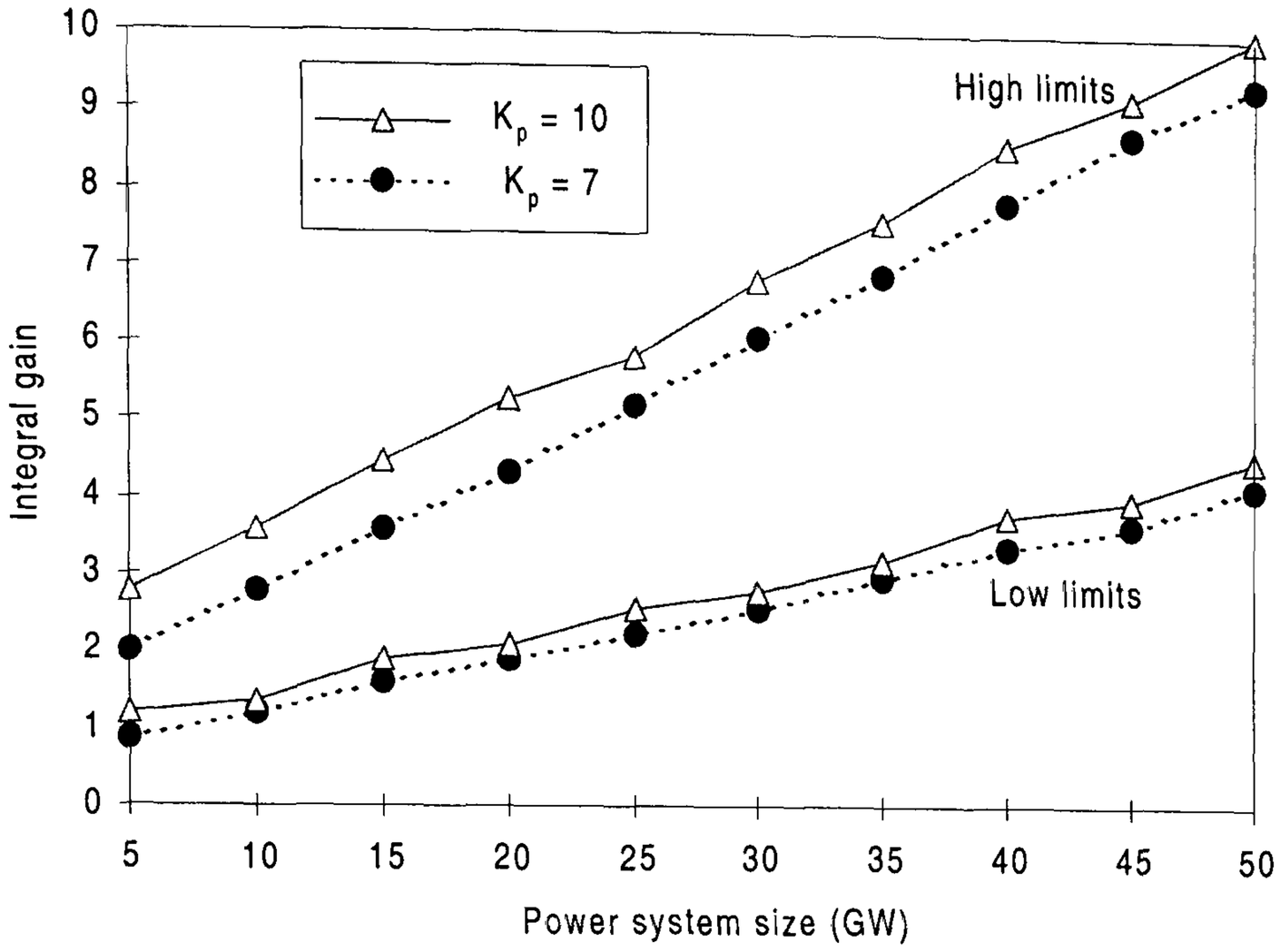

Figure 7-10: Gain limits versus the power system size

The high limits represent the cases when operating with droop setting of 1% and produce fast stable responses with acceptable overshoots. Here the response depends on the power system size and the bigger the system the higher the gains that can be used. Increasing the proportional gain leads to an increase in the integral gain to speed up the response further. However there is a limit to the expansion of the proportional gain, as it causes a reduction in the phase margin if it is increased further, as describe in Section 6.3.2.

Figure 7-11 shows the effect of the power system size on the response of a frequency regulation unit generating 150MW and responding to a 150MW step load change in the power system. The unit is operating with 1% droop and the governor settings were $K_p = 10$, $K_i = 8$ and $K_d = 4$. From these results, it can be seen that a faster rise time is achieved when the power system is lightly loaded but it has a higher overshoot and longer settling time. The size of the power system is therefore a significant factor in determining the response of the unit for any given governor settings [66].

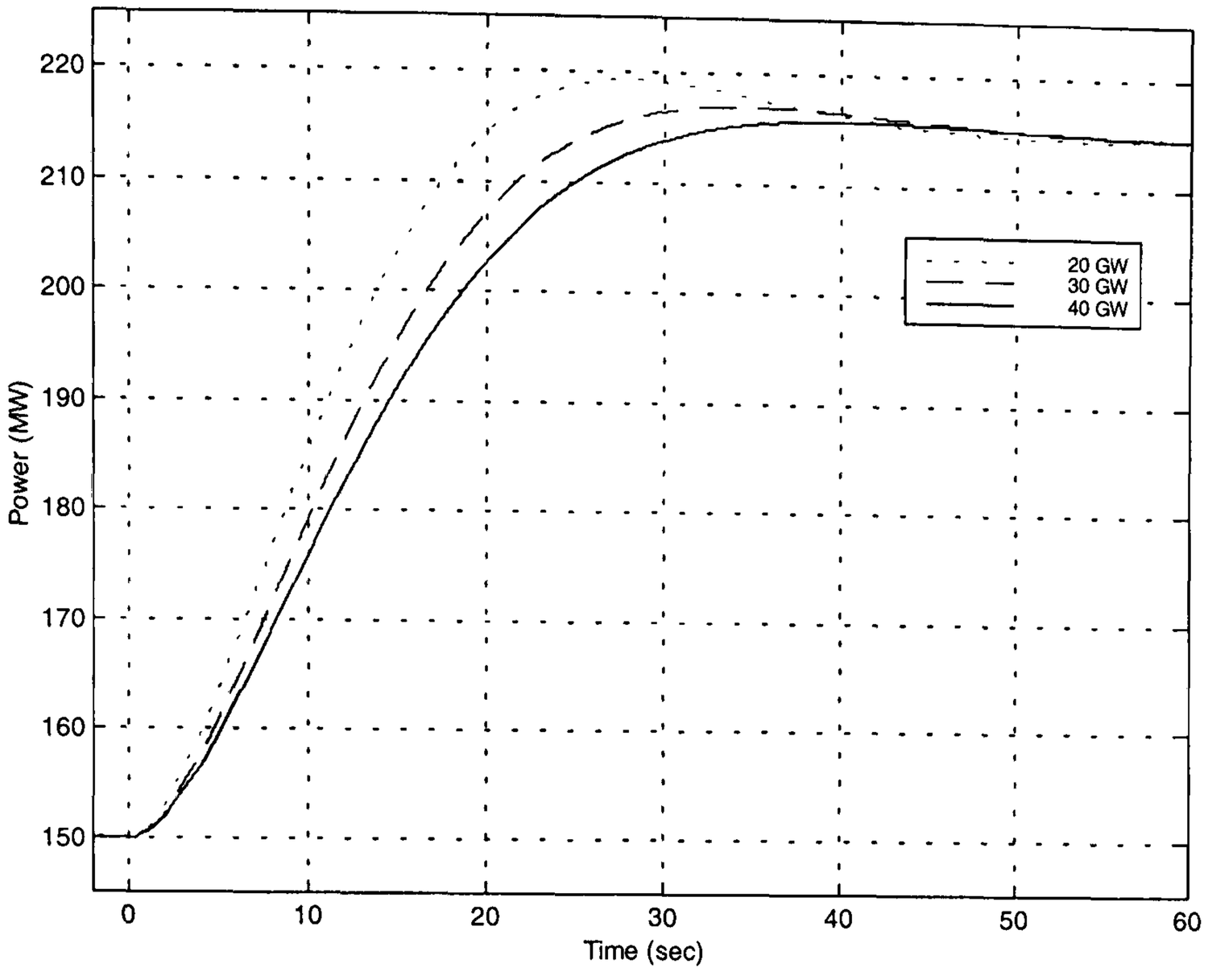

Figure 7-11: *Unit responses as a function of power system size*

7.5 Conclusions

This chapter emphasises the contribution made by the simulation to improving operations at Dinorwig. Three main benefits arise from this exercise. First, a black-start model for Dinorwig was developed which is used to predict the performance of the two units used to provide the initial generation and frequency control needed to restore a shutdown power system. The results indicate that this configuration can act to limit frequency swings to within permitted values for a 15% unit rating load insertions. This regime is currently implemented at Dinorwig for power system restoration.

The second benefit is representation of observed behaviour of the station under certain operating conditions where the interactions between the units resulted in oscillatory variation of power output. The major conclusions regarding the simulation of the pressure oscillations at the turbine inlet are:

- The results of the simulation reflect the recorded responses of the real system.
- The droop settings of the operating units have a significant effect on the response of the power station. Using a lower droop value tends to stabilise the overall response of

the station. The oscillation are more likely to occur when more than one unit is set to operate with a droop of 4% and is near full load.

- Adding a derivative term to the governor loop when operating with a dead-band tends to reduce the oscillation and make the system more damped.

- The onset of oscillatory behaviour is sensitive to the water time constant of the common tunnel. Since it occurs when the water time constant is that corresponding to more than three units online, it suggests that the governor gains should be scheduled according to the number of unit on-line.

The third application is a nonlinear simulation based stability analysis and the results obtained from the simulation have been demonstrated to produce an evaluation of the link between power system size and the unit governor settings when operating as a frequency regulator. The response is influenced by the power system size and the gains should be adjusted accordingly. To fulfil the station's commercial obligation, high gain settings are required to speed the response but this causes higher undesirable overshoots and therefore, a compromise should be made between the two. Because of this investigation, governor gain scheduling with regard to the power system size is planned for the future. This is subject to the availability of the power system-loading conditions from the NGC.

Chapter 8

Hardware-in-the-Loop Simulation

8.1 Introduction

The final goal of this work is the implementation of real-time control applied on the station model using an actual station governor, giving so-called *hardware-in-the-loop simulation* (**HIL**). Working with HIL includes both the capability to model the system entirely as a simulation " off-line" as well as being able to use **real** components running on-line in parallel with simulations of other components.

The chapter begins by describing real-time control of the plant model with the **model** governor. The model governor is subsequently replaced with a real governor from Dinorwig, which is used to control the simulated plant in response to changes in the system conditions. It is then possible to compare the response using the real governor with that of the off-line simulation both to further validate the model and to establish the optimum settings for the governor under a range of operating conditions before these are tested on the power station itself [67].

This is similar to the approach of Throckmorton [68] who developed a model-based DSP real-time simulator that can be used to evaluate the performance of the speed governor and the effect of the sampling time on quantisation errors. However, Throckmorton's simulator is based on the simulation of two linear models in real-time and was not connected to plant hardware. The advantage of the HIL arrangement is that

the real behaviour of that part of the system is obtained without assumption or approximation.

8.2 Real-Time Systems

Real-time systems are those in which the correctness of the system depends not only on the logical results of computation but also on the time at which the results are produced. Typically, a real-time system consists of a controlling system and a controlled system. A computer based controlling system interacting with real-world plant is based on the information from various sensors and inputs which measure the actual state of the plant. The information presented to the computer must be consistent with the actual state of the environment, or the actions of the controlling system can be disasters. In many real-time systems, severe consequences result if the timing and logical correctness requirements of the system are not satisfied. The timing correctness requirements arise from the system's role as a controller. For example, in the case of Dinorwig, if the computer controlling the actuator does not command it to stop at a certain position on time, the unit will generate more power than required due to the guide vane opening. This makes the periodic monitoring of the environment and the timely processing of the data an essential.

A real-time system must be able to handle time constraints which are commonly divided into two categories: hard real-time systems and soft real-time systems. In hard systems, timing correctness is critically important and may not be sacrificed for other gains. In some cases, the timing correctness may be so important that criteria on logical correctness may be relaxed in favour of achieving timing correctness. In soft real-time system, time correctness is important but not critical. An occasional failure to observe it should not result in serious consequences. Soft real-time tasks are performed as fast as possible, but are not constrained by absolute deadlines, and their timing correctness may be sacrificed under special circumstances such as peak demands on the processor or the communication medium [69].

The most common timing constraints for tasks are either *periodic* or *aperiodic*. An aperiodic task has a deadline by which it must finish or start, or it may have a constraint on both start and finish times. With a periodic task, a period might mean "once per period T" or "exactly T time units apart".

8.3 Development of the Real-Time HIL System

The system is built using the dSPACE® real-time environment, which is based on a dSPACE I/O board allowing the processor to interact directly with the sensors during real-time simulation. The real-time interface tool (RTI) connects Simulink and the Real-Time Workshop (RTW) with dSPACE's real-time systems to form a ready-to-use environment for real-time applications. The RTI runs through all steps necessary to prepare the application for the real-time test. The last step loads the application into the dSPACE processor. The RTW is used to convert the Simulink models to real-time C code and automatically builds programs that can be run from the real-time system environment. The RTW includes a tool called the Target Language Compiler (TLC), which works as a text processor used to transform an intermediate form of a Simulink model (*.rtw) and the target files (*.tlc)[#] into C code. The program is then loaded into the real-time target, the DS1102 control board that is built around the Texas Instruments TMS320C31 floating-point DSP processor. Figure 8-1 describes the relationship of the dSPACE system [70] and the Matlab development software [46].

When operating in real-time the DS1102 board allows the variables to be transferred between the controller and the controlled system using the A/D and D/A converter. The resolution of D/A converter was set to 14 bits to obtain a resolution of ± 1 Bit in 16348, while the A/D resolution was set to 16 Bit that gives ± 1Bit in 65536. The RTI generates a file with references to signal and parameters, which gives easy access to the dSPACE software such as Cockpit and Trace.

The Cockpit (Virtual Instrument Panel) software gives a high degree of user control over the real-time experiment. It allows the user to modify and display all the variables represented in a processor or controller board memory, including Simulink block inputs/outputs and block parameters. Trace is a data acquisition and variable display tool, which tracks all variables on a dSPACE processor without interrupting the real-time application, including Simulink block inputs/outputs and block parameters.

[#] Target files are set of files that are interpreted by the TLC to transform RTW code (*.rtw) into C code.

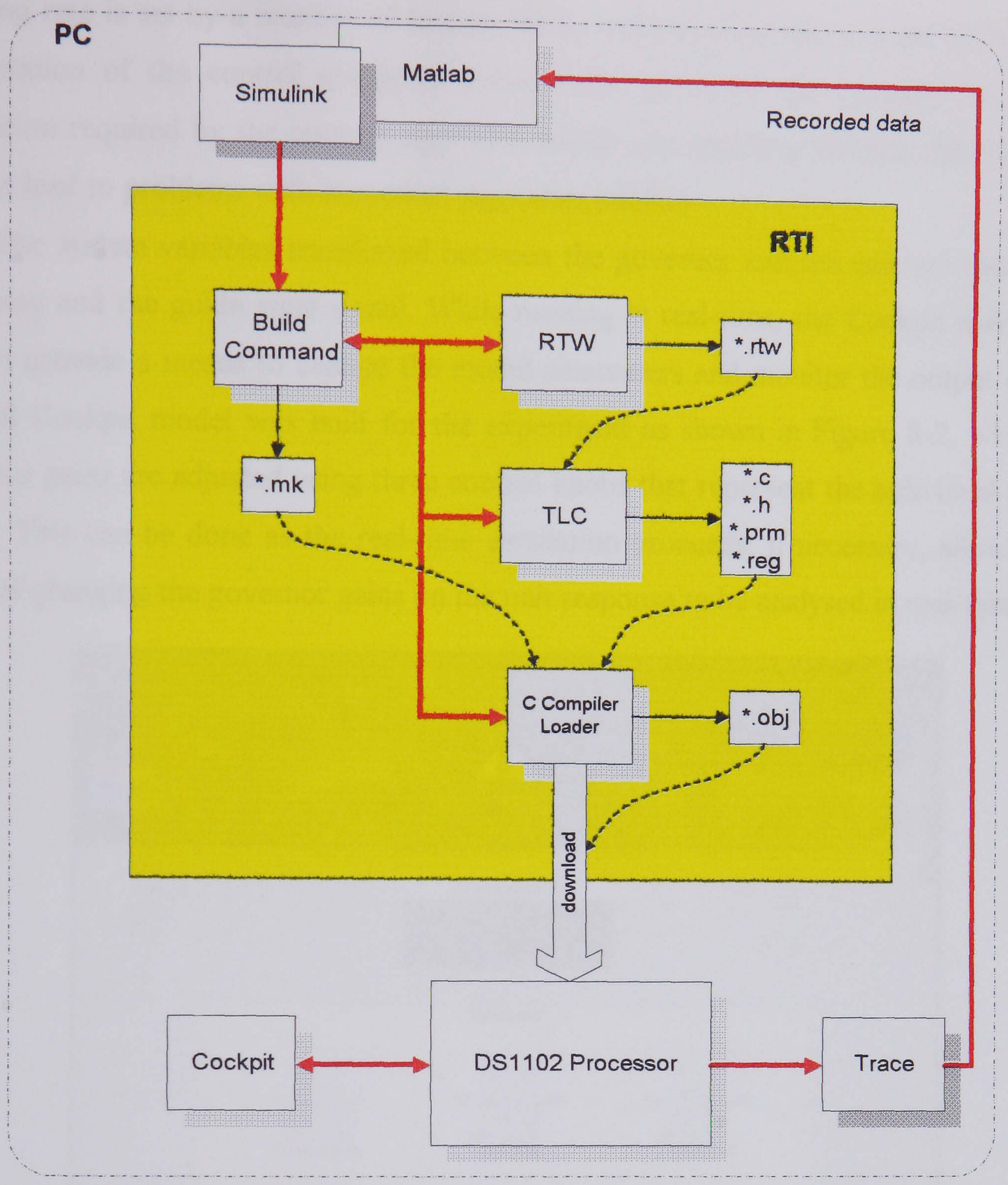

Figure 8-1: *Development of DSP real-time system*

8.3.1 Real-time implementation using models for the governor and unit

As a preliminary to proper HIL simulation, real-time closed loop control of a single generating unit supplying an isolated load was implemented using simulink **models** for both the governor and unit. This test is conducted to evaluate the effect of the computer-sampling rate on the unit response when operating in real-time. This is done to ensure that the sampling rate is short enough for accuracy of the response. An appropriate limit to the

sampling rate is set by a number of factors. First, a physical limitation is set by the speed of operation of the control computer because the processor has to carry out all the calculation required by the control algorithm within one sampling interval. Sampling too fast can lead to problems with numerical algorithm stability.

The system variables transferred between the governor and the unit are the system frequency and the guide vane signal. While running in real-time, the Cockpit software is used to provide a means to change the model parameters and monitor the output signals. A small Cockpit model was built for the experiment as shown in Figure 8-2, where the governor gains are adjusted using three control knobs that represent the individual control action. This can be done as the real-time simulation proceeds, if necessary, allowing the effect of changing the governor gains on the unit response to be analysed in real-time.

Figure 8-2: *Cockpit instrument panel*

The power generated by the Unit was displayed using a digital indicator. The Trace software was used to monitor the power generated and the frequency of the unit in addition to the guide vane position and the controller output signal as the simulation progressed.

8.3.2 Test results

A single unit model of the station based on the nonlinear representation of the water column described in Section 5.2.1.2, and a standard Dinorwig governor model were used in this experiment utilising an isolated operation governor gain settings $K_p = 2.5$, $K_i = 0.8$ and $K_d = 4$. The first step in moving towards a real-time simulation was the selection of the solver and its step size. The first attempt was a simple first order integration algorithm (Euler) with fixed step size selected as 0.1s.

The real-time and off-line simulation responses to a 30MW step load change were compared. Figure 8-3(a), shows the responses of both runs where it can be seen that there are some discrepancies between the two responses because of the choice of the solver and integration time. This problem was corrected by choosing an ode5 (Dormand-Prince) solver and adjusting the step size to 100μs which gives good agreement between the real-time response and the off line simulation as shown in Figure 8-3(b). These solver type and integration step sizes were used in subsequent tests.

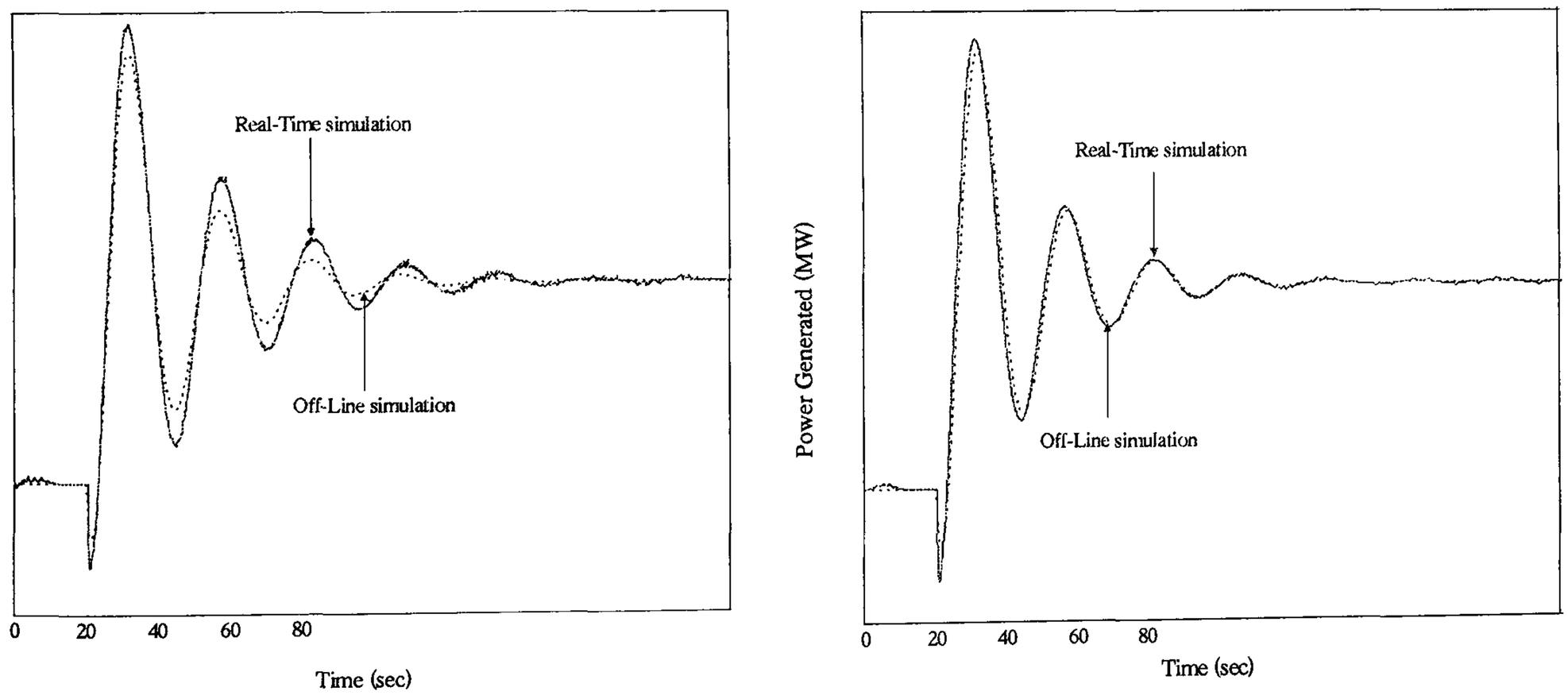

Figure 8-3: *Responses of a single unit connected to an isolated load*

The effects of the governor-sampling time during the real-time simulation on the unit response were also investigated by trying different sampling times. The results shown in Figure 8-4 reveal that the value of 50ms currently in use at Dinorwig gives good agreement with the offline simulation. However, sampling at slow rates such as 0.3s the response is unstable.

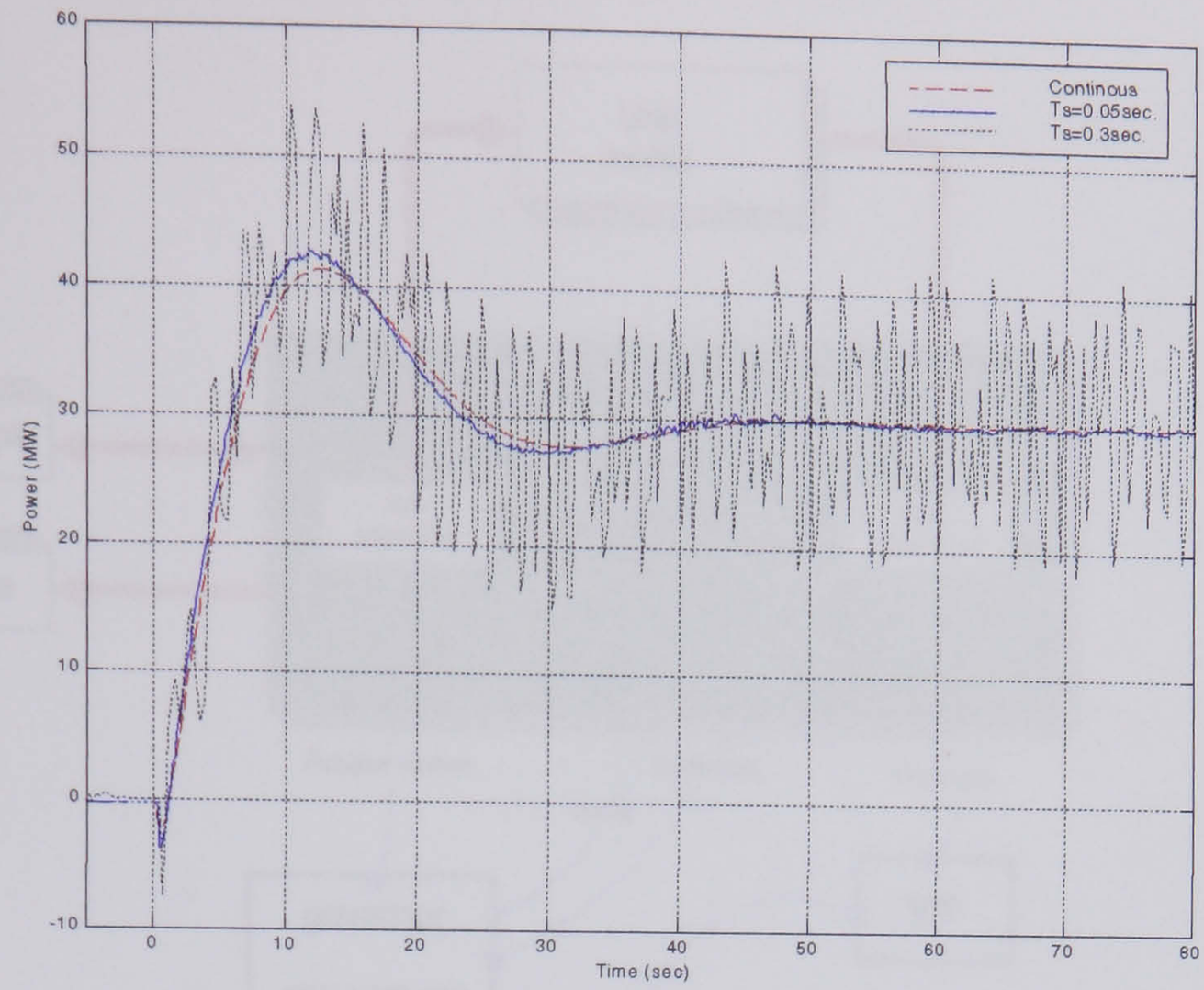

Figure 8-4: *The effect of the sampling rate on the unit response*

8.3.3 Connecting the real governor to the plant model

The next stage was to utilise a spare governor (type ABB-HPC 640) identical to the one used in operation at Dinorwig to control the unit model. The governor was loaded with the latest version of the PC diagram control algorithm program [42] Figure 8-5 shows the system setup, where a power system frequency signal is generated from the model and fed into the governor via the voltage/frequency converter mentioned earlier (Section 4.3.1). The governor output control signal corresponding to the actuator position is fed into the model to regulate the generating unit. Two additional signals are fed back to the governor directly from the model. The first represents the total power generated by the unit and the second is the guide vane position to complete the feedback loop of the governor hardware. This configuration allows the governor settings and the effects of modifying the governor strategy on the system responses to be investigated.

One of the key steps in modifying the model itself towards a real-time HIL implementation was definition of the signals that must be passed to and from the real governor via the dSPACE I/O board. This was a relatively simple task in principle but one which was complicated in practice by the need to fully understand the voltage and current signals associated with the governor.

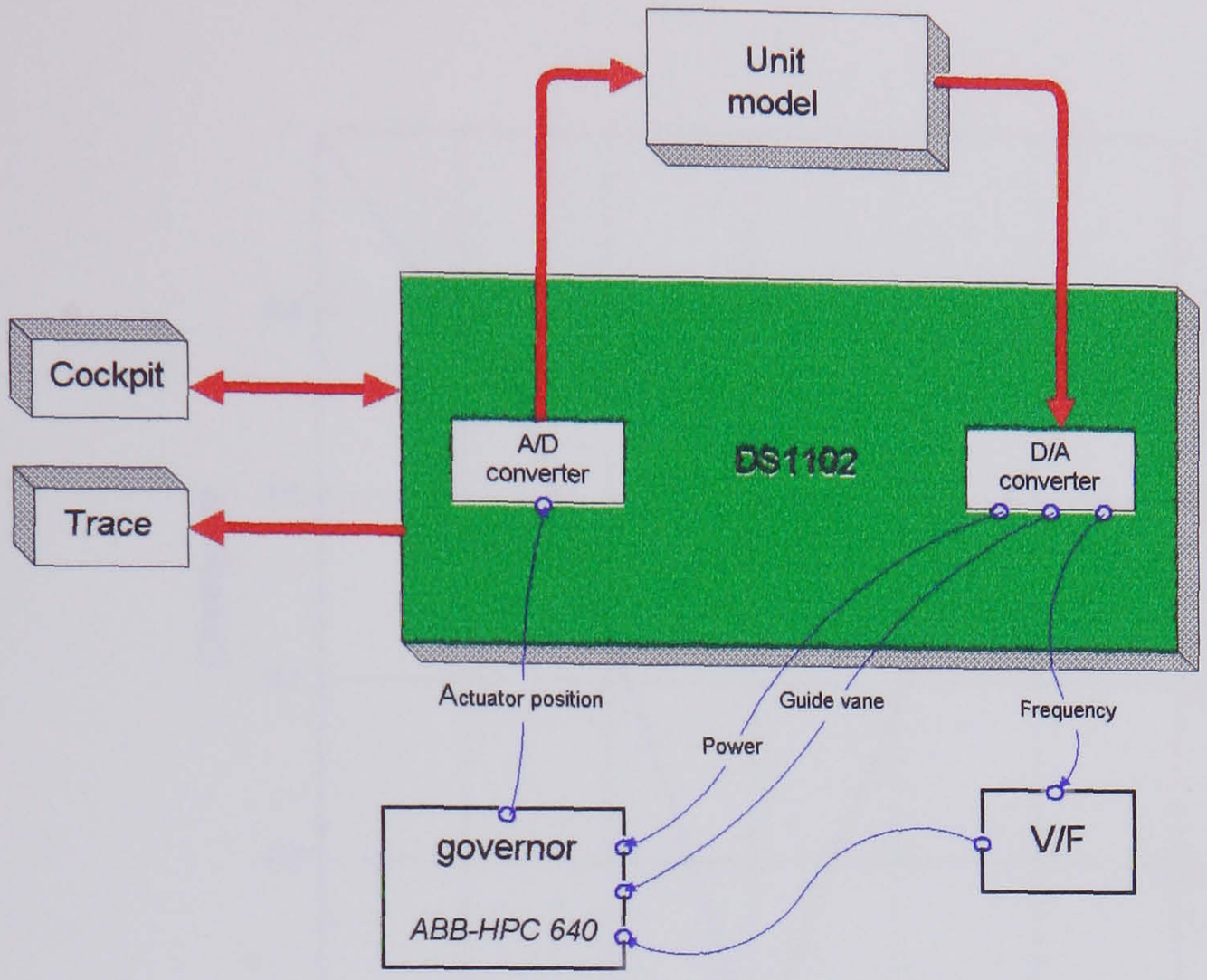

Figure 8-5: *Real governor control configuration*

The governor output is a ±10V analogue signal corresponding to the actuator servo being fully closed to fully open. In practice, this signal is later converted to a ±60mA current signal to control the actuator servo valve. The guide vane opening and closing rates depend on the servo valve characteristics (opening/closing rates), which were obtained by conducting a test on Unit #1, by applying voltage signals into the servo valve and calculating its opening and closing rates. The results are shown in Figure 8-6, which indicates that the closing rate is faster than the opening rate and when the current signal is near ±2mA, the servo will be moving at a very slow rate (near standstill). Thus the actuator servo signal normally operates near zero current and when an extra load occurs on the system the current value will increase and the servo will start opening at a rate dependent upon the current until the guide vane reaches its required position and the control signal is decreased to near zero current. A similar action occurs when the guide vane closes, the only difference being that the current sign will be negative and a faster closing rate. It was therefore necessary to modify to the unit actuator model to accommodate these servomechanism characteristics by adding an additional Simulink block called "actuator signal conversion" as shown in Figure 8-7, which is a lookup table

corresponding to the opening/closing rates dependent upon the input signal from the governor.

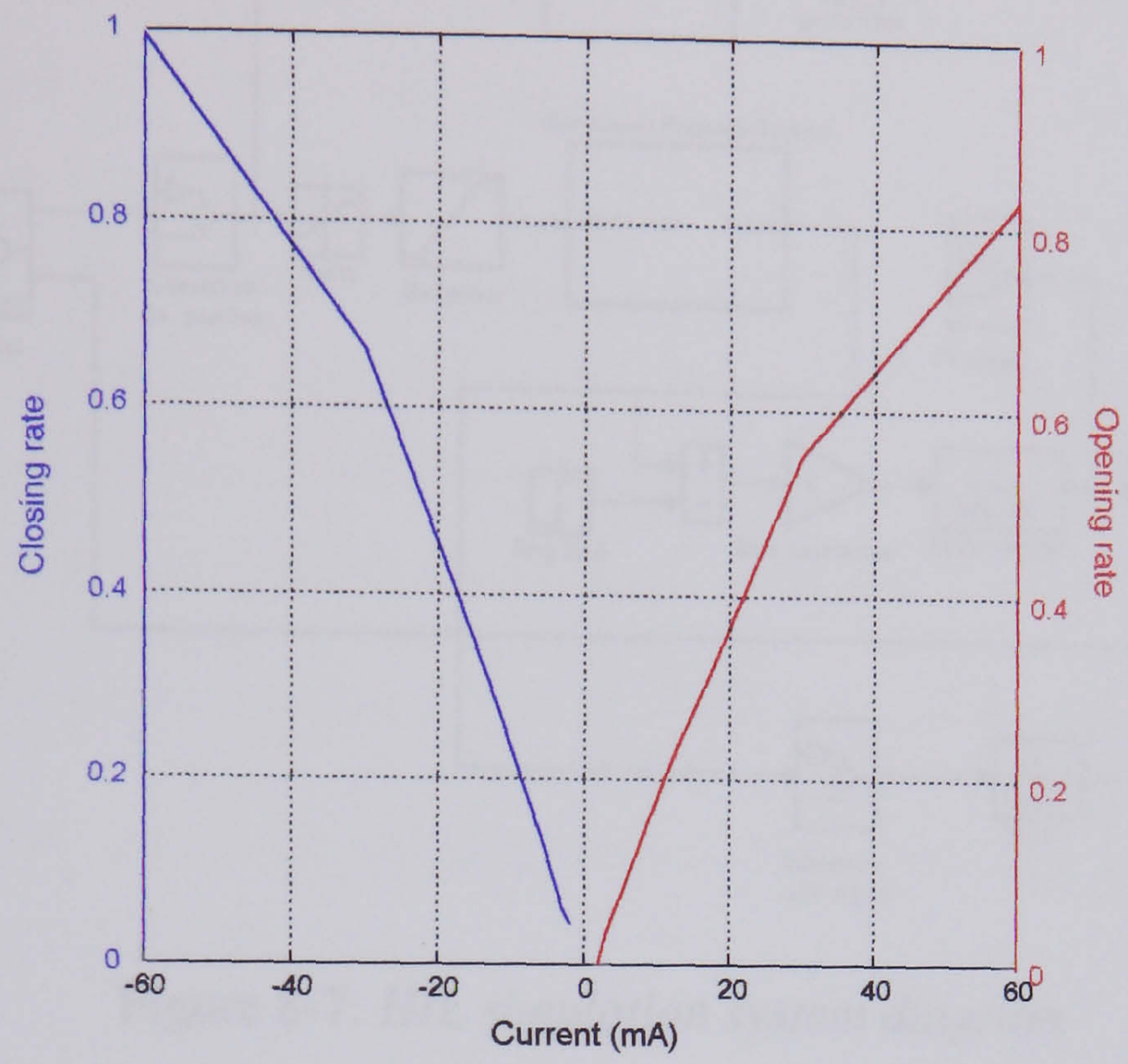

Figure 8-6: *Servo valve characteristics*

The power system frequency signal into the governor was obtained from the model via the DAC #1, which is connected to the V/F circuit to convert it to a pulsed frequency signal. The 5V supply block produces a signal equivalent to 50Hz frequency and the frequency deviation in the Power System due to changes in loading conditions is added to it. The actuator position signal that is fed back to the governor is ±10V and this is obtained directly from the model (±1 in Simulink = ±10V analogue). Meanwhile the power value generated by the 'Nonlinear Penstock Turbine' block unit is converted to a ±2V signal then passed through a power transducer filter and connected to the governor via DAC #3. Since the power generated in the model is based on the per unit format, a "pu/MW conversion" block is used to display it in MW's.

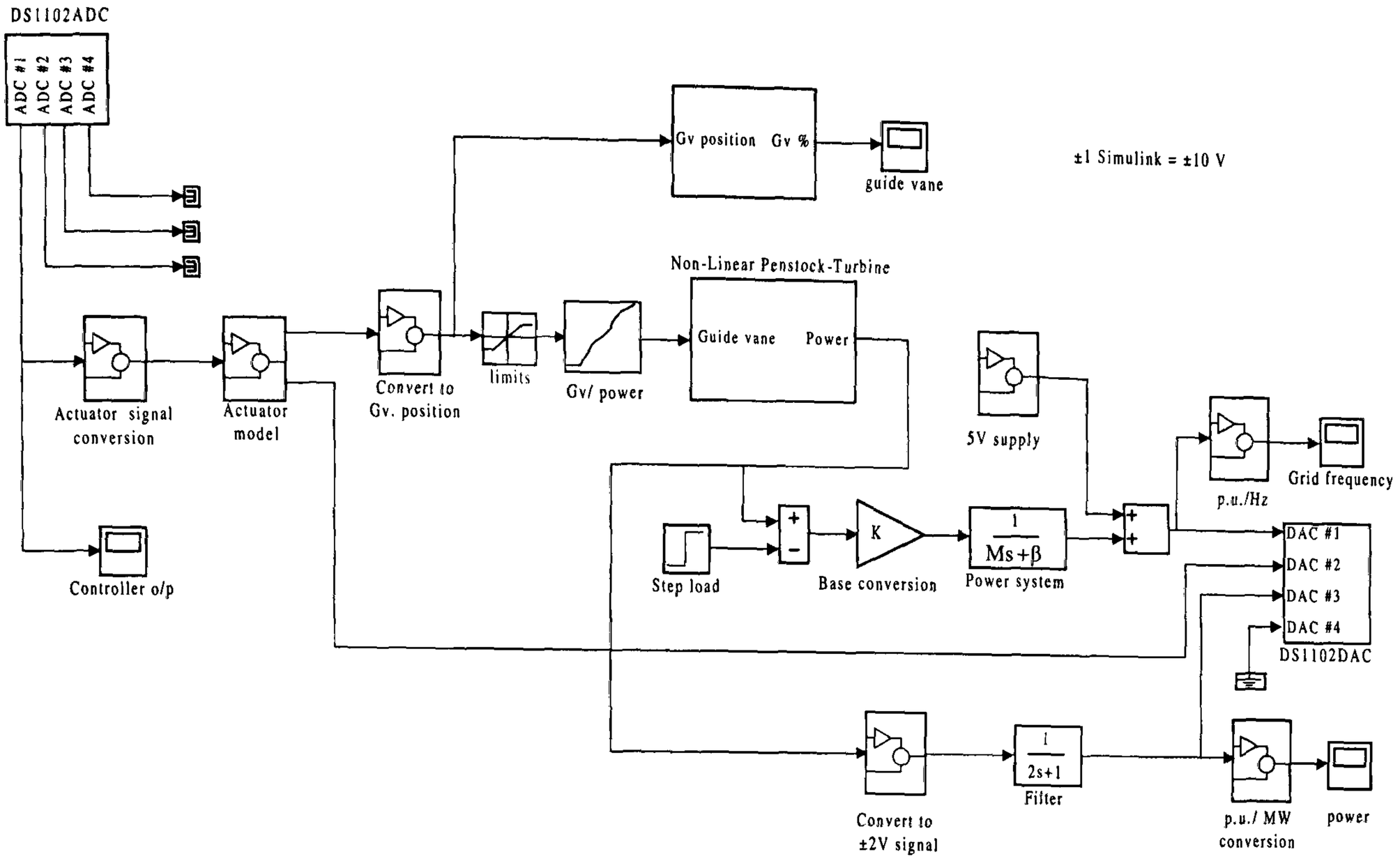

Figure 8-7: *HIL simulation system diagram*

8.3.4 Test results

Once the model and its interfaces were developed within SIMULINK®, it was a straightforward task to build the real-time code and download it to the DS1102 board. With the real-time program running on the dSPACE® hardware connected to the real governor via interface mentioned earlier, it was possible to exercise the functionality of the governor. The test was conducted on a plant model with the nonlinear representation of the water column with multiple penstocks as described in detail in Section 5.2.2. The investigation was based on three units connected to the power system, two of which are operating near full load with deadband on and speed droop of 1%. The third is used as a test unit to analyse its response to system parameter changes for a variety of operating conditions.

The equipment setup is shown in Figure 8-8 where the Trace software was used to monitor the system responses such as the power, frequency, the actuator position and the control signal from the governor. The touch-sensitive screen control panel, identical to the one used by the station operator in the control room, was linked to the governor to alter the system variables such as the power and frequency references in addition to the speed droop setting. The control panel is also used to display the system frequency, the unit

power generated, the guide vane position and the system operating limits. It is also used to add/remove the deadband in the control loop.

Tests were carried out for typical power system arrangements with total load capacity of 35GW at 50Hz, with load varying 1% for every 1% change in the frequency (D = 1). The system has 1000MW of spinning reserve and only 10% of the total generation is from units operating as frequency regulators, with their droop set at 4%. The rest of the generators are operating with valves wide open. Operating with this configuration, the generation contributing to the regulation is equal to 3600MW and using equation (3.22) the system composite frequency response characteristic (stiffness β) is equal to $2500\frac{\text{MW}}{\text{Hz}}$, which represents $3.57\frac{\text{p.u.MW}}{\text{p.u.Hz}}$. The power system total inertia used in the simulation (M) was set to 10s and the hydraulic system parameters were obtained from Table 2-1 and Table 2-2.

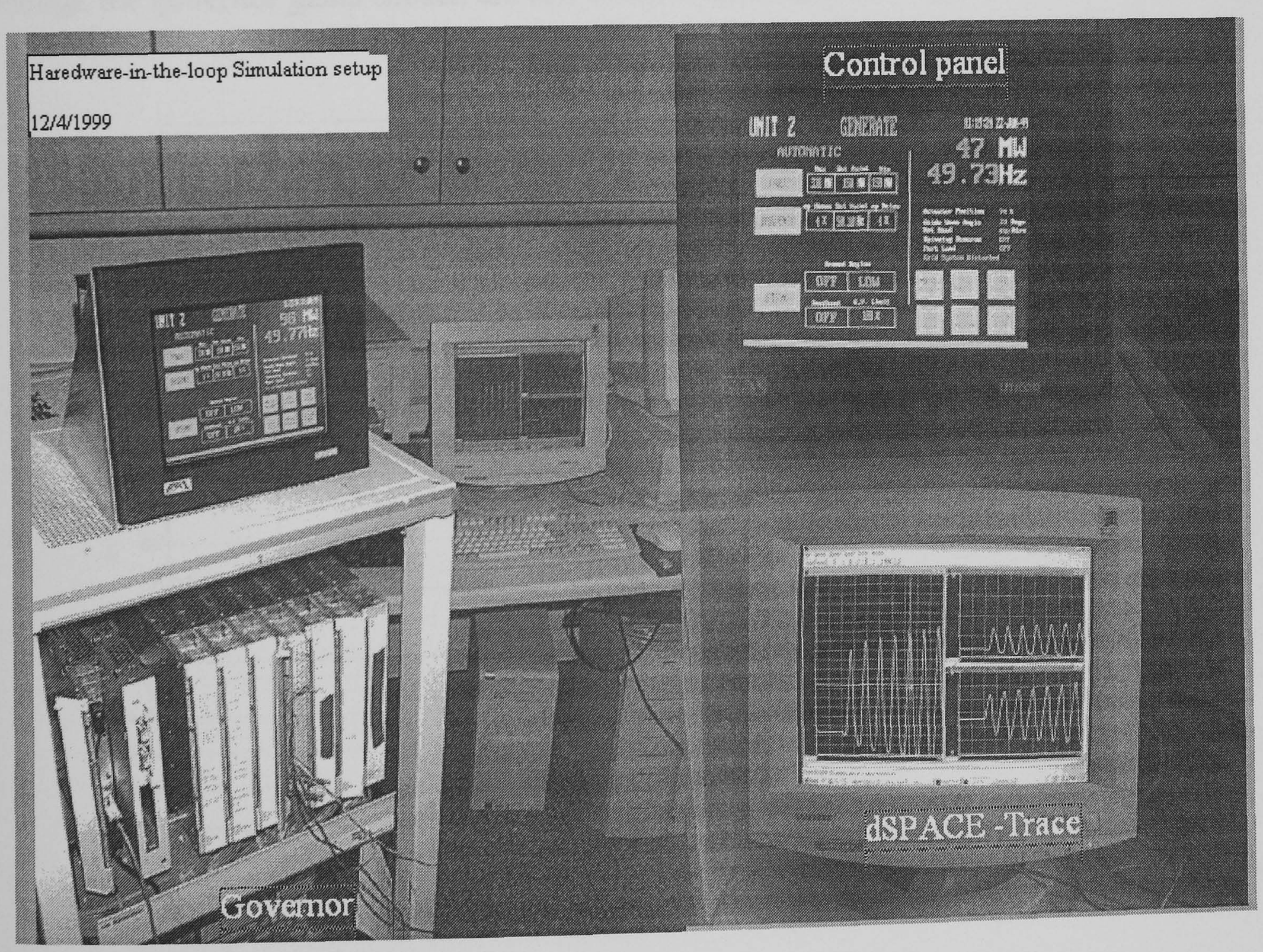

Figure 8-8: *Test equipment*

The first test was to study the deadband response of the unit being instructed to increase the generation from 150MW to 288MW. Successive runs were performed for different operating conditions using the gain schedule shown in Table 8-1, which represents those in current use at Dinorwig.

Table 8-1: Unit parameters

	Droop	K_p	K_i	K_d
Case-1	4%	7	3	4
Case-2	1%	10	8	2

Figure 8-9 shows two cases of simulation runs, case-1 using 4% droop and case-2 using 1% droop with their corresponding gain schedules. It clearly demonstrates that using high droop gain with a deadband on will prompt the response to be very active even though the governor gains chosen are low compared to case-2.

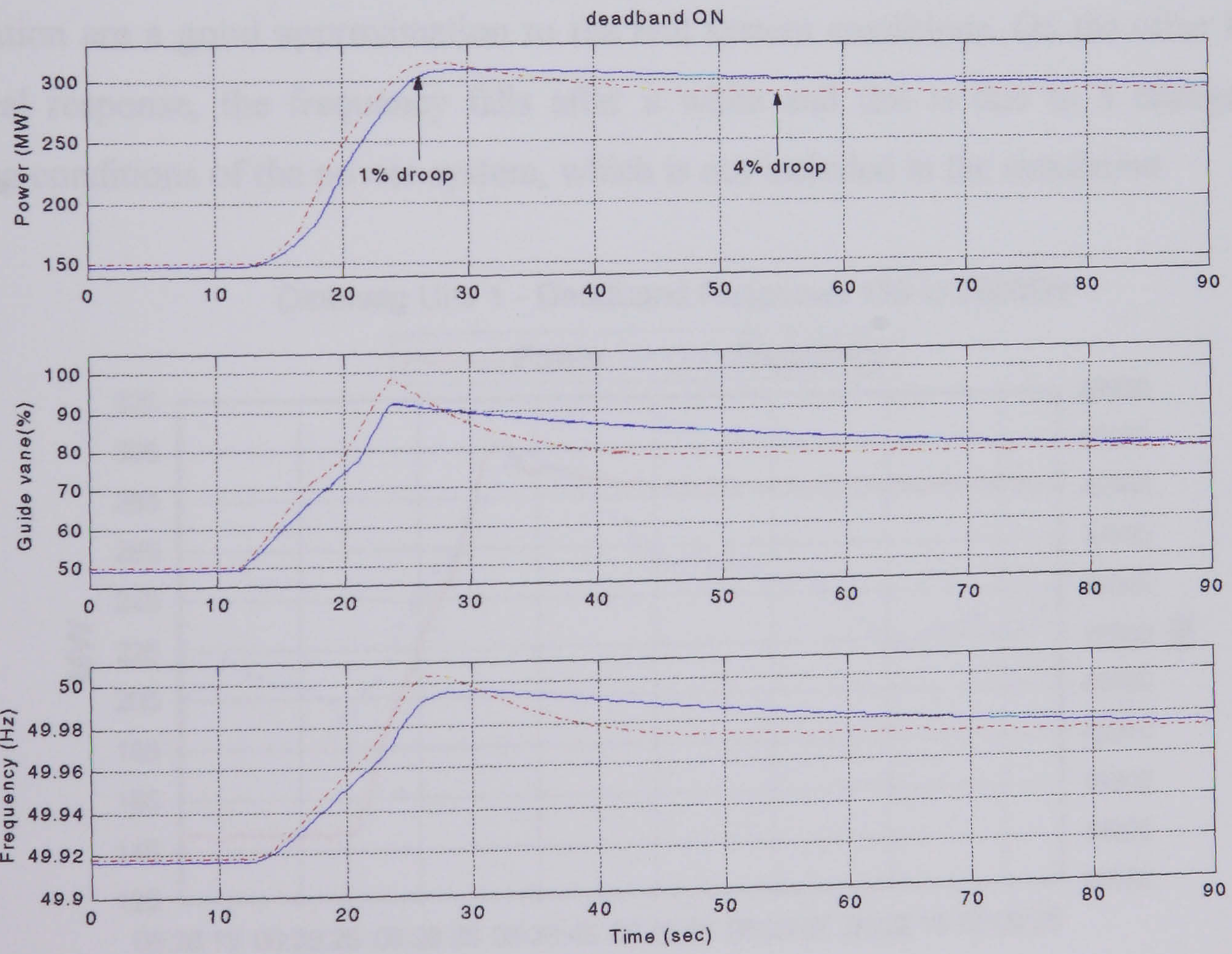

Figure 8-9: *Unit deadband responses*

There are some benefits associated with this as the response rise time and the settling time are faster, but there are disadvantages too which are the high overshoots which, in certain operating conditions, may lead to instability (as discussed in Section 7.3). In both cases, the frequency is boosted by a value of 0.054Hz, which can be calculated from the composite frequency response characteristic (β).

A measured response of Unit #1 operating at 4% droop with deadband on is shown in Figure 8-10, the Unit is generating 150MW and at time 06:28:30, it is initiated to increase the generation to 288 MW. The response rise time is about 9 seconds and the time taken to reach the maximum overshoot $T_p \approx 12$ seconds while the ±2% settling time is about 25seconds. Comparing this response with the simulated response of Figure 8-9 clearly shows the similarity between the two. However, there are some discrepancies between the two especially in relation to the size of the overshoot. In the actual response, the power overshoots by 12MW while the simulated response overshoots by 20MW. As far as the power system frequency is concerned there is about 0.05Hz boost in the frequency in both responses which verifies that the power system parameters used in the simulation are a good approximation to the real system conditions. On the other hand, in the real response, the frequency falls after a while and this is due to a change in the loading conditions of the power system, which is not included in the simulation.

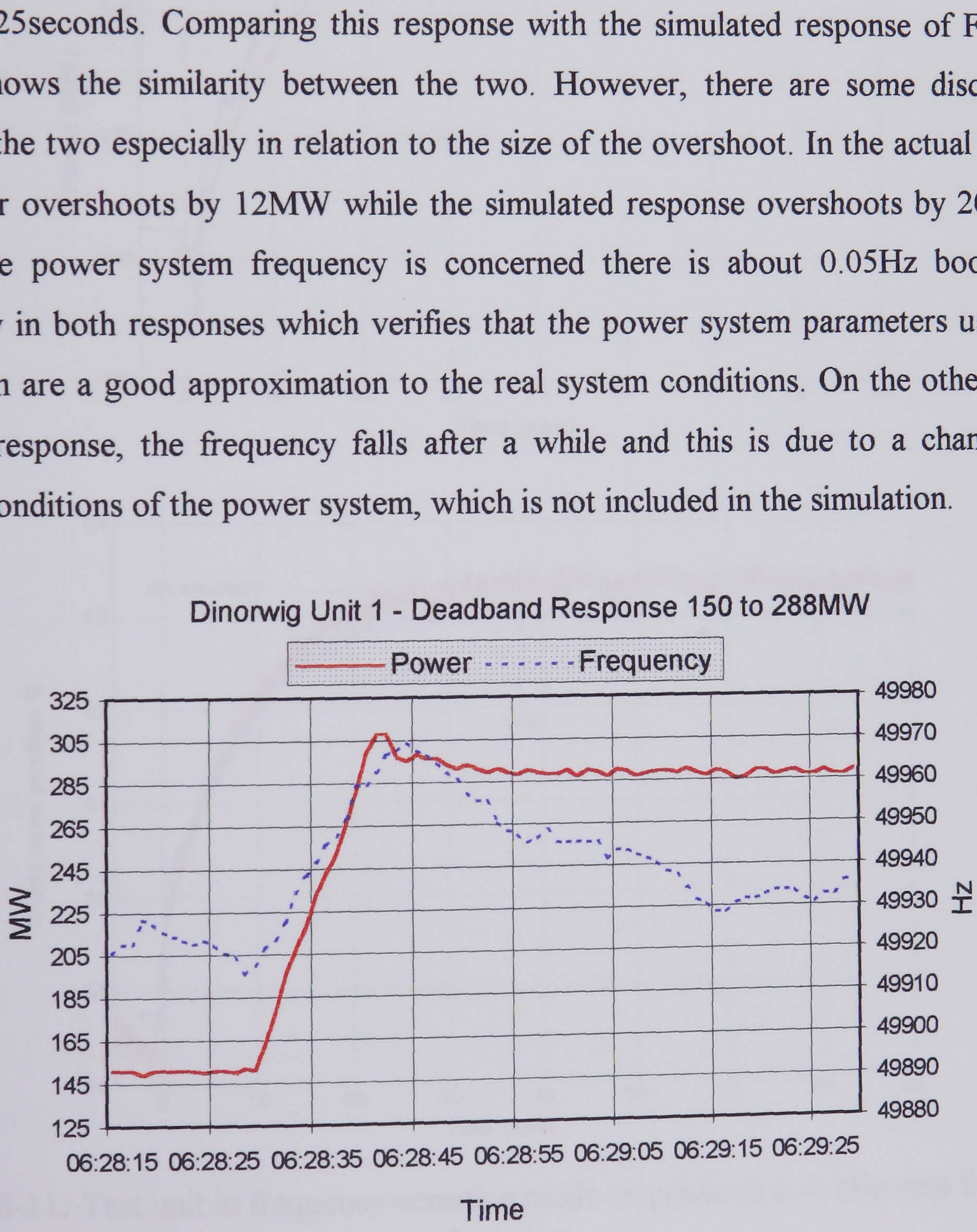

Figure 8-10: *Unit #1 deadband response 150MW – 288MW*

The system is used to investigate the plant dynamic frequency response[#]. In this case, a step frequency error signal of – 0.1Hz is inserted into the governor frequency-control loop in the HIL simulation. The unit under test is initially loaded at 230MW and operating with 4% droop but now the deadband on the grid frequency measurement is NOT included. The results shown in Figure 8-11 exhibit very good agreement between the measured and simulated responses.

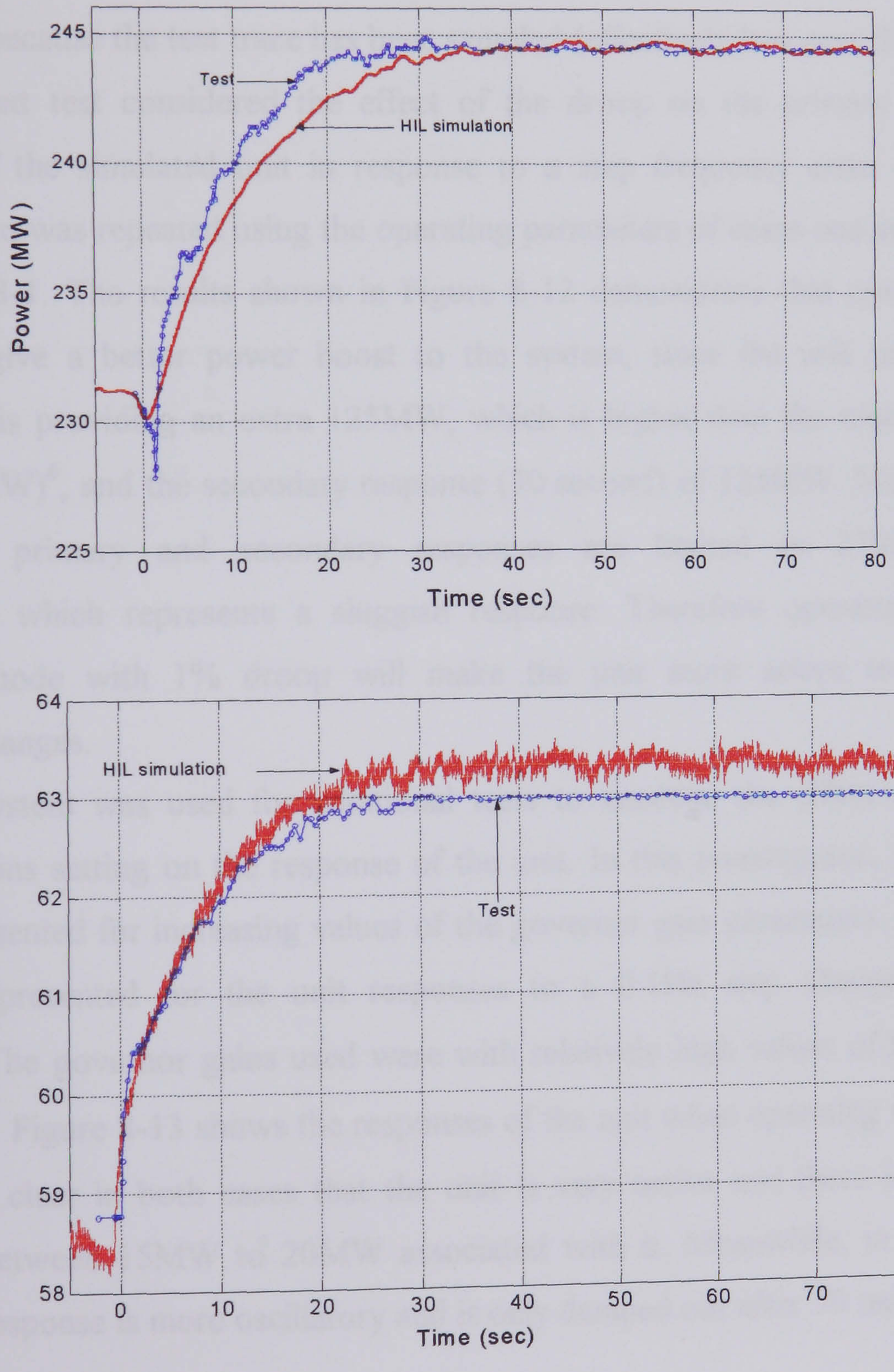

Figure 8-11: Test unit in frequency-sensitive mode response to a -0.1Hz step frequency deviation

---

[#] This represents the test described in Section 5.3.4 to establish Dinorwig frequency response capabilities.

Both exhibit the initial non-minimum phase drop in generated power as the guide vane begins to open although the measured drop is more pronounced than predicted by the simulation. This is followed by a load pickup of 13MW occurring over the next 25 seconds, while the guide vane opens from 58.5% to 63.8%. Note the noisy fluctuation on the guide vane position signal which is absent in the off-line simulation; this is partly due to chattering in the actuator characteristic's deadband and partly due to noise in the electronic hardware. This actually occurs in practice too although this is not shown in Figure 8-11 because the test trace has been sampled (effectively low pass filtered).

The next test considered the effect of the droop on the primary and secondary responses of the simulated unit in response to a step frequency error of -0.3Hz. The simulation run was repeated using the operating parameters of cases one and two obtained from Table 8-1. The results shown in Figure 8-12 demonstrate that operating with 1% droop will give a better power boost to the system, since the unit primary response (10 second) is providing an extra 125MW, which is higher than the requirements of the NGC (111MW)[#], and the secondary response (30 second) of 125MW. Meanwhile the 4% droop unit primary and secondary responses are limited to 27MW and 43MW respectively, which represents a sluggish response. Therefore operating in frequency regulation mode with 1% droop will make the unit more active to power system frequency changes.

The system was used for additional tests to examine the effect of changing the governor gains setting on the response of the unit. In this investigation, three simulation runs are presented for increasing values of the governor gain parameters. In the first two, results are presented for the unit responses to a 0.1Hz step change in the system frequency. The governor gains used were with relatively high values of $K_p = 10$, $K_i = 12$ and $K_d = 10$. Figure 8-13 shows the responses of the unit when operating with 1% and 4% droop. It is clear in both cases that the unit is very active and there is an undesirable overshoot between 15MW to 20MW associated with it. Meanwhile, in the case of 4% droop, the response is more oscillatory and is only damped out after 50 seconds.

[#] This value is obtained from the FHC contract with NGC.

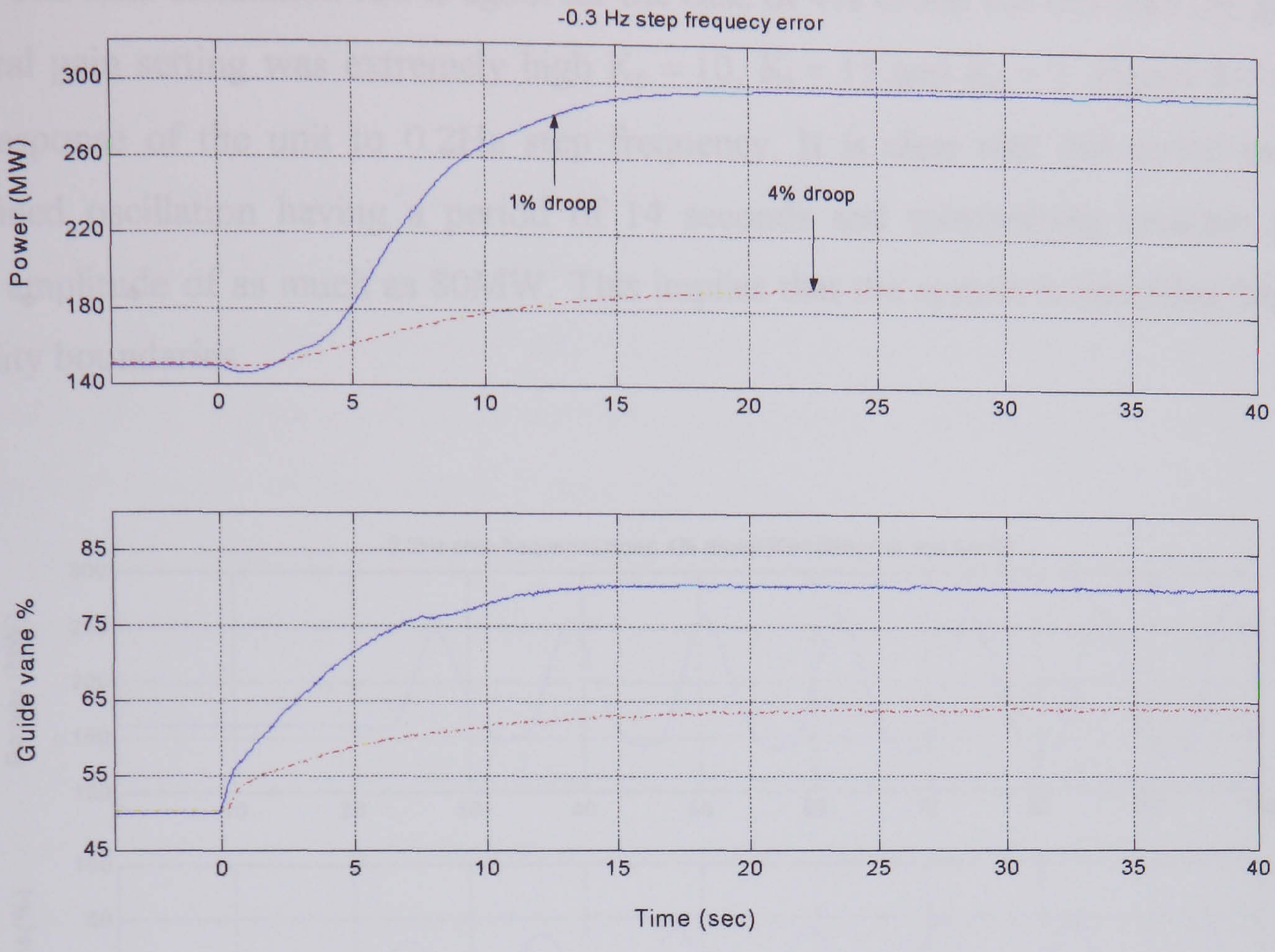

Figure 8-12: *HIL simulation response to -0.3Hz step frequency*

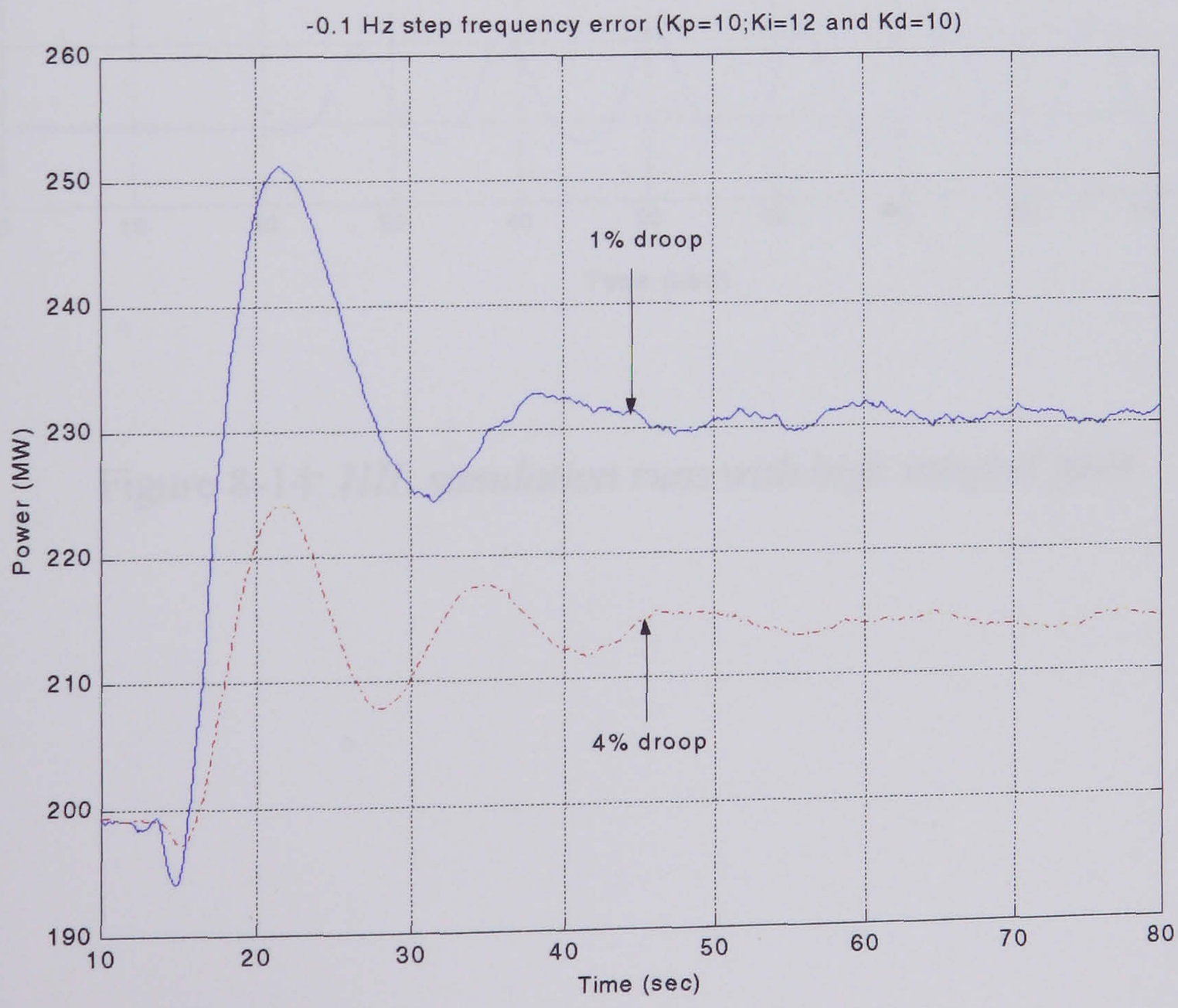

Figure 8-13: *HIL simulation runs with new governor gains*

The final simulation run is again for the case of 4% droop but this time the governor integral gain setting was extremely high $K_p = 10$, $K_i = 15$ and $K_d = 2$. Figure 8-14 shows the response of the unit to 0.2Hz step frequency. It is clear that this action induces a sustained oscillation having a period of 14 seconds and substantially constant peak to peak amplitude of as much as 80MW. This implies that the system is operating beyond its stability boundaries.

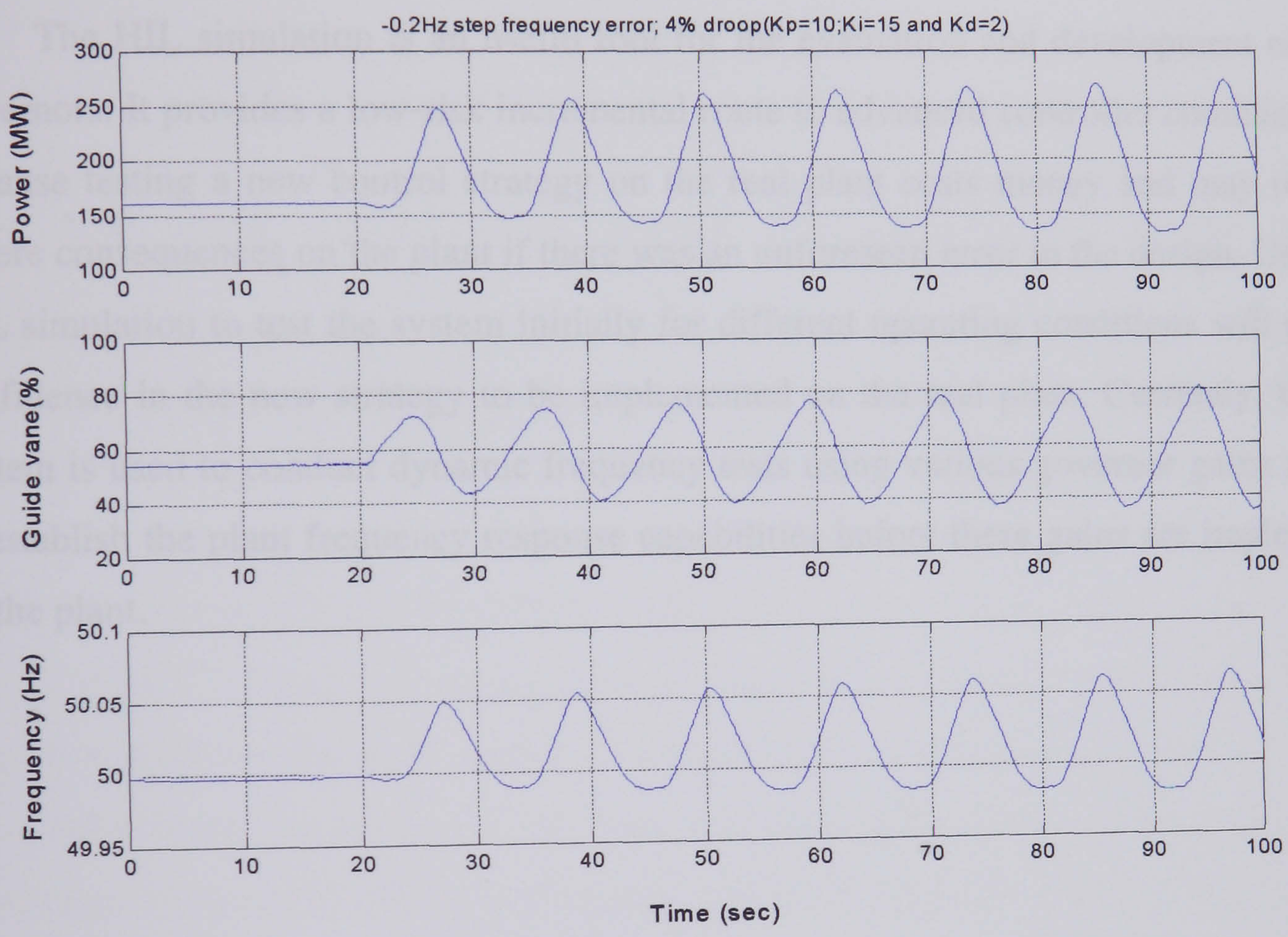

Figure 8-14: *HIL simulation runs with high integral gain*

8.4 Conclusions

The purpose of this work is to investigate whether a hardware-in-the-loop simulation can be applied to the pumped storage station nonlinear model. It has been demonstrated that it is possible to build representative plant models based on the Dinorwig power station that are capable of real-time execution and which result in excellent accuracy compared with the real system responses, such as the dead-band response of Figure 8-9 and the dynamic frequency response of the plant of Figure 8-11.

The HIL simulation is an useful tool for the evaluation and development of speed governors. It provides a low-risk incremental route to advanced controller commissioning because testing a new control strategy on the real plant costs money and may result in severe consequences on the plant if there was an unforeseen error in the design. Using the HIL simulation to test the system initially for different operating conditions will provide confidence in the new strategy to be implemented on the real plant. Currently, the HIL system is used to conduct dynamic frequency tests using various governor gains settings to establish the plant frequency response capabilities before these gains are implemented on the plant.

Chapter 9

Conclusions and Future Work

9.1 Review of Thesis

This thesis has described a nonlinear computer model of Dinorwig Power Station constructed using MATLAB® /SIMULINK® software which has also been integrated using dSPACE® as part of a real-time HIL simulation. The thesis shows that this work has helped to improve the performance of Dinorwig. The modelling process has yielded information about the system which helps to define, and provide understanding of, the interaction between its different elements. Chapter 1 explains that the motivation for investigating Dinorwig in detail is the economic situation since deregulation of the electricity market and the importance for the generation companies of improving their responses.

Chapter 2 considers the development of equations that represent the hydraulic system. Emphasis is given to describing and modelling the water hammer phenomenon in the water column and the hydraulic coupling between the units sharing the same tunnel, as is the case at Dinorwig. The chapter presents the most accepted methods of modelling the system in addition to investigating their advantages and disadvantages. The system parameters, namely the water starting time, water travelling time and head loss coefficients, are calculated for each part of the system. This is a very important exercise as the accuracy of the model and hence the simulation depends on it. The chapter

concludes that using a nonlinear model is more accurate than using a simple linearised representation in simulation studies.

Chapter 3 gives a short overview of the electrical system theory necessary to understand its operation and control. Modelling the power system is a very complex issue, because it involves the effects of all generating units, the links between the grids in multi-area power systems the loads on the system and their dynamics. In the thesis more emphasis is given to active power control because Dinorwig is used for load frequency control (LFC). Thus, differential equations relating the generator speed to acceleration torque are developed using the swing equation. The load effects are based on a static load constant current model where the power varies with voltage in a linear manner. The internal machine oscillations, which indicate the stiffness of the unit's coupling with the power system, are also taken into account.

Chapter 4 describes the speed governor that is based on a three-term controller. An investigation into the Dinorwig control system is carried out where two control loops per turbine are implemented for frequency and power respectively, and the governor setting used is the same for all operating conditions. The governor is a digital based controller with very complex PLC programming. The results of swept-frequency test carried out on the governor verify its mathematical representation. The results also reveal two additional filters in the system - one for signal averaging (frequency signal) and the second to limit the derivative gain. The chapter proceeds with modelling of the guide vane where a step response is used to obtain the system model. The guide vane actuators have nonlinear dynamics due to the physical limitation on their movement and this effect is incorporated in the model. The chapter highlights the benefits of system identification techniques for obtaining a low order linearised model.

Chapters 2 to 4 constitute a review and application of established theory which leads to an original study into methods to integrate the complete system model as described in Chapter 5. Here step-by-step model integration is presented, and the disadvantages of using linear models for simulation study are highlighted. Methods of system verification are introduced and the results increase the confidence in the model to be used for off-line simulation study.

Governor tuning is described in Chapter 6 which derives an optimum governor setting to enhance the station responses for different operating conditions. An analysis of isolated operation based on the Routh-Hurwitz criterion and root locus method reveals

that using derivative action would increase the stability boundaries and hence improves the response of the Units. The investigation expands the limits of derivative gain as predicted by Hagihara et al [48]. The effects of the power system on the Dinorwig governor gain is also investigated using Gain and Phase margins analysis. The results show that the grid loading has a critical influence on the plant response and hence the required governor gains. For a larger grid size, high governor gains are desirable while the gains should be reduced for smaller grid sizes. However, when operating with dead-band on, the droop setting mainly influences the Unit response and a high droop gain is required for this mode of operation. This finding could be used for gain scheduling control (see future work). This will have big impact on Dinorwig as it will be able to deliver fast and stable responses for all operation conditions, which implies more financial gains in return.

The focus of Chapter 7 is on the application of the simulation. A new black–start (energising the power system after a black out) scheme was designed for Dinorwig. This configuration can act to limit frequency swings for a 15% cold load insertion to within permitted values. The simulation was then used to investigate and duplicate a sustained oscillation incident of all the units on-line that occurred at Dinorwig. The results show that the problem could be avoided if the droop setting of the units with dead band on was set to a higher value, an assumption that agreed with the prediction of the previous chapter. The chapter concludes by extensive simulation carried out to predict the stability limits for the governor in order to improve the plant performance for a wide range of operating conditions.

The final chapter is used to integrate the off-line simulation model with the hardware governor system to establish a real-time HIL simulation. The work involved extensive Simulink model enhancement to interface it with the hardware so that the correct type of information (input/output data) was passed between the two. The results show good agreement in the responses of the HIL configuration and real plant. The HIL configuration is used as a test bed for any governor control alteration on the existing system at Dinorwig.

9.2 Future Work

The system models and the off-line/real-time simulation developed within this project have proven to be powerful tools for analysing the performance of Dinorwig. The models developed are generic and, with little modification, could be applied to any hydro plant. Some improvement could be made to the linearised models used in control system design by applying the system identification techniques described in Chapter 4 to obtain authentic simplified models of the hydraulic system over the complete range of operating conditions.

Modelling of the power system as used in this work is based on the collective performance of all the generators connected. However, to investigate the effect of other plants online operating as frequency regulators on Dinorwig's performance, it is necessary to include them in the model as individual units. This was a difficult task to achieve because the information is not available from the NGC for commercial reasons. Another factor which could improve the model is to include the base load units being shut down or coming on-line, as this will affect the manner that a Dinorwig part-load unit will pick up or shed load.

The work has highlighted the limitation of the present PID governors where the control system design is done by means of linearised transfer functions. The plant is a highly nonlinear system and advanced control techniques could be implemented to give Dinorwig more robust control. The first approach is the use of an open loop adaptive (gain-scheduling) controller to counteract the large time-constant variations which occur when different numbers of turbine-generators are on-line. A limited form of gain scheduling is currently implemented at Dinorwig when operating with the dead-band. The study shows that Dinorwig has a hydraulic coupling which arises from a common supply tunnel which adversely affects the system stability. To reduce the interaction between the units, a multivariable controller could be used which yields better stability margins and gives a clear advantage over single loop PID controllers [71]. Adaptive self-tuning control involving continuous estimation of grid size is another possibility to investigate.

A new generation of governor could be designed based on the technique of modular neuro-fuzzy systems [72]. The adoption of a modular strategy will support the design of complex controllers involving multiple inputs and outputs. This will involve:

- Evaluation of the range of operating conditions and constraints for Dinorwig and establishment of appropriate data collection methods to monitor these conditions.
- Evaluation of the embedded knowledge regarding the plant and the station operation currently available within the personnel at Dinorwig and the incorporation of that knowledge into the new governor.
- Application of neuro-fuzzy methods to control the generation in order to build a governor capable of autonomously responding to changes in system conditions and to imposed constraints.

The 'hardware-in-the-loop' configuration could be used to evaluate the new governor where a prototype system of the governor will be connected to the simulation plant model.

A decline in efficiency of the plant costs money in terms of water energy loss, maintenance and overhaul costs. Therefore, operating the turbo-generator units at optimum efficiency and with minimum maintenance costs is an important issue for the First Hydro Company. Assessment of overall long-term performance of individual Units can be achieved by condition monitoring, where the measured responses are compared to establish if any Unit is operating more efficiently than the others. Any long-term changes in an Unit's performance can also be spotted as a possible indication of imminent malfunction or need for maintenance due to wear and tear.

Appendix-I

Linearised turbine-penstock model

The first order linear model of turbine-penstock used in Section 2.4.1 is derived by linearising equations (2-4) and (2-11), which is achieved by substituting $x = x_0+\Delta x$ for each variable, dropping the initial conditions and any terms higher than Δx. For equation (2-4)

$$\left(\bar{q}_0+\Delta\bar{q}\right)=\left(\bar{G}_0+\Delta\bar{G}\right)\sqrt{\bar{h}_0+\Delta\bar{h}} \tag{I-1}$$

The terms under the radical can be linearised using Taylor expansion of a polynomial raised to the ½ power,

$$(x_0+\Delta x)^{1/2}=\sqrt{x_0}\left(1+\frac{\Delta x}{2x_0}\right) \tag{I-2}$$

therefore;

$$\bar{q}_0+\Delta\bar{q}=\left(\bar{G}_0+\Delta\bar{G}\right)\sqrt{\bar{h}_0}\left(1+\frac{\Delta\bar{h}}{2\bar{h}_0}\right) \tag{I-3}$$

$$\bar{q}_0+\Delta\bar{q}=\bar{G}_0\sqrt{\bar{h}_0}+\bar{G}_0\frac{\Delta\bar{h}\sqrt{\bar{h}_0}}{2\bar{h}_0}+\Delta\bar{G}\sqrt{\bar{h}_0}+\frac{\Delta\bar{G}\Delta\bar{h}\sqrt{\bar{h}_0}}{2\bar{h}_0}$$

Dropping the initial conditions and the terms higher than Δx yields,

$$\Delta\bar{q}=\Delta\bar{G}\sqrt{\bar{h}_0}+\bar{G}_0\frac{\Delta\bar{h}\sqrt{\bar{h}_0}}{2\bar{h}_0} \tag{I-4}$$

In equation (2-11) h_i is constant therefore,

$$\Delta\bar{h}=-\Delta\bar{q}T_w s \tag{I-5}$$

Substituting $\Delta \bar{h}$ in equation (I-4) gives,

$$\Delta \bar{q} = \Delta \bar{G} \sqrt{\bar{h}_0} - \frac{\bar{G}_0 \sqrt{\bar{h}_0}}{2\bar{h}_0} T_w s \Delta \bar{q} \tag{I-6}$$

Solving for $\Delta \bar{q}$ gives

$$\Delta \bar{q} = \Delta \bar{G} \frac{\sqrt{\bar{h}_0}}{1 + \frac{\bar{G}_0 \sqrt{\bar{h}_0}}{2\bar{h}_0} T_w s} \tag{I-7}$$

The equation for mechanical power developed in the turbine is,

$$\overline{P_m} = A_t \bar{q} \bar{h} \tag{I-8}$$

Linearising equation (I-8) yield,

$$\Delta \overline{P_m} = A_t q_0 \Delta h + A_t \Delta q h_0 \tag{I-9}$$

Substituting equation (I-5) into (I-9) for $\Delta \bar{h}$ yields,

$$\Delta \overline{P_m}(s) = A_t \left(\bar{h}_0 - \bar{q}_0 T_w s \right) \Delta \bar{q} \tag{I-10}$$

Substituting equation (I-7) for $\Delta \bar{q}$ into equation (1-10) gives

$$\frac{\Delta \overline{P_m}(s)}{\Delta \bar{G}(s)} = \frac{A_t \left(\bar{h}_0 - \bar{q}_0 T_w s \right) \sqrt{\bar{h}_0}}{1 + \frac{\bar{G}_0 \sqrt{\bar{h}_0}}{2\bar{h}_0} T_w s} \tag{I-11}$$

However, $\bar{q}_0 = \bar{G}_0 \sqrt{\bar{h}_0}$

$$\frac{\Delta\overline{P_m}(s)}{\Delta\overline{G}(s)} = \frac{A_t \bar{h}_0 \sqrt{\bar{h}_0}\left(1 - \frac{\bar{q}_0}{\bar{h}_0} T_w s\right)}{1 + \frac{\bar{q}_0}{2\bar{h}_0} T_w s} = A_t \bar{h}_0 \sqrt{\bar{h}_0}\left(\frac{1 - T_{w0}.s}{1 + 0.5T_{w0}.s}\right) \quad \text{(I-12)}$$

Note since $T_w = \frac{Lq_{base}}{gAh_{base}}$, $\bar{q}_0 = \frac{q_0}{q_{base}}$ and $\bar{h}_0 = \frac{h_0}{h_{base}}$

The water starting time in equation (I-12) is $T_{w0} = \frac{\bar{q}_0}{\bar{h}_0} T_w = \frac{Lq_0}{gAh_0}$

which corresponds to the unit's operating condition rather than the rated conditions. Thus to accurately model the water column in stability simulations, it would be necessary to adjust the value of T_w each time the dispatch of the hydroelectric units was changed in the initial condition load flow.

Appendix-II

Comparison between model and test responses

Additional model verification is presented by comparing the simulation model and the plant responses during the dynamic frequency test, carried out by the NGC, at Dinorwig to asses its frequency response capabilities as described in Section 5.3.4. Test B0 was carried out by injection of a simulated frequency error signal of - 0.5Hz ramped in 10s into the governor of Unit #2. The Unit was initially loaded to 150MW operating at specific governor gains of $K_p = 9$, $K_i = 5$, $K_d = 2$ and 4% droop. Figure (II-1) shows the amount of power being picked up by the Unit as a response to the negative frequency signal (extra load). The Unit picks up an extra load of 50MW after 10s and 72MW after 30s. While the guide vane moves from 38% to 55% as shown in Figure (II-2). The test scenario was applied to the simulation model and the results illustrates good agreement for both the power and guide vane movement.,

Test B2 was carried out using ± 0.2Hz error signal ramped in 10s. The Unit was initially loaded to 230MW, operating at governor gains of $K_p = 10$, $K_i = 8$, $K_d = 2$ and with a droop of 4%. The power picked up by the Unit is shown in Figure (II-3), here the Unit picks up an extra load of 26MW after 10s and 30MW after 30s. Then during the positive error signal the Unit shed 23MW in 10s. The guide vane moves as shown in Figure (II-4) from 57% to 65%, corresponding to the extra generation. As before, the test was simulated and the results demonstrate once more the good agreement with the test, however, the simulated power is rather less damped than the measured response. This may be due to change in the operational conditions of the plant, as another unit is brought on-line.

Test A4 represents Unit #2 loaded with 150MW and operating at governor gains of $K_p = 10$, $K_i = 8$, $K_d = 2$ and 1% droop, responding to –0.2Hz step error signal. The results are shown in Figure (II-5) and Figure (II-6) where the Unit picks up load of 75MW after 10s and 110MW after 30s. Appling the test to the simulation model results in responses agree with the test result.

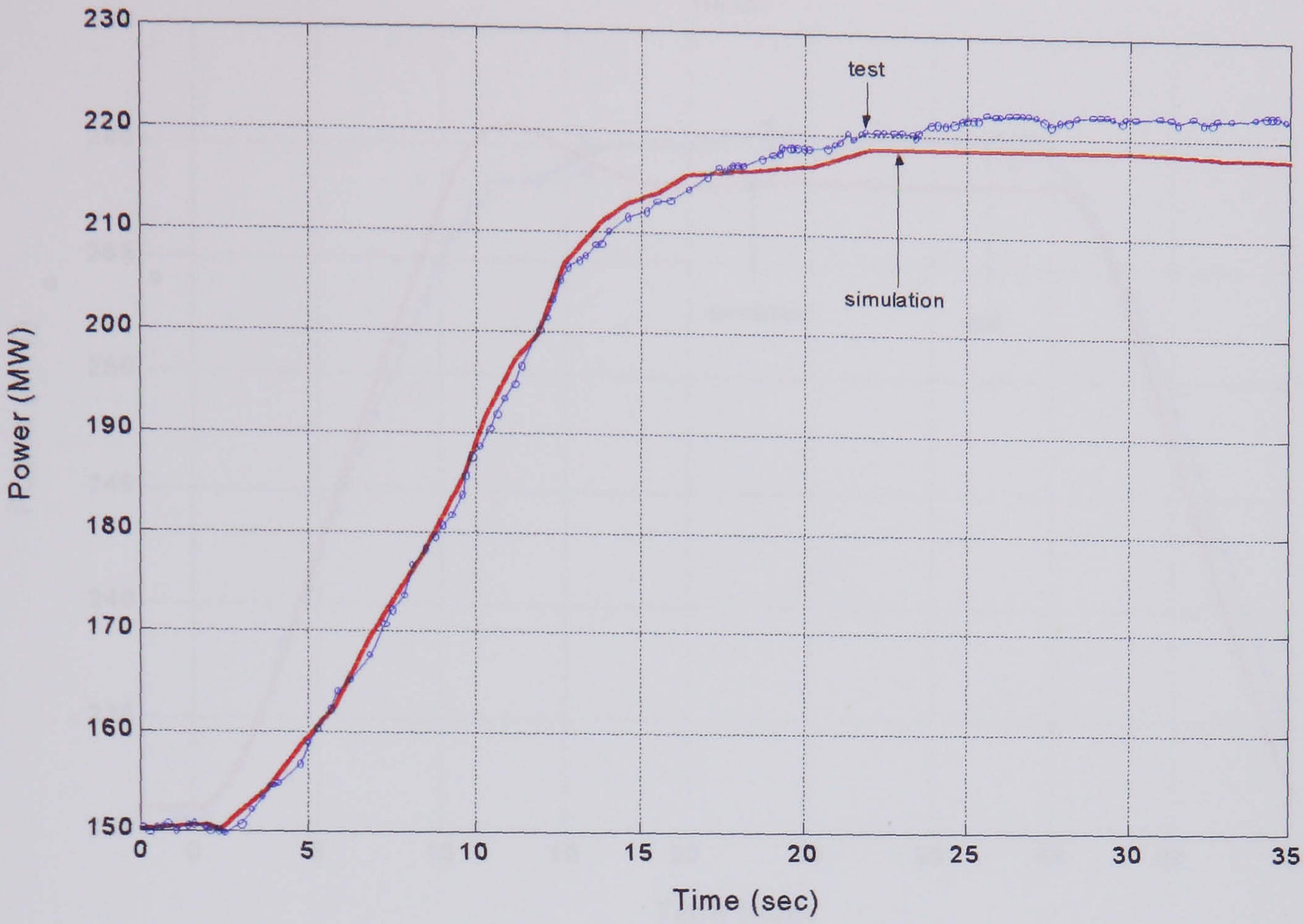

Figure II-1: *Test B0 unit loading*

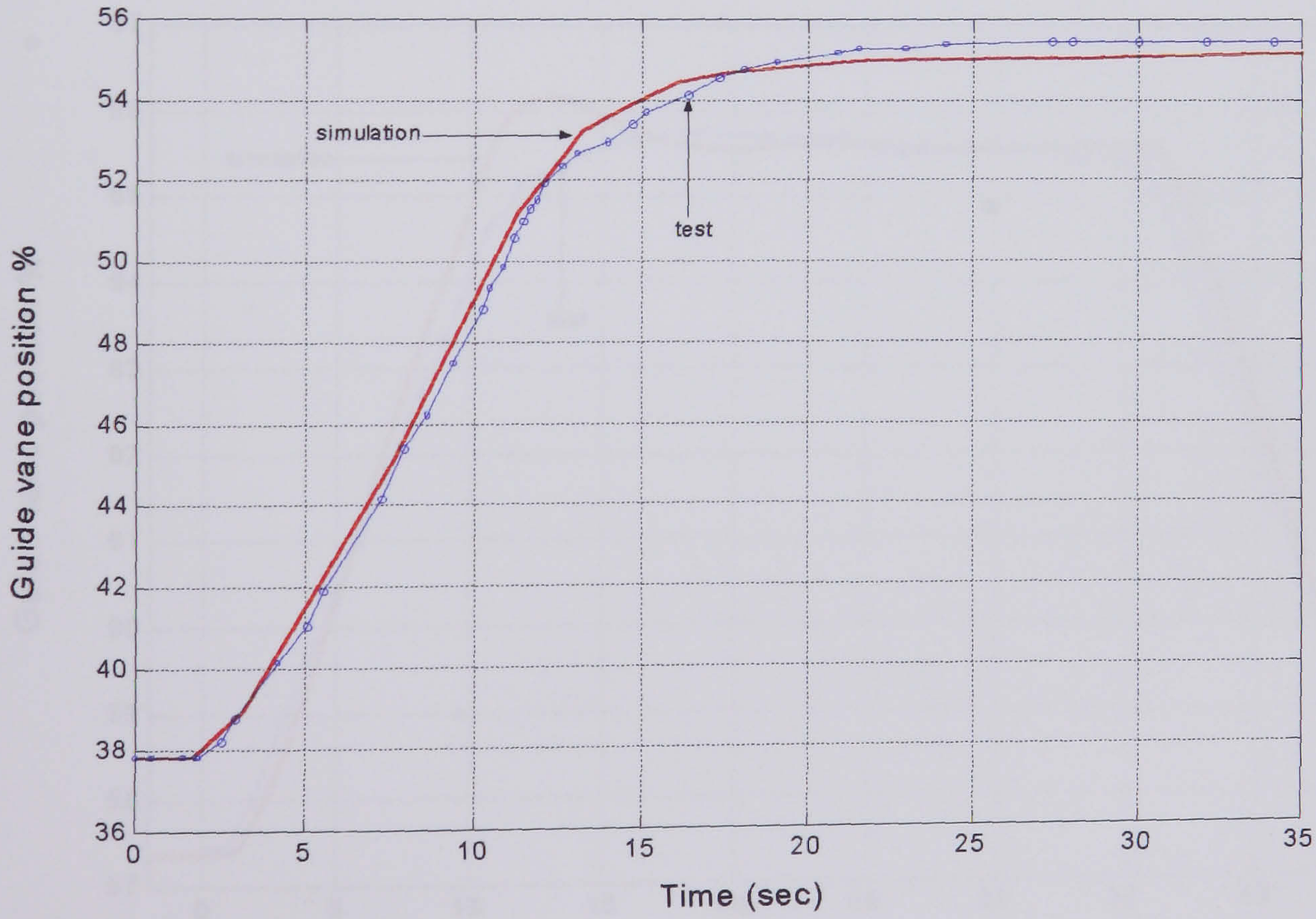

Figure II-2: *Test B0 unit guide vane movement*

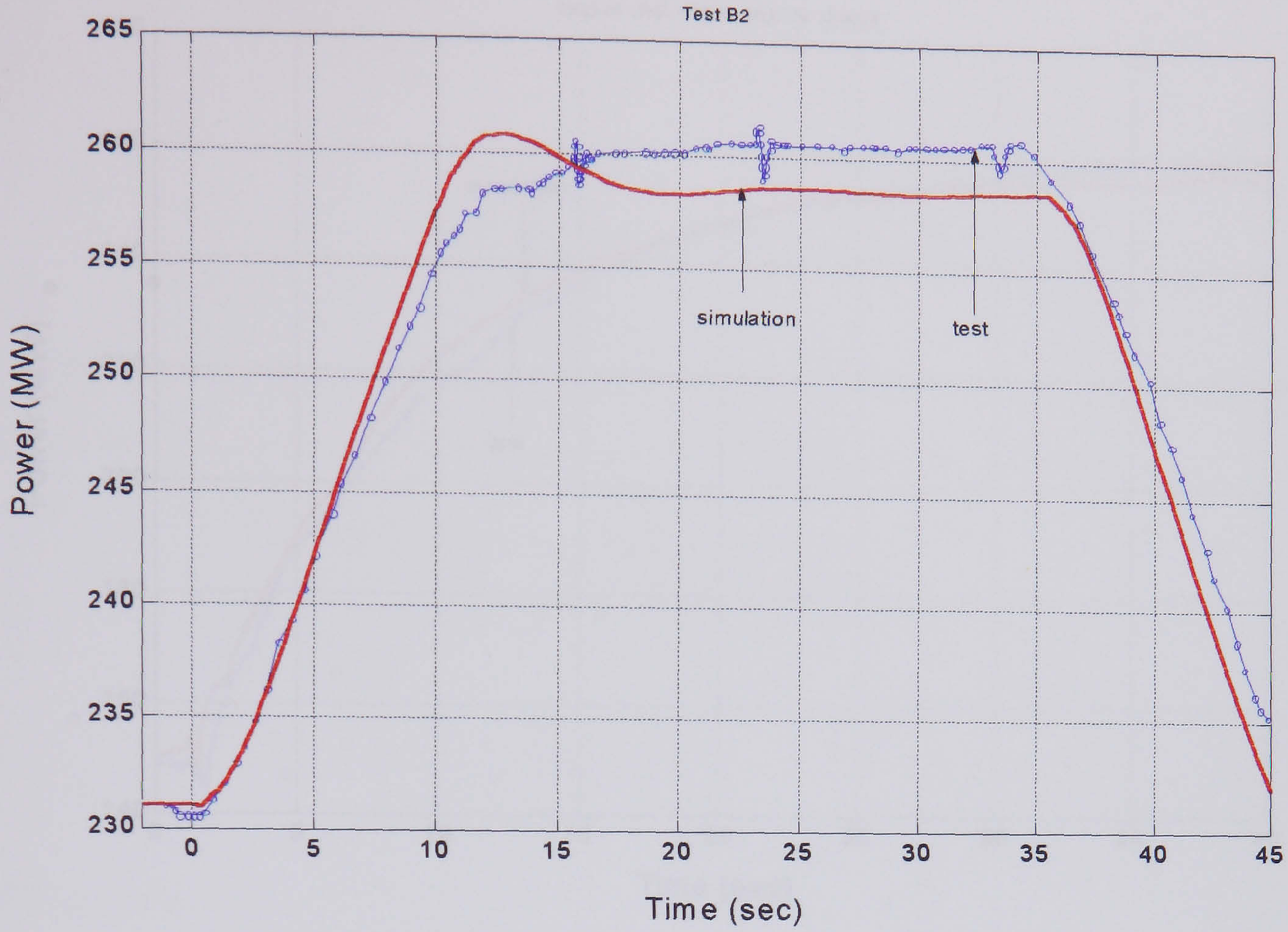

Figure II-3: *Test B2 unit loading*

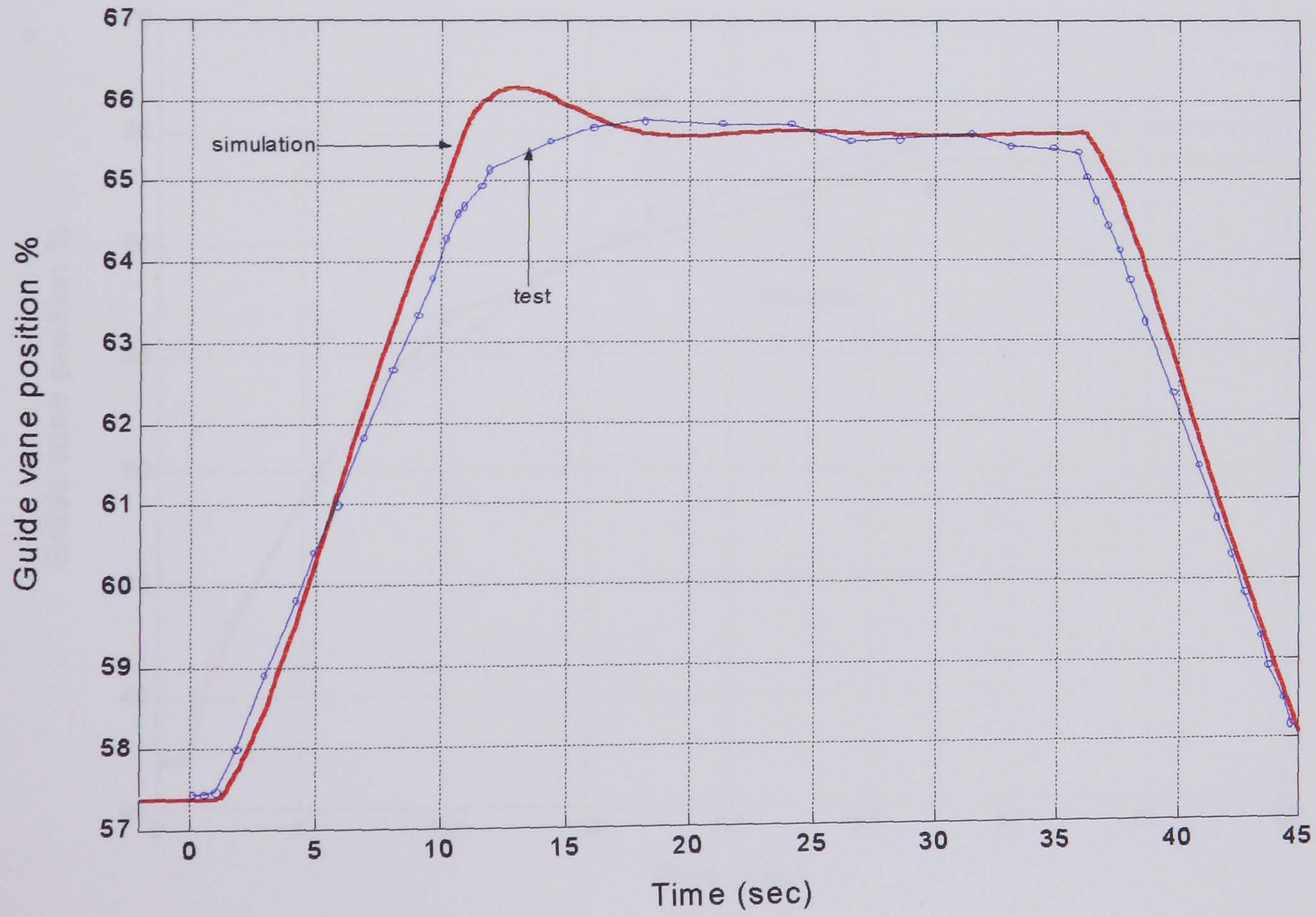

Figure II-4: *Test B2 unit guide vane movement*

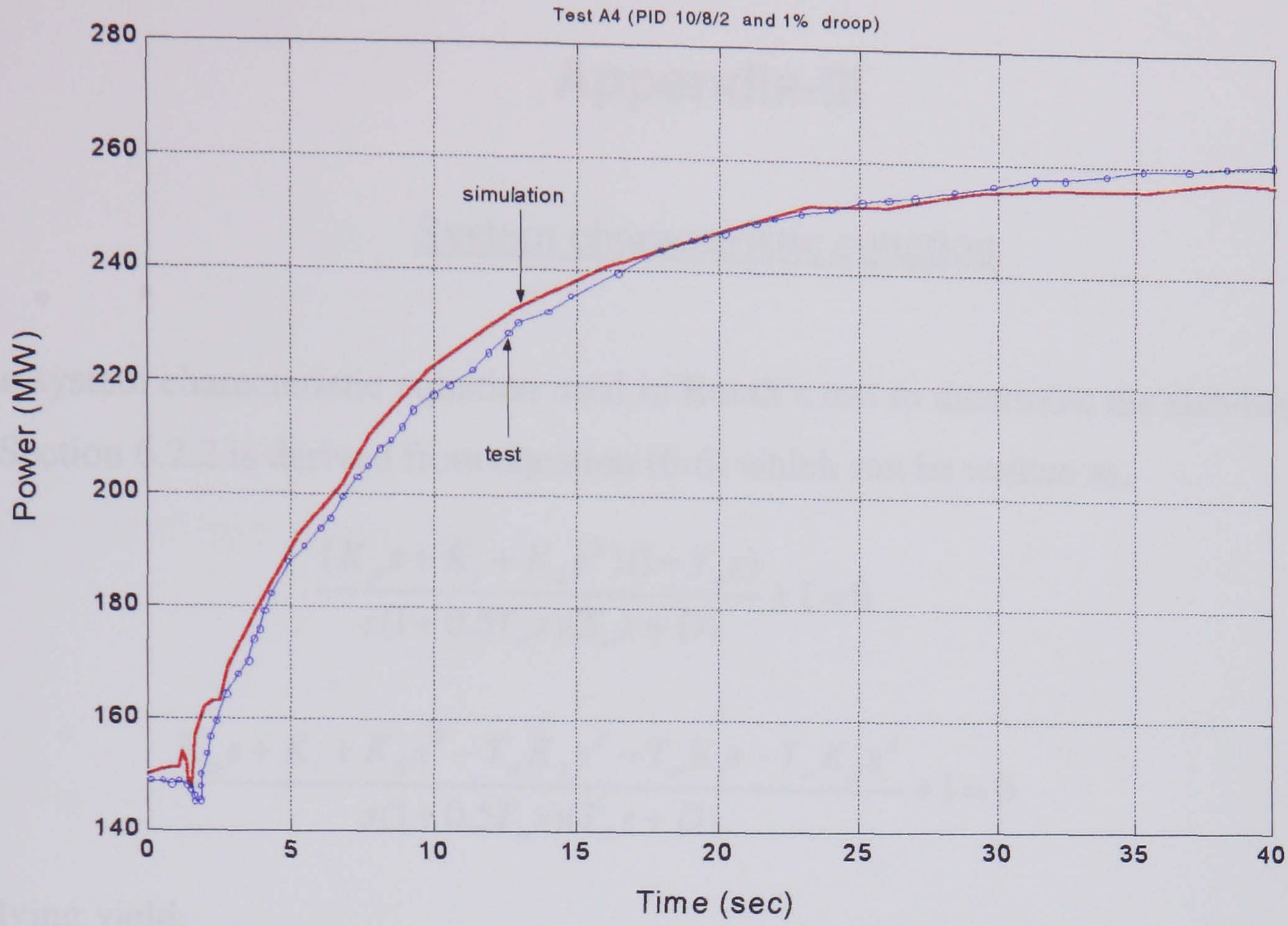

Figure II-5: *Test A4 unit loading*

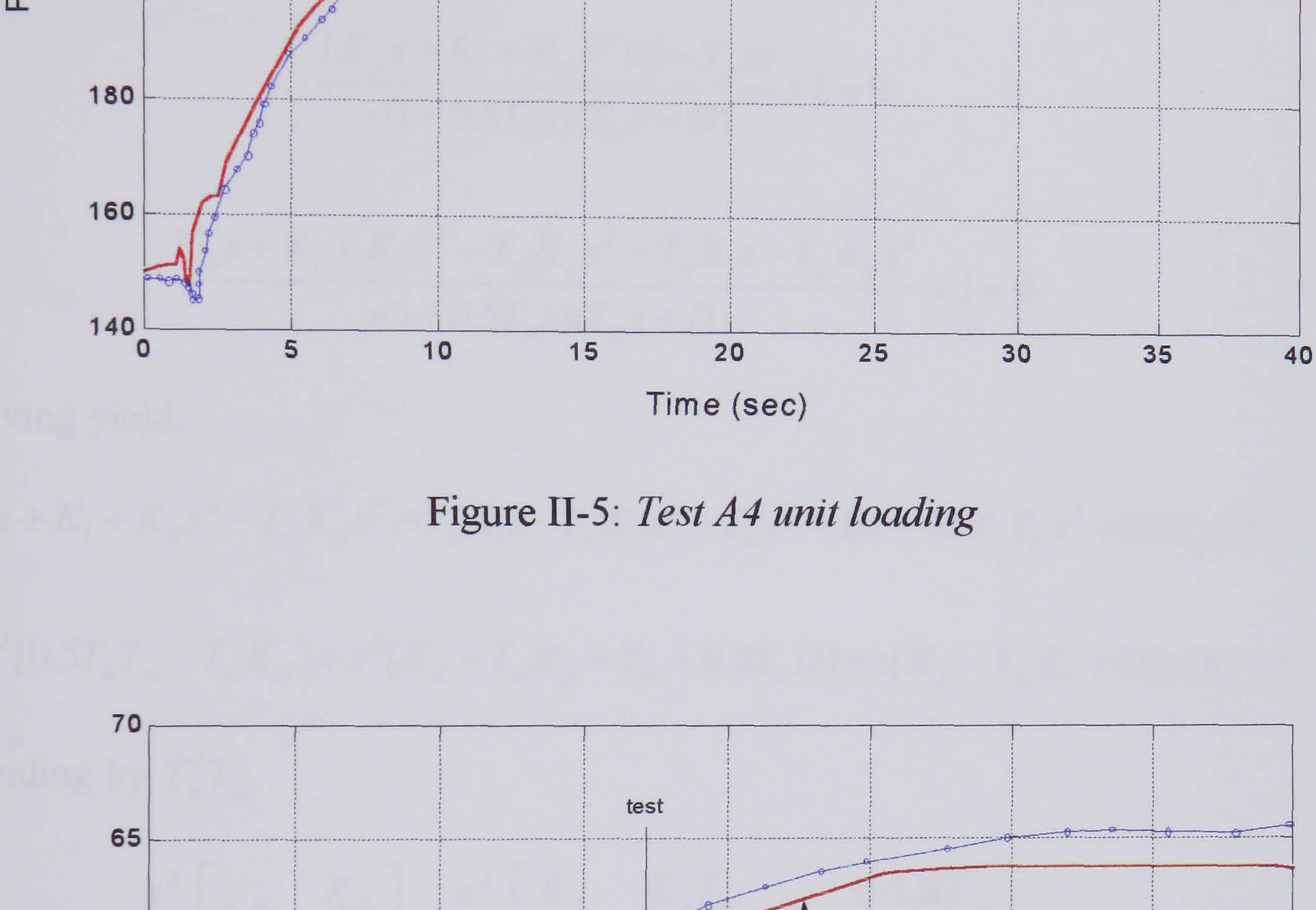

Figure II-6: *Test A4 unit guide vane movement*

Appendix-III

System characteristic equation

The system characteristic equation used in Routh's test to determine the stability margins in Section 6.2.2 is derived from equation (6-6) which can be written as,

$$\frac{(K_p s + K_i + K_d s^2)(1 - T_w s)}{s(1 + 0.5T_w s)(T_m s + D)} + 1 = 0 \qquad \text{(III-1)}$$

$$\frac{K_p s + K_i + K_d s^2 - T_w K_p s^2 - T_w K_i s - T_w K_d s^3}{s(1 + 0.5T_w s)(T_m s + D)} + 1 = 0 \qquad \text{(III-2)}$$

Solving yield,

$$K_p s + K_i + K_d s^2 - T_w K_p s^2 - T_w K_i s - T_w K_d s^3 + T_m s^2 + Ds + 0.5T_w T_m s^3 + 0.5T_w D s^2 = 0 \qquad \text{(III-3)}$$

$$s^3[0.5T_w T_m - T_w K_d] + s^2[K_d - T_w K_p + T_m + 0.5T_w D] + s[K_p - T_w K_i + D] + K_i = 0 \qquad \text{(III-4)}$$

Dividing by $T_w^2 T_m$

$$\frac{s^3}{T_w}\left[0.5 - \frac{K_d}{T_m}\right] + \frac{s^2}{T_w^2}\left[\frac{K_d}{T_m} - \frac{K_p T_w}{T_m} + 1 + \frac{0.5DT_w}{T_m}\right] + \frac{s}{T_w^3}\left[\frac{K_p T_w}{T_m} - \frac{K_i T_w^2}{T_m} + \frac{DT_w}{T_m}\right] + \frac{1}{T_w^4}\left[\frac{K_i T_w^2}{T_m}\right] = 0 \qquad \text{(III-5)}$$

Set $X_1 = \frac{K_p T_w}{T_m}$; $X_2 = \frac{K_i T_w}{K_p}$; $X_3 = \frac{K_d}{T_m}$; $X_4 = D\frac{T_w}{T_m}$

The T_w may be eliminated by scaling the Laplace variable $s_{new} = sT_w$

$$s^3(0.5 - X_3) + s^2(X_3 - X_1 + 1 + 0.5X_4) + s(X_1 - X_1 X_2 + X_4) + X_1 X_2 = 0 \qquad \text{(III-6)}$$

Equation (III-6) is used to determine the Routh array.

Appendix-IV

Open loop transfer function of the system

The appendix describe the derivation of the open loop transfer function of the system used in Section 6.2.3 to obtain the optimum system setting using root loci. The system transfer function of equation (6-3) is

$$G(s) = \frac{(K_p s + K_i + K_d s^2)(1 - T_w s)}{s(1 + 0.5 T_w s)(T_m s + D)}$$

Solving yield,

$$G(s) = \frac{-T_w K_d s^3 + s^2(K_d - T_w K_p) + s(K_p - T_w K_i) + K_i}{s(1 + 0.5 T_w s)(T_m s + D)} \qquad \text{(IV-1)}$$

dividing by $T_m T_w^2$ yield,

$$G(s) = \frac{-\frac{s^3}{T_w}\left(\frac{K_d}{T_m}\right) + \frac{s^2}{T_w^2}\left(\frac{K_d}{T_m} - \frac{T_w K_p}{T_m}\right) + \frac{s}{T_w^3}\left(\frac{K_p T_w}{T_m} - \frac{K_i T_w^2}{T_m}\right) + \frac{1}{T_w^4}\left(\frac{K_i T_w^2}{T_m}\right)}{\frac{s}{T_m T_w^2}(1 + 0.5 T_w s)(T_m s + D)} \qquad \text{(IV-2)}$$

eliminate T_w by scaling the Laplace variable $s_{new} = sT_w$

$$G(s) = \frac{-s^3\left(\frac{K_d}{T_m}\right) + s^2\left(\frac{K_d}{T_m} - \frac{T_w K_p}{T_m}\right) + s\left(\frac{K_p T_w}{T_m} - \frac{K_i T_w^2}{T_m}\right) + \left(\frac{K_i T_w^2}{T_m}\right)}{\frac{s}{T_m}(1 + 0.5 s)(T_m s + T_w D)} \qquad \text{(IV-3)}$$

rearranging

$$G(s) = \frac{-s^3\left(\frac{K_d}{T_m}\right) + s^2\left(\frac{K_d}{T_m} - \frac{T_w K_p}{T_m}\right) + s\left(\frac{K_p T_w}{T_m} - \frac{K_i T_w^2}{T_m}\right) + \left(\frac{K_i T_w^2}{T_m}\right)}{s(1 + 0.5 s)(s + \frac{T_w}{T_m} D)} \qquad \text{(IV-4)}$$

substituting $X_1 = \frac{K_p T_w}{T_m}$; $X_2 = \frac{K_i T_w}{K_p}$; $X_3 = \frac{K_d}{T_m}$; $X_4 = D\frac{T_w}{T_m}$ $X_1 X_2 = K_i \frac{T_w^2}{T_m}$

$$G(s)=\frac{-s^3X_3+s^2\left(X_3-X_1\right)+s\left(X_1-X_1X_2\right)+X_1X_2}{s(1+0.5s)(s+X_4)} \tag{IV-5}$$

Bibliography

[1] K. H. Fasol and G. M. Pohl, "Simulation, controller design and field tests for a hydropower plant - a case study", Automatica, vol. 3, pp. 475-485, 1990.

[2] K. H. Fasol, "Stabilization and re-engineering of a hydroelectric power plant - a case study", Control Engineering Practice, vol. 5(1), pp. 109-115, 1997.

[3] O. C. Symons, "Dinorwig Power Station -ASEA Governor Performance", Central electricity Generating Board PL-ST/28/76, 1976.

[4] D. N. Konidaris and J. Tegopoulos, "Investigation of Oscillatory Problems of Hydraulic Generating Units Equipped with Francis Turbines", IEEE Transaction on Energy Conversion, vol. 12, pp. 419-425, 1997.

[5] J. F. Douglas and R. D. Mathews, "Fluid Mechanics", 2. Addison Wesley Longman Ltd.: 1996.

[6] J. Undrill and J. Woodward, "Calculation for Determining Temporary Droop", PAS-86, pp. 443-451, 1966.

[7] Central Electricity Generating Board, "Report on Studies for Hydraulic System", Merz & McLellan 1975.

[8] J. L. Woodward, "Hydraulic-Turbine Transfer Function for use in Governing Studies", Proc. IEE, vol. 115, pp. 424-426, 1968.

[9] Thorne D.H and Hill E.F, "Field Testing and Simulation of Hydraulic Turbine Governing Performance", IEEE Transaction on Power Apparatus and Systems, PAS-93, pp. 1183-1191, 1974.

[10] J. R. Smith and et al, "Assessment of hydro-turbine models for power-systems studies", IEE Proceeding, vol. 130, Part C, pp. 1-6, 1983.

[11] Kvaerner Boving Ltd., "Commissioning Report for Unit #1 Replacement Governors", National Grid 20043, 15-6-1995 1995.

[12] F. R. Schleif and A. B. Wilbor, "The Coordination of Hydraulic Turbine Governors for Power System Operation", IEEE Transaction on Power Apparatus and Systems, PAS-85, pp. 750-756, 1966.

[13] Working Group on Prime, "Hydraulic Turbine and Turbine Control Models for System Dynamic Studies", IEEE Transaction on Power Systems, vol. 7, pp. 167-179, 1992.

[14] IEEE Committee Report, "Dynamic Models for Hydro Turbines in Power System Studies", IEEE Transaction on Power Apparatus and Systems, 1973.

[15] C. Vournas and A. Zaharakis, "Hydro Turbine Transfer Functions with Hydraulic Coupling", IEEE Transaction on Energy Conversion, vol. 8, pp. 527-532, 1993.

[16] D. G. Ramey and J. W. Skooglund, "Detailed Hydro-governor Representation for System Stability Studies", IEEE Transaction on Power Apparatus and Systems, PAS-89, pp. 106-112, 1970.

[17] C. C. Warnick, "Hydropower Engineering". Prentice-Hall Ltd.: 1984.

[18] L. Wozniak and G. H. Fett, "Conduit Representation in Closed loop Simulation of Hydraulic Systems", ASME Publication, vol. 71-WA/FE-26, pp. 1-5, 1971.

[19] L. N. Hannett, J.W. Feltes, B. Fardanesh, and W. Crean, "Modelling and Control Tuning of a Hydro Station with Units Sharing a Common Penstock Section", IEEE Transaction on Power Systems, vol. 14, pp. 1407-1414, 1999.

[20] L. N. Hannett, "Field Tests to Validate Hydro Turbine-Governor Model Structure and Parameters", IEEE Transaction on Power Systems, vol. 9, pp. 1744-1750, 1994.

[21] K. Dutton, S. Thompson, and B. Barraclough, "The Art of Control Engineering", 2nd edition. Addison-Wesley: 1998.

[22] C. K. Sanathanan, "Accurate Low Order Model for Hydraulic Turbine - Penstock", IEEE Transaction on Energy Conversion, vol. EC-2, pp. 196-200, 1987.

[23] R. E. Goodson, "Distributed System Simulation Using Infinite Product Expansions", Simulation, vol. 15, pp. 255-263, 1970.

[24] P. Azoury, M. Baasiri and H. Najm, "Effects of Valve-Closure Schedule on Water Hammer", vol. 112, pp. 890-903, 1984..

[25] H. M. Paynter, "Methods and Results from M.I.T Studies in Unsteady Flow", BSCE Journal, vol. 39, pp. 224-227, 1952.

[26] C. S. Kung and X. L. Yang, "Energy Interpretation of Hydraulic Transients in Power Plant with Surge Tank", Journal of Hydraulic Research, vol. 31, pp. 825-839, 1993.

[27] C. D. Vournas and G. Papaioannou, "Modelling and Stability of a Hydro Plant with two Surge Tanks", IEEE Transaction on Energy Conversion, vol. 10, pp. 368-375, 1994.

[28] J. Parmakian, "Water Hammer Analysis", Dover Publication, New York: 1963.

[29] R. H. Sabersky and A. J. Acosta, "Fluid flow", The Macmillan Company New York: 1975.

[30] FHC Report D21, "Head loss Calculation for Dinorwig System", First Hydro Company, 1995.

[31] F. P. deMello and C. Concordia, "Concepts of Synchronous Machine Stability as Affected by Excitation Control", IEEE Transaction on Power Apparatus and Systems, PAS-88, pp. 316-329, 1969.

[32] Kvaerner Boving Ltd., "Governor- influence of derivative gain on the optimisation of proportional & integral gains", Report-22664, 1996.

[33] C. Concordia, "Load representation in power system stability studies", IEEE Transaction on Power Apparatus and System, PAS-101, pp. 969-977, 1982.

[34] G. L. Berg, "Power system load representation", Proc.IEE, vol. 120, pp. 344-348, 1973.

[35] IEEE Task Force, "Load Representation for Dynamic Performance Analysis", IEEE Transaction on Power Systems, vol. 8, pp. 472-481, 1993.

[36] B. Delfino, G. B. Denegri, E. C. Bonini, R. Marconato, and P. Scarpellini, "Black-Start and Restoration of a Part of the Italian HV Network: Modelling and Simulation of a Field Test", IEEE Transaction on Power Systems, vol. 11, pp. 1371-1379, 1996.

[37] L. Basanez, J. Riera, and J. Ayza, "Modelling and Simulation of Multiarea Power System Load-Frequency Control", Mathematics and Computers in Simulation, pp. 54-62, 1984.

[38] O. L. Elgerd and C. H. Fosha, "Optimum Megawatt-Frequency Control of Multiarea Electric Energy Systems", IEEE Transaction on Power Apparatus and Systems, PAS-89, pp. 556-563, 1970.

[39] T. Inoue, H. Taniguchi, Y. Ikeguchi, and K. Yoshida, "Estimation of Power System Inertia Constant and Capacity of Spinning -reserve Support Generators Using Measured Frequency Transients", IEEE Transaction on Power Systems, vol. 12, pp. 136-143, 1997.

[40] R. M. Wright, "Understanding Modern Governor Control", IEEE Transaction on Energy Conversion, vol. 4, pp. 453-458, 1989.

[41] C. C. Bissell, "Control Engineering", 2nd edition, Chapman & Hill, London: 1994.

[42] Instruction Manual, "ABB Turbine Governor HPC640 PC diagram", ABB Generation, Sweden 1995.

[43] P. E. Wellstead and M. B. Zarrop, "Self-Tuning Systems", Wiley: 1991.

[44] Solartron Instruments, "1253 Gain-Phase Analyser Operating Manual", Schlumberger Technologies, 1987.

[45] Instruction Manual "Analogue Devices Voltage-to-Frequency convertor AD537".

[46] User's Guide, "MATLAB System Toolboxes", Version 5, 3rd edition, The Math Works Inc., MA, USA: 1996.

[47] J. M. Undrill and W. Strauss, "Influence of Hydro Plant Design on Regulating and Reserve Response Capacity", IEEE Transaction on Power Apparatus and Systems, PAS-93, pp. 1192-1200, 1974.

[48] G. F. Franklin and J. D. Powell, "Feedback Control of Dynamic Systems", 3rd edition, Addison-Wesley Publishing Company.

[49] S. Hagihara, "Stability of a Hydraulic Turbine Generating Unit Controlled by P.I.D Governor", IEEE Transaction on Power Apparatus and Systems, PAS-98, pp. 2294-2298, 1979.

[50] S. P. Mansoor, D. I. Jones, D. A. Bradley, C. Aris, and G. Jones, "Modelling of a Pumped Storage Hydro Power Station for Stability Studies", The International Journal on Hydropower & Dams "Hydropower into the Next Century", pp. 535-544, 1999.

[51] S. P. Mansoor, "Modelling of a Multiple Pump-Storage Units connected to a Power System", Conference Proceeding PREP"99, pp. 412-415, 1999.

[52] A. P. Boldy, "Dinorwig Power Station Parametric Study", Hydrosim Consultants HYS-RP112, 1998.

[53] I. A. Erinmez, D. O. Bickers, G. F. Wood, and W. W. Hung, "NGC Experience with Frequency Control in England and Wales - Provision of Frequency Response by Generators", IEEE PES 1999 Winter Meeting, vol. 1, pp. 590-593, 1998.

[54] L. Wozniak, "A Graphical Approach to Hydro-generator Tuning", IEEE Transaction on Energy Conversion, vol. 5, pp. 417-421, 1990.

[55] L. M. Hovey and L. A. Bateman, "Speed-Regulation Tests on a Hydro Station Supplying an Isolated Load", AIEE, vol. 62, pp. 364-371, 1962.

[56] L. M. Hovey, "Optimum Adjustment of Hydro Governors on Manitoba Hydro System", AIEE, pp. 581-585, 1962.

[57] H. M. Paynter, "The Analogue in Governor Design, I, a restricted problem Governor A Palimpsest on Electronic Analogue Art", Printed by A. Philbrick Researches, Inc., Boston, MA., pp. 224-227, 1960.

[58] J. E. Van Ness, "Root Loci of Load Frequency Control Systems", IEEE Transaction on Power Apparatus and Systems, vol. S82, pp. 712-724, 1963.

[59] D. Graham and R. C. Lathrop, "The Synthesis of Optimum Responses: Criteria and Standard Forms", Trans. Am. Inst. Electrical Engineering, vol. 72, pp. 273-288, 1953.

[60] S. J. Mason, "Feedback Theory: Some Properties of Signal Flow Graphs", Proc. IRE, vol. 41, pp. 1144-1156, 1953.

[61] IEEE Standard 122-1991, "Recommended Practice for Functional and Performance Characteristics of Control Systems for Steam Turbine-Generator Units", February 1992.

[62] S. P. Mansoor, D. I. Jones, D. A. Bradley, C. Aris, and G. Jones, "Stability of a Pump Storage Hydro-Power Station Connected to a Power System", IEEE power Winter Meeting 1999, New York, pp. 646-650, 1999.

[63] A Task Force Report, "Power System Restoration", IEEE Transaction on Power Systems, vol. PWRS-2, pp. 271-276, 1987.

[64] P. F. Arnold, "Summery of system restoration plan for Pacific Northwest Power System", Power System Restoration T.F.Mtg., 1984.

[65] S. P. Mansoor, D. I. Jones, D. A. Bradley, C. Aris, and G. Jones, "Simulation of Oscillatory Behaviour at Dinorwig Pumped Storage Hydro Power Station", The International Journal on Hydropower & Dams "Hydropower into the Next Century", pp. 587-594, 1999.

[66] S. P. Mansoor, D. A. Bradley, C. Aris, and G. Jones, "The Influence of the Grid on the Response of Pump Storage Hydro-Power Station", World Scientific, Recent Advances in Circuits and Systems, pp. 259-263, 1998.

[67] S. P. Mansoor, D. A. Bradley, C. Aris, and G. Jones, "The Development of a Hardware-In-The-Loop Simulation of a Pump Storage Hydro Power Station", Proceedings of Mechatronics '98, pp. 633-638, 1998.

[68] P. J. Throckmorton and L. Wozniak, "A Generic DSP-Based Real-Time Simulator with Application to Hydro-generator Speed Controller Development", IEEE Transaction on Energy Conversion, vol. 9, pp. 238-242, 1993.

[69] S. Bennett, "Real-Time Computer Control", 1st edition, Prentice Hall International, Hertfordshire, UK: 1988.

[70] dSPACE User's Guide. dSPACE GmbH, Paderborn, Germany, 1996.

[71] D. I. Jones, "Multivariable control analysis of a hydraulic turbine", Trans Inst MC, vol. 21 (2/3), pp. 122-136, 1999.

[72] R.B. Nukala, "Neuro-fussy controllers for unstable systems", PhD Thesis, University of Lancaster.